



UNIVERSITAT^{DE}
BARCELONA

Advances in high throughput and affordable phenotyping for adapting maize and wheat to climate change

Adrián Gracia Romero



Aquesta tesi doctoral està subjecta a la llicència **Reconeixement 4.0. Espanya de Creative Commons.**

Esta tesis doctoral está sujeta a la licencia **Reconocimiento 4.0. España de Creative Commons.**

This doctoral thesis is licensed under the **Creative Commons Attribution 4.0. Spain License.**

Doctoral thesis

Advances in high throughput and affordable phenotyping for adapting maize and wheat to climate change



Adrian Gracia Romero

Universitat de Barcelona, 2021



UNIVERSITAT DE
BARCELONA

Advances in high throughput and affordable phenotyping for adapting maize and wheat to climate change

Memòria presentada per Adrian Gracia Romero per a optar al grau de Doctor per la Universitat de Barcelona.

Aquest treball s'emmarca en el programa de doctorat de Ecologia, Ciències Ambientals i Fisiologia Vegetal del Departament de Biologia Evolutiva, Ecologia i Ciències Ambientals (BEECA) de la Facultat de Biologia de la Universitat de Barcelona.

El present treball ha estat realitzat en el grup de recerca Integrative Crop Ecophysiology Group, sota la direcció del Dr. José Luis Araus Ortega i del Dr. Shawn C. Kefauver.

Adrian Gracia Romero

Doctorant

José Luis Araus Ortega

**Dr. José Luis Araus
Ortega**

Director i tutor

**Dr. Shawn Carlisle
Kefauver**

Director

26 d'abril 2021

A mi padre y a mi madre, quienes me lo han dado todo.

*A la Jessica, qui em fa despendrem de totes les meves inseguretats
i em treu el millor de mi.*

ABSTRACT

Supplying sufficient food to an increasing population is one of the most important challenges over the next century. To meet this demand, crop productivity will need to increase while it is being threatened by climate change effects like the increase of temperatures and the intensity of drought periods. Improving crop performance is key for an efficient adaptation to these challenging growing conditions, with crop breeding being one of the pillars. In that sense selecting more productive varieties for specific environments requires a better understanding of plant acclimation to stress conditions, including efficient phenotyping approaches. Plant phenotyping research pursues the development of new methods with high-throughput capacity and affordable to characterize non-destructively plant traits of interest. The main focus of this thesis was to develop and study versatile and precise methodologies with high-throughput capacity in order to improve crop performance assessments, while saving time and costs in the phenotyping tasks of two of the most important cereal crops: maize and wheat. The use of unmanned aerial vehicles (UAV) equipped with imaging sensors (including RGB, multispectral and thermal) permits covering simultaneously hectares of experimental fields fast, precisely, and in a non-destructive way. However, ground evaluations may still be an alternative in terms of cost and spatial resolution. The performance of these methodologies to assess genotypic differences in grain yield was evaluated in maize and wheat under different agronomical and environmental growing conditions such as nutrient deficiency, conservation agriculture, drought and heat stress. On one side, maize studies were performed in trials in Zimbabwe focused on the evaluation of genotypes under either low and normal phosphorus conditions or the application of conservation agriculture together with different top-dressing nitrogen fertilization regimes, to overcome the nutrient poverty of soils. In these studies, vegetation indices, related to

parameters informing on the above-ground biomass and assessed during early stages of development, performed well as grain yield indicators. Moreover, during more advanced phenological stages, indices informing on the leaf and the canopy color were the traits that reported a better association with grain yield and N content in leaves. For the case of wheat, evaluations were performed in different latitudes in Spain covering a range of environments and grown under different management conditions, and sampling was performed during the reproductive stage (heading, anthesis and grain filling). In general terms, biomass indicators, such as canopy green biomass inferred from vegetation indices, together with water status indicators, such as canopy temperature, were the most critical traits predicting GY. The delay of senescence in water-limited environments and the photosynthetic efficiency measured by multispectral indices like the photochemical reflectance index (PRI) during anthesis were also relevant traits for GY under the rainfed and late-planting trials, respectively.

ACKNOWLEDGEMENTS

All the work presented in this doctoral thesis is the result of a teamwork, that It couldn't be finish without the help and contribution of my directors and colleagues. Firstly, I would like to thank both of my directors.

Professor **Josep Lluís Araus** has been the greatest mentor I could have for this journey. From the moment I started working with him during my bachelor, he always had a moment for me, and he offered everything I needed. He has encouraged me all the time and made me feel very motivated. I have always felt as an important part of the research, as he always considered my opinion, and I had his trust when I had to make important decisions.

To doctor **Shawn C. Kefauver** I have to thank all the skills I have acquired during this doctorate, from statistical analysis, programming, image analysis, flight operations with the drone, scientific writing skills, data visualization... Moreover, thanks to him, I got the best opportunities in relation to courses, conferences and travels.

At the same level, the assistance of my colleagues from the Integrative Ecophysiology Group have been fundamental. From each of them I take something. **Omar Vergara** was the first person I met, the one who had an enormous patience to introduce me to the research and from whom I learned all the basics of the field work. From **Rut Sanchez** I got the confidence to manage myself as a researcher, always being open to help. Even coinciding in a short period, **Susan Merino** gave me lots of important advice of how to cope with the doctorate during our long talks. From **Jose Armando** I have taken how to take the bright side of the things, always with the right words to cheer everybody up. I spent long periods in the laboratory with **Fadia Chairi**, were we laughed a lot, making the time go faster during tedious work. **Fatima Zahra Rezzouk** and **Luisa Buchailot**

have been my two PhD colleagues. When they arrived as master's students, I was the one with the patience, but since then we have evolved together. The last to arrive, **Joel Segarra**, is someone who's always ready to discuss about anything and our talks have been a learning for me. Thanks to **Melissa Chang, Cristina Caldelas, Thomas Vatter** and **Rubén Vicente** for their support along these years. I would also like to thank all the visiting students that joined us, **Samuel Kamphorst, Ludovico Caracciolo, Valter, Maissa** and **Yassine**, it was a pleasure meeting them, and sharing with them not only a bit of knowledge but also a friendship. I would like to thank the contribution from **Dra. Maria Dolors Serret** and **Dr. Jordi Bort**. We made a great team, and I will always remember the good times in the office, our travels, the long car trips singing all kind of songs, the also long field works and the great dinners after, the conferences, the participation in courses... All of them became really good friends and made my PhD much easier and a great experience.

In addition, I thank the rest of PhD students, researchers, technicians and the professors from the **Unit of Fisiologia Vegetal**, the experimental field facilities of the greenhouse and the *Serveis Científicotecnics UB*, especially the support and guidance of **Dra. Ma Lluïsa Moisset** since I got into to the master.

I also wanted to thank all our collaborators and the working staff in the research stations. On one side, we got a lot of support from **Jesús Merida** and **Natalia Marín** from INIA-Coria del Río, **Maria Teresa Nieto "Mariate"** from INIA-Colmenar de Oreja and **Nieves Aparicio** from ITACyL-Valladolid, not only for their involvement on the field management, but also they were always ready to help in the field. I would also like to thank to all the team in Valladolid, especially **Ismael, Raquel** and **Yessica**. On the other side, thanks to **Jill Cairns, Mainassara Zaman-Allah, Christian Thierfelder** and

Boddupalli M. Prasanna from CIMMYT-Harare, who received us in Zimbabwe and Kenia, and they were always very disposed to collaborate with us.

I would like to extend my sincere thanks to **Prof. Pablo Zarco Tejada** who opened the doors of his research group in Melbourne and gave me the opportunity from learning from them. Thanks to **Dra. Lola Suarez, Dr. Tomas Poblete, Anne Wang, Andrew R. Longmire, Anirudh Belwalkar, Xiaojin Qian** and **Wey Yao Wong**, who spend time to teach me about lots of techniques and methodologies that were new to me and also ensured all the time that I had a great stay. My time in Australia was a very inspirational experience from which I keep lots of good memories.

Thanks to my friends **Adri Sanchez, Àlex Pereira, Pere Galimany, Celeste Chalk, Silvia Alvarez, Eira Pasqual** and the guys from **La LMS**, who have accompanied me during these years, and they always had time for a beer or two. Thanks to my colleagues of **Ambientals**, who are a very important part of my life.

Thanks to all of my **family** for their continuous love, help and support.

Thanks to **my parents**, their dedication and guidance were more valuable than they could ever imagine.

Lastly, thanks to **Jessica**, her unqualified support, love and encourage have been crucial during these years.

TABLE OF CONTENTS

ABBREVIATIONS	1
INTRODUCTION	3
Food Security in the face of Climate Change	5
Challenges for maize and wheat breeding	8
Closing yield gaps through plant phenotyping	9
Basis of Remote Sensing techniques for Plant Phenotyping	12
Formulation of spectral vegetation indices	13
Low-cost assessment of VI through conventional RGB cameras	14
Canopy temperature as an indicator of crop water status	16
UAV as high-throughput plant phenotyping tools	17
Isotope composition as laboratory analysis to complement VI	18
OBJECTIVES	21
Specific aims	23
REPORT OF THE THESIS DIRECTORS	27
CHAPTER 1. Comparative performance of ground vs. aerially assessed RGB and multispectral indices for early-growth evaluation of maize performance under phosphorus fertilization	39
CHAPTER 2. Phenotyping conservation agriculture management effects on ground and aerial remote sensing assessments of maize hybrids performance in Zimbabwe	55
CHAPTER 3. UAV and ground image-based phenotyping: a proof of concept with durum wheat agriculture: a case of study with maize in Zimbabwe	79
CHAPTER 4. Leaf versus whole-canopy remote sensing methodologies for crop monitoring under conservation agriculture: a case of study with maize in Zimbabwe	107
CHAPTER 5. High-throughput phenotyping to define of durum wheat ideotypes adapted to Mediterranean environments	127
DISCUSSION	173
Breeding for yield, a phenotypically complex trait	175
Remote sensing ability to assess genotypic differences in yield under different growing conditions	178

Multispectral VIs performance determining differences in grain yield	179
RGB Indices performance determining differences in grain yield	180
Canopy Temperature performance determining differences in grain yield	181
Comparative Performance of Ground Versus Aerially Assessed Indices	184
Assessment of plant traits across the crop season: when is the best moment to measure	186
Challenges and opportunities of GY prediction models based on phenotyping data	187
CONCLUSIONS	191
RESUM GENERAL DE LA TESI	197
REFERENCES	201

ABBREVIATIONS

AN , Ammonium Nitrate	d¹⁵N , nitrogen stable isotope composition
ANOVA , analysis of variance	DF/Fm' , Effective Fluorescence Quantum yield
Anth , anthocyanins	FAO , Food and Agriculture Organization
ARI , anthocyanin reflectance index	Flav , flavonoids
CA , conservation agriculture	GA , green area
CARI , chlorophyll absorption ratio index	GGA , greener area
CCI , chlorophyll content index	GLI , green leaf index
Chl , chlorophyll	GY , grain yield
CIMMYT , International Maize and Wheat Improvement Center	H² , heritability
CP , conventional ploughed	HIS , Hue-Intensity-Saturation
CRI , carotenoid reflectance index	HTPP , High-Throughput Plant Phenotyping
CSI , crop senescence index	ICPOES , Inductively Coupled Plasma Optical Emission Spectroscopy
CT , canopy temperature	INIA , Instituto Nacional de Investigación y Tecnología Agraria y Alimentaria
CTD , canopy temperature depression	
CTV , contribution to total variation	
d¹³C , carbon stable isotope composition	

IPCC, Intergovernmental Panel on
Climate Change

LASSO, least absolute shrinkage and
selection operator

LCC, leaf chlorophyll content

MAE, mean absolute error

MAPAMA, Ministerio de Agricultura y
Pesca Alimentación y Medio Ambiente

masl, meters above sea level

MCARI, chlorophyll absorption ratio
index

MET, multi-environment trials

NBI, nitrogen balance index

Ndab. normalized difference $a*b^*$

NDVI, normalized difference
vegetation index

NGRDI, normalized green-red
difference index

NIR, near-infrared

OSAVI, optimized soil adjusted
vegetation index

PRI, photochemical reflectance index

RGB, Red-Green-Blue

RMSE, root mean square error

SAVI, soil adjusted vegetation index

SIAR, Sistema de Información
Agroclimática para el Regadío

SSA, Sub-Saharan Africa

TCARI, transformed chlorophyll
absorption ratio index

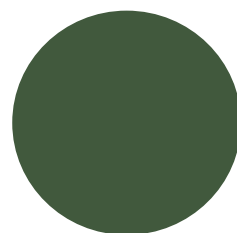
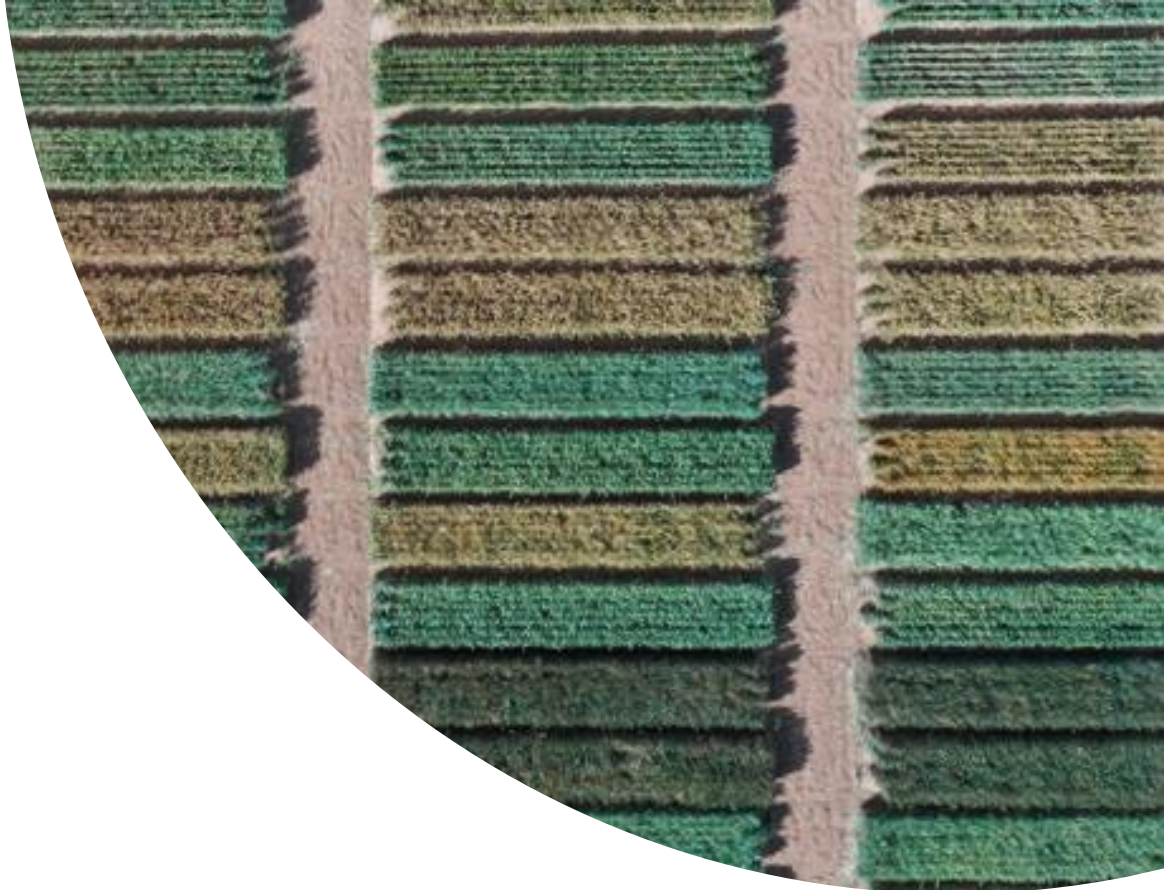
TGI, triangular greenness index

TIR, thermal infrared radiation

UAV, unmanned aerial vehicle

VIs, vegetation indices

WBI, water band index



INTRODUCTION

INTRODUCTION

Food Security in the face of Climate Change

During the past half-century, a marked growth in food production helped to keep pace with the increase on food demand despite a doubling of the total world population. The so-called Green Revolution involved a conjunction of advances, such as the development of high yielding varieties, the massive synthesis and use of chemicals fertilizers, as well as an increase in the level of mechanization in cultivation that led to an unprecedented increase in agricultural productivity (Khush, 1999). Nevertheless, prospects show that global food security is not ensured for the near future (McKersie, 2015). The Food and Agriculture Organization (FAO) of the United Nations defined food security as when all people, at all times, have physical, social and economic access to sufficient, safe and nutritious food that meets their dietary needs and food preferences for an active and healthy life (FAO, IFAD, UNICEF, WFP, 2020). Current demands for crop production are experiencing an acceleration, mainly driven by trends in population growth, which anticipate that humans will reach near 11.2 billion by 2100 (Figure 1). Also hampered with a shift of diets away from staples and increasingly towards livestock and dairy products, vegetables and fruit, and fats and oils, and a greater competition for land, water, and energy for biofuel production (Cole et al., 2018). This has placed pressure on food production globally, which would need to be increased by 60%–110% to meet these increasing demands (Figure 2). However, the current rates of yield increase are insufficient to meet the anticipated demands, as agricultural production is being highly limited by biotic and abiotic stresses (i.e., diseases and water, nutrient and energy scarcity) as result of the impact of climate change (Charles et al., 2010). These constraints have very diverse effects on global agriculture due to a very strong regional component, but also vary by crop. For example, to optimize the attainable yields of the main staple

crops in Sub-Saharan Africa would primarily require addressing nutrient deficiency for maize, while in the Mediterranean Basin there has been observed a co-limitation of both nutrient and water for wheat (Mueller et al., 2012).

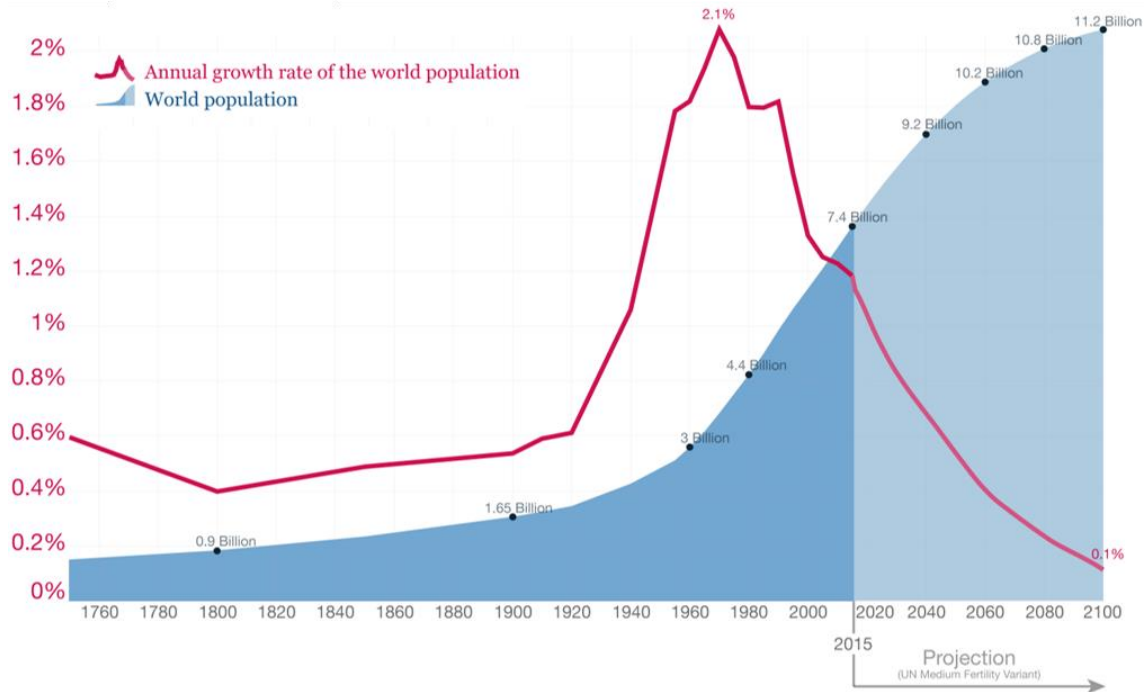


Figure 1. World population growth rate (red line) and total world population (blue shaded area) from 1950 to 2100. Figure adapted from the source “Our World in Data”.

The principal factors that will contribute most to the productivity of agricultural crops are changes in precipitation and temperature (Von Braun, 2007; Calzadilla et al., 2013). Variations in rainfall patterns determine the availability of freshwater and soil moisture, critical for crop growth, particularly in rainfed agriculture. At global scale, according to the last report of the Intergovernmental Panel on Climate Change (IPCC) human-induced global warming is likely to reach 1.5°C between 2030 and 2052 (IPCC, 2019). Temperature determines the length of growing season and control the crop’s development with higher temperatures shortening the frost period and promoting cultivation in cool-climate marginal croplands but reducing crop cycles and yields in semi-arid areas (IPCC, 2019).

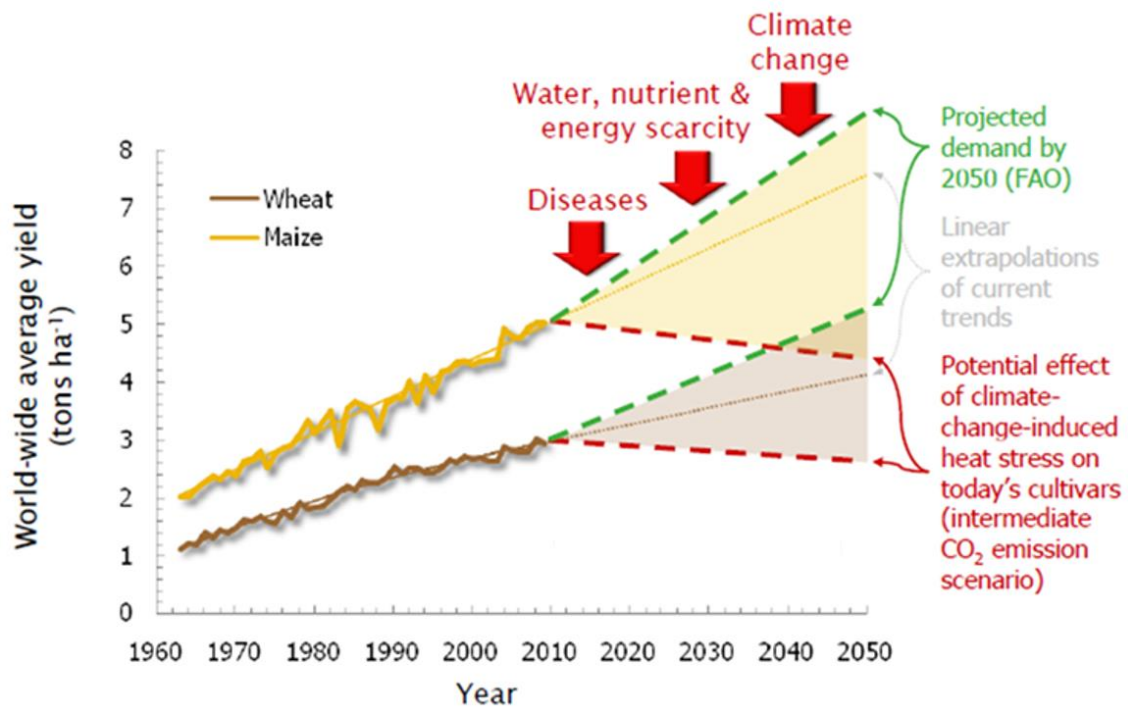


Figure 2. World-wide average yield trends in wheat (brown line) and maize (yellow line) from the period 1960-2015 measured in tonnes per hectare. From the period 2015-2050, brown and yellow lines represent the linear extrapolations of the current trends for wheat and maize, respectively. Green line represents the projected food demand by 2050 and the red line the potential effect of climate change on the yield trends. Figure adapted from FAO resources.

For the Sub-Saharan Africa (SSA) region, together with increasing threats of climate change with more frequent dry spells and increased heat stress, the loss of soil and its fertility is expected to become more critical makes particularly vulnerable due the low adaptive capacity of their current cropping systems. Traditional practices of monoculture and soil tillage have led to a decline in soil fertility (Thierfelder et al., 2015), causing the use of phosphorus and nitrogen fertilizers to become essential. Yet, this situation cannot be considered sustainable given the economic and environmental impact associated with high fertilization rates.

In the case of southern Europe, projected changes in temperature and precipitation patterns in the coming decades are positioning the Mediterranean Basin as one of the most prominent climate change hotspots (Diffenbaugh and Giorgi, 2012), where severe impacts on agriculture are expected (Asseng et al., 2015). Of particular concern for the Iberian Peninsula is an increase in the frequency and severity of droughts associated with a decrease in precipitation and coupled with an increase in evapotranspiration caused by rising temperatures (Vicente-Serrano et al., 2014). For wheat, the success of breeding in the second half of the last century was made possible by the introduction of dwarf genes, increasing the harvest index and thus yield. However, since then, the rate of genetic advance has declined. Focusing on drought and temperature stress, one key factor to increasing wheat may be extending the duration of grain filling by maintaining healthy green.

Challenges for maize and wheat breeding

Accelerating crop improvement is an issue of increasing urgency to satisfy the ever-increasing global food demand and for that purpose wheat and maize breeding success depends on developing high-yielding varieties better adapted to the changing climate conditions. How crop yields are affected by the stress conditions caused by climate change has received a great deal of attention (Mittler, 2006; Mosa et al., 2017; Lamers et al., 2020), as the effect of abiotic stress can lead to deficiencies in growth, crop yields or permanent damage.

One of the major abiotic stressors that affects crops growth is water deficit. Water stress is primarily caused when the water supply to the roots becomes limiting or the transpiration rates becomes excessive (Osakabe et al., 2014). When an episode of drought shock occurs, the osmotic and metabolic imbalance of the plant leads to turgor loss and stomatal closure. In addition to the degree of the water deficit experienced, the timing of

the stress is crucial at certain development stages that are particularly sensitive for cereals. Water stress during early phenological stages will comprise a reduction in cell growth and leaf area with a consequent decrease in photosynthetic area. Drought events affecting heading and flowering time will reduce yield potential (Snape et al., 2001), as it is when number of kernels is determined. Finally, water stress will cause a shortening of the grain filling period and results in early senescence (Christopher et al., 2014). Usually, in field conditions, crops are subjected to a combination of different stresses, and it is very common to encounter drought together with heat stress under semi-arid areas. Episodes of elevated temperatures cause an acceleration of plant development, dysfunctional photosynthesis, lower fertility and poor fruit formation, having subsequent effects on crop yield (Asseng et al., 2015).

Deficiencies of major nutrients like nitrogen or phosphorus are usual in agroecosystems and can cause containment for normal growth and development of plants (Evans, 1983; Carstensen et al., 2018). As N represents a large portion of the photosynthetic proteins and phosphorus is a key element for the formation of ATP during photosynthesis, the insufficient availability will reduce the photosynthetic capacity leading to symptoms chlorosis, necrosis, reduced growth and reduced tillering.

Therefore, the intrinsic uncertainty of climate change predictions poses a challenge to achieve the target increase for wheat and maize production.

Closing yield gaps through plant phenotyping

The main approaches by which productivity of staple crops can be boosted include both the continued exploitation of the natural genetic variability and the adoption of better management practices (Araus et al., 2018). From the beginning of the development of agriculture, humanity evolved with crop species by the selection of most favorable plants available leading to a continuous improvement of production. Likewise, strategies to deal

with future environmental scenarios include the breeding selection of crop varieties, shifting plant characteristics to increase their resilience and reduce risks of yield shortfalls (Araus and Kefauver, 2018). Contemporary plant breeding programs require the analysis of hundreds of lines to develop new crop varieties with high yield and quality. Alternatively, the other pathway involves adjusting agronomic management practices for mitigating the exposure of crops to environmental stresses. The alteration of agronomy practices may include actions ranging from the implementation of more efficient irrigation and fertilization schemes, adjusting cultivation in terms of sowing and harvest times to adapt the whole cropping system to the application of the principles of other agronomic planning as the conservation agriculture (CA) (i.e., minimum soil disturbance, permanent soil cover and diversified crop rotations).

Phenotyping is the foundation of any breeding selection process. Plant phenotyping comprise the assessment of complex traits such as growth, development, stress tolerance and resistance, architecture, physiology, and yield, in order to study the of phenotypes with the spatially and temporally dynamic environment (Costa et al., 2019). To identify the adequate implementation of phenotyping is required hundreds of genotypic lines grown under diverse environmental scenarios, making the characterization of each plant phenome the main bottleneck for the crop improvement process (Araus and Cairns, 2014). The main object of field phenotyping is to capture information on structure, function and performance of a plant to characterize the plasticity of its phenome (genome x environment) when exposed to a range of growing conditions. Plant phenotyping purchases the generation of generate high-throughput and valuable phenotypic plant traits trough the development of and application of the suite of tools and methods together with their environment, to finally develop models able to assist in genotype selection, precision agriculture and yield forecast (Crain et al., 2017). Modern

plant phenotyping aims to guide the genome selection in basis of genetics, epigenetics, environmental pressures and crop management (Costa et al., 2019). The characterization of the plant phenotype includes diverse structural and functional traits related to growth, yield and adaptation to stress, from molecular to canopy assessments. Due to the integration of a diversity of information, phenotyping is considered at the forefront of plant breeding and selection.

High-throughput phenotyping programs (HTPP) imply the use of different non-invasive remote sensing (RS) approaches (Atzberger, 2013; Reynolds and Langridge, 2016), which enable the screening larger populations faster and more precisely than conventional phenotyping procedures. Traditional phenotyping procedures were based on the measurement on observable crop characteristics while is growing (i.e., crop establishment or date of flowering) and agronomical and yield traits after the harvest (i.e., harvest index), which are not only laborious and time-consuming but also the monitoring by eye was subjective and error-prone.

The evaluation of chlorophyll (Chl) concentration always has been one of the more common measurement made by plant scientists, traditionally assessed by the extraction of leaf materials and after by spectrophotometric determination. The development of hand-held and portable devices like the SPAD-502 from Minolta-Konica led the assessment Chl concentration from leaf transmittance in a fast and non-destructive manner. Habitually, SPAD readings have been used as indicators of crop nutritional status, such as chlorophyll concentration is strongly related to the N status of the plant (Bullock and Anderson, 1998). The SPAD-502 meter utilizes two light-emitting diodes (650 and 940 nm) and a photodiode detector to sequentially measure transmission through leaves of red and infrared light (Markwell et al., 1995). A newer alternative is the three-in-one instrument Dualex from Force-A, that, besides chlorophylls (Chl a + b), also

measures leaf epidermal flavonoids (Flav) and anthocyanins (Anth) (Cerovic et al., 2012). More recently, a newly leaf-clip sensor called MultispeQ has been developed, that apart from assessing pigment content, works as a fluorimeter that provides photosynthetic parameters, as well as environmental and location information (Kuhlgert et al., 2016). Leaf Chl readings are useful to diagnose nutrient restrictions, especially when N is the limiting factor (Buchailot et al., 2019) as changes in leaf N content result in changes in the photosynthetic proteins, that represents a large portion of the total leaf N (Evans, 1983). Despite this, operating at leaf level might be time-consuming and with low repeatability, as it only can be measured in 5-10 leaf flags.

Basis of remote sensing techniques for plant phenotyping

For that reason, remote sensing tools have received more attention as a fast and non-destructive method to estimate plant traits by the characterization of the spectral reflectance of light to determine the amount and condition of the above biomass of a crop (Xie et al., 2020). Plants have a characteristic spectral behavior as most of the radiation in the near-infrared region is reflected in contrast to the visible wavelengths where absorption is predominant (Figure 2). Thus, the interaction of light as electromagnetic radiation is measured as transmittance at leaf level and reflectance at both leaf and canopy level has been demonstrated to provide quantitative and robust information of the physiological status of a plant.

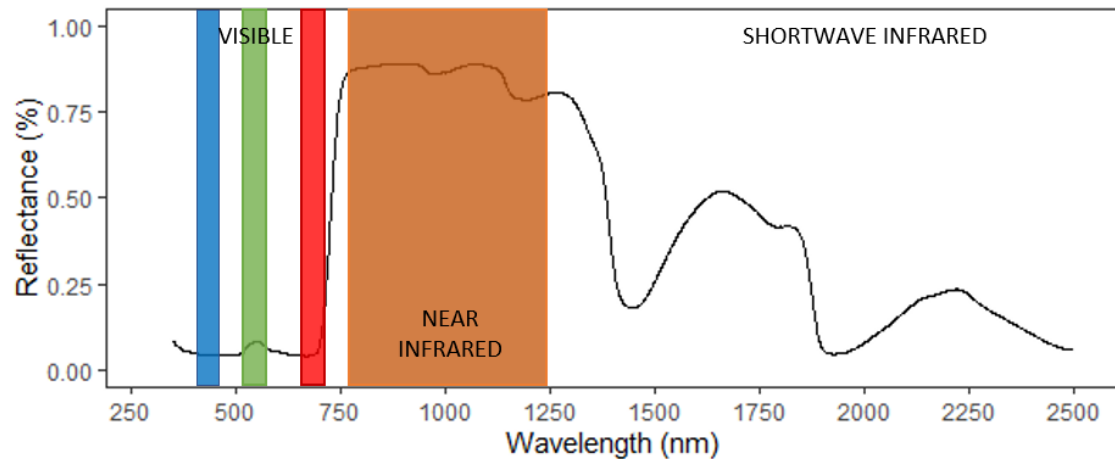


Figure 2. Typical spectral reflectance curve for vegetation.

Formulation of spectral vegetation indices

Vegetation indices (VIs) use two or more spectral bands formulated to enhance a particular vegetation signal, while reducing the solar irradiance and soil background effects (Table 1). One of the formulations most used is an index based on the combination of the characteristic low reflectance in the visible region of the spectrum (400 – 700nm) and the high reflectance in the near-infrared (NIR) (700-1100nm) region (Hassan et al., 2019). The normalized difference vegetation index (NDVI) is extensively used for measurements of vegetative cover and vigor, as well as indicators of biotic/abiotic stress levels. There are an elevated number of reformulations of the NDVI, including slight modifications and other spectral parameters to decrease the effect of soil or the problem of saturation with dense canopies. Beyond morphological and plant architecture aspects, another of the main focuses of the formulation of vegetation indices is the assessment of plant pigment content, including chlorophylls, carotenoids and anthocyanins, using reflectance information from the visible region (Gitelson et al., 2001). VI that use reflectance information at the red region (625-700nm) of the spectrum, apart from being indicators of chlorophyll content, are also used as N content predictors (Frels et al., 2018). The assessment of the photosynthetic capacity is also possible using specific narrow

bands from 510 to 550nm that are very sensitive to changes in the de-epoxidation of the xanthophyll cycle, as the case of the photochemical reflectance index (PRI) (Penuelas et al., 1993). Concerning to the NIR wavelengths, the reflectance is determined by other biochemical characteristics as water content, protein or sugar content. For example, the turgor of the leaves, as a water absorption indicator, can be assessed with the water band index (WBI) using information from the 900 and 950nm (Penuelas et al., 1993). Hence, a better understanding of the different reflectivity patterns and peaks for the calculation of vegetation indices is of a critical importance to improving the assistance to model and predict crop yields.

Low-cost assessment of VI through conventional RGB cameras

Besides the use of multispectral or hyperspectral information, further opportunities are found in the use of information derived from conventional digital Red–Green–Blue (RGB) cameras for the calculation of VI based on the color properties of the canopy. Despite being a low-cost and a low-technology methodology, RGB-derived indices have demonstrated their potential assessing plant traits for the forecasting of yield by formulating VI in relation to assess the canopy greenness according to different color model representations. The versatility, in addition to the affordable costs, of these technologies makes its application in expansion (Araus and Kefauver, 2018).

Table 1. Plant physiological traits and the spectral information used to assess them, a list of example indices and their possible applications in phenotyping studies.

Target trait	Spectral Information	Example indices	Applications
<i>Vegetation cover, Plot greenness</i>	RGB; HIS color model, CIElab color model Red, NIR	GA, GGA, Hue, CSI, Ndab, NGRI, TGI, GLI NDVI, SAVI, OSAVI	Stress detection Canopy cover, LAI Shoot green biomass Growth dynamics Senescence Canopy greenness Agronomic and yield traits Plant emergence Phenology Stress detection Chlorophyll content Leaf nitrogen content
<i>Chlorophyll content</i>	Green, Red, NIR	CARI, TCARI, MCARI, TCARI/OSAVI	Shoot green biomass Senescence Canopy greenness Stress detection Chlorophyll content Leaf nitrogen content
<i>Anthocyanin and carotenoids content</i>	Blue, Red, NIR	ARI, ARI2, CRI, CRI2	Photosynthetic status Chlorophyll content Anthocyanin and carotenoids content Leaf nitrogen content Stress detection
<i>Photosynthesis traits</i>	Green, NIR	PRI, CCI	Photosynthetic status Senescence Chlorophyll content Stress detection
<i>Water content</i>	Water content	WBI, WDVl	WBI, WDVl

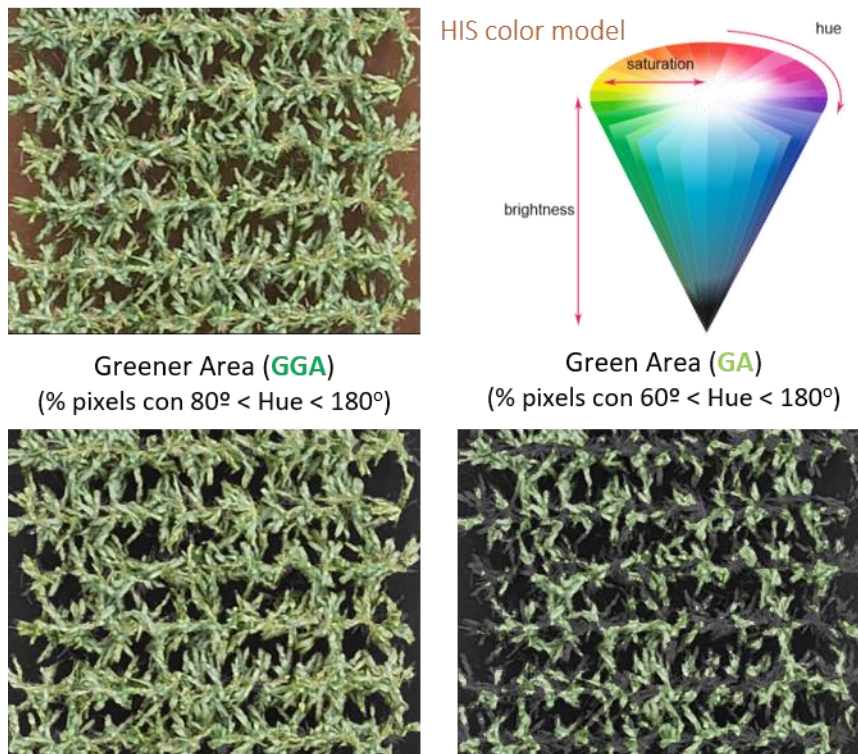


Figure 3. RGB image of a maize canopy and the calculations of the GA and GGA indices based on the HIS color model.

Canopy temperature as an indicator of crop water status

Alternative applications of RS methodologies involve the assessment of the canopy temperature (CT) through measurements of emitted thermal infrared radiation (TIR). CT can be measured by infrared thermometry (Idso et al., 1981) or thermography (Jones, 2002), both methodologies detecting radiation in the long range of the electromagnetic spectrum (9–14 μm). CT measurements are used for the detection of changes in stomatal conductance as a response to the water status of the plant, since transpiration is the main factor used for balancing leaf temperature (Jackson et al., 1988; Moran et al., 1994). As stomatal regulation is highly influenced by the environmental conditions, the stomata closure will cause an increase of CT. Thus, low CT values (i.e. cooler canopies) have been associated to higher stomatal conductance and maximum photosynthetic rates under non-water-limited conditions (Fischer et al., 1998), and

therefore CT performs as a good estimator of phenotypic differences of yield (Pinto et al., 2017). Another common expression of CT is through the difference between the air and the canopy temperature, known as canopy temperature depression (CTD) (Smith et al., 1986).

UAVs as high-throughput plant phenotyping tools

In recent years, there is an increasing number of multiscale phenotyping studies that focus on the discussion of the potential use of different reflectance measurement platforms to assess crop parameters related to yield (Araus et al., 2018). VI can be formulated from leaf level using leaf-clip instruments (e.g. *Spectrapen*, *PhotosynQ*) or from canopy level, using cameras or sensors (e.g. *GreenSeeker*) at ground or aerial level (from a drone, an airborne or a satellite). In large experiments, the use of hand-held instruments is laborious, time-consuming and the measurements can be sensitive to weather fluctuations over time. While the number of measurements at the leaf scale may be limited, canopy measurements permit assessing the whole plot variability at once, but depending on the distance from the target, the spatial resolution could affect the precision of the VIs calculated. Other limitations associated with the canopy measurements at ground level are related to the maintenance of a constant view angle of the sensor/camera to the crop canopy. Hence, unmanned aerial vehicles (UAV) platforms (Figure 4) allow the simultaneous characterization of larger number of cultivars faster than the conventional phenotyping procedures and minimizing the effect of the changing environmental conditions (Araus et al., 2018).

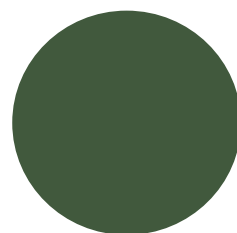
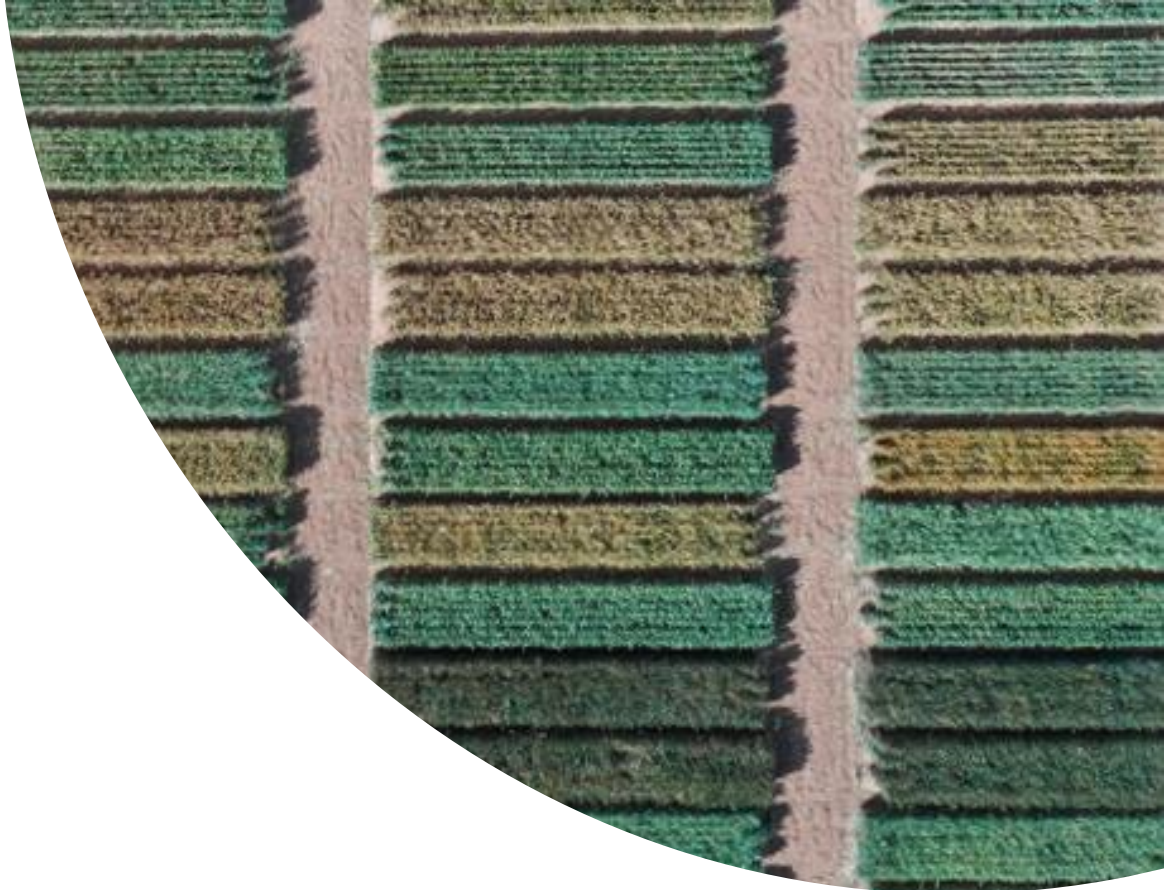


Figure 4. OktoXL 6S12 unmanned aerial platform equipped with the Tetracam multispectral sensor.

Isotope composition as laboratory analysis to complement VI

In order to improve the knowledge on the genome adaptation on the HTPP, the application of RS approaches can be complemented with the analysis of stable isotopes. Although these techniques can be considered costly, time-consuming and require extensively laboratory work, their application could be reliable information for phenotyping purposes (Araus et al., 2013a) as it constitutes an integrative indicator of plant status over the crop cycle (Farquhara and Richardsb, 1984). The stable carbon ($\delta^{13}\text{C}$) and nitrogen ($\delta^{15}\text{N}$) isotope compositions, when analyzed in plant matter, inform on the water regimen and nitrogen metabolism conditions, respectively, of the plant (Yousfi et al., 2012). On one hand, the $\delta^{13}\text{C}$ is an indicator of the water status of the plant, that provide information of photosynthesis and transpiration efficiency decreasing with stress (Yousfi et al., 2016). The values of $\delta^{13}\text{C}$ are different for wheat and maize, as the plants with a photosynthetic metabolism C3 show smaller values than the C4 plants (Farquhar, 1983). On the other hand, the $\delta^{15}\text{N}$ is used to study dynamics of N in soil–plant systems (Choi et al., 2002), with $\delta^{15}\text{N}$ reporting values closer to zero when the origin of the N-fertilizer is synthetic (Bateman et al., 2005). The evaluation of C and N isotope composition in dry matter is a

promising phenotyping tool, exhibiting high heritability and genetic correlation with yield in several studies (Condon et al., 2004; Araus et al., 2013b), and some others highlighting their synergies when are measured in conjunction to canopy vegetation indices (Vergara-Díaz et al., 2016; Yousfi et al., 2016, 2019). The procedure of isotope analysis requires the oven-dry and grind the samples, a precision weighing sealing at the lab prior to detection with an isotope-ratio mass-spectrometry elemental analyzer.



OBJECTIVES

OBJECTIVES

The main objective of this thesis is to advance in the implementation of phenotyping in practice, with the focus placed in maize and wheat, the two main crops worldwide. To this end, this work studied the development of a versatile phenotyping platform, of high capacity and moderate cost, consisting of an unmanned aerial vehicle (UAV) carrying thermal, multispectral and RGB cameras. The performance of wheat and maize genotypes was assessed using this platform under a range of growing conditions. A further objective was to deepen into the relationship between the remote sensing (RS) measurements and the physiological mechanisms involved in the adaptative response of durum wheat and maize genotypes against a wide range of environmental conditions. Moreover, RS measurements from ground were used to calibrate the aerial platforms and thus, evaluate the benefits and disadvantages of the UAV assessments. In addition, stable carbon and nitrogen isotopes were assessed as time-integrated proxies for water performance and nitrogen metabolism. Furthermore, we worked on the development of applications to facilitate the transfer of information from the platform and enhance the use of RGB images as powerful alternative for phenotyping.

Specific aims

Chapter 1. The aim of this study was to test the efficiency of different remote sensing methods and tools in assessing the yield performance and the phosphorus status of a total of 26 maize hybrids under optimum and no phosphorus fertilization at the seedling stage. Different categories of sensors were tested, including RGB cameras (placed on an aerial platform as well as at ground level), alongside a multispectral camera (on the aerial platform) and a spectrometer with an active sensor designed to measure the NDVI at ground level. Field trials were carried out at the Southern Africa regional station of

CIMMYT (International Maize and Wheat Improvement Center) located in Harare, Zimbabwe.

Chapter 2. The aim of this study was to evaluate the efficiency of a set of remote sensing indexes in assessing the yield differences of different maize hybrids at early growth stages under conventionally ploughed (CP) and zero-tillage (conservation agriculture, CA) conditions. Different categories of sensors were tested, including RGB cameras (placed on an aerial platform as well as at ground level), alongside multispectral and thermal cameras (both installed on the aerial platform) and an active sensor portable field spectrometer designed to measure the NDVI at ground level. Additionally, canopy temperature, leaf chlorophyll content, and dry matter isotopic composition were evaluated. The effect of the different CA practices (as the soil vegetation cover) on the imaging sensor was also evaluated. Field trials were carried out at the Southern Africa regional station of CIMMYT (International Maize and Wheat Improvement Center) trial located in Domboshawa, Zimbabwe.

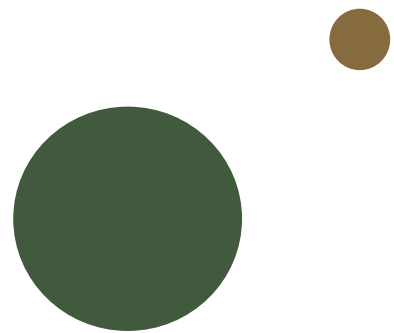
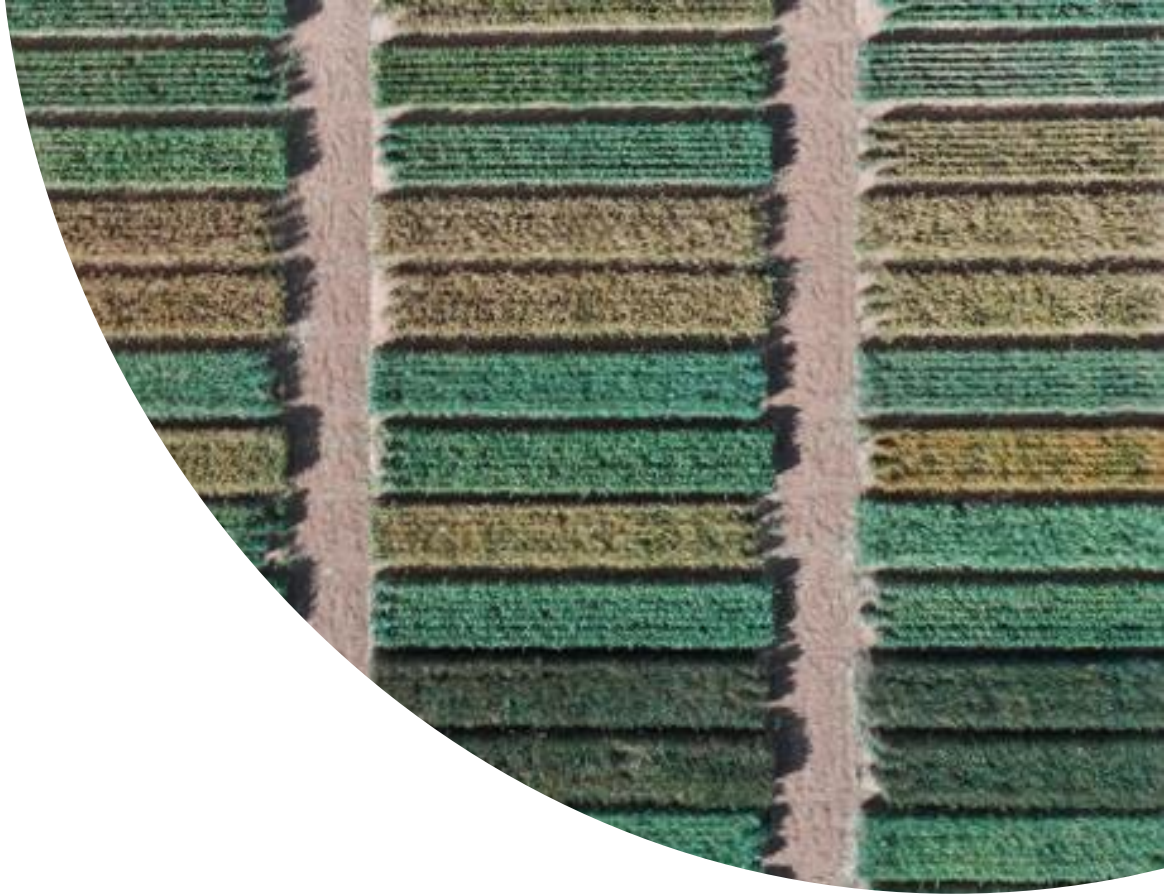
Chapter 3. The aim of this study was to compare the performance of different UAV remote sensing technologies (RGB, multispectral, and thermal) measured during the reproductive stage for assessing the genotypic performance of durum wheat under Mediterranean conditions. To that end a wide range of growing conditions (supplementary irrigation, rainfed, or late-planting) were tested. Field trials were carried out at the experimental station of the Instituto Nacional de Investigación y Tecnología Agraria y Alimentaria (INIA) of Colmenar de Oreja situated at 40 km south of Madrid, Spain. For the processing of this large amount of data we also present the MosaicTool software, for high-throughput data extraction and processing of UAV phenotyping data. The final objective was to provide guidance as to the appropriate RGB, multispectral, and thermal image indexes (i.e., appropriate traits) for the identification of high-yielding as

well as resilient varieties. Besides studying phenotypic correlations, the heritability of these traits and their genetic correlations with grain yield have been analyzed. Moreover, the benefits and disadvantages of the use of phenotyping platforms in terms of aerial versus ground positioning were evaluated for their potential to discriminate between cultivars and also regarding their throughput capacity and cost.

Chapter 4. The aim of this study was to compare the performance of a set of single-leaf and canopy-based remote sensing indices for assessing the influence of the top-dressing levels and the combination of tillage and residue levels on maize grain yield and leaf nitrogen content. Two different specialized portable leaf pigment-meters, as well as leaf scans for measuring the color of the leaves were used to assess the leaf N content. Concerning the canopy-scale assessments, RGB images were taken at the ground level, using a pheno-pole, and from the aerial level, using a UAV. As a complementary selection strategy, carbon and nitrogen stable isotope signatures were analyzed in the leaves, as a potential tool for evaluating water and nitrogen status or differences in N assimilation. Field trials were carried out at the Southern Africa regional station of CIMMYT (International Maize and Wheat Improvement Center) located in Harare, Zimbabwe.

Chapter 5. The aim of this study was to evaluate the performance of a set of wheat cultivars grown in a wide range of Spanish latitudes for three consecutive crop seasons, with very diverse climatic conditions, and in trials under different growing conditions (well-irrigated, rainfed, late-planting and low-nitrogen). Apart from the GY, the evaluation was carried out through leaf pigments readings and canopy field evaluation using RGB (Red-Green-Blue) and multispectral vegetation indices and thermal measurements evaluated from ground and using a unmanned aerial vehicle. Measurements were performed at different phenological stages during the reproductive part of the crop, since Mediterranean agro-environments are characterized by the

occurrence of terminal (i.e. during the last part of the crop cycle) stresses, such as drought and heat. Thereafter, variables measured were used to perform GY prediction models within environments using the LASSO model and the detection rate was used to the design of wheat ideotypes.



REPORT OF THE THESIS DIRECTORS

REPORT OF THE THESIS DIRECTORS

Integrative Crop Ecophysiology Group

<https://integrativecropecophysiology.com>

Plant Physiology Section, Department of Evolutionary Biology, Ecology and Environmental Sciences, Faculty of Biology, University of Barcelona, Diagonal 643, 08028, Barcelona, Spain. Tel. 934 021 465

Dr. José Luis Araus and Dr. Shawn Carlisle Kefauver, as directors of the thesis entitled “*Advances in high throughput and affordable crop phenotyping for adapting maize and wheat to climate change*” which was developed by the doctoral student Adrian Gracia Romero, report about the impact factor and the participation of the doctoral student in the different chapters included in this doctoral thesis.

Chapter 1. The article “**Comparative performance of ground vs. aerially assessed RGB and multispectral indices for early-growth evaluation of maize performance under phosphorus fertilization**” published in *Frontiers in Plant Science* in 2017 with an impact factor of 3.677, is a journal placed within the first decile of the Science Area: Agricultural and Biological Sciences: Plant Science. To date, this work has accumulated 53 citations (Google Scholar, revised in April 2021). In this study, we evaluated the performance of a set of remote sensing indices derived from Red-Green-Blue (RGB) images and multispectral (visible and infrared) data as phenotypic traits and crop monitoring tools for early assessment of maize performance under phosphorus fertilization. This work reinforces the effectiveness of canopy remote sensing for plant phenotyping and crop management of maize under different phosphorus nutrient conditions and suggests that the RGB indices are the best option. Adrian Gracia-Romero

took a role participating in the field evaluation, and further processing the information and had a key role writing the draft of the manuscript.

Chapter 2. The article “**Phenotyping conservation agriculture management effects on ground and aerial remote sensing assessments of maize hybrids performance in Zimbabwe**” published in *Frontiers in Plant Science* in 2018 with an impact factor of 4.106, is a journal placed within the first decile of the Science area: Agricultural and Biological Sciences: Plant Science. To date, this work has accumulated 25 citations (Google Scholar, revised in April 2021). We present the results of a study in which Red-Green-Blue (RGB) and multispectral indexes were evaluated for assessing maize genotype performance under conventional ploughing (CP) and CA practices. Most of the calculated indexes (e.g., Green Area, GA) and Normalized Difference Vegetation Index, NDVI)) were significantly affected by tillage conditions increasing their values from CP to CA. Indexes derived from the RGB-images related to canopy greenness performed better at assessing yield differences, potentially due to the greater resolution of the RGB compared with the multispectral images, although this performance was more evident for CP than CA. As in the first Chapter, Adrian Gracia-Romero took a role participating in the field evaluation, and further processing the information and writing the draft.

Chapter 3. The article “**UAV and ground image-based phenotyping: a proof of concept with Durum wheat**” published in *Remote Sensing* in 2019 with an impact factor of 4.509, is a journal placed within the first decile of the area: Earth and Planetary Science. To date, this work has accumulated 33 citations (Google Scholar, revised in April 2021). We compared the performance of red–green–blue (RGB), multispectral, and thermal data of individual plots captured from the ground and taken from an UAV, to assess genotypic differences in yield. Our results showed that crop vigor, together with the amount and duration of the canopy green biomass that contributed to grain filling, were critical

phenotypic traits for the selection of germplasm that is better adapted to present and future Mediterranean conditions. The effect from platform proximity (distance between the sensor and crop canopy) was evaluated on the vegetation indexes, and both ground and aerial measurements performed similarly in assessing yield. Again, Adrian Gracia-Romero took an active role in the field evaluation and further data processing, and he was the responsible of writing the draft.

Chapter 4. The article “**Leaf versus whole-canopy remote sensing methodologies for crop monitoring under conservation agriculture: a case of study with maize in Zimbabwe**” published in Scientific Reports in 2020 with an impact factor of 3.998, is a journal placed within the first decile of the science area: Multidisciplinary. To date, this work has not been cited. This study compares maize leaf and canopy-based approaches for assessing N fertilization performance under different tillage, residue coverage and top-dressing conditions in Zimbabwe. Canopy measurements from both ground and aerial platforms performed very similar, but indices assessed from the UAV performed best in capturing the most relevant information from the whole plot and correlations with GY and leaf N content were slightly higher than similar indices measured at ground level. Leaf-based measurements demonstrated utility in monitoring N leaf content, though canopy measurements outperformed the leaf readings in assessing GY parameters, while providing the additional value derived from the affordability and easiness of using a pheno-pole system or the high-throughput capacities of the UAV. As before, Adrian Gracia-Romero took an active role in the field evaluation and further data processing, and he was the responsible of writing the draft.

Chapter 5. The article “**High-throughput phenotyping to define of durum wheat ideotypes adapted to Mediterranean environments**” will be submitted to date to The Plant Journal, with an impact factor of 6.141. This study aimed the evaluation of the

performance of a set of wheat cultivars grown in a wide range of Spanish latitudes for three consecutive crop seasons, with very diverse climatic conditions, and in trials under different growing conditions (well-irrigated, rainfed, late-planting and low-nitrogen). Measurements were performed at different phenological stages during the reproductive part of the crop, since Mediterranean agro-environments are characterized by the occurrence of terminal (i.e. during the last part of the crop cycle) stresses, such as drought and heat. Together with GY, the evaluation was carried out through leaf pigments readings and canopy field evaluation using RGB (Red-Green-Blue), multispectral vegetation indices and thermal measurements evaluated from ground and using a unmanned aerial vehicle. Thereafter, variables measured were used to perform GY prediction models within environments using the LASSO model and the detection rate across 100 validations was used to the design of wheat ideotypes. Adrian Gracia-Romero took an active role in the field evaluation and further data processing, and he has been the responsible of writing the draft.

Other articles where the doctoral student participated as a co-author:

- Rezzouk, F.Z., Gracia-Romero, A. et al. Ideotypic characteristics of durum wheat grown in Mediterranean environments differing in water and temperature condition. (under review).
- Kamphorst, S. H. et al. Heterosis and reciprocal effects for physiological and morphological traits of popcorn plants under different water conditions (under review)
- Jairo, V., Gracia-Romero, A. et al. Adaptation of high yielding European wheat cultivars to Mediterranean conditions (under review).

- Segarra, J., Gracia-Romero, A. et al. Multiscale monitoring of wheat grain nitrogen content (under review).
- Ben-Jabeur, M., Gracia-Romero, A., et al. 2020. The promising MultispeQ device for tracing the effect of seed coating with biostimulants on growth promotion, photosynthetic state and water–nutrient stress tolerance in durum. *Euro-Mediterranean Journal for Environmental Integration* 6 (1), 1-11
- Rezzouk, FZ., Gracia-Romero, A., et al. 2020. Remote sensing techniques and stable isotopes as phenotyping tools to assess wheat yield performance: Effects of growing temperature and vernalization. *Plant Science* (IF: 3.785) 10.1016/j.plantsci.2019.110281
- Ben-Jabeur, M., Gracia-Romero, A., et al. 2019. A Novel Aspect of Essential Oils: Coating Seeds with Thyme Essential Oil induces Drought Resistance in Wheat. *Plants* (IF: 2.632) 8 (10), 371 doi:10.3390/plants8100371
- Yousfi, S., Gracia-Romero, A., et al. (2019). Combined use of low-cost remote sensing techniques and $\delta^{13}\text{C}$ to assess bread wheat grain yield under different water and nitrogen conditions. *Agronomy* (IF: 1.419) 9(6), 285; DOI: 10.3390/agronomy9060285
- Buchaillot, ML., Gracia-Romero, A., et al. 2019. Evaluating the performance of different commercial and pre-commercial maize varieties under low nitrogen conditions using affordable phenotyping tools. *Sensors* (IF: 2.475) 19(8), 1815. DOI: 10.3390/s19081815
- Fernandez-Gallego, JA. et al. (2019). Cereal crop ear counting in field conditions using zenithal RGB images. *JoVE (Journal of Visual. Experiments)*. (IF: 1.325) (144), e58695 DOI: 10.3791/58695

- Yousfi, S., Gracia-Romero, A., et al. 2016. Comparative performance of remote sensing methods in assessing wheat performance under Mediterranean conditions. *Agricultural Water Management* (IF: 3.182). 164 (2016) 137–147

Internships

- 09/2019 - 12/2019. PhD Student, research visit in Hyperspectral Remote Sensing & Precision Agriculture Laboratory (Univ. of Melbourne, Australia).
School of Agriculture and Food, Faculty of Veterinary and Agricultural Sciences (FVAS), and Department of Infrastructure Engineering, Melbourne School of Engineering (MSE), University of Melbourne, Melbourne, Victoria 3010, Australia. Under the guidance of Professor Pablo J. Zarco-Tejada

Training courses, courses and workshops:

- 01/2020. Workshop on “Writing effective research manuscripts”, organized by the Dep. Evolutive Biology, Ecology and Environmental Sciences of the University of Barcelona, Barcelona, Spain.
- 01/2020. Course “Statistical tools for plant phenomic data analysis”, organized by IAMZ-CIHEAM with the collaboration of the European Plant Phenotyping Network (EPPN2020), Zaragoza, Spain.
- 10/2019. Course “Learn Python in a Day” - Simpliv courses, organized by the University of Melbourne, Melbourne, Australia.
- 10/2018. Course “Training course for new teachers UB”, organized by the Institut de Desenvolupament Professional (IDP-ICE) – UB in Barcelona.
- 09/2018. Course “Harmonized UAS techniques Training Course: Introduction to data acquisition and preprocessing”, organized by the HARMONIOUS COST

Action on UAS Data Preparation and Calibration and held by Svarmi Efh, Reykjavik, Iceland.

- 01/2018. Course “Accredited Drone Pilot Course 5-15kg” approved by AESA, organized by HEMAV, Castelldefels, Spain.
- 02/2017. Course “Breeding Small Grain Cereal Crops in A Climate Change Scenario”, organized by the International Center for Agricultural Research in the Dry Areas (ICARDA) in Zaragoza (Spain)

Communications in symposiums and conferences

- Gracia-Romero, A. et al. (2020). Assessing relationships between hyperspectral imagery and wheat parameters. Oral presentation. III Spanish Symposium on Cereal Physiology and Breeding. Pamplona, Spain. November 14th – 15th 2020.
- Rezzouk F.Z., Gracia-Romero A. et al. (2020). Durum wheat ideotypes to Spanish environments differing in water and temperature conditions. Oral presentation. III Spanish Symposium on Cereal Physiology and Breeding. Pamplona, Spain. November 14th – 15th 2020.
- Kefauver, S.C., Gracia Romero, A. et al. (2020). Tailor-made software to meet challenges of phenotyping. Oral presentation. III Spanish Symposium on Cereal Physiology and Breeding. Pamplona, Spain. November 14th – 15th 2020.
- Kefauver, S.C., Gracia Romero, A. et al. (2020). (September 26 - October 2, 2020, Virtual Symposium). OPEN-SOURCE SOFTWARE FOR CROP PHYSIOLOGICAL ASSESSMENTS USING HIGH RESOLUTION RGB IMAGES. In Proceedings of the IGARSS 2020 IEEE International Geoscience and Remote Sensing Symposium (In press). IEEE.

- Formiga, D., Gracia-Romero, A. et al. (2019). Remote Sensing Techniques for the Future of Plant Science. In the VIII Jornada Ambiental. Universitat de Barcelona and Bodegas Torres. Poster presentation. 5 May 2019.
- Silva-Sánchez, A., Gracia-Romero, A., et al. (2019). Comparison of Proximal Remote Sensing Devices for Estimating Eggplant response to Root-Knot Nematodes. Online presentation and Proceedings Paper. 3rd International Electronic Conference on Remote Sensing, 22 May – 5 June.
- Gracia-Romero, A., et al. (2019). Leaf vs. Whole-Canopy Remote Sensing Methodologies for Nitrogen Monitoring and Grain Yield Prediction: A Case of Study with Maize in Zimbabwe. Oral presentation. II Simposio Español de Fisiología y Mejora de Cereales, Córdoba (Spain), 6-7 March 2019.
- Rezzouk, F. Z., Gracia-Romero, A., et al. (2019). Remote sensing techniques and stable isotopes as phenotyping tools to assess wheat yield performance: effects of growing temperature and vernalization needs. Oral presentation. II Simposio Español de Fisiología y Mejora de Cereales, Córdoba (Spain), 6-7 March 2019.
- Gracia-Romero, A., et al. (2018). Aerial versus ground phenotyping quiz: a proof of concept with durum wheat. Oral presentation and poster. In Evolution of Mediterranean Agriculture: Interdisciplinary Perspectives on Historical Developments and Future Visions, Barcelona (Spain), 22-24 November 2018.
- Gracia-Romero, A., et al. (2018). Smartphones to estimate plant water status CerealMobile app. Oral presentation. In Iwater International Integrated Water Cycle Show, Barcelona (Spain), 13-15 November 2018.
- Kefauver, SC., Gracia-Romero, A., et al. (2018). Technology Industry and Education: Citizen Science. Oral presentation. In Geoscience and Remote Sensing Symposium, 2018. IGARSS 2018. (presented July 2018 – Forum Session Chair).

- Gracia-Romero, A. and Rezzouk, FZ. Phenotyping under Drought Stress. Oral presentation in III Workshop Young Researchers of the Institut de Recerca del Aigua (IdRA), Barcelona (Spain), 24 May 2018.
- Gracia-Romero, A. et al. Remote Sensing Phenotyping for Estimating Grain Yield of Wheat Growing Under Different Water and Temperature Conditions. Poster. In I Spanish Symposium on Cereal Physiology and Breeding, Zaragoza (Spain), 9-10 April 2018.
- Kefauver, SC., Gracia-Romero, A. et al. UAV and Proximal Sensing for Phenotyping Maize in African Breeding Programs. Oral Presentation. In I Spanish Symposium on Cereal Physiology and Breeding, Zaragoza (Spain), Spain 9-10 April 2018.
- Pallavicini, Y., Gracia-Romero, A. et al. Aerial platforms as a new approach to select resistant lines for yellow rust in bread wheat breeding program. Oral Presentation. In I Spanish Symposium on Cereal Physiology and Breeding, Zaragoza (Spain), 9-10 April 2018.
- Martinez-Peña, R., Gracia-Romero, A. Canopy Vegetation Indices to assess yield in durum wheat. Poster. In I Spanish Symposium on Cereal Physiology and Breeding, Zaragoza (Spain), 9-10 April 2018.
- Gracia-Romero, A. et al. Phenotyping agriculture management effects on remote sensing assessments of maize hybrids performance. Online presentation. In 2nd International Electronic Conference on Remote Sensing, 22 March – 5 April 2018.
- Kefauver, SC., Gracia-Romero, A. et al. UAV Phenotyping and Proximal Sensing for Maize Assessments in Breeding Programs. Oral presentation. ES1309 OPTIMISE COST Action - Final Conference, Sofia, Bulgaria, 19 February 2018.

- Plant Phenotyping Symposium. Next generation plant phenotyping for trait discovery, breeding and beyond: transnational access European platform. Public attendance. European Plant Phenotyping Network, Barcelona, Spain, 11-12 November 2015.

To certify this for corresponding purposes,

Dr. José Luis Araus Ortega

Dr. Shawn C. Kefauver



CHAPTER 1

Comparative Performance of Ground vs. Aerially Assessed RGB and Multispectral Indices for Early-Growth Evaluation of Maize Performance under Phosphorus Fertilization

Adrian Gracia-Romero, Shawn C. Kefauver, Omar Vergara-Díaz, Mainassara A. Zaman-Allah, Boddupalli M. Prasanna, Jill E. Cairns and José L. Araus

Published in:
Frontiers Plant Science (2017) 8:2004.



Comparative Performance of Ground vs. Aerially Assessed RGB and Multispectral Indices for Early-Growth Evaluation of Maize Performance under Phosphorus Fertilization

Adrian Gracia-Romero¹, Shawn C. Kefauver¹, Omar Vergara-Díaz¹, Mainassara A. Zaman-Allah², Boddupalli M. Prasanna², Jill E. Cairns² and José L. Araus^{1*}

¹ Integrative Crop Ecophysiology Group, Plant Physiology Section, Faculty of Biology, University of Barcelona, Barcelona, Spain, ² International Maize and Wheat Improvement Center, CIMMYT Southern Africa Regional Office, Harare, Zimbabwe

OPEN ACCESS

Edited by:

Yanbo Huang,
United States Department of
Agriculture, United States

Reviewed by:

Jingcheng Zhang,
Hangzhou Dianzi University, China
Maria Balota,
Virginia Tech, United States

*Correspondence:

José L. Araus
jaraus@ub.edu

Specialty section:

This article was submitted to
Technical Advances in Plant Science,
a section of the journal
Frontiers in Plant Science

Received: 06 September 2017

Accepted: 10 November 2017

Published: 27 November 2017

Citation:

Gracia-Romero A, Kefauver SC, Vergara-Díaz O, Zaman-Allah MA, Prasanna BM, Cairns JE and Araus JL (2017) Comparative Performance of Ground vs. Aerially Assessed RGB and Multispectral Indices for Early-Growth Evaluation of Maize Performance under Phosphorus Fertilization. *Front. Plant Sci.* 8:2004. doi: 10.3389/fpls.2017.02004

Low soil fertility is one of the factors most limiting agricultural production, with phosphorus deficiency being among the main factors, particularly in developing countries. To deal with such environmental constraints, remote sensing measurements can be used to rapidly assess crop performance and to phenotype a large number of plots in a rapid and cost-effective way. We evaluated the performance of a set of remote sensing indices derived from Red-Green-Blue (RGB) images and multispectral (visible and infrared) data as phenotypic traits and crop monitoring tools for early assessment of maize performance under phosphorus fertilization. Thus, a set of 26 maize hybrids grown under field conditions in Zimbabwe was assayed under contrasting phosphorus fertilization conditions. Remote sensing measurements were conducted in seedlings at two different levels: at the ground and from an aerial platform. Within a particular phosphorus level, some of the RGB indices strongly correlated with grain yield. In general, RGB indices assessed at both ground and aerial levels correlated in a comparable way with grain yield except for indices a^* and u^* , which correlated better when assessed at the aerial level than at ground level and Greener Area (GGA) which had the opposite correlation. The Normalized Difference Vegetation Index (NDVI) evaluated at ground level with an active sensor also correlated better with grain yield than the NDVI derived from the multispectral camera mounted in the aerial platform. Other multispectral indices like the Soil Adjusted Vegetation Index (SAVI) performed very similarly to NDVI assessed at the aerial level but overall, they correlated in a weaker manner with grain yield than the best RGB indices. This study clearly illustrates the advantage of RGB-derived indices over the more costly and time-consuming multispectral indices. Moreover, the indices best correlated with GY were in general those best correlated with leaf phosphorus content. However, these correlations were clearly weaker than against grain yield and only under low phosphorous conditions. This work reinforces the effectiveness of canopy remote sensing for plant phenotyping and crop management of maize under different phosphorus nutrient conditions and suggests that the RGB indices are the best option.

Keywords: maize, remote sensing, UAV, RGB Vis, multispectral Vis, phosphorous fertilization

INTRODUCTION

Sub-Saharan Africa (SSA) has one of the world's fastest growing populations but the growth rate of food production has not kept pace with this, leading to a food deficit (McIntyre et al., 2009). Low levels of soil phosphorous (P) and nitrogen (N), are the main constraints to crop growth in these areas (Buerkert et al., 2001). Phosphorous fertilizers are relatively costly in SSA and are scarce in some countries, partly due to poorly developed markets, and so phosphorous application is low (1 kg ha^{-1} compared with 14.3 kg ha^{-1} in Asia) (Smalberger et al., 2006). Plant scientists face the challenge of solving these limitations while taking into account the additional implications of climate change on food security (Cairns et al., 2012, 2013a). In that sense, affordable technologies capable of monitoring crop performance for agronomical purposes, yield prediction or to assess phenotypic variability for breeding are bottlenecks in the pathway to full exploitation of this technology (Reynolds et al., 2012; Araus and Cairns, 2014).

Remote sensing has become an important methodology for the application of agricultural monitoring and to improve precision and throughput in phenotyping. There is a growing body of literature demonstrating the usefulness of remote sensing for a wide range of applications in agriculture: growth monitoring, yield prediction, stress detection, nutrient deficiency diagnosis, and control of plant diseases (Fiorani and Schurr, 2013). In the case of phenotyping, these methodologies offer the opportunity to screen large numbers of genotypes at a lower cost and faster than conventional phenotyping and provide to breeding programs the opportunity to assess genetic diversity under field conditions. Remote sensing methods enable detailed non-invasive information to be captured throughout the plant life cycle. Among the different remote sensing techniques, the most usual indices used are derived from Red-Blue-Green (RGB) images (Casadesús et al., 2007) and multispectral (Thenkabail et al., 2002), hyperspectral (Blackburn, 2007) and thermal sensors and images (Araus and Cairns, 2014; Deery et al., 2016). However, large differences exist in the price of the different equipment deployed (e.g., spectrometers vs. conventional red/green/blue cameras).

The traditional procedure has involved the use of multispectral sensors and the development of numerous vegetation indices associated with vegetation parameters such as above-ground biomass, water and nutrient deficiency, and

crop yield (Petropoulos and Kalaitzidi, 2012). The Normalized Difference Vegetation Index (NDVI) is one of the most well-known vegetation indices derived from multispectral remote sensing, as it includes visible and near infrared radiation. Although, it was originally developed for satellite remote vegetation sensing, it has also been found useful in ground-based and aerial applications. In fact, several groups of spectral variables have been identified as being of value in characterizing plant performance and empirical indices have been defined. Among these, some are modifications of the NDVI that takes atmospheric effects and/or soil influences into account in order to increase their sensitivity, like the Soil-adjusted Vegetation Index (SAVI) or the Renormalized Vegetation Index (RDVI) (Wu, 2014). Others, like the Photochemical Reflectance Index (PRI), aim to assess how efficiently the radiation is used by plants during photosynthesis, while the Modified Chlorophyll Absorption in Reflectance Index (MCARI) or the Transformed Chlorophyll Absorption in Reflectance Index (TCARI) (Haboudane et al., 2002), are focused on quantifying photosynthetic pigments. Further, other indices also have been used to determine the water status of plants, like the Water Index (WI) (Peñuelas et al., 1993; Babar et al., 2006).

The use of information derived from conventional digital RGB (of red, green, blue) images may represent a low-cost alternative to the use of multispectral or hyperspectral information for formulating vegetation indices. The images can be processed to convert RGB values into indices based on the models of Hue-Intensity-Saturation (HIS), CIELab, and CIELuv cylindrical-coordinate representations of colors. The RGB indices implementation has been extensive and successful for providing a wide-range of phenomic data about genotypic performance under different growing conditions (Casadesús et al., 2007; Casadesús and Villegas, 2014; Vergara-Díaz et al., 2015, 2016; Zaman-Allah et al., 2015; Zhou et al., 2015; Yousfi et al., 2016).

The environmental variability throughout the day, like changes in radiation, temperature or the occurrence of clouds, affects the phenotypic observations inconsistently and may limit the accuracy of the time-consuming proximal measurements at ground level (e.g., the relative chlorophyll content). The incorporation of these methodologies into aerial based platforms enables the simultaneous characterization of a larger number of plots (i.e., spectral reflectance at solar noon), which may help to minimize the effect of changing environmental conditions (Araus and Cairns, 2014). This becomes extremely important with regards to the increasing demand to support and accelerate progress in breeding for novel traits, which at the same time requires accurate high throughput phenotyping of a large numbers of plants. Furthermore, the added cost of the aerial platforms may be offset by time savings by reducing manual field labor.

The vegetation indices, formulated from the visible and infrared spectrum of the light reflected by plants or derived from RGB conventional digital images are the most usual remote sensing method to assess plant nutrient status (Vergara-Díaz et al., 2016). However, while most studies that have focused on the spectral evaluation of nutrient deficiencies of crops have

Abbreviations: SSA, Sub-Saharan Africa; RGB, Red-Blue-Green; NDVI, Normalized Difference Vegetation Index; UAV, Unmanned aerial Vehicle; GY, Grain yield; VIs, Vegetation Indices; HIS, Hue-Intensity-Saturation; GA, Green Area; GGA, Greener Area; AN, Ammonium Nitrate; CIMMYT, International Maize and Wheat Improvement Center; masl, meters above sea level; CP-OES, Inductively Coupled Plasma Optical Emission Spectroscopy; P content, Phosphorous content; LCC, Chlorophyll Content; PRI, Photochemical Reflectance Index; SAVI, Soil Adjusted Vegetation Index; MCARI, Modified Chlorophyll Absorption Ratio Index; WBI, Water Band Index; RDVI, Renormalized Difference Vegetation Index; EVI, Enhanced Vegetation Index; ARI2, Anthocyanin Reflectance Index 2; CRI2, Carotenoid Reflectance Index 2; TCARI, Transformed Chlorophyll Absorption in Reflectance Index; OSAVI, Optimized Soil-Adjusted Vegetation Index; $\Delta F/Fm'$, Effective Fluorescence Quantum yield; NIR, Near-Infrared.

concerned analysis of nitrogen content, such evaluations are far less common with other nutrients, including phosphorous (Osborne et al., 2002; Mahajan et al., 2014). In addition to the reduction in the total biomass, the lack of other mineral nutrients can also influence the color of leaves. In the case of phosphorus, it is well-known that leaf darkening is caused by a phosphorous deficiency, but the relationship between symptoms and leaf color is less evident than for nitrogen deficiency.

Because maize is among the major crops globally, and the main staple for direct human consumption in SSA (Cairns et al., 2013b), the aim of this study was to test the efficiency of different remote sensing methods and tools in assessing the yield performance and the phosphorus status of a total of 26 maize hybrids under optimum and no phosphorus fertilization. The performance of remote sensing assessment from an unmanned aerial platform and from the ground was compared. Different categories of sensors were tested, including RGB cameras (placed on an aerial platform as well as at ground level), alongside a multispectral camera (on the aerial platform) and a spectrometer with an active sensor designed to measure the NDVI at ground level. Measurements were performed at the seedling stage in order to assess early predictions of plant performance and yield. Phosphorus fertilization affects plant growth which subsequently may alter water status (e.g., through differences in the amount transitive area or in root development) and nitrogen uptake and assimilation. In that sense, the stable isotope compositions of C and N ($\delta^{13}\text{C}$ and $\delta^{15}\text{N}$) were measured in leaf samples as a complementary selection traits, aiming to assess any effect of phosphorous assimilation on the water status and nitrogen metabolism of the plant. Thus, for a C4 species such as maize in spite $\delta^{13}\text{C}$ composition while barely reflects genotypic variability in water performance, it may still catch differences between treatments in the plant water status (Cabrera-Bosquet et al., 2009); while $\delta^{15}\text{N}$ may reflect the effect of the treatment on the uptake and further assimilation of N (Evans, 2001).

MATERIALS AND METHODS

Plant Material and Growing Conditions

Field trials were carried out at the Southern Africa regional station of CIMMYT (International Maize and Wheat Improvement Center) located in Harare (−17.800, 31.050, 1498 masl), Zimbabwe. The soil in the station is characterized by a pH slightly lower than 6, nitrogen as nitrate (NO_3^-) of around $4 \mu\text{g g}^{-1}$ and phosphorous contents of nearly $20 \mu\text{g g}^{-1}$ (Vergara-Díaz et al., 2016).

A set of 25 maize hybrids developed at CIMMYT plus a local check (CZH131001, CZH0524, CZH141042, CZH0631, CZH131002, CZH0513, CZH131007, CZH03042, CH12716, CZH03004, CZH15020, SC513, CZH132210, CZH142125, CZH132218, CZH142153, CZH142159, SC719, CZH142186, CZH142212, CZH142074, CZH142003, CZH142206, CZH142195, and CZH142210) were sown during the wet season on December 2015. These maize hybrids reflect a large variability in plant performance to different phosphorous conditions. The experimental design consisted of two separated

phosphorous treatments with 26 plots each corresponding to each maize genotype studied (52 plots in total).

Seeds were planted on December 21st 2015, in three rows per plot; rows were 4 m long and 75 cm apart ($9 \text{ m}^2/\text{plot}$), with 17 plants per row and 25 cm between plants in each a row. A split-plot in a randomized complete block design without replicates was used. The field was fertilized with $200 \text{ kg}\cdot\text{ha}^{-1}$ of ammonium nitrate (AN) and $250 \text{ kg}\cdot\text{ha}^{-1}$ of muriate of potash before sowing (basal fertilizer), followed with $250 \text{ kg}\cdot\text{ha}^{-1}$ AN for top dressing. In order to generate differential phosphorus conditions, $400 \text{ kg}/\text{ha}$ of superphosphate fertilizer were added at pre-sowing to one half of the trial, corresponding to the optimum phosphorous fertilized conditions (OP). The other part of the trial corresponded to the non-phosphorus fertilized conditions (NPF). The trial was depleted of phosphorus for 1 year. A two-row border of a commercial maize variety was sown on the edges of the trial to prevent border effects. Trials were gathered following the standard procedures of CIMMYT. The central 3.5 m of each row was harvested discarding 2 plants at each end, thus the collected grain yield ($\text{t}\cdot\text{ha}^{-1}$) corresponded to the weight of 7.87 m^2 .

In addition, these hybrids were also tested in other trials in Zimbabwe under optimal fertilization conditions comparable to those of the OP trial of the experimental station. Evaluations were performed at the Agricultural Research Trust site in Harare (−17.716, 31.716, 1,516 masl). For these trials, the fertilization conditions were basically the same than at the OP conditions of the main study (CIMMYT Station).

Proximal and Aerial Data Collection

Remote sensing evaluations were performed on seedlings (<5 leaves) during the last week of January. Vegetation indices derived from RGB images were evaluated for each plot at ground and aerial levels. At ground level one conventional digital picture was taken per plot, holding the camera about 80 cm above the plant canopy in a zenithal plane and focusing near the center of each plot. The digital camera used was an Olympus OM-D (Olympus, Tokyo, Japan). Pictures were acquired at a 16-megapixel resolution with a sensor using a 14-mm focal length, triggered at a speed of 1/125 s with the aperture programmed in automatic mode. NDVI was also determined on individual plots at ground level using a portable spectrometer (GreenSeeker handheld crop sensor, Trimble, USA). Additionally, the leaf chlorophyll content (LCC) of the last developed leaf was measured using a Minolta SPAD-502 portable chlorophyll meter (Spectrum Technologies Inc., Plainfield, IL, USA). Eight leaves were measured for each plot (four per row), each leaf being the last fully expanded within a plant. For each leaf four measurements were taken from the middle portion of the lamina.

Further, RGB and multispectral aerial images were acquired using an unmanned aerial vehicle (UAV) (Mikrokopters OktoXL, Moormerland, Germany) flying under remote control at around 50 m (Figure 1). The camera used for the aerial images was a Lumix GX7 (Panasonic, Osaka, Japan), a digital single lens mirrorless camera with an image sensor size of $17.3 \times 13.0 \text{ mm}$. Images were taken at 16-megapixel resolution using a 20-mm focal length. In addition, a multispectral camera covering

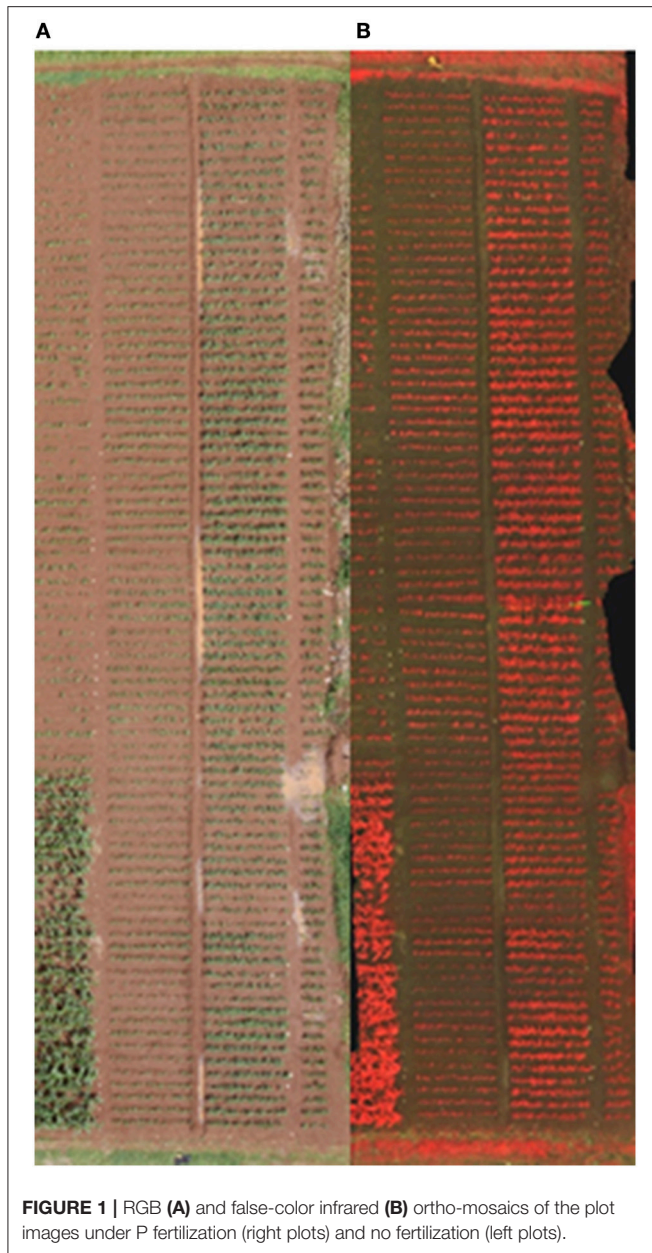


FIGURE 1 | RGB (A) and false-color infrared (B) ortho-mosaics of the plot images under P fertilization (right plots) and no fertilization (left plots).

wavelengths in the visible and near infrared regions of the spectrum (MCA12, Tetracam Inc., Chatsworth, CA, US) was also mounted in the drone. The camera consisted of 12 independent image sensors, and optics with user configurable filters. It captured 15.6-megapixels of image data and transferred this to 12 separate flash memory cards. Both RGB and multispectral images were taken at the rate of one every 5 s.

Image Processing

To obtain correct image mosaics from the multispectral images a 3D reconstruction approach was needed to produce an accurate ortho-mosaic and remove the effects of the UAV flight. Agisoft PhotoScan Professional (Agi-soft LLC, St. Petersburg, Russia) was employed for this task using 20–30 overlapping images for

both mosaics (RGB and multispectral) with at least 80% overlap. Through the open source image analysis platform FIJI (Fiji is Just ImageJ; <http://fiji.sc/Fiji>), regions of interest were established at each row for the plots to be cropped.

RGB pictures were subsequently analyzed using a version of the Breedpix 0.2 software adapted to JAVA8 and integrated as a plugin within FIJI; <https://github.com/George-haddad/CIMMYT>). This software enables the extraction of RGB vegetation indices (VIs) in relation to different properties of color (Casadesús et al., 2007). Essentially, the indices are based on either the average color of the entire image, in diverse units related to its “greenness,” or on the fraction of pixels classified as green canopy relative to the total number of pixels in the image. In HSI color space, the Hue (H) component describes the color itself traversing the visible spectrum in the form of an angle between 0° and 360°, where 0° means red, 60° means yellow, 120° means green and 180° means cyan. Derived from the Hue, Green Area (GA), and Greener Area (GGA) analyze the proportion of green pixels in the image. GA is the percentage of pixels in the image in the hue range from 60 to 180°, that is, from yellow to bluish green. Meanwhile, GGA is somewhat more restrictive because the range of hue considered by the index is from 80 to 180°, excluding yellowish-green tones. In the CIELab color space model, dimension L* represents lightness, and the green to red range is expressed by the a* component, with a more positive value representing a purer red, and conversely a more negative value indicating a greener color. Meanwhile, blue to yellow is expressed by the b* component, where the more positive the value the closer it is to a pure yellow, whereas the more negative the value the closer it is to blue. Similarly, in the CIELuv color space model, dimensions u* and v* are perceptually uniform coordinates, where the visible spectrum starts with blue at the bottom of the space, moving through green in the upper left (mostly scaled by v*) and out to red in the upper right (mostly scaled by u*). The multispectral indices, formulated with the Tetracam camera and detailed in **Table 1**, were calculated from the multispectral images using a custom FIJI macro code.

Leaf Phosphorous Content

Similar leaves to those used for leaf chlorophyll measurements were sampled and subsequently oven dried at 70°C for 24 h and ground to a fine powder. For the analysis of P content, a total of 100 mg of sample were digested in acid for 24 h at 90°C within Teflon vessels, using 2 ml of HNO_3 and 0.5 ml of hydrogen peroxide, with samples subsequently re-suspended in 30 ml of deionized water. Analyses were performed by Inductively Coupled Plasma Optical Emission Spectroscopy (ICP-OES) using a Perkin-Elmer Optima 3200RL Spectrometer (Perkin-Elmer, Massachusetts, EEUU) at the Scientific Facilities of the University of Barcelona. Leaf phosphorous content was expressed in mg of P per g of dry mass.

Total Nitrogen Content and Carbon and Nitrogen Stable Isotope Compositions

The same ground material was also used to analyze the total nitrogen content together with the stable isotopic abundances of carbon and nitrogen in the leaves. Samples of about

TABLE 1 | Indices derived from the multispectral visible and near infrared bands.

Target group	Index	Equation	Wavelengths	References
Broadband greenness	Normalized difference vegetation index (NDVI)	$(B840 - B670)/(B840 + B670)$	Red, NIR	Rouse et al., 1973
	Soil adjusted vegetation index (SAVI)	$(B840 - B670)/(B840 + B670 + L) * (1 + L)$ Low vegetation, L = 1, intermediate, 0.5, and high 0.25	Red, NIR	Huete, 1988
	Optimized soil-adjusted vegetation index (OSAVI)	$((1 + 0.16) * (B780 - B670)) / ((B780 + B670 + 0.16))$	Red, NIR	Rondeaux et al., 1996
	Renormalized difference vegetation index (RDVI)	$(B840 - B670) / ((B840 + B670)^{1/2})$	Red, NIR	Roujean and Breon, 1995
	Enhanced vegetation index (EVI)	$2.5 * (B840 - B670) / (B840 + (6 * B670) - (7.5 * B450) + 1)$	Blue, Red, NIR	Huete et al., 2002
Light Use efficiency	Photochemical reflectance index (PRI)	$(B550 - B570) / (B550 + B570)$	Green	Gamon et al., 1997
Leaf pigments	Modified chlorophyll absorption ratio index (MCARI)	$[(B700 - B670) - 0.2 * (B700 - B550)] * B700 / B670$	Green, Red	Daughtry, 2000
	Transformed chlorophyll absorption in reflectance index (TCARI)	$3 * (B700 - B670) - 0.2 * (B700 - B550) * (B700 / B670)$	Green, Red, NIR	Haboudane et al., 2002
	Anthocyanin reflectance index 2 (ARI2)	$B840 * (1 / B550 - 1 / B700)$	Blue, Red, NIR	Gitelson et al., 2001
	Carotenoid reflectance index 2 (CRI2)	$1 / B550 - 1 / B700$	Blue, Red	Gitelson et al., 2002
Canopy water content	Water band index (WBI)	$(R840 - B670) / (B840 + B670)^{1/2}$	Red, NIR	Peñuelas et al., 1993

0.7 mg of dry matter and reference materials were weighed into tin capsules, sealed, and then loaded into an elemental analyzer (Flash 1112 EA; ThermoFinnigan, Schwerte, Germany) coupled with an isotope ratio mass spectrometer (Delta C IRMS, ThermoFinnigan), operating in continuous flow mode. Measurements were carried out at the Scientific Facilities of the University of Barcelona. The $^{13}\text{C}/^{12}\text{C}$ ratios (R) of plant material were expressed in composition ($\delta^{13}\text{C}$) notation (Coplen, 2008) as follows:

$$\delta^{13}\text{C} (\text{‰}) = [(R \text{ sample} / R \text{ standard}) - 1] \times 1000 \quad (1)$$

Where: sample refers to plant material and standard to Pee Dee Belemnite (PDB) calcium carbonate. International isotope secondary standards of a known $^{13}\text{C}/^{12}\text{C}$ ratio (IAEA CH7, polyethylene foil, IAEA CH6 sucrose and USGS 40 l-glutamic acid) were calibrated against Vienna Pee Dee Belemnite calcium carbonate (VPDB) with an analytical precision of 0.1‰. The $^{15}\text{N}/^{14}\text{N}$ ratios of plant material were also expressed in δ notation ($\delta^{15}\text{N}$) using international secondary standards of known $^{15}\text{N}/^{14}\text{N}$ ratios (IAEA N1 and IAEA N2 ammonium sulfate and IAEA NO₃ potassium nitrate), with analytical precision of about 0.2‰. Further, the C/N ratio was obtained from these analyses.

Statistical Analysis

Statistical analyses were conducted using the open source software, RStudio 1.0.44 (R Foundation for Statistical Computing, Vienna, Austria). Data for the set of physiological traits were subjected to factorial analyses of variance (ANOVAs) to test the effects of growing conditions on the different traits studied. A bivariate correlation procedure was used to calculate the Pearson correlation coefficients of the different remote sensing indices against the grain yield and the leaf phosphorus

content. Multiple regressions were calculated via a forward stepwise method with GY and P content as dependent variables and the different indices as independent parameters. The figures were also drawn using the Rstudio software.

RESULTS

The Effect of Phosphorous Availability on Grain Yield and Leaf Parameters

Omission of phosphorous fertilizer significantly decreased yield from a mean value (across genotypes) of 7.50 to 5.64 t ha⁻¹ under optimum and no-phosphorous fertilizer conditions, respectively (Table 2). Moreover, the varieties presented a wide range of yield and leaf phosphorus content within the fertilization conditions. Despite this, the phosphorus content of the leaves only correlated significantly against grain yield under non-phosphorus-fertilized conditions (Supplementary Figure 1).

The effect of phosphorous fertilization was also significant for the different leaf parameters studied. Thus, leaf total phosphorous content (P content) and chlorophyll content (LCC) strongly decreased in response to a lack of phosphorous fertilizer. The total nitrogen content (N) also decreased significantly ($P < 0.000$), although in a weaker manner, whereas the total carbon content (C) together with the C/N ratio increased slightly without phosphorous fertilizer, and the stable carbon and nitrogen isotopic composition did not change.

The Effect of Phosphorous Fertilization and the Sensor Altitude on Vegetation Indices

Phosphorous-input also affected the RGB and multispectral indices (Table 3). All RGB indices derived from aerial images were significantly affected by phosphorous fertilization except v*. For the RGB indices measured from the ground, only Hue,

TABLE 2 | Effect of supplemental phosphorus fertilization on the grain yield (GY), leaf chlorophyll content (LCC), phosphorous content (P), leaf carbon and nitrogen concentration (C and N), leaf C/N ratio, and the stable carbon ($\delta^{13}\text{C}$) and nitrogen ($\delta^{15}\text{N}$) composition within the non-phosphorous fertilized (NPF) and the optimal phosphorous (OP) conditions.

	NPF	OP	p-value
GY (t ha ⁻¹)	5.64 ± 0.20	7.5 ± 0.20	0.000***
LCC	32.01 ± 0.99	46.19 ± 0.78	0.000***
P (mg/g DW)	2.06 ± 0.08	4.81 ± 0.11	0.000***
C (%)	43.62 ± 0.10	43.03 ± 0.23	0.021*
N (%)	3.95 ± 0.04	4.30 ± 0.06	0.000***
C/N	11.08 ± 0.11	10.06 ± 0.13	0.000***
$\delta^{13}\text{C}$ (‰)	-11.66 ± 0.03	-11.61 ± 0.04	0.428
$\delta^{15}\text{N}$ (‰)	-1.32 ± 0.23	-1.09 ± 0.30	0.541

Values are means ± standard error of the 26 hybrids. Levels of significance: * $P < 0.05$; *** $P < 0.001$.

Saturation, a*, u*, GA and GGA were significantly affected. Regardless of how images were collected, GA and GGA exhibited the strongest changes, decreasing more than the half with the absence of phosphorous fertilization. In contrast, the CIE-XYZ color space indices, particularly a* and u*, increased significantly in absence of phosphorous fertilization ($P < 0.0001$). Besides, the values of the vegetation indices varied significantly ($P < 0.0001$) with imaging height (ground vs. UAV), except for GA (ground/aerial; GA: NPF 0.08/0.07, OP 0.21/0.20; GGA: NPF 0.08/0.02, OP 0.20/0.12). Hue and GGA were lower when they were assessed on the ground rather than from the aerial platform, while the other indices showed the opposite behavior.

The multispectral index NDVI also decreased significantly ($P < 0.0001$) as response to lack of phosphorus fertilizer (Table 3). The values of NDVI were slightly lower when this index was measured with the hand-held sensor at ground level compared with the same index assessed from the multispectral camera placed in the aerial platform. Apart from EVI, which was not affected by phosphorus fertilization, the values of the other multispectral indices measured via the UAV's multispectral images (Table 1) were also significantly smaller ($P < 0.000$) in the absence of phosphorous fertilizer compared with optimum phosphorous.

Correlations between the remote sensing indices Hue, a*, u*, GA, GGA, and NDVI assessed at ground level against the same indices measured from the UAV were very strong (Table 4). Moreover, most of these indices exhibited a slope close to 1 (Supplementary Figure 2). In contrast, relationships reported for the remaining RGB indices (Intensity, Saturation, Lightness, b*, and v*) were much lower.

Performance of Remote Sensing Indices Assessing Grain Yield and Leaf Phosphorous

Correlation coefficients for the relationships of grain yield with both the RGB (Table 5) and the multispectral indices (Table 6) were calculated. Within both phosphorus conditions and regardless of the imaging height (ground or from UAV) of

TABLE 3 | Effect of phosphorous fertilization on remote sensing indices derived from RGB and spectral measurements within the non-phosphorous fertilized (NPF) and the optimal phosphorous (OP) conditions.

	NPF	OP	p-value
RGB INDICES/GROUND			
Intensity	0.36 ± 0.00	0.36 ± 0.00	0.861
Hue	30.63 ± 0.45	39.34 ± 1.23	0.000***
Saturation	0.19 ± 0.00	0.18 ± 0.00	0.000***
Lightness	42.35 ± 0.11	42.67 ± 0.25	0.243
a*	1.18 ± 0.15	-1.93 ± 0.37	0.000***
b*	18.88 ± 0.23	18.48 ± 0.20	0.200
u*	10.82 ± 0.22	6.34 ± 0.49	0.000***
v*	20.38 ± 0.24	20.65 ± 0.26	0.440
GA	0.08 ± 0.01	0.21 ± 0.01	0.000***
GGA	0.08 ± 0.00	0.20 ± 0.01	0.000***
RGB INDICES/UAV			
Intensity	0.50 ± 0.00	0.49 ± 0.00	0.003**
Hue	23.53 ± 0.37	29.64 ± 0.72	0.000***
Saturation	0.24 ± 0.00	0.22 ± 0.00	0.000***
Lightness	55.13 ± 0.25	53.94 ± 0.40	0.014**
a*	9.39 ± 0.22	4.42 ± 0.42	0.000***
b*	26.53 ± 0.22	25.18 ± 0.23	0.000***
u*	28.05 ± 0.34	19.54 ± 0.69	0.000***
v*	28.28 ± 0.24	27.82 ± 0.25	0.192
GA	0.07 ± 0.01	0.20 ± 0.01	0.000***
GGA	0.02 ± 0.00	0.12 ± 0.01	0.000***
SPECTRAL INDICES			
NDVI _g	0.30 ± 0.03	0.49 ± 0.03	0.000***
NDVI	0.35 ± 0.01	0.50 ± 0.01	0.000***
SAVI	0.16 ± 0.01	0.24 ± 0.01	0.000***
OSAVI	0.23 ± 0.01	0.34 ± 0.01	0.000***
RDVI	0.16 ± 0.00	0.25 ± 0.01	0.000***
EVI	0.22 ± 0.01	0.35 ± 0.01	0.000***
PRI	0.16 ± 0.01	0.18 ± 0.00	0.001**
MCARI	0.05 ± 0.04	0.06 ± 0.00	0.000***
TCARI	0.08 ± 0.00	0.09 ± 0.00	0.012*
TCARI/OSAVI	0.36 ± 0.01	0.26 ± 0.01	0.000***
ARI ₂	0.75 ± 0.02	0.67 ± 0.02	0.010*
CRI ₂	6.65 ± 0.12	6.03 ± 0.20	0.009**
WBI	0.92 ± 0.00	0.94 ± 0.01	0.000***

These indices are defined at section Material and Methods. Values are means ± SE of the individual values of the 26 genotypes. Levels of significance: * $P < 0.05$; ** $P < 0.01$; *** $P < 0.001$.

data acquisition, GA and GGA were best correlated with grain yield, followed by Hue and a*. The u* index also correlated well with grain yield but only when measured from the aerial platform. The rest of the RGB indices correlated far more weakly or did not correlate with grain yield, irrespective of the phosphorus fertilization status or the imaging height of index assessment. Combining both fertilization levels also gave similar results. The correlations of these indices against leaf phosphorus content within both phosphorus treatments were in general weak or absent. It was only under the combination of both fertilization levels that the remote sensing indices had a clearly improved

TABLE 4 | Regression coefficients (r) of the relationships between the remote sensing indices measured at ground against the same VIs measured at aerial level.

	<i>r</i>	<i>p</i> -value
Intensity	0.275	0.000***
Hue	0.902***	0.000***
Saturation	0.466	0.000***
Lightness	0.126	0.000***
<i>a</i>	0.919***	0.000***
<i>b</i>	0.316	0.000***
<i>u</i>	0.903***	0.000***
<i>v</i>	0.310	0.000***
GA	0.970***	0.509
GGA	0.942***	0.000***
NDVI	0.889***	0.000***

Correlations were studied across plots within both trials conditions in combination. Levels of significance: ****P* < 0.001.

TABLE 5 | Regression coefficients of the relationships between the RGB-indices, measured at ground and aerial levels, with grain yield and P content.

	Grain yield			P content		
	NPF	OP	Comb.	NPF	OP	Comb.
RGB INDICES/GROUND						
Intensity	0.194	-0.217	-0.084	-0.014	-0.067	-0.041
Hue	0.777***	0.732***	0.827***	0.336	-0.370	0.594*
Saturation	0.468*	-0.027	-0.179	0.065	0.247	-0.429*
Lightness	0.459*	-0.014	0.205	0.086	-0.152	0.126
<i>a</i> *	-0.601**	-0.725***	-0.818***	-0.334	0.405*	-0.643**
<i>b</i> *	0.572**	0.226	0.171	0.110	-0.020	-0.157
<i>u</i> *	-0.300	-0.729***	-0.786***	-0.267	0.425*	-0.667**
<i>v</i> *	0.642***	0.362	0.434**	0.151	-0.152	0.094
GA	0.816***	0.817***	0.878***	0.111	-0.369	0.707**
GGA	0.822***	0.816***	0.877***	0.122	-0.367	0.711**
RGB INDICES/AERIAL						
Intensity	-0.223	-0.715***	-0.620***	0.166	0.021	-0.359
Hue	0.731***	0.798***	0.868***	-0.062	-0.361	0.624**
Saturation	0.149	0.266	-0.235	-0.539*	-0.112	-0.581*
Lightness	-0.102	-0.653***	-0.526***	0.109	-0.047	-0.316
<i>a</i> *	-0.856***	-0.784***	-0.883***	-0.284	0.339	-0.750**
<i>b</i> *	0.192	0.002	-0.292*	-0.466*	-0.221	-0.575*
<i>u</i> *	-0.830***	-0.777***	-0.873***	-0.424*	0.284	-0.777**
<i>v</i> *	0.318	0.084	0.016	-0.333	-0.337	-0.283
GA	0.837***	0.814***	0.891***	0.139	-0.343	0.693**
GGA	0.790***	0.752***	0.837***	0.206	-0.309	0.697**

Correlations were studied across plots within the non-phosphorus fertilization (NPF) and the optimal phosphorus (OP) trials, as well as both in combination (Comb.). Levels of significance: **P* < 0.05; ***P* < 0.01; ****P* < 0.001.

correlation with leaf P concentration, particularly for the indices that exhibited the best correlations with grain yield. However, the correlations against P content were in all cases weaker than with grain yield.

Concerning NDVI, and regardless the fertilization level, the highest correlation with GY was found with ground

TABLE 6 | Regression coefficients of the relationships between the multispectral-indices and the multispectral with grain yield, P and N content.

	Grain Yield			P Content		
	NPF	OP	Comb.	NPF	OP	Comb.
MULTISPECTRAL INDICES						
NDVI _{ground}	0.734***	0.711***	0.863***	0.058	-0.423*	0.669***
NDVI	0.628***	0.643***	0.823***	0.324	-0.347	0.800***
SAVI	0.652***	0.644***	0.823***	0.159	-0.269	0.790***
OSAVI	0.657**	0.655**	0.829***	0.216	-0.303	0.797***
RDVI	0.658***	0.650***	0.829***	0.198	-0.286	0.795***
EVI	0.613***	0.529**	0.798***	0.119	-0.220	0.782***
PRI	0.039	0.312	0.406**	0.428*	0.032	0.466*
MCARI	0.358	-0.019	0.452**	-0.035	-0.033	0.463*
TCARI	0.172	-0.200	0.238	-0.147	0.055	0.314
TCARI/OSAVI	-0.401*	-0.618**	-0.748***	-0.368	0.283	-0.700***
ARI2	-0.012	0.286	-0.133	-0.286	-0.002	-0.363
CRI2	0.016	0.359	-0.091	-0.162	-0.064	-0.364
WBI	0.241	0.595**	0.598***	-0.014	-0.064	0.414*
MULTISPECTRAL BANDS						
B450	-0.348	-0.688***	-0.638***	-0.459	0.318	-0.383
B550	0.261	-0.505**	-0.102	-0.205	0.371	0.036
B570	0.032	-0.529**	-0.419**	-0.498*	0.212	-0.354
B670	-0.302	-0.566**	-0.739***	-0.540*	0.398	-0.731***
B700	-0.116	-0.525**	-0.602***	-0.463*	0.324	-0.567**
B720	0.269	-0.045	0.153	-0.319	0.125	0.047
B780	0.465*	0.477*	0.741***	-0.020	-0.122	0.688***
B840	0.496*	0.550**	0.779***	0.010	-0.137	0.744***
B860	0.442*	0.492*	0.753***	-0.051	-0.129	0.736***
B900	0.425*	0.537**	0.761***	-0.063	-0.083	0.739***
B950	0.390*	0.411*	0.724***	-0.024	-0.091	0.741***

Correlations were studied across plots within the non-phosphorus fertilization (NPF) and the optimal phosphorus (OP) trials, as well as both in combination (Comb.). Levels of significance: **P* < 0.05; ***P* < 0.01; ****P* < 0.001.

spectroradiometer measurements, although the NDVI derived from the UAV was still highly correlated with GY (Table 6). Multispectral indices SAVI, RDVI, OSAVI, EVI, and WBI were also significantly correlated with GY within the two phosphorus conditions alone, or when both levels were combined. Individual multispectral bands presented significant correlations with yield, particularly under optimal phosphorus. Correlations of these indices with leaf P content were weak or absent, regardless of the phosphorus level, whereas spectral bands around 570, 670, and 700 nm significantly, but weakly, correlated with P content at the low fertilization level. In the case of the RGB indices, combining both treatments strongly increased the correlations between the multispectral indices and P content, particularly for the indices that best correlated with grain yield (NDVI, SAVI, RDVI, EVI, or OSAVI). However, the strengths of the correlations were always lower than for grain yield.

For the purpose of testing how the combination of different indices measured from the aerial platform may improve the strength and accuracy of the assessment of grain yield and phosphorous concentration, stepwise regressions were performed (Table 7). The best predictive equations of grain yield were achieved using RGB indices, which were the most significant

TABLE 7 | Multilinear regression (stepwise) of grain yield (GY) as dependent variable and the different categories of remote sensing traits (RGB VIs, multispectral VIs, and specific multispectral bands) measured from the unmanned aerial vehicle within the non-phosphorus fertilization (NPF) and the optimal phosphorus (OP) trials.

			Equation	R ²	RSE	p-value	Portion of variance
GY	NPF	Aerial RGB VIs	$GY = -0.25 \cdot u^* + 13.99 \cdot GA + 11.65$	0.821	0.590	0.000	$u^* = 0.49$ $GA = 0.50$
		Multispectral VIs	$GY = 59.08 \cdot MCARI - 12.46 \cdot TCARI/OSAVI + 7.38$	0.463	0.769	0.000	$MCARI = 0.46$ $TCARI/OSAVI = 0.53$
	OP	Aerial RGB VIs	$GY = 12.31 \cdot GA + 5.00$	0.662	0.596	0.000	$GA = 1.00$
		Multispectral VIs	$GY = -43.94 \cdot NDVI + 189.93 \cdot RDVI - 59.62 \cdot EVI + 3.36$	0.652	0.632	0.000	$NDVI = 0.31$ $RDVI = 0.40$ $EVI = 0.28$
P content	NPF	Aerial RGB VIs	$P \text{ content} = -0.26 \cdot Hue - 0.49 \cdot a^* + 13.00$	0.436	0.337	0.001	$Hue = 0.41$ $a^* = 0.58$
		Multispectral VIs	$P \text{ content} = -146.66 \cdot NDVI - 995.36 \cdot SAVI + 1289 \cdot RDVI + 0.53$	0.311	0.381	0.038	$NDVI = 0.39$ $SAVI = 0.29$ $RDVI = 0.31$
	OP	Aerial RGB VIs	$P \text{ content} = 0.47 \cdot b^* - 0.56 \cdot v^* + 8.82$	0.210	0.520	0.065	$b^* = 0.34$ $v^* = 0.65$
		Multispectral VIs	$P \text{ content} = 77.16 \cdot SAVI - 86.16 \cdot RDVI + 7.20$	0.151	0.539	0.150	$SAVI = 0.46$ $RDVI = 0.53$

R², determination coefficient; RSE, Residual Standard Error.

measurements in the absence of phosphorous fertilizer. The multispectral bands and indices performed better at predicting grain yield under optimum phosphorus conditions than the non-fertilized conditions. In contrast, the prediction of P was not as good as GY and the only significant equations were found at the non-phosphorous fertilization conditions ($P < 0.050$).

In order to check the ability of the remote sensing indices to predict genotypic differences in yield, we correlated the genotypic values of the different categories of remote sensing traits evaluated in the seedlings with the yield of each hybrid determined from multi-location trials developed in parallel (Table 8). Every index that correlated with yield in our experiment, in either the absence of phosphorous fertilizer or in optimum conditions, also showed significant correlations with the genotypic yield data of the multilocation study. The correlation coefficients calculated with the RBG and the multispectral indices against the yield of the multilocation study were very similar to those found between these indices and the grain yield in the present study. The best correlated RGB VIs were GA and GGA again, both ground and aerial measurements. Also, the spectral indices associated with the greenness and density measurements correlated greatly with the genotypic yield, and to a similar extent as the correlation with grain yield in the same trials. On the other hand, the RDVI and the WBI correlated even better with grain yield from the multilocation trials than with the grain yield of the present remote sensing trial.

DISCUSSION

Phosphorus Fertilization Effect on Grain Yield

Phosphorous is an essential nutrient for plant growth and development (Manschadi et al., 2014). For that reason, the yield of the hybrids was strongly affected by the lack of phosphorus

fertilizer, and leaf phosphorous content correlated with grain yield across hybrids in the non-phosphorus-fertilized trial. The large variability in plant performance across the hybrids that was revealed in our results presumably reflects differences in P use efficiency as well as genotypic differences in yield potential (i.e., productivity under optimal agronomical conditions). In general, most reports state that P deficiency reduces photosynthetic capacity and efficiency through different mechanisms (Brooks et al., 1988).

Yield variations caused by differences in the water status of the plants can be ruled out through the lack of differences in $\delta^{13}C$. Even for a C4 plant like maize, differences in plant water status, and intrinsic photosynthetic metabolism may be reflected in the $\delta^{13}C$ of the plant matter, with $\delta^{13}C$ decreasing in response to water stress (Farquhar et al., 1989; Monneveux et al., 2007). We did not find differences in $\delta^{13}C$ associated to fertilization. In contrast, significant differences between the two fertilization conditions were detected in the WBI values. This index uses the reflectance spectra at the near and far-infrared region as an indication of water absorption. Hence, higher WBI values indicate a better water status. Optimal growing conditions had enabled faster seedling growth and therefore turgid leaves (i.e., more watered), although past studies have also indicated that WBI can predict the leaf area index (Roberts et al., 1998; Qiu et al., 2007). Thus, higher WBI values at optimum P conditions must be due to a larger canopy area rather than water status differences. Nevertheless, some reports have indicated that phosphorus fertilization can help crops to use water more efficiently under limited moisture conditions (Waraich et al., 2011).

Phosphorous and nitrogen content in the leaves correlated within each fertilization levels (Supplementary Figure 3) and both contents were higher under optimal compared with non-phosphorous fertilization conditions. Differences in

TABLE 8 | Regression coefficients (*r*) of the relationships across the genotypes of the VI's measured in seedlings at non-phosphorus fertilization (NPF) and optimal phosphorous (OP) conditions in this study against grain yield data from other trials.

	NPF	OP
RGB INDICES/GROUND		
<i>Intensity</i>	0.079	-0.237
<i>Hue</i>	0.494*	0.695***
<i>Saturation</i>	0.562**	-0.039
<i>Lightness</i>	0.311	-0.047
<i>a*</i>	-0.232	-0.677***
<i>b*</i>	0.592**	0.187
<i>u*</i>	0.057	-0.685***
<i>v*</i>	0.602**	0.314
GA	0.738***	0.830***
GGA	0.741***	0.828***
RGB INDICES/UAV		
<i>Intensity</i>	-0.465*	-0.643***
<i>Hue</i>	0.767***	0.766***
<i>Saturation</i>	0.491**	0.360
<i>Lightness</i>	-0.317	-0.570**
<i>a*</i>	-0.705***	-0.721***
<i>b*</i>	0.423*	0.137
<i>u*</i>	-0.625***	-0.692***
<i>v*</i>	0.450*	0.209
GA	0.848***	0.779***
GGA	0.785***	0.730***
SPECTRAL INDICES		
NDVI g	0.752***	0.594**
NDVI	0.656***	0.629***
PRI	-0.207	0.223
SAVI	0.658***	0.630***
MCARI	0.399*	-0.017
WBI	0.486*	0.573**
RDVI	0.721***	0.630***
EVI	0.403*	0.334
ARI2	0.133	0.162
CRI2	0.112	0.243
TCARI	0.304	-0.157
OSAVI	0.552**	0.611***

Levels of significance: * $P < 0.05$; ** $P < 0.01$; *** $P < 0.001$.

nitrogen content may account for the variation across genotypes and fertilization levels in LCC and the fact that at least under NPF chlorophyll content and phosphorous content correlated positively.

Comparative Performance of Ground vs. Aerially Assessed Indices at Determining Genotypic Differences in Grain Yield

The vegetation indices derived from conventional digital RGB images have been proposed as a means of estimating green biomass and grain yield in maize and other cereals under stress conditions (Ahmad and Reid, 1996). As the ground and aerial

measurements were taken at the same time on the same day, variation in environmental variables such as light intensity and brightness can be almost negligible. Thus, the main differences are due to the resolution of the pictures (Figure 2). Besides using cameras with the same sensor size (17.3×13 mm) that capture images at the same resolution (16-megapixels), the final resolution of the images was also affected (by the square of) the distance between the camera and the object (in this case the plots). While the images collected in our study from the UAV only reached a resolution of 488×193 pixels per plot, the spatial resolution of the images taken from the ground was $4,608 \times 3,072$ pixels per plot. When the spatial resolution is very high, plants in the image are well-defined; however, when the spatial resolution is poorer, the boundaries between plants and soil are fuzzy, and consequently, there is usually a higher portion of pixels including information of both vegetation and bare soil (Torres-Sánchez et al., 2014). Despite such differences in resolution, some indices like *a** and *u** assessed aerially correlated better against grain yield, whereas others exhibited similar performance to ground determined indices, except for GGA which correlated slightly weaker when assessed from the aerial platform. The *a** and *u** indices are more likely to reflect color components that are more sensitive to the scene's illumination and the camera's self-adjustments (Casadesús et al., 2005), thus being more limited by soil lightness and therefore performing better at the aerial level with reduced image resolution. Conversely, a reduction in the number of pixels in the image makes it more difficult to identify differences in vegetation color, so GGA performed better at ground level. Nevertheless, advances in digital photography allow sufficiently high resolution for low-altitude aerial imaging to be a viable and economical monitoring tool for agriculture (Sankaran et al., 2015). Moreover, aerial photographs enable coverage of the whole plot (which usually is not the case for images taken at ground level) and therefore, to some extent, may compensate for the loss of spatial resolution. In this sense, correlations with grain yield by indices derived from aerial imaging were generally only slightly weaker than indices measured at ground level. Some of the RGB indices like Hue, *a**, *u**, GA, or GGA and the NDVI, produced correlation coefficients higher than $R^2 = 0.900$ when compared to the same indices measured at ground level and from the aerial platform (Supplementary Figure 2). This is despite the methodological differences between index determination at ground level (on an individual plot basis) and the aerial platform (across a whole trial and further segmented into individual plots). Therefore, both approaches are able to offer essentially similar kinds of information.

Comparative Performance of the RGB vs. Multispectral Indices at Determining Genotypic Differences in Grain Yield

The RGB-based indices, GA and GGA, were the best at GY prediction, outperforming other RGB indices, NDVI and the rest of the spectral indices. Considering that the data of our study was collected at an early phenological stage, the plants were not able to cover the soil completely. Therefore, the superior performance of these indices should be attributable, at least in

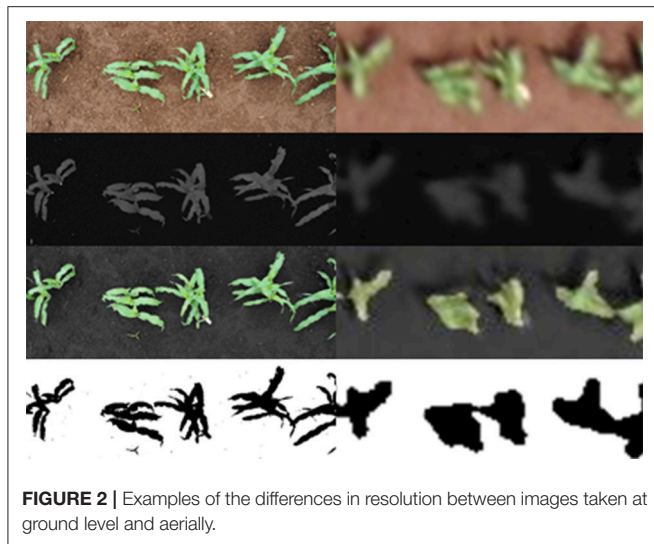


FIGURE 2 | Examples of the differences in resolution between images taken at ground level and aerially.

part, to their insensitivity to soil color (Casadesús et al., 2007). GA quantifies the portion of green pixels to the total pixels of the image and is a reliable estimator of vegetation cover (Lukina et al., 1999). By contrast, GGA does not incorporate the yellowish green fraction of vegetation when the GA becomes saturated during late phenological periods. Therefore, elevated GA and GGA indices, probably driven by a higher biomass, seem to be more relevant for predicting higher yield. Although these indices performed in a very similar way at both measurement locations, when the GGA was measured at ground level it tended to be more highly correlated to GY. Besides other considerations the far higher resolution of the RGB compared with the multispectral images may be also relevant when working from an aerial platform.

A recent study has concluded that RGB images performed better than NDVI in determining genotypic differences in hybrid maize yield under different nitrogen fertilization conditions (Vergara-Díaz et al., 2016). The results of our research include the NDVI and its reformulations as the SAVI, OSAVI, EVI, and RDVI indices, which were best correlated with GY. These indices, which are based on the strong contrast between the near infrared (NIR) and (R) bands, are optical measurements of canopy greenness and canopy cover (Tucker, 1979). NDVI is a widely accepted approximation for assessing crops under different growing conditions, but it can fail to distinguish changes in soil cover and plant density from changes in vegetation color (Steven et al., 1996). As our study was made at an early stage of development, the plants did not have enough biomass to cause this saturation problem. The SAVI was developed as a modification of the NDVI, to correct the brightness incidence of the soil (Huete, 1988). Notwithstanding the reduction in soil noise problems, correlations of the SAVI with GY were not improved in comparison to the NDVI. The optimization of this index, which applied an adjusting coefficient (Rondeaux et al., 1996) that resulted in the OSAVI, also did not improve the correlation with GY, but rather caused the opposite. The RDVI and the EVI are another indices based on the NDVI,

which have been developed with the intention of correcting the rapid saturation due to dense vegetation (Liu and Huete, 1995). Even though this was not a problem in our study, the fact that those indices emphasize the vigor of vegetation has enabled achieving quite strong correlations, similar to NDVI.

MCARI is an index that measures the depth of chlorophyll absorption at 670 nm relative to the reflectance at 550 and 700 nm (Daughtry, 2000). TCARI is a transformation developed to counteract the effect of soil background (Haboudane et al., 2002). However, both indices are still sensitive to the background reflectance properties. The plots studied were particularly characterized by a low leaf area index, so neither the MCARI nor the TCARI were adequate for our experiment. Anthocyanin and carotenoid pigments were also detected by the ARI2 and the CRI2 indices, but no valuable information has been obtained.

The complementary metal-oxide-semiconductor (CMOS) image sensor of the micro-MCA12 camera is optimized to collect wavelengths at ~ 800 nm, dropping in a smooth curve to a low relative efficiency at 400 nm in the visible wavelengths and a smaller reduction in efficiency at 1050 nm in the NIR, at the limits of its range. As a consequence, the efficiency of the measurements in the blue band (450 nm) is considerably lower (20%) in comparison to the measurements of the NIR or the R bands (85% both). Due to this limitation in the blue region sensitivity, more noise is included in the measurements of the blue band. Moreover, inadequate phosphorus content can result in a darkening of the leaves to a purple color. This would explain why the single band measurement in the blue region correlated with GY at optimum conditions but it failed to do so under non-fertilized conditions. The correlation analysis between each multispectral band and yield has identified sensitive wavelengths under both phosphorus levels, and this ranges from 780 to 950 nm of the near-infrared (NIR, 750–1,350 nm) region of the spectrum.

The results obtained proved that measurements at an early growing date, while the plants are still seedlings, are optimal for the assessment of the future yield.

Performance of RGB and Multispectral Indices at Determining Genotypic Differences Derived from Leaf Phosphorus Concentration

The strength of the correlations inside each treatment between the indices and the P content were far lower than of these indices with GY. Distribution of values is not uniform and in fact the linear correlation has not any sense besides to show these vegetation indices are able to clearly differentiate between the two different groups of phosphorous fertilization (but not across genotypes within each fertilization level). The same happened with the LCC and the leaf nitrogen content (Supplementary Figure 3). The two different fertilization levels caused differences in leaf phosphorous content but indirectly also differences in leaf chlorophyll and total nitrogen contents (and at that with an abundance of N fertilizer applied to

both treatments). Therefore, differences in leaf color between treatments are evident (less chlorophyll and nitrogen content in the leaves on non-phosphorous fertilized plants). However, similar to a^* , GA, and GGA (Supplementary Figure 4), leaf chlorophyll and nitrogen contents did not correlate or just did marginally (SPAD values within NPF) against leaf phosphorous content. Again, the differences between fertilization levels accounted for the significant relationship of leaf chlorophyll and N contents against leaf phosphorous content when data of both fertilization levels were combined. Moreover, there is a lack of consistency between the ground and aerial RGB index correlations in regard to phosphorous content (Table 5). In contrast, the correlations with grain yield follow the same patterns for both fertilization levels. Therefore, the significance of the correlations of the indices with phosphorus concentration may be related to the relationship between leaf phosphorus concentration and green biomass due to phosphorous is an essential element in plant growth (Manschadi et al., 2014; Gemenet et al., 2016). Indices better assessed differences in leaf phosphorous concentration at the low phosphorous conditions compared to optimum conditions due to the primary capacity of these indices to strongly correlate with green biomass and thus grain yield.

Similarly, the multispectral indices didn't show significant correlations with P content within each fertilization level, while several of these indices correlated with GY. Only the PRI correlated with leaf phosphorous content (and just under low P conditions). The PRI is a spectral index increasingly used as an indicator of photosynthetic efficiency because it is based on the short-term reversible xanthophyll pigment cycle (Peñuelas et al., 2011). Low phosphorus levels can lead to an increase in the de-epoxidation process, which augments the relative amount of zeaxanthin and decreases violaxanthin (Goodwin, 1980; Tambussi et al., 2002). Zeaxanthin is essential for dissipation of excess energy as heat in chloroplasts (Demmig-Adams et al., 2013). The weak but still significant correlations between the PRI and the P content suggest a similar photoprotection response. In other studies, similar findings have been reported that associate nutrient deprivation with increased zeaxanthin levels and thus lower PRI values (Filella et al., 1996). In reference to the multispectral bands, only the bands located at 570, 670, and 700 nm correlated with the leaf phosphorous content, and these were a weakly correlation with the leaf phosphorous content. These bands correspond to the green (570 nm) and red regions (670 and 700 nm) and they have been used to assess non-stressed vegetation (Thenkabail et al., 2002). Higher values of reflection at these bands might correspond to vigorous plants with higher P content. These results are in conflict with the results obtained by Osborne et al. (2002), who reported a significant spectral response in the NIR region to the P concentration in corn.

CONCLUSIONS

There is a need for phenotyping tools which increase the selection efficiency and to understand mechanisms of phosphorous tolerance. This study clearly shows a genotypic variability for

low phosphorous tolerance, with a reduction in yields of 25% in average in comparison with the optimum conditions. Previous studies in the literature suggests that only when reduction is 75% or more, selecting for specific adaptation to tolerance to low nutrient availability is the strategy (Bänziger et al., 1997; Masuka et al., 2012). However, selecting for yield potential instead than for specific adaptation to low phosphorous, still makes sense when the yield reduction associated was moderate, like in this study, which is the usual situation in agronomical scenarios. Hence, indices also correlated with the yield of the hybrids when they were performed under the high yielding conditions.

This study emphasizes the capabilities of RGB vegetation indices as phenotypic traits for predicting maize performance during early stages of crop growth. GA was the vegetation index best correlated with grain yield across maize hybrids and regardless the phosphorous fertilization level and therefore this index may serve to select the most productive hybrids for the SSA. RGB indices assessed at ground level were comparable to those measured from an aerial platform. Moreover, RGB indices performed better than multispectral vegetation indices. The use of vegetation indices derived from RGB images may represent a very affordable approach for phenotyping and may become even more economical due to the similarity between results obtained from ground evaluation and those achieved from aerial platforms. The phenotypic correlations found between the remote sensing indices of seedlings and the genotypic yield data collected in the multi-location trials confirm their usefulness. Despite its comparatively low tech and low-cost nature, digital photography is a promising approach, and its derived indices have demonstrated potential for the assessment of crop management in maize, making it ideal for developing countries in particular.

Additionally, RGB-derived vegetation indices are also amenable for monitoring the effects of phosphorous fertilizer applications. However, only some of the indices best correlated with grain yield exhibited significant, albeit weaker, correlations with leaf phosphorus content. Moreover, these correlations were only present under low phosphorus fertilization, which suggests that they were linked to differences in biomass and grain yield caused by phosphorous fertilization.

AUTHOR CONTRIBUTIONS

MZ-A, BP, and JC managed and directed the maize trials at the Southern Africa regional office of CIMMYT in Harare, Zimbabwe. SK carried out the UAV flights for the obtainment of aerial measurements. OV-D and JA conducted the field measurements and the collection of samples. AG-R processed the images, analyzed the samples and wrote the paper under the supervision of JA and SK and with the contributions from all the other authors.

FUNDING

This article was supported by grants from the MAIZE CGIAR Research Program and the AGL2016-76527-R Project from

the Ministerio de Economía y Competitividad of the Spanish Government. We also acknowledge the support from IdRA and the Universitat de Barcelona.

ACKNOWLEDGMENTS

We thank the personnel from the CIMMYT Southern Africa Regional Office at Harare for their support during the field measurements and sampling. The trials were planted under

the Bill and Melinda Gates funded project, Improved Maize for African Soils. Finally, we thank Dr. Jaume Casadesús for providing the BreedPix software.

SUPPLEMENTARY MATERIAL

The Supplementary Material for this article can be found online at: <https://www.frontiersin.org/articles/10.3389/fpls.2017.02004/full#supplementary-material>

REFERENCES

- Ahmad, I. S., and Reid, J. F. (1996). Evaluation of Colour Representations for Maize Images. *J. Agric. Eng. Res.* 63, 185–195. doi: 10.1006/jaer.1996.0020
- Araus, J. L., and Cairns, J. E. (2014). Field high-throughput phenotyping: the new crop breeding frontier. *Trends Plant Sci.* 19, 52–61. doi: 10.1016/j.tplants.2013.09.008
- Babar, M. A., Reynolds, M. P., Ginkel, M., Van Klatt, A. R., Raun, W. R., and Stone, M. L. (2006). Spectral reflectance to estimate genetic variation for In-season biomass, leaf chlorophyll, and canopy temperature in wheat. *Crop Sci.* 46, 1046–1057. doi: 10.2135/cropsci2005.0211
- Bänziger, M., Betrán, F. J., and Lafitte, H. R. (1997). Efficiency of high-nitrogen selection environments for improving maize for low-nitrogen target environments. *Crop Sci.* 37, 1103–1109. doi: 10.2135/cropsci1997.0011183X003700040012x
- Blackburn, G. A. (2007). Hyperspectral remote sensing of plant pigments. *J. Exp. Bot.* 58, 855–867. doi: 10.1093/jxb/erl123
- Brooks, A., Woo, K. C., and Wong, S. C. (1988). Effects of phosphorus nutrition on the response of photosynthesis to CO₂ and O₂, activation of ribulose biphosphate carboxylase and amounts of ribulose biphosphate and 3-phosphoglycerate in spinach leaves. *Photosyn. Res.* 15, 133–141. doi: 10.1007/BF00035257
- Buerkert, A., Bationo, A., and Piepho, H. P. (2001). Efficient phosphorus application strategies for increased crop production in sub-Saharan West Africa. *Field Crops Res.* 72, 1–15. doi: 10.1016/S0378-4290(01)00166-6
- Cabrera-Bosquet, L., Molero, G., Nogués, S., and Araus, J. L. (2009). Water and nitrogen conditions affect the relationships of $\Delta^{13}\text{C}$ and $\Delta^{18}\text{O}$ to gas exchange and growth in durum wheat. *J. Exp. Bot.* 60, 1633–1644. doi: 10.1093/jxb/erp028
- Cairns, J. E., Crossa, J., Zaidi, P. H., Grudloyma, P., Sanchez, C., Araus, J. L., et al. (2013a). Identification of drought, heat, and combined drought and heat tolerant donors in maize. *Crop Sci.* 53, 1335–1346. doi: 10.2135/cropsci2012.09.0545
- Cairns, J. E., Hellin, J., Sonder, K., Araus, J. L., MacRobert, J. F., Thierfelder, C., et al. (2013b). Adapting maize production to climate change in sub-Saharan Africa. *Food Security* 5:345. doi: 10.1007/s12571-013-0256-x
- Cairns, J. E., Sanchez, C., Vargas, M., Ordoñez, R., and Araus, J. L. (2012). Dissecting maize productivity: ideotypes associated with grain yield under drought stress and well-watered conditions. *J. Integr. Plant Biol.* 54, 1007–1020. doi: 10.1111/j.1744-7909.2012.01156.x
- Casadesús, J., Biel, C., and Savé, R. (2005). Turf color measurement with conventional digital cameras. *Int. J. Remote Sens.* 26, 804–811.
- Casadesús, J., Kaya, Y., Bort, J., Nachit, M. M., Araus, J. L., Amor, S., et al. (2007). Using vegetation indices derived from conventional digital cameras as selection criteria for wheat breeding in water-limited environments. *Ann. Appl. Biol.* 150, 227–236. doi: 10.1111/j.1744-7348.2007.00116.x
- Casadesús, J., and Villegas, D. (2014). Conventional digital cameras as a tool for assessing leaf area index and biomass for cereal breeding. *J. Integr. Plant Biol.* 56, 7–14. doi: 10.1111/jipb.12117
- Coplen, T. B. (2008). *Explanatory Glossary of Terms used in Expression of Relative Isotope Ratios and Gas Ratios. IUPAC Recommendations 2008.* International Union of Pure and Applied Chemistry Inorganic Chemistry Division, Commission on Isotopic Abundances and Atomic Weights: Research Triangle Park, NC.
- Daughtry, C. (2000). Estimating corn leaf chlorophyll concentration from leaf and canopy reflectance. *Remote Sens. Environ.* 74, 229–239. doi: 10.1016/S0034-4257(00)00113-9
- Deery, D. M., Rebetzke, G. J., Jimenez-Berni, J. A., James, R. A., Condon, A. G., Bovill, W. D., et al. (2016). Methodology for high-throughput field phenotyping of canopy temperature using airborne thermography. *Front. Plant Sci.* 7:1808. doi: 10.3389/fpls.2016.01808
- Demmig-Adams, B., Cohu, C. M., Amiard, V., van Zadelhoff, G., Veldink, G. A., Muller, O., et al. (2013). Emerging trade-offs - impact of photoprotectants (PsbS, xanthophylls, and vitamin E) on oxylipins as regulators of development and defense. *New Phytol.* 197, 720–729. doi: 10.1111/nph.12100
- Evans, R. D. (2001). Physiological mechanisms influencing plant nitrogen isotope composition. *Trends Plant Sci.* 6, 121–126. doi: 10.1016/S1360-1385(01)01889-1
- Farquhar, G. D., Ehleringer, R., and Hubick, K. T. (1989). Carbon isotope discrimination and photosynthesis. *Annu. Rev. Plant Physiol. Plant Mol. Biol.* 40, 503–537. doi: 10.1146/annurev.pp.40.060189.002443
- Fillella, I., Amaro, T., Araus, J. L., and Penuelas, J. (1996). Relationship between photosynthetic radiation-use efficiency of barley canopies and the photochemical reflectance index (PRI). *Physiol. Plant.* 96, 211–216. doi: 10.1111/j.1399-3054.1996.tb00204.x
- Fiorani, F., and Schurr, U. (2013). Future scenarios for plant phenotyping. *Annu. Rev. Plant Biol.* 64, 267–291. doi: 10.1146/annurev-arplant-050312-120137
- Gamon, J. A., Serrano, L., and Surfus, J. S. (1997). The photochemical reflectance index: an optical indicator of photosynthetic radiation use efficiency across species, functional types, and nutrient levels. *Oecologia* 112:492. doi: 10.1007/s004420050337
- Gemenet, D. C., Leiser, W. L., Beggi, F., Herrmann, L. H., Vadez, V., Rattunde, H. F. W., et al. (2016). Overcoming phosphorus deficiency in west African pearl millet and sorghum production systems: promising options for crop improvement. *Front. Plant Sci.* 7:1389. doi: 10.3389/fpls.2016.01389
- Gitelson, A. A., Merzlyak, M. N., and Chivkunova, O. B. (2001). Optical properties and nondestructive estimation of anthocyanin content in plant leaves. *Photochem. Photobiol.* 74, 38–45. doi: 10.1562/0031-8655(2001)074<0038:OPANEO>2.0.CO;2
- Gitelson, A. A., Zur, Y., Chivkunova, O. B., and Merzlyak, M. N. (2002). Assessing carotenoid content in plant leaves with reflectance spectroscopy. *Photochem. Photobiol.* 75, 272–281. doi: 10.1562/0031-8655(2002)075<0272:ACCIPL>2.0.CO;2
- Goodwin, T. W. (1980). *The Biochemistry of the Carotenoids.* London: Chapman and Hall.
- Haboudane, D., Miller, J. R., Tremblay, N., Zarco-Tejada, P. J., and Dextraze, L. (2002). Integrated narrow-band vegetation indices for prediction of crop chlorophyll content for application to precision agriculture. *Remote Sens. Environ.* 81, 416–426. doi: 10.1016/S0034-4257(02)00018-4
- Huete, A. (1988). A soil-adjusted vegetation index (SAVI). *Remote Sens. Environ.* 25, 295–309. doi: 10.1016/0034-4257(88)90106-X

- Huete, A., Didan, K., Miura, T., Rodriguez, E. P., Gao, X., and Ferreira, L. G. (2002). Overview of the radiometric and biophysical performance of the MODIS vegetation indices. *Remote Sens. Environ.* 83, 195–213. doi: 10.1016/S0034-4257(02)00096-2
- Liu, H. Q., and Huete, A. (1995). A feedback based modification of the NDVI to minimize canopy background and atmospheric noise. *IEEE Trans. Geosci. Remote Sens.* 33, 457–465. doi: 10.1109/36.377946
- Lukina, E. V., Stone, M. L., and Raun, W. R. (1999). Estimating vegetation coverage in wheat using digital images. *J. Plant Nutr.* 22, 341–350. doi: 10.1080/01904169909365631
- Mahajan, G. R., Sahoo, R. N., Pandey, R. N., Gupta, V. K., and Kumar, D. (2014). Using hyperspectral remote sensing techniques to monitor nitrogen, phosphorus, sulphur and potassium in wheat (*Triticum aestivum* L.). *Precision Agric.* 15, 499–522. doi: 10.1007/s11119-014-9348-7
- Manschadi, A. M., Kaul, H.-P., Vollmann, J., Eitzinger, J., and Wenzel, W. (2014). Developing phosphorus-efficient crop varieties—An interdisciplinary research framework. *Field Crops Res.* 162, 87–98. doi: 10.1016/j.fcr.2013.12.016
- Masuka, B., Araus, J. L., Das, B., Sonder, K., Cairns, J. E., and Cairns, J. E. (2012). Phenotyping for abiotic stress tolerance in maize. *J. Integr. Plant Biol.* 54, 238–249. doi: 10.1111/j.1744-7909.2012.01118.x
- McIntyre, B. D., Herren, H. R., and Wakhungu, R. T. W. J. (2009). *Agriculture at a Crossroads: International Assessment of Agricultural Knowledge, Science and Technology for Development (IAASTD)*. Sub-Saharan Africa (SSA): IAASTD Report.
- Monneveux, P., Sheshshayee, M. S., Akhter, J., and Ribaut, J. (2007). Using carbon isotope discrimination to select maize (*Zea mays* L.) inbred lines and hybrids for drought tolerance. *Plant Sci.* 173, 390–396. doi: 10.1016/j.plantsci.2007.06.003
- Osborne, S. L., Schepers, J. S., Francis, D. D., and Schlemmer, M. R. (2002). Detection of phosphorus and nitrogen deficiencies in corn using spectral radiance measurements. *Agron. J.* 94, 1215–1221. doi: 10.2134/agronj2002.1215
- Peñuelas, J., Filella, I., Biel, C., Serrano, L., and Savé, R. (1993). The reflectance at the 950–970 nm region as an indicator of plant water status. *Int. J. Remote Sens.* 14, 1887–1905.
- Peñuelas, J., Garbulsky, M. F., and Filella, I. (2011). Photochemical reflectance index (PRI) and remote sensing of plant CO₂ uptake. *New Phytol.* 191, 596–599. doi: 10.1111/j.1469-8137.2011.03791.x
- Petropoulos, G. P., and Kalaitzidi, C. (2012). Multispectral vegetation indices in remote sensing: an overview. *Ecol. Modell.* 2, 15–39.
- Qiu, H.-L., Sanchez-Azofeifa, A., and Gamon, J. (2007). “Ecological applications of remote sensing at multiple scales,” in *Functional Plant Ecology, 2nd Edn*, Books in Soils, Plants, and the Environment (Boca Raton, FL: CRC Press), 655–675.
- Reynolds, M., Foulkes, J., Furbank, R., Griffiths, S., King, J., Murchie, E., et al. (2012). Achieving yield gains in wheat. *Plant Cell Environ.* 35, 1799–1823. doi: 10.1111/j.1365-3040.2012.02588.x
- Roberts, D. A., Brown, K., Green, R., Ustin, S., and Hincley, T. (1998). “Investigating the relationship between liquid water and leaf area in clonal Populus,” in *Summaries of the 7th Annual JPL Earth Science Workshop*, JPL (Pasadena, CA).
- Rondeaux, G., Steven, M., and Baret, F. (1996). Optimization of soil-adjusted vegetation indices. *Remote Sens. Environ.* 55, 95–107. doi: 10.1016/0034-4257(95)00186-7
- Roujean, J.-L., and Breon, F.-M. (1995). Estimating PAR absorbed by vegetation from bidirectional reflectance measurements. *Remote Sens. Environ.* 51, 375–384. doi: 10.1016/0034-4257(94)00114-3
- Rouse, J. W., Hass, R. H., Schell, J. A., and Deering, D. W. (1973). “Monitoring vegetation systems in the great plains with ERTS,” in *Third Earth Res. Technol. Satellite Symp. Vol. 1*, 309–317.
- Sankaran, S., Khot, L. R., Espinoza, C. Z., Jarolmasjed, S., Sathuvalli, V. R., Vandemark, G. J., et al. (2015). Low-altitude, high-resolution aerial imaging systems for row and field crop phenotyping: a review. *Eur. J. Agronomy.* 70, 112–123. doi: 10.1016/j.eja.2015.07.004
- Smalberger, S. A., Singh, U., Chien, S. H., Henao, J., and Wilkens, P. W. (2006). Development and validation of a phosphate rock decision support system. *Agron. J.* 98, 471–483. doi: 10.2134/agronj2005.0244
- Steven, M. D., Malthus, T. J., Demetriades-Shah, T. H., Danson, F. M., and Clark, J. A. (1996). “High-spectral resolution indices for crop stress,” in *Applications of Remote Sensing in Agriculture*, in eds M. D. Steven and J.A. Clark (London: Butterworths), 209–228.
- Tambussi, E. A., Casadesus, J., Munné-Bosch, S., and Araus, J. L. (2002). Photoprotection in water-stressed plants of durum wheat (*Triticum turgidum* var. durum): Changes in chlorophyll fluorescence, spectral signature and photosynthetic pigments. *Funct. Plant Biol.* 29, 35–44. doi: 10.1071/PP01104
- Thenkabail, P. S., Smith, R. B., Pauw, E., and De, De Pauw, E. (2002). Evaluation of narrowband and broadband vegetation indices for determining optimal hyperspectral wavebands for agricultural crop characterization. *Photogramm. Eng. Remote Sensing* 68, 607–621.
- Torres-Sánchez, J., Peña J. M., de Castro, A. I., and López-Granados, F. (2014). Multi-temporal mapping of the vegetation fraction in early-season wheat fields using images from UAV. *Comp. Elec. Agric.* 103, 104–113. doi: 10.1016/j.compag.2014.02.009
- Tucker, C. J. (1979). Red and photographic infrared linear combinations for monitoring vegetation. *Remote Sens. Environ.* 8, 127–150. doi: 10.1016/0034-4257(79)90013-0
- Vergara-Díaz, O., Kefauver, S. C., Elazab, A., Nieto-Taladriz, M. T., and Araus, J. L. (2015). Grain yield losses in yellow-rusted durum wheat estimated using digital and conventional parameters under field conditions. *Crop J.* 3, 200–210. doi: 10.1016/j.cj.2015.03.003
- Vergara-Díaz, O., Zaman-Allah, M. A., Masuka, B., Hornero, A., Zarco-Tejada, P., Prasanna, B. M., et al. (2016). A novel remote sensing approach for prediction of maize yield under different conditions of nitrogen fertilization. *Front. Plant Sci.* 7:666. doi: 10.3389/fpls.2016.00666
- Waraich, E. A., Ahmad, R., Ashraf, M. Y., and Saifullah, A. (2011). Improving agricultural water use efficiency by nutrient management in crop plants Acta Agriculturae Scandinavica, Section B — Soil and Plant. *Science* 61, 291–304. doi: 10.1080/09064710.2010.491954
- Wu, W. (2014). The Generalized Difference Vegetation Index (GDVI) for dryland characterization. *Remote Sens.* 6, 1211–1233. doi: 10.3390/rs6021211
- Yousfi, S., Kellas, N., Saidi, L., Benlakehal, Z., Chaou, L., Siad, D., et al. (2016). Comparative performance of remote sensing methods in assessing wheat performance under Mediterranean conditions. *Agric. Water Manag.* 164, 137–147. doi: 10.1016/j.agwat.2015.09.016
- Zaman-Allah, M., Vergara, O., Araus, J. L., Tarekge, A., Magorokosho, C., Zarco-Tejada, P. J., et al. (2015). Unmanned aerial platform-based multi-spectral imaging for field phenotyping of maize. *Plant Methods* 11:35. doi: 10.1186/s13007-015-0078-2
- Zhou, B., Elazab, A., Bort, J., Vergara, O., Serret, M. D., and Araus, J. L. (2015). Low-cost assessment of wheat resistance to yellow rust through conventional RGB images. *Comp. Elec. Agric.* 116, 20–29. doi: 10.1016/j.compag.2015.05.017

Conflict of Interest Statement: The authors declare that the research was conducted in the absence of any commercial or financial relationships that could be construed as a potential conflict of interest.

Copyright © 2017 Gracia-Romero, Kefauver, Vergara-Díaz, Zaman-Allah, Prasanna, Cairns and Araus. This is an open-access article distributed under the terms of the Creative Commons Attribution License (CC BY). The use, distribution or reproduction in other forums is permitted, provided the original author(s) or licensor are credited and that the original publication in this journal is cited, in accordance with accepted academic practice. No use, distribution or reproduction is permitted which does not comply with these terms.



CHAPTER 2



Phenotyping Conservation Agriculture Management Effects on Ground and Aerial Remote Sensing Assessments of Maize Hybrids Performance in Zimbabwe

Adrian Gracia-Romero, Omar Vergara-Díaz,
Christian Thierfelder, Jill E. Cairns, Shawn C.
Kefauver and José L. Araus

Published in:
Remote Sensing (2018), 10(2), 349

Article

Phenotyping Conservation Agriculture Management Effects on Ground and Aerial Remote Sensing Assessments of Maize Hybrids Performance in Zimbabwe

Adrian Gracia-Romero ¹, Omar Vergara-Díaz ¹ , Christian Thierfelder ², Jill E. Cairns ², Shawn C. Kefauver ^{1,*}  and José L. Araus ¹

¹ Integrative Crop Ecophysiology Group, Plant Physiology Section, Faculty of Biology, University of Barcelona, 08028 Barcelona, Spain; adriangraciaromero@hotmail.com (A.G.-R.); omarvergaradiaz@gmail.com (O.V.-D.); jaraus@ub.edu (J.L.A.)

² International Maize and Wheat Improvement Center, CIMMYT Southern Africa Regional Office, P.O. Box MP163, Harare, Zimbabwe; c.thierfelder@cgiar.org (C.T.); j.cairns@cgiar.org (J.E.C.)

* Correspondence: sckefauver@ub.edu

Received: 27 December 2017; Accepted: 14 February 2018; Published: 24 February 2018

Abstract: In the coming decades, Sub-Saharan Africa (SSA) faces challenges to sustainably increase food production while keeping pace with continued population growth. Conservation agriculture (CA) has been proposed to enhance soil health and productivity to respond to this situation. Maize is the main staple food in SSA. To increase maize yields, the selection of suitable genotypes and management practices for CA conditions has been explored using remote sensing tools. They may play a fundamental role towards overcoming the traditional limitations of data collection and processing in large scale phenotyping studies. We present the result of a study in which Red-Green-Blue (RGB) and multispectral indexes were evaluated for assessing maize performance under conventional ploughing (CP) and CA practices. Eight hybrids under different planting densities and tillage practices were tested. The measurements were conducted on seedlings at ground level (0.8 m) and from an unmanned aerial vehicle (UAV) platform (30 m), causing a platform proximity effect on the images resolution that did not have any negative impact on the performance of the indexes. Most of the calculated indexes (Green Area (GA) and Normalized Difference Vegetation Index (NDVI)) were significantly affected by tillage conditions increasing their values from CP to CA. Indexes derived from the RGB-images related to canopy greenness performed better at assessing yield differences, potentially due to the greater resolution of the RGB compared with the multispectral data, although this performance was more precise for CP than CA. The correlations of the multispectral indexes with yield were improved by applying a soil-mask derived from a NDVI threshold with the aim of corresponding pixels with vegetation. The results of this study highlight the applicability of remote sensing approaches based on RGB images to the assessment of crop performance and hybrid choice.

Keywords: maize; remote sensing; UAV; RGB; multispectral; conservation agriculture; Africa

1. Introduction

Traditional practices of land preparation involve soil tillage through moldboard ploughing to soften the seedbed, ensure uniform germination, remove weed plants, and release soil nutrients through mineralization and oxidation. However, this mechanical disturbance is leading to a decline in organic matter, an increase of the loss of water by runoff, and, finally, to soil erosion [1]. Together with increasing threats of climate change, the loss of soil and its fertility is expected to become more critical for global agricultural production [2]. Over the next century, Sub-Saharan Africa (SSA) is expected to

be particularly vulnerable due to the range of projected impacts: e.g., the multiple stresses and low adaptive capacity of current cropping systems, as well as population increase [3]. Maize (*Zea mays* L.) is the principal staple food crop in large parts of SSA and is usually grown in small-holder farming systems under rainfed conditions. The limited availability of inputs is a leading factor that contributes to low yields that in turn are not able to keep pace with the food demand [4]. Hence, one of the most effective pathways for adaptation is to focus on breeding new varieties and also on changing crop management [5–8].

In light of soil degradation, conservation agriculture (CA) practices have been proposed as an alternative to tillage-based agriculture in SSA as a pragmatic solution to increasing production while conserving the natural resource base [9]. CA is a set of core principles, including minimum soil disturbance, permanent soil cover, and diversified crop rotations supported by integrated soil, crop, and water management, which aims to reduce and/or revert many negative effects of conventional farming practices [10]. Besides the control of soil erosion, CA has become increasingly popular as the crop management system conserves soil moisture, reduces fossil fuel use, lowers costs and, once established, increases yield permanently [11]. Recent literature has shown the potential of CA to improve resilience against seasonal drought events and thereby reduce the risk of crop failure in SSA [8,12–16]. However, most crop cultivars currently grown under CA have been developed under conventional or full tillage conditions, and it is likely that relevant genetic adaptations of CA conditions may have been removed during previous breeding efforts. Furthermore, large scale phenotyping studies under zero-tillage conditions are missing.

For the selection of genotypes with high-performing yield components under CA, accurate phenotyping tools capable of estimating yield at early crop stages are needed. During early growth stages, environmental factors such as temperature or soil moisture have a vital influence on germination rate, seedling vigor, and, consequently, on yield [17]. However, assessing those traits usually requires destructive laboratory measurements and/or visual scoring assessments that are laborious under field conditions. They are also prone to be subjective and incur additional associated costs.

Specialized sensors have become an important component for crop monitoring, particularly for improving precision, efficiency, and throughput in phenotyping [18]. Remote sensing indexes have largely demonstrated their various applications in agriculture, including yield prediction, stress detection, and control of plant diseases under a wide range of growing and environmental conditions [19]. The classical approach has involved the use of multispectral data for the development of numerous vegetation indexes to measure biomass (e.g., Normalized Difference Vegetation Index, NDVI), water content (e.g., Water Band Index, WBI), or pigment composition (e.g., Modified Chlorophyll Absorption Ratio Index, MCARI) in yield studies. At present, the use of information derived from RGB images (using red, green, and blue color bands) acquired with conventional digital cameras represents a low-cost alternative. The images can be processed to convert RGB values into indexes based on the models of Hue-Intensity-Saturation (HIS), CIE Lab, and CIE Luv cylindrical coordinate representations of colors [20]. Moreover, recent technological advances have led the incorporation of these sensors into aerial based platforms, enabling the simultaneous characterization of specific crop physiological traits for a larger number of plots, which may help to minimize the effect of changing environmental conditions during critical sampling moments [18,21–24].

Alternative applications of remote sensing techniques include the measurement of canopy temperature [25]. This can provide high-value information of the crop water status, since transpiration is a principal factor reducing the leaf's temperature. The use of thermal cameras has been proposed as an easy approach in crop management, and in breeding it can replace other more laborious techniques like the use of stable isotopes, which are costly, time-consuming, and require extensive laboratory work [26]. Moreover, in case of C4 crops like maize, the usefulness of stable isotopes for breeding is questionable [27]. The possibility of applying these methodologies in CA systems could be critical in improving our knowledge and supporting the full implementation of crop phenotyping for CA in developing countries.

The aim of the present study was to evaluate the efficiency of a set of remote sensing indexes in assessing the yield differences of different maize hybrids at early growth stages under conventionally ploughed (CP) and zero-tillage (CA) conditions. Different categories of sensors were tested, including RGB cameras (placed on an aerial platform as well as at ground level), alongside multispectral and thermal cameras (both installed on the aerial platform) and an active sensor portable field spectrometer designed to measure the NDVI at ground level. Additionally, canopy temperature, leaf chlorophyll content, and dry matter isotopic composition were evaluated.

2. Materials and Methods

2.1. Site Description

The experiment was conducted at Domboshawa Training Centre (17°37'S, 31°10'E and 1560 m.a.s.l.), situated at the north-east of Harare (Zimbabwe), during the 2015/2016 crop season (Figure 1). This site is characterized by moderately deep Arenosols and Luvisols under FAO classification [28]. It has approximately 5% clay content and is derived from granite parent material [29]. The climate conditions correspond to the Zimbabwean agro-ecological region II [30], with generally long dry periods (April to October), in which April to July is cool and August to October is warm. This region receives an average rainfall of between 700 and 1000 mm and mean maximum daily temperatures of 32 °C during summer.

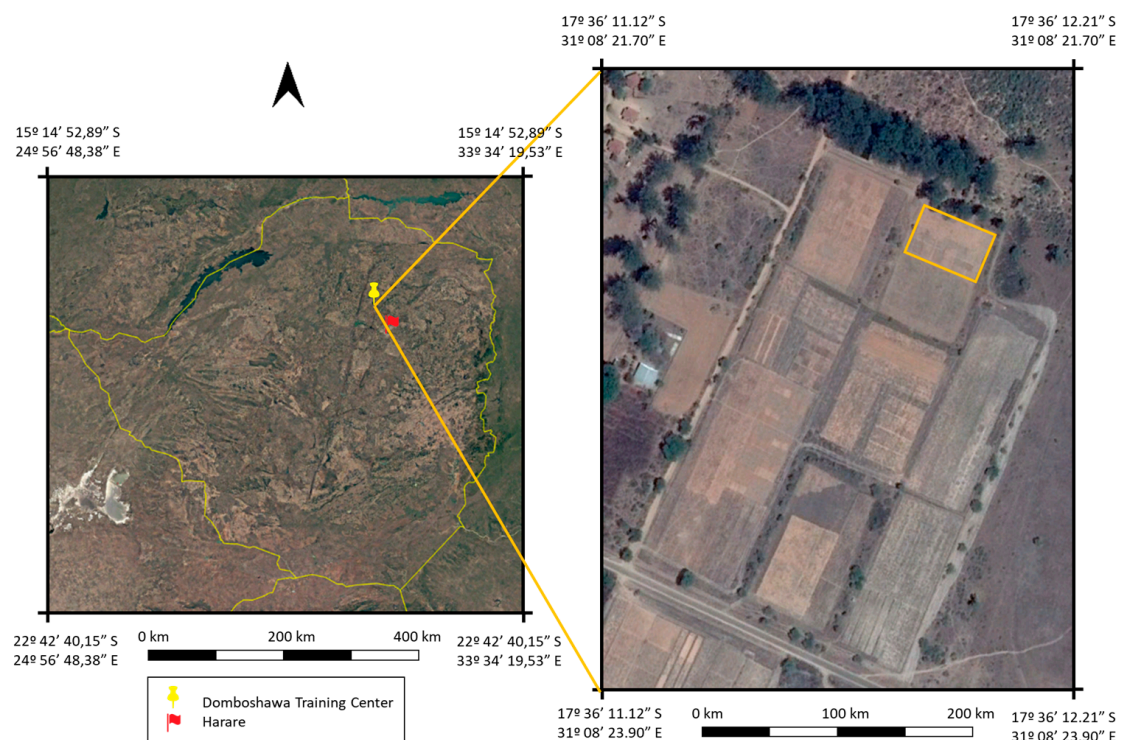


Figure 1. Landsat satellite (left) and CNES Airbus (right) images of the study area acquired using Google Earth Pro. The photographs are from the 31st of December 2015. The image on the left shows the location of the Domboshawa Training Center in Zimbabwe. The image on the right shows the field site.

2.2. Plant Materials and Experimental Design

Seven maize drought tolerant commercial hybrids (SC621, Pan53, 30G19, Zap55, Pristine601, PGS61, and Zap61) and one drought-sensitive commercial control variety (SC513) were manually planted on 14 December 2015 in plots of 23 m² (5 × 4.6 m) with four lines per plot. Two differential plot management regiments have been applied to the field since 2009 (Figure 2). One half was managed

using no-tillage and the application of 2.5–3.0 Mg ha⁻¹ of maize stover to all the plots. Rotation, a critical component for CA, was not practiced in this trial. Weed control was done by applying a combination of 2.5 L ha⁻¹ of glyphosate, 3 L ha⁻¹ of atrazine, and 1 L ha⁻¹ of dual immediately after planting, if there were weeds present. The other half was conventionally ploughed and without any residue management.

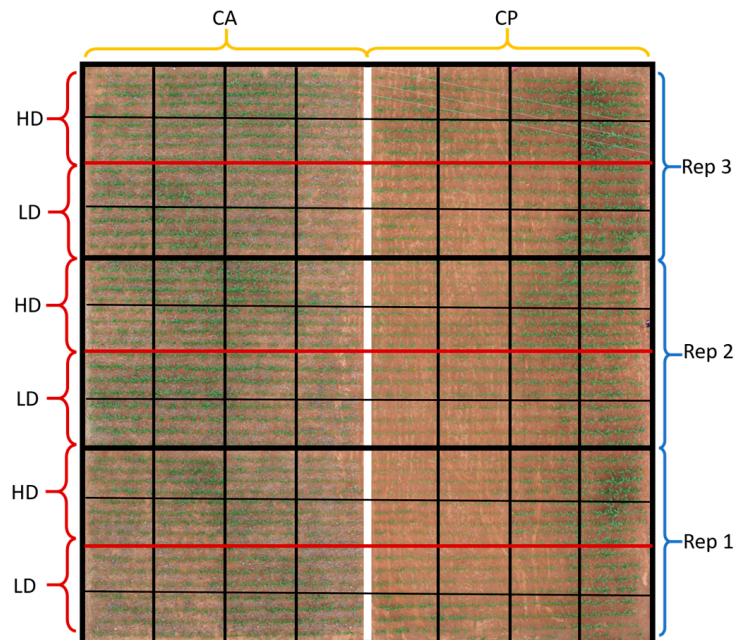


Figure 2. Map of the experimental design showing alternating High Density (HD) and Low Density (LD) plots per replicate, with Conservation Agriculture (CA) on the left and Conventional Ploughing (CP) on the right. Each square corresponds one plot dedicated to each of the different hybrids used. Complete details of the experimental design are explained in Section 2.2.

Both cropping systems were fertilized twice equally with 200 kg ha⁻¹ using Compound D (7:14:7) as a basal NPK dressing and top dressed with ammonium nitrate (200 kg ha⁻¹, 46% N) in a split application four weeks and seven weeks after seeding. Maize plants seeded at different density sub-treatments were applied: one low-planting density (44,444 plants ha⁻¹) and one high-planting density (53,333 plants ha⁻¹). Each sub-treatment was repeated in three replicates in which varieties were ordered in a completely randomized block design. A total of 96 plots were studied (2 agricultural practices × 2 density conditions × 8 varieties × 3 replicates, 24 plots per growing conditions).

2.3. Agronomical Traits and Proximal (Ground) Data Collection

The crop was harvested at physiological maturity. Grain yield (Mg ha⁻¹) and total above-ground biomass (Mg ha⁻¹) were determined as corresponding to the central 3.6 m of the two central rows of each plot (6.48 m²), omitting the border plants. The harvest index was calculated as grain yield as a portion of total biomass.

Proximal (ground) data was collected 45 days after sowing on 28 January 2016 when the hybrids reached the stage of 4 to 6 leaves. Leaf chlorophyll content (LCC) was measured using a Minolta SPAD-502 portable chlorophyll meter (Spectrum Technologies Inc., Plainfield, IL, USA). For each plot, five leaves were selected randomly (being the last fully expanded leaf within a plant) and were measured in the middle portion of the lamina and averaged. The Normalized Difference Vegetation Index was determined at ground level using a portable spectrometer (GreenSeeker handheld crop sensor, Trimble, Sunnyvale, CA, USA) by passing the sensor over the middle of each plot at a constant height of 0.5 m above and perpendicular to the canopy (NDVI.g).

One RGB picture was taken per plot, holding the camera at 80 cm above the plant canopy in a zenithal plane and focusing near the center of each plot. The conventional digital camera used was an Olympus OM-D (Olympus, Tokyo, Japan), a digital single lens mirrorless camera with an image sensor size of 17.3 × 13.0 mm of 16-megapixel (MP) resolution. The images were saved in JPEG format with a resolution of 4608 × 3072 pixels. As the plots were too big for a single photograph, three different images samples were taken of each central row.

RGB images were subsequently analyzed using a version of the Breedpix 2.0 software (Jaume Casadesús, <https://bio-protocol.org/e1488>, IRTA, Lleida, Spain) adapted to JAVA8 and other RGB image analyses together integrated as freely available CIMMYT MaizeScanner plugin within FIJI (<https://imagej.net/Fiji> and <https://github.com/George-haddad/CIMMYT>). This software enables the extraction of RGB vegetation indexes in relation to different color properties [20]. Essentially, the indexes are based on either the average color of the entire image, in diverse units related to its “greenness”, or on the fraction of pixels classified as green canopy relative to the total number of pixels in the image. In HIS color space, the Hue (H) component describes the color value itself by traversing the visible spectrum in the form of an angle between 0° and 360°. Derived from the Hue portion of HIS color space, Green Area (GA) and Greener Area (GGA) analyze the proportion of green/yellow and green pixels in the image. GA is the percentage of pixels in the image in the hue range from 60° to 180°, that is, from yellow to bluish green. Meanwhile, GGA is somewhat more restrictive, because the range of hue considered by the index is from 80° to 180°, thus excluding the yellowish-green tones. Additionally, those two indexes are used to formulate the Crop Senescence Index (CSI), which provides a scaled ratio between yellow and green vegetation pixels [31], as follows:

$$CSI = \frac{(GA - GGA)}{GA} \times 100$$

In the CIELab color space model, dimension L* represents lightness, and the green to red range is expressed by the a* component, with a more positive value representing a purer red, and conversely a more negative value indicating a greener color. Meanwhile, blue to yellow is expressed by the b* component, in which the more positive the value the closer it is to a pure yellow, whereas the more negative the value the closer it is to blue. Similarly, in the CIELuv color space model, dimensions u* and v* are perceptually uniform coordinates, in which the visible spectrum starts with blue at the bottom of the space, moving through green in the upper left (mostly scaled by v*) and out to red in the upper right (mostly scaled by u*) [32].

2.4. Aerial Data Collection

Furthermore, aerial measurements were acquired during the same visit as the ground data using an unmanned aerial vehicle (UAV) (Mikrokopter OktoXL 6S12, Moormerland, Germany) flying under manual remote control at an altitude of 30 m (Figure 3). Two flights were performed; on one flight only, the RGB digital camera was mounted, and the other included both the multispectral and thermal cameras.

The RGB aerial images were obtained using a Lumix GX7 (Panasonic, Osaka, Japan) digital mirrorless camera with an image sensor size of 17.3 × 13.0 mm using a 20 mm lens. Images were taken at 16-MP and were saved in JPEG format, on this occasion with a resolution of 4592 × 3448 pixels. For the multispectral data, a Tetracam micro-MCA (Tetracam Inc., Chatsworth, CA, USA) was used. The camera consists of twelve independent image sensors and optics each with user configurable filters of center wavelengths and full-width half-max band-width (450 ± 40, 550 ± 10, 570 ± 10, 670 ± 10, 700 ± 10, 720 ± 10, 780 ± 10, 780 ± 10, 840 ± 10, 860 ± 10, 900 ± 20, 950 ± 40 nm), and one sensor dedicated to calibration (Light Incident Sensor, ILS). That sensor uses micro-filters housed in the ILS module behind a diffusor plate that corresponds to the same spectral characteristic of the 11 downwards looking sensors, thus providing an accurate band-by-band reflectance calibration in real-time. It captures 15.6-MP of image data as 12 × 1.3-MP images transferred to twelve separate flash

memory cards. The multispectral images acquired were aligned and calibrated to reflectance using PixelWrench II version 1.2.2.2 (Tetracam, Chatsworth, CA, USA). Canopy temperature was measured using a FLIR Tau2 640 (FLIR Systems, Nashua, NH, USA) with a VOx uncooled microbolometer equipped with a TEAX Thermal Capture model (TEAX Technology, Wilnsdorf, Germany) for recording of full resolution thermal video (640×520 pixels at 20 frames per second). The thermal images were first exported using the TeAx ThermoViewer v1.3.12 (TeAx Technology, Wilnsdorf, Germany) to raw 16-bit TIFF format as Kelvin $\times 10,000$ and converted to 32-bit temperature in Celsius using a custom batch processing macro function in FIJI [33].



Figure 3. Mikrokopter OktoXL 6S12 unmanned aerial platform equipped with the micro-MCA12 Tetracam multispectral sensor, showing the placement of the Incident Light Sensor (ILS) module with white diffuser plate connected by a fiber optic cable to the top of the UAV facing upwards while the other 11 multispectral sensors are positioned on a dual axis gimbal camera platform for zenithal/nadir image capture. The RGB (Red-Green-Blue) and TIR (thermal infrared) cameras were alternately mounted on the same gimbaled platform for image capture.

To obtain an accurate orthomosaic of the pre-processed aerial images from each sensor, a 3D reconstruction was produced using Agisoft PhotoScan Professional (Agisoft LLC, St. Petersburg, Russia, www.agisoft.com) [34]. A total of 30 overlapped images were needed for each orthomosaic. Then, the procedure of cropping the plots was done using the open source image analysis platform FIJI (Fiji is Just ImageJ; <http://fiji.sc/Fiji>), in which regions of interest were established at each plot and then exported, taking care that exactly the same ground area was segmented for each plot across all treatments. The RGB aerial exported plots were processed the same way as the ground images as described previously in Section 2.3. For the formulation of the different multispectral indexes, as detailed in Table 1, we developed a customized FIJI macro code. This macro code enabled the calculation of the multispectral indexes through two different approaches: on the one hand, measuring the mean value of the plot image of each band (plot measurements), and on the other hand, in order to make more accurate measurements, we applied a threshold of NDVI values of 0.4–1 to focus the measurements of all the indexes on only the pixels corresponding to maize and lower NDVI values (<0.4) corresponding to bare-ground; other background image components were discarded. Therewith, percentage of vegetation cover was estimated by the inverse of the implementation of the soil mask. Finally, the thermal average temperature of the whole exported plots was also measured using FIJI.

Table 1. Indexes derived from the multispectral visible and near infrared bands. The wavelengths used in the formulation of the indexes are adapted slightly based on the multispectral micro-MCA Tetracam camera. * Note that for the PRI index, B550 is used instead of the original B531 by the cited reference study.

Group	Index	Equation	Wavelengths	References
Broadband Greenness	Normalized Difference Vegetation Index (NDVI)	$\frac{(B840 - B670)}{(B840 + B670)}$	Red, NIR	[35]
	Soil Adjusted Vegetation Index (SAVI)	$\frac{(B840 - B670)}{(B840 + B670 + L)}$ Intermediate vegetation, $L = 0.5$	Red, NIR	[36]
	Optimized soil-adjusted vegetation index (OSAVI)	$\frac{(1 + 0.16) \cdot (B780 - B670)}{(B780 + B670 + 0.16)}$	Red, NIR	[37]
	Renormalized Difference Vegetation Index (RDVI)	$\frac{(B840 - B670)}{\sqrt{(B840 + B670)}}$	Red, NIR	[38]
	Enhanced Vegetation Index (EVI)	$\frac{2.5 \cdot (B840 - B670)}{(B840 + (6 \cdot B670) - (7.5 \cdot R450) + 1)}$	Blue, Red, NIR	[39]
Light Use Efficiency	Photochemical Reflectance Index (PRI) *	$\frac{(B550 - B570)}{(B550 + B570)}$	Green	[40]
Leaf Pigments	Modified Chlorophyll Absorption Ratio Index (MCARI)	$(B700 - R670) - 0.2 \cdot (B700 - B550) \cdot \left(\frac{B700}{B670}\right)$	Green, Red, NIR	[41]
	Chlorophyll Content Index (CCI)	$\frac{(B550 - B670)}{(550 + B670)}$	Green, NIR	[42]
	Transformed Chlorophyll Absorption Ratio Index (TCARI)	$3 \cdot (B700 - B670) - 0.2 \cdot (B700 - B550) \cdot \left(\frac{B700}{B670}\right)$	Green, Red, NIR	[43]
		$\frac{TCARI}{OSAVI}$	Green, Red, NIR	
	Anthocyanin Reflectance Index 2 (ARI2)	$B840 \cdot \left(\frac{1}{B550} - \frac{1}{B700}\right)$	Blue, Red, NIR	[44]
	Carotenoid Reflectance Index 2 (CRI2)	$\left(\frac{1}{B550} - \frac{1}{B700}\right)$	Blue, Red	[45]
Water Content	Water Band Index (WBI)	$\left(\frac{B970}{B900}\right)$	Red, NIR	[46]

2.5. Carbon and Nitrogen Stable Isotope Compositions

Similar leaves were sampled for LCC, carbon, and nitrogen measurements, and were subsequently oven dried at 70 °C for 24 h and ground to a fine powder. Samples of approximately 0.7 mg of dry matter and reference materials were weighed into tin capsules, sealed, and then loaded into an elemental analyzer (Flash 1112 EA; ThermoFinnigan, Schwerte, Germany) coupled with an isotope ratio mass spectrometer (Delta C IRMS, ThermoFinnigan), operating in continuous flow mode. Measurements were carried out at the Scientific Facilities of the University of Barcelona. The $^{13}\text{C}/^{12}\text{C}$ ratios (R) of plant material were expressed in composition ($\delta^{13}\text{C}$) notation [47] as follows:

$$\delta^{13}\text{C} (\text{‰}) = [(R_{\text{sample}}/R_{\text{standard}}) - 1] \times 1000$$

in which sample refers to plant material and standard to Pee Dee Belemnite (PDB) calcium carbonate. International isotope secondary standards of a known $^{13}\text{C}/^{12}\text{C}$ ratio (IAEA CH7, polyethylene foil, IAEA CH6 sucrose and USGS 40 l-glutamic acid) were calibrated against Vienna Pee Dee Belemnite calcium carbonate (VPDB) with an analytical precision of 0.1‰. The $^{15}\text{N}/^{14}\text{N}$ ratios of plant material were also expressed in δ notation ($\delta^{15}\text{N}$) using international secondary standards of known $^{15}\text{N}/^{14}\text{N}$ ratios (IAEA N1 and IAEA N2 ammonium sulfate and IAEA NO₃ potassium nitrate), with analytical precision of about 0.2‰. Furthermore, total carbon and nitrogen (%) were analyzed in the same samples, and the C/N ratio was calculated.

2.6. Statistical Analysis

Statistical analyses were conducted using the open source software, R and RStudio 1.0.44 (R Foundation for Statistical Computing, Vienna, Austria). Data for the set of physiological traits were subjected to factorial completely randomized analyses of variance (ANOVAs) to test the effects of growing conditions on the different traits studied. A bivariate correlation procedure was used to calculate the Pearson correlation coefficients of the different remote sensing indexes against the grain yield. Multiple linear regressions were calculated via a forward stepwise method with GY as the dependent variable and the different indexes as independent parameters. The figures were also drawn using the RStudio software.

3. Results

3.1. Differences in Yield Parameters and Conventional Phenotyping Measurements within Growing Conditions and Genotypes

Means of yield, biomass, and traits informing on the water and nitrogen status of the crop are presented in Table 2. Grain yield was significantly greater under CA conditions ($p < 0.0001$), by almost 20% relative to the CP. Harvest index was also significantly higher, but no differences were found for biomass between the two treatments. Concerning planting density, it did not affect any yield parameter. Even so, the highest-yielding conditions were recorded at high-density CA plots (3.07 Mg ha^{-1} on average), and the least on low-density CP plots (2.29 Mg ha^{-1}). The genotypic variability for grain yield (Table 3) was only significant under CA ($p < 0.001$) at high density conditions ($p < 0.01$).

ANOVA analysis showed no significant differences in LCC between management practices or density levels. Meanwhile, canopy temperature showed a significant increase in plots grown under CA ($p < 0.05$) and when the plant density was high ($p < 0.001$), although the increment was small. Finally, neither the percentage of carbon nor nitrogen nor their isotopic signatures showed significant changes across the different growing conditions.

3.2. The Effect of Conservation and Conventional Agricultural Practices and the Sensor Altitude on Vegetation Indexes

The mean of the RGB and multispectral indexes for the ground and aerial images at each growing condition are shown in Tables 4 and 5. There were no significant differences across the indexes reported due to changes of planting density; mean data of low and high densities is not presented. The differential tillage practices, however, affected all the RGB indexes for both sensor levels (Table 4). Hue increased greatly from the CP to the CA (ground 20.22%/aerial 21.89%), and its derived indexes GA and GGA also showed a similar rise of their values. Otherwise, the indexes derived from the CIE-Lab and CIE-Luv reduced their values, particularly a^* and u^* . The height level from which the indexes were measured (either from ground or the aerial platform) affected their values at both agricultural practices conditions, except for the Saturation (Supplementary Table S1). Differences were highly evidenced in the Hue and GGA values, which decreased greatly when they were calculated from the aerial images in comparison to the ground images. Even considering those differences, the correlations between the measurements from both platforms were very strong in general, only showing low relationship coefficients with Intensity, Lightness, and the v^* index. Moreover, the correlations were higher at CP conditions in comparison with CA.

Table 2. Effect of the tillage conditions and planting density conditions on the yield parameters (GY, Biomass and Harvest Index), leaf chlorophyll content (LCC), leaf carbon and nitrogen concentration (C and N), leaf C/N ratio and the stable carbon ($\delta^{13}\text{C}$), and nitrogen ($\delta^{15}\text{N}$) isotopic composition. Values are means \pm standard error. Level of significance (p -value): *, $p < 0.05$; ***, $p < 0.001$. Treatments: CA, conservation agriculture; CP, conventional agriculture; LD, low density; HD, high density.

	GY	Biomass	Harvest Index	SPAD	Temperature	C	$\delta^{13}\text{C}$	N	$\delta^{15}\text{N}$	C/N
	(Mg ha ⁻¹)	(Mg ha ⁻¹)			(°C)	(%)	(‰)	(%)	(‰)	
Treatment										
CA	2.99 \pm 0.10	2.66 \pm 0.11	0.49 \pm 0.01	42.71 \pm 0.38	25.02 \pm 0.10	45.8 \pm 0.50	-11.98 \pm 0.03	3.77 \pm 0.04	0.52 \pm 0.08	12.14 \pm 0.06
CP	2.42 \pm 0.14	2.50 \pm 0.14	0.44 \pm 0.01	42.24 \pm 0.38	24.64 \pm 0.15	44.64 \pm 0.49	-11.93 \pm 0.03	3.69 \pm 0.04	0.59 \pm 0.07	12.11 \pm 0.05
p -value	0.000 ***	0.351	0.000 ***	0.395	0.017 *	0.097	0.287	0.161	0.518	0.673
Density										
LD	2.61 \pm 0.12	2.45 \pm 0.12	0.47 \pm 0.01	42.37 \pm 0.36	24.59 \pm 0.12	45.32 \pm 0.58	-11.95 \pm 0.03	3.74 \pm 0.05	0.51 \pm 0.07	12.13 \pm 0.05
HD	2.81 \pm 0.13	2.71 \pm 0.13	0.46 \pm 0.01	42.45 \pm 0.40	25.14 \pm 0.11	45.08 \pm 0.41	-11.96 \pm 0.03	3.72 \pm 0.04	0.59 \pm 0.08	12.12 \pm 0.06
p -value	0.230	0.145	0.820	0.712	0.000 ***	0.724	0.922	0.760	0.453	0.988
Combinations										
CA * LD	2.92 \pm 0.13	2.59 \pm 0.17	0.49 \pm 0.01	42.61 \pm 0.56	24.80 \pm 0.13	46.64 \pm 0.48	-11.97 \pm 0.04	3.83 \pm 0.04	0.53 \pm 0.11	12.18 \pm 0.07
CA * HD	3.07 \pm 0.14	2.73 \pm 0.15	0.49 \pm 0.01	42.81 \pm 0.52	24.32 \pm 0.21	44.99 \pm 0.85	-11.98 \pm 0.04	3.72 \pm 0.07	0.50 \pm 0.12	12.10 \pm 0.09
CP * LD	2.29 \pm 0.19	2.31 \pm 0.18	0.44 \pm 0.01	42.14 \pm 0.47	25.25 \pm 0.13	44.1 \pm 0.97	-11.94 \pm 0.04	3.66 \pm 0.08	0.49 \pm 0.09	12.07 \pm 0.08
CP * HD	2.55 \pm 0.20	2.69 \pm 0.21	0.44 \pm 0.01	42.34 \pm 0.61	24.99 \pm 0.17	45.18 \pm 0.08	-11.93 \pm 0.05	3.72 \pm 0.02	0.68 \pm 0.11	12.14 \pm 0.07
p -value	0.751	0.484	0.931	0.999	0.489	0.051	0.812	0.146	0.312	0.353

Table 3. Genotypic yield variability of the eight maize hybrids for each growing condition. Values are means \pm standard error. Level of significance: **, $p < 0.01$. Treatments: CA, conservation agriculture; CP, conventional agriculture; LD, low density; HD, high density.

	CA	CP	LD	HD
SC513	2.50 \pm 0.18	1.52 \pm 0.19	2.12 \pm 0.34	1.90 \pm 0.20
SC621	2.32 \pm 0.18	2.60 \pm 0.39	2.54 \pm 0.19	2.38 \pm 0.40
PAN53	3.26 \pm 0.13	2.71 \pm 0.36	2.82 \pm 0.23	3.16 \pm 0.33
30G19	2.52 \pm 0.15	2.12 \pm 0.34	2.22 \pm 0.26	2.42 \pm 0.29
Zap55	3.72 \pm 0.18	3.03 \pm 0.39	3.23 \pm 0.36	3.52 \pm 0.31
Pristine 601	3.16 \pm 0.26	2.02 \pm 0.37	2.19 \pm 0.39	2.98 \pm 0.34
PGS61	3.23 \pm 0.25	2.61 \pm 0.29	2.76 \pm 0.25	3.07 \pm 0.34
Zap61	3.24 \pm 0.29	2.74 \pm 0.53	2.95 \pm 0.51	3.03 \pm 0.35
p -value	0.001 **	0.147	0.155	0.007 **

Table 4. Effect of tillage practices and placement of the sensors (ground versus aerial) on the RGB indexes. These indices are defined in Materials and Methods. Values are means \pm standard error. Level of significance (p -value): ***, $p < 0.001$. Treatments: CA, conservation agriculture; CP, conventional agriculture.

		Intensity	Hue	Saturation	Lightness	a*	b*	u*	v*	GA	GGA	CSI
Ground	CA	0.37 \pm 0.00	48.04 \pm 0.97	0.19 \pm 0.00	44.01 \pm 0.23	-4.44 \pm 0.28	20.14 \pm 0.35	3.59 \pm 0.42	22.91 \pm 0.36	0.26 \pm 0.01	0.24 \pm 0.01	8.83 \pm 0.60
	CP	0.36 \pm 0.00	39.96 \pm 0.91	0.25 \pm 0.00	42.81 \pm 0.19	-1.27 \pm 0.38	23.13 \pm 0.24	9.12 \pm 0.57	24.79 \pm 0.21	0.19 \pm 0.01	0.18 \pm 0.01	6.48 \pm 0.46
	p -value	0.000 ***	0.000 ***	0.000 ***	0.000 ***	0.000 ***	0.000 ***	0.000 ***	0.000 ***	0.000 ***	0.000 ***	0.000 ***
Aerial	CA	0.49 \pm 0.00	38.25 \pm 0.75	0.19 \pm 0.00	54.96 \pm 0.35	-0.54 \pm 0.32	24.21 \pm 0.13	11.67 \pm 0.54	28.10 \pm 0.14	0.22 \pm 0.01	0.15 \pm 0.01	32.87 \pm 1.19
	CP	0.49 \pm 0.00	31.38 \pm 0.49	0.25 \pm 0.00	55.25 \pm 0.48	4.99 \pm 0.39	28.77 \pm 0.27	22.2 \pm 0.76	31.34 \pm 0.27	0.16 \pm 0.01	0.10 \pm 0.01	42.43 \pm 2.41
	p -value	0.000 ***	0.000 ***	0.000 ***	0.000 ***	0.000 ***	0.000 ***	0.000 ***	0.000 ***	0.000 ***	0.000 ***	0.000 ***

Table 5. Effect of tillage practices (CA versus CP) and the application of the soil mask (plot measurements versus vegetation measurements) on the multispectral indexes. These indexes are defined in Materials and Methods. Values are means \pm standard error. Level of significance (p -value): *, $p < 0.05$; **, $p < 0.01$; ***, $p < 0.001$. Treatments: CA, conservation agriculture; CP, conventional agriculture.

		Vegetation	NDVI _g	NDVI	SAVI	OSAVI	RDVI	EVI	PRI	MCARI	CCI
Plot	CA	66.25 \pm 0.93	0.55 \pm 0.01	0.42 \pm 0.01	0.27 \pm 0.01	0.34 \pm 0.01	4.19 \pm 0.10	0.54 \pm 0.01	0.16 \pm 0.00	19.54 \pm 0.47	0.08 \pm 0.01
	CP	72.30 \pm 1.04	0.48 \pm 0.01	0.38 \pm 0.01	0.25 \pm 0.01	0.31 \pm 0.01	3.85 \pm 0.11	0.39 \pm 0.01	0.13 \pm 0.00	16.89 \pm 0.38	-0.01 \pm 0.01
	p -value	0.000 ***	0.000 ***	0.006 **	0.031 *	0.013 *	0.026 *	0.000 ***	0.000 ***	0.000 ***	0.000 ***
Vegetation	CA			0.66 \pm 0.01	0.45 \pm 0.01	0.55 \pm 0.01	6.85 \pm 0.11	0.88 \pm 0.02	0.21 \pm 0.00	32.16 \pm 0.66	0.27 \pm 0.01
	CP			0.62 \pm 0.01	0.44 \pm 0.01	0.53 \pm 0.01	6.68 \pm 0.11	0.74 \pm 0.01	0.19 \pm 0.00	31.74 \pm 0.61	0.20 \pm 0.01
	p -value			0.001 **	0.343	0.049 *	0.263	0.000 ***	0.000 ***	0.624	0.000 ***
		TCARI	TCARI/OSAVI	ARI2	CRI2	WBI					
Plot	CA	36.40 \pm 0.67	0.42 \pm 0.01	0.47 \pm 0.01	0.01 \pm 0.00	0.94 \pm 0.01					
	CP	35.68 \pm 0.74	0.47 \pm 0.02	0.73 \pm 0.01	0.01 \pm 0.00	0.93 \pm 0.00					
	p -value	0.461	0.030 *	0.000 ***	0.000 ***	0.558					
Vegetation	CA	46.75 \pm 0.82	0.33 \pm 0.01	0.23 \pm 0.02	0.00 \pm 0.00	1.01 \pm 0.01					
	CP	50.15 \pm 1.10	0.38 \pm 0.01	0.51 \pm 0.02	0.01 \pm 0.00	0.99 \pm 0.00					
	p -value	0.012 *	0.001 **	0.000 ***	0.000 ***	0.06					

Excluding WBI and TCARI and the vegetation measurement of SAVI, RDVI, and MCARI, all the vegetation indexes based on multispectral data could distinguish the plots where different agricultural practices were applied (Table 5). The indexes considered as indicators of green biomass, like NDVI (both ground and aerial), SAVI, or OSAVI, exhibited a large increase ($p < 0.050$) in their values at the CA plots in comparison with CP. Contrary to this, CA showed a significant decrease ($p < 0.001$) in the percentage of vegetation cover (CA 66.25%/CP 72.30%). Indexes more related to leaf pigments, like PRI or MCARI, were also significantly higher under CA compared with CP, but it was much less pronounced. Conversely, the stress index ARI2 decreased significantly ($p < 0.0001$) from the CA to the CP. The application of soil mask, to direct the multispectral measurements to only the vegetation, resulted in significant variation in vegetation index values. The mean values of the green biomass and the vegetation pigments indexes both increased regardless of tillage conditions; the differences between the two growing conditions was much less severe than when they were measured at the whole plot level. In comparison with measurements made by GreenSeeker, raw NDVI measurements taken with the UAV were slightly lower, while those where NDVI was calculated through the mask were higher. The relationships between the measurements of NDVI at both platform levels were robust, but the correlation using the masked values were stronger (Supplementary Table S1). Moreover, these correlations were higher under CP conditions as compared with CA.

3.3. Performance of Remote Sensing Index as Predictors of Grain Yield

To test the accuracy of remote sensing indexes for assessing differences in yield, correlations are presented for grain yield against indexes. RGB indexes measured on the CP plots, regardless of height level of image taking; Hue and its derived indexes were the ones that correlated best with grain yield. Indeed, nearly all aerial indexes worked very similarly as the ground indexes, showing almost identical correlation coefficients (Table 6). Only b^* and v^* correlations varied considerably, going from low (ground) to extremely strong (aerial) correlations. On the other hand, even though these indexes performed much better under the conventional practices, some significant and strong correlations could be found under CA. For both ground and aerial levels, those indexes related to the greenness of the vegetation color, as Hue, GA, GGA, a^* , and u^* were best correlated to yield.

Likewise, as happened with the RGB, multispectral indexes performed better when assessing yield at the conventional tillage conditions (Table 7). However, in this case CA conditions showed much lower correlations in comparison with the RGB derived indexes. Under CP conditions, NDVI and its optimized indexes (SAVI, OSAVI and RDVI) were very closely related to GY, but the strongest correlation was found with the combination of two indexes, TCARI/OSAVI ($R = -0.779$, $p < 0.0001$). For both tillage conditions, CA and CP, the application of the soil mask helped to improve the correlation between indexes related to the light use efficiency (PRI) and to the leaf pigments (TCARI) and grain yield.

In terms of density conditions, both RGB and multispectral indexes worked slightly better with higher plant densities compared to the low-density conditions. Moreover, a deeper analysis of the results showed that the best conditions in which to correlate the remote sensing indexes was the combination of high density planting at the CP plots. Under these conditions, most of the R^2 coefficients were near or even higher than 0.800.

The ability of remote sensing indexes assessing grain yield was further tested by multivariate linear models (Table 8). All the equations presented were obtained using four or less indexes, all of them measured from the UAV. The best predictive equation was achieved using CP data, explaining 75.6% of the variation in yield. Besides this, the equation derived from the CA plots could only explain 35.1% of yield variation. Equations derived from the high-planting density conditions predicted yields more efficiently than low density conditions (65.4 and 52.6%, respectively).

Table 6. Regression coefficients of the relationships between the RGB-indices, measured at ground and aerial levels, with grain yield. These indices are defined at section Material and Methods. Level of significance (p -value): *, $p < 0.05$; **, $p < 0.01$; ***, $p < 0.001$. Treatments: CA, conservation agriculture; CP, conventional agriculture; LD, low density; HD, high density.

		Intensity	Hue	Saturation	Lightness	a*	b*	u*	v*	GA	GGA	
Ground measurements	<i>Tillage</i>											
		CA	−0.065	0.484 ***	−0.317 *	−0.021	−0.509 *	−0.226	−0.544 ***	−0.137	0.487 ***	0.507 ***
		CP	0.503 ***	0.741 ***	−0.478 ***	0.568 ***	−0.742 ***	−0.206	−0.717 ***	0.157	0.777 ***	0.783 ***
		<i>Planting density</i>										
		LD	0.342 *	0.597 ***	−0.483 ***	0.366 *	−0.633 ***	−0.350 *	−0.623 ***	−0.152	0.660 ***	0.662 ***
		HD	0.361 *	0.754 ***	−0.509 ***	0.410 **	−0.785 ***	−0.326 *	−0.771 ***	−0.100	0.767 ***	0.767 ***
		<i>Combinations</i>										
		CA * LD	−0.054	0.422 *	−0.386	−0.032	−0.498 *	−0.310	−0.539 **	−0.213	0.511*	0.513 *
		CA * HD	−0.054	0.580 **	−0.247	0.020	−0.570 **	−0.138	−0.585 **	−0.052	0.493 *	0.528 **
		CP * LD	0.419 *	0.622	−0.304	0.456 *	−0.596 **	−0.032	−0.567 **	0.218	0.627 **	0.636 ***
		CP * HD	0.565 **	0.827 ***	−0.594 **	0.671 ***	−0.850 ***	−0.318	0.830 ***	0.176	0.894 ***	0.898 ***
	Aerial measurements	<i>Tillage</i>										
		CA	−0.393 **	0.548 ***	−0.149	−0.363 *	−0.567 ***	−0.265	−0.554 *	−0.145	0.562 ***	0.561 ***
		CP	−0.776 ***	0.754 ***	−0.719 ***	−0.777 ***	−0.796 ***	−0.818 ***	−0.812 ***	−0.794 ***	0.784 ***	0.798 ***
		<i>Planting density</i>										
		LD	−0.555 ***	0.614 ***	−0.495 ***	−0.565 ***	−0.651 ***	−0.606 ***	−0.658 ***	−0.617 ***	0.653 ***	0.664 ***
		HD	−0.627 ***	0.684 ***	−0.440 **	−0.631 ***	−0.739 ***	−0.667 ***	−0.751 ***	−0.697 ***	0.776 ***	0.786 ***
		<i>Combinations</i>										
		CA * LD	−0.468 *	0.582 **	−0.292	−0.444 *	−0.600 **	−0.395	−0.594 **	−0.296	0.578 **	0.572 **
		CA * HD	−0.360	0.519 **	−0.105	−0.331	−0.544 **	−0.262	−0.533 **	−0.116	0.545 **	0.557 **
		CP * LD	−0.606 **	0.577 **	−0.649 ***	−0.610 **	−0.654 ***	−0.694 ***	−0.674 ***	−0.662 ***	−0.662 **	0.633 ***
	CP * HD	−0.907 ***	0.881 ***	−0.793 ***	−0.906 ***	−0.900 ***	−0.920 ***	−0.913 ***	−0.905 ***	0.916 ***	0.920 ***	

Table 7. Regression coefficients of the relationships between the multispectral-indices, measured at ground and aerial levels, with grain yield. These indices are defined at section Material and Methods. Level of significance (*p*-value): *, *p* < 0.05; **, *p* < 0.01; ***, *p* < 0.001. Treatments: CA, conservation agriculture; CP, conventional agriculture; LD, low density; HD, high density.

		Vegetation area	NDVI.g	NDVI	SAVI	OSAVI	RDVI	EVI	PRI	MCARI	CCI	TCARI	TCARI/OSAVI	ARI2	CRI2	WBI		
Plot measurements	<i>Tillage</i>																	
		CA	−0.386 **	0.490 **	0.361 *	0.389 **	0.379 **	0.390 **	0.368 *	0.435 **	0.215	0.355 *	0.094	−0.334 *	−0.321	−0.299 *	0.116	
		CP	−0.727 ***	0.812 ***	0.751 ***	0.729 ***	0.747 ***	0.734 ***	0.676 ***	0.697 ***	0.105	0.710 ***	−0.454 **	−0.785	−0.479	0.066	0.412 **	
		<i>Planting density</i>																
			LD	−0.592 ***	0.740 **	0.577 ***	0.477 ***	0.532 ***	0.493 ***	0.488 ***	0.641 ***	0.127	0.610 ***	−0.253	−0.671 ***	−0.549 ***	−0.372 *	0.269
			HD	−0.737 ***	0.795 **	0.750 ***	0.748 ***	0.753 ***	0.749 ***	0.714 ***	0.713 ***	0.495 ***	0.731 *	−0.285	−0.755 ***	−0.500 ***	−0.26	0.364 *
		<i>Combinations</i>																
			CA * LD	−0.38	0.464 *	0.298	0.281	0.289	0.285	0.251	0.398	0.108	0.327	0.006	−0.379	−0.483 *	−0.359	0.065
			CA * HD	−0.393	0.526 *	0.402	0.481 *	0.444 *	0.475 *	0.528 *	0.473 *	0.415	0.397 *	0.143	−0.367	−0.263	−0.19	0.284
			CP * LD	−0.602 **	0.793 **	0.630 ***	0.582 **	0.614 **	0.590 **	0.490 **	0.617 **	−0.079	0.589 **	−0.445 *	−0.726 ***	−0.478 *	0.033	0.622 **
			CP * HD	−0.850 ***	0.850 ***	0.860 ***	0.847 ***	0.858 ***	0.849 ***	0.830 *	0.780 ***	0.363	0.818 ***	−0.587 **	−0.869	−0.488 *	0.141	0.443 *
	Vegetation measurements	<i>Tillage</i>																
		CA			0.383 **	0.390 **	0.395 **	0.396 **	0.29	0.456 **	0.13	0.344 *	0.072	−0.234	−0.38	−0.390 **	0.107	
		CP			0.767 ***	0.664 ***	0.731 ***	0.673 ***	0.507 ***	0.729 ***	−0.323 *	0.738	−0.641 ***	−0.785 ***	−0.695	−0.643 ***	0.445 **	
		<i>Planting density</i>																
			LD			0.617 ***	0.358 *	0.489 ***	0.384 **	0.333 *	0.620 ***	−0.234	0.599 ***	−0.516 ***	−0.704 ***	−0.608	−0.533 ***	0.238
			HD			0.791 ***	0.717 ***	0.768 ***	0.723 ***	0.640 ***	0.801 ***	−0.062	0.803 ***	−0.562 ***	−0.752 ***	−0.74	−0.740 ***	0.503 ***
		<i>Combinations</i>																
			CA * LD			0.324	0.257	0.273	0.254	0.175	0.328	−0.021	0.245	−0.097	−0.404	−0.307	−0.248	0.011
			CA * HD			0.468 *	0.579 **	0.543 *	0.577 **	0.388	0.614 **	0.222	0.541 **	0.131	−0.238	−0.609	−0.658 ***	0.344
		CP * LD			0.650 ***	0.489 ***	0.588 ***	0.505 *	0.245	0.613 **	−0.402	0.596 **	−0.610 **	−0.732 ***	−0.614	−0.517 **	0.444 *	
		CP * HD			0.866 ***	0.788 ***	0.837 ***	0.793 ***	0.702 **	0.828 ***	−0.374	0.854 ***	−0.787 ***	−0.874 ***	−0.763	−0.738 ***	0.582 **	

Table 8. Multilinear regression (stepwise) of grain yield (GY) as dependent variable and the remote sensing traits (RGB and multispectral vegetation indexes) measured from the unmanned aerial vehicle as independent variables. These indexes are defined at section Material and Methods. R^2 , determination coefficient; RSE, Residual Standard Error.

	Equation	R^2	RSE	p -Value
Conservation	$GY = -4.37 + 0.11 \cdot \text{Lightness} + 9.23 \cdot \text{GA} - 0.04 \cdot \text{MCARI}$	0.351	0.521	0.000
Portion of variance	Lightness GA MCARI	0.237 0.164 0.159		
Conventional	$GY = 16.56 - 0.36 \cdot b^* - 16.28 \cdot \text{SAVI} + 2.06 \cdot \text{RDVI} - 0.02 \cdot \text{TCARI/OSAVI}$	0.757	0.491	0.000
Portion of variance	b^* SAVI RDVI TCARI/OSAVI	0.237 0.164 0.159 0.195		
Low density	$GY = 5.36 - 0.26 \cdot b^* + 10.21 \cdot \text{OSAVI} - 13.99 \cdot \text{CCI}$	0.516	0.609	0.000
Portion of variance	b^* OSAVI CCI	0.203 0.166 0.147		
High density	$GY = 0.517 + 6.44 \cdot \text{GGA} + 3.14 \cdot \text{OSAVI}$	0.654	0.531	0.000
Portion of variance	GGA OSAVI	0.353 0.300		

4. Discussion

4.1. Implications of Growing Conditions on Yield Parameters

Conservation agriculture practices have been proposed as potential systems to increase crop yield, [1,2,48,49]). As can be seen in our results, CA plots out-yielded conventional agriculture. Positive responses to CA are principally the result of the interacting effect of soil characteristics and climate [1]. One of these benefits is attributed to the water-harvesting effects of minimum-tillage practices [50,51]. Underwater limited conditions increased soil moisture, leading to comparably higher yields under CA [9]. We did not report any water data in our study but indirectly derived these through sensors that measure related parameters. We attributed significant differences in plot temperature due to residue cover under CA. It is very likely that the residue cover, even though it helps to maintain the humidity of the top-layers of the soil, dries faster than the soil and thus presents a higher temperature than both soil and vegetation. Also, better water availability of CA should have been reflected in a significant decrease in the carbon isotopic composition of the leaves of this C4 species in comparison with CP agriculture plots due to a decrease of the leakiness of the bundle-sheath cells or by an increase of the C_i/C_c as a consequence of an increase of the photosynthetic capacity [27]. Therefore, due to the fact that the trial has been running under CA since 2009, yield improvements were likely not related due to increased soil moisture or decreased temperature but due to a long-term improvement in soil health and fertility.

Since crop management has led to a considerable increase in yield, changes in genotype may be an option to make use of the enhanced yield potential provided by this environmental factor. While the literature related to CA is mostly focused on crop management, the study of the genetic crop adaptation is limited and usually concludes that the interaction between the tillage practice and the genotype is absent [7,52–54]. Crops have been grown on conventional tillage for many years and genes governing the adaptation to CA either have been lost over time through untargeted selection or have become redundant [55]. However, the varieties used in this experiment only showed significant differences in yield under CA, not under conventional agriculture management (CP). This may suggest the existence of some traits linked to tillage with a direct effect on improving yield. Herrera et al. (2013) [56] conclude that traits associated with emergence (early vigor) and resistance to diseases may increase

genotype performance under CA. Thus, these results reinforce the need to further evaluate genotypic performance of varieties developed and selected in CP and test them under no-tillage conditions.

4.2. Comparative Performance of the Vegetation Indexes at Determining Differences in Grain Yield under CP and CA Conditions

RGB imaging and processing have become a major tool for phenotyping, and its ability to determine plant performance in terms of biomass and yield has been demonstrated again in this study. The indexes that performed better in assessing differences in yield were the ones more related to canopy greenness (such as a^* or GGA) and thus to vegetation cover [20]. Therefore, elevated values of these indexes, driven by higher biomass levels, help to anticipate higher yields even at early growing stages [57]. Just like RGB, the multispectral indexes that are more sensitive to the green biomass (e.g., NDVI) and its reformulations such as the SAVI, OSAVI, and RDVI were the best correlated with GY. Those indexes contain information from the red reflectance region [35,37,38], which increases with a reduction of the biomass density, making them ideal for identifying differences in vigor at early growing stages.

Other multispectral indexes that worked well in assessing differences in GY were PRI and TCARI/OSAVI. The Photochemical Reflectance Index (PRI) is a spectral index increasingly used as an indicator of photosynthetic efficiency [58], because it is closely related to $\Delta F/F_m'$ [59,60]. Low PRI values reflect a lower light use efficiency of PSII that will finally be translated in a yield loss. Meanwhile, the Transformed Chlorophyll Absorption in Reflectance Index (TCARI), based on the Modified Chlorophyll Absorption in Reflectance Index (MCARI), is a depth measure of the chlorophyll absorption at 670 nm relative to the reflectance at 550 and 700 nm [43]. This pigment index did not correlate with yield until the background was corrected and normalized with the OSAVI. The TCARI/OSAVI ratio is an index very sensitive to changes in chlorophyll content but very resistant to the variations in LAI at the same time [43].

Although significant results were obtained, these indexes did not perform equally when assessing yield differences within the different tillage growing conditions. The strengths of the indexes' (both RGB and multispectral) correlations against yield were much lower in CA compared with CP. The reason for this is assumed to be the added noise derived from the crop residue coverage of the soil. According to the FAO definition, the soil surface has to be covered at least by 30% to qualify as CA in principle [61], which may have influenced remote sensing readings under CA. Due to this fundamental difference between CA and CP, it is difficult to segregate the biomass from the plant and residue cover. The application of an NDVI mask on the multispectral images effectively reduced background reflectance and increased their correlations statistically, although the improvements were minor (Figure 4). Indexes linked to the pigment content such as the CCI, ARI2, and CRI2 benefited most from the use of a soil mask. As can be seen in Figure 5, even with its distinct color, the CA background influenced the images mildly and supported the assessment of vegetation area, particularly in RGB images that are based on the portion of green pixels of the image.

Meanwhile, the use of the near-infrared (NIR) region by some spectral indexes, which greatly decreases its reflectance over soil, helps to increase the sensibility to the canopy cover [62]. Despite these appreciations, the RGB-based indexes GA and GGA outperformed NDVI and the rest of spectral indexes at predicting GY under CA conditions. The far higher resolution of the RGB compared with the multispectral images may be the critical factor here when working from an aerial platform (Figure 2) [33,57].

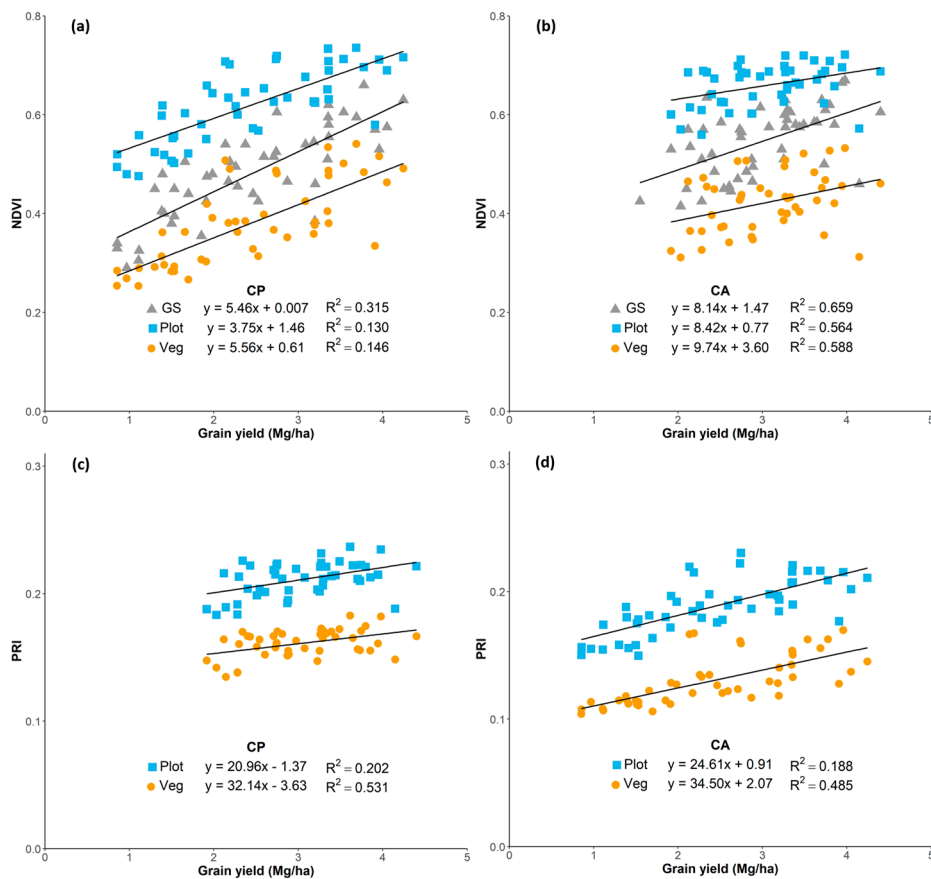


Figure 4. Relationship between grain yield with the Normalized Difference Vegetation Index (NDVI), measured with the GreenSeeker and calculated from the aerial multispectral images (a,b) and with the Photochemical Reflectance Index (PRI), measured from the aerial multispectral images (c,d).

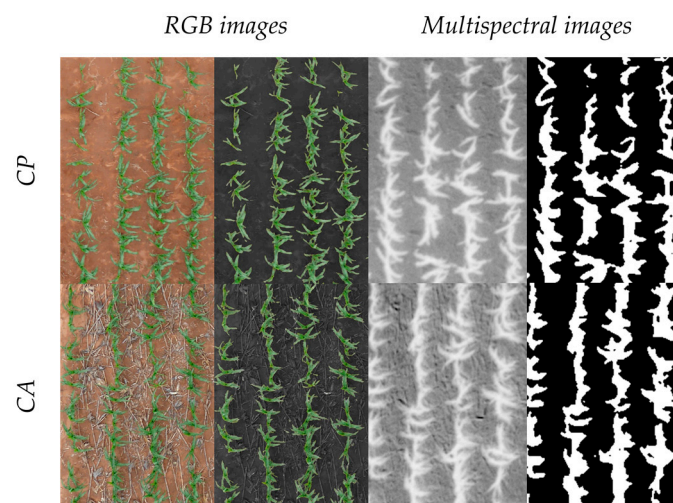


Figure 5. Examples of the differences in the vegetation area identification with the RGB and multispectral images with at the conservation (ca) and conventional (CP) plots.

4.3. Platform Proximity Effects on the Performance of the Vegetation Indexes Assessing Grain Yield Differences

The possibility to incorporate remote sensing methodologies onto unmanned aerial based platforms enables the characterization of a larger number of plots in much less time, helping to

minimize the effect of the changing environmental conditions during the sampling [18]. Moreover, aerial photographs facilitate the coverage of the whole plot (which usually is not possible for the images taken at ground level, particularly with tall crops such as maize). Yet, the altitude of the sensor from the canopy of the crop has a negative effect on the resolution of the images when using cameras with the same resolution (16-megapixels with both airborne and ground). While the RGB images collected from the UAV only reached a resolution of 825×1210 pixels per plot, the spatial resolution of the images taken from the ground was of 4608×3072 pixels per plot. Despite this loss of resolution, aerial indexes performed very similarly or even better than the ground measurements. This may also help to explain why the ground to aerial correlation for the RGB data was higher in CP than in CA, especially if the added background complexity of CA requires higher spatial resolution for accurate quantification. Limited resolution due to the height level can also constrain the performance of NDVI. Our results show how the use of an active sensor (i.e., with its own source of light), such as the GreenSeeker at ground level, helped to improve the correlation with GY in comparison with the NDVI formulation from the aerial images, although this improvement was rather small. This may be due to the improved normalization of the light and other environmental conditions while using field sensors that take some time to cover all of the study plots.

5. Conclusions

Conservation agriculture management practices had a positive effect on increasing yields as compared to conventional ploughed system. These results may help support the adoption of CA to combat declining yields that affect SSA agriculture. Henceforth, in order to fully exploit the yield potential, future efforts should focus on the study of the impact of the genotype selection for a particular management system (e.g., Genotype \times Environment \times Management interaction). The main point of field phenotyping is to understand the genotypic responses and dissect that traits associated with a better performance under CA as a management system. Thus, further work is required before breeding programs invest resources into a whole new management system.

The use of remote sensing technologies, as presented here, would be increasingly useful for large-scale phenotyping studies. The results suggest, even at early crop growth stages, that the different RGB and multispectral indexes have the potential to effectively assess yield differences under CA conditions, even if their performance is lower than under CP conditions. This is assumed to be mainly due to the residue cover effect on the measurements; however, applying a soil (and stover) mask to the images could help in overcoming this technical problem, which may be best accomplished by the fusion of high resolution RGB with multispectral and/or thermal data or by employing advanced image segmentation algorithms not explored in this study. Nevertheless, the performance of the RGB indexes in predicting yield was less affected by tillage conditions than the multispectral indexes. The indexes that best correlated with yield were mostly related to the greenness of the canopy vegetation, such as the RGB indexes GA and a^* , and the multispectral indexes NDVI and RDVI. Finally, the platform proximity effect on the image resolution did not have a negative impact on the performance of the indexes, reinforcing the usefulness of UAV and its associated image processing for high throughput plant phenotyping studies under field conditions.

Supplementary Materials: The following are available online at www.mdpi.com/2072-4292/10/2/349/s1, Table S1: Regression coefficients (r) and P-value from ANOVA for the relationships between the remote sensing indexes measured at ground against the same indexes measured at aerial level within the conservation (CA), conventional (CP) and the combination of both conditions. These indexes are defined in detail in the Material and Methods. GA, Greener Area; GGA, Greener Green Area; NDVI, Normalized Difference Vegetation Index.

Acknowledgments: We thank the personnel from the CIMMYT Southern Africa Regional Office at Harare for their support during the field measurements and sampling. The trials were financially supported by CRP MAIZE (www.maize.org). We also acknowledge Stress Tolerant Maize for Africa funded by the Bill & Melinda Gates Foundation and USAID for open-access publication support. Finally, we thank Jaume Casadesús for providing the BreedPix software and Regina Hlatywayo for being instrumental in trial implementation.

Author Contributions: C.T. and J.C. managed and directed the maize trials at the Domboshawa Training Center, Zimbabwe. S.K. carried out the UAV flights for the obtainment of aerial measurements. O.V.-D. and J.A. conducted the field measurements and collection of samples. A.G.-R. processed the images, analyzed the samples and wrote the paper under the supervision of J.A. and S.K. and with the contribution from all the other authors.

Conflicts of Interest: The authors declare no conflict of interest.

Abbreviations

The following abbreviations are used in this manuscript:

SSA	Sub-Saharan Africa
RGB	Red-Blue-Green
CA	conservation agriculture
CP	conventional ploughed
NDVI	Normalized Difference Vegetation Index
UAV	unmanned aerial vehicle
GY	grain yield
HIS	Hue-Intensity-Saturation
GA	Green Area
GGA	Greener Area
CSI	Crop Senescence Index
CIMMYT	International Maize and Wheat Improvement Center
m.a.s.l.	meters above sea level
CP-OES	Inductively Coupled Plasma Optical Emission Spectroscopy
LCC	leaf chlorophyll content
PRI	Photochemical Reflectance Index
SAVI	Soil Adjusted Vegetation Index
MCARI	Modified Chlorophyll Absorption Ratio Index
WBI	Water Band Index
RDVI	Renormalized Difference Vegetation Index
EVI	Enhanced Vegetation Index
ARI2	Anthocyanin Reflectance Index 2
CRI2	Carotenoid Reflectance Index 2
TCARI	Transformed Chlorophyll Absorption in Reflectance Index
OSAVI	Optimized Soil-Adjusted Vegetation Index
$\Delta F/F_m'$	Effective fluorescence quantum yield
NIR	near-infrared.

References

1. Thierfelder, C.; Rusinamhodzi, L.; Ngwira, A.R.; Mupangwa, W.; Nyagumbo, I.; Kassie, G.T.; Cairns, J.E. Conservation agriculture in Southern Africa: Advances in knowledge. *Renew. Agric. Food Syst.* **2015**, *30*, 328–348. [[CrossRef](#)]
2. Farooq, M.; Flower, K.C.; Jabran, K.; Wahid, A.; Siddique, K.H.M. Crop yield and weed management in rainfed conservation agriculture. *Soil Tillage Res.* **2011**, *117*, 172–183. [[CrossRef](#)]
3. Cairns, J.E.; Hellin, J.; Sonder, K.; Araus, J.L.; MacRobert, J.F.; Thierfelder, C.; Prasanna, B.M. Adapting maize production to climate change in sub-Saharan Africa. *Food Secur.* **2013**, *5*, 345–360. [[CrossRef](#)]
4. Fess, T.L.; Kotcon, J.B.; Benedito, V.A. Crop breeding for low input agriculture: A sustainable response to feed a growing world population. *Sustainability* **2011**, *3*, 1742–1772. [[CrossRef](#)]
5. Martín, M.M.S.; Olesen, J.E.; Porter, J.R. A genotype, environment and management (GxExM) analysis of adaptation in winter wheat to climate change in Denmark. *Agric. For. Meteorol.* **2014**, *187*, 1–13. [[CrossRef](#)]
6. Studnicki, M.; Wijata, M.; Sobczyński, G.; Samborski, S.; Gozdowski, D.; Rozbicki, J. Effect of genotype, environment and crop management on yield and quality traits in spring wheat. *J. Cereal Sci.* **2016**, *72*, 30–37. [[CrossRef](#)]

7. Thierfelder, C.; Rusinamhodzi, L.; Setimela, P.; Walker, F.; Eash, N.S. Conservation agriculture and drought-tolerant germplasm: Reaping the benefits of climate-smart agriculture technologies in central Mozambique. *Renew. Agric. Food Syst.* **2016**, *31*, 414–428. [[CrossRef](#)]
8. Thierfelder, C.; Chivenge, P.; Mupangwa, W.; Rosenstock, T.S.; Lamanna, C.; Eyre, J.X. How climate-smart is conservation agriculture (CA)?—Its potential to deliver on adaptation, mitigation and productivity on smallholder farms in southern Africa. *Food Secur.* **2017**, *9*, 537–560. [[CrossRef](#)]
9. Thierfelder, C.; Wall, P.C. Investigating Conservation Agriculture (CA) Systems in Zambia and Zimbabwe to Mitigate Future Effects of Climate Change. *J. Crop Improv.* **2010**, *24*, 113–121. [[CrossRef](#)]
10. Farooq, M.; Siddique, K. *Conservation Agriculture*; Springer: Cham, Switzerland; Heidelberg, Germany; New York, NY, USA; Dordrecht, The Netherlands; London, UK, 2015; Volume 1.
11. Govaerts, B.; Verhulst, N.; Castellanos-Navarrete, A.; Sayre, K.D.; Dixon, J.; Dendooven, L. Conservation Agriculture and Soil Carbon Sequestration: Between Myth and Farmer Reality. *Crit. Rev. Plant Sci.* **2009**, *28*, 97–122. [[CrossRef](#)]
12. Giller, K.E.; Witter, E.; Corbeels, M.; Tittonell, P. Conservation agriculture and smallholder farming in Africa: The heretics' view. *Field Crops Res.* **2009**, *114*, 23–34. [[CrossRef](#)]
13. Stevenson, J.R.; Serraj, R.; Cassman, K.G. Evaluating conservation agriculture for small-scale farmers in Sub-Saharan Africa and South Asia. *Agric. Ecosyst. Environ.* **2014**, *187*, 1–10. [[CrossRef](#)]
14. Steward, P.R.; Dougill, A.J.; Thierfelder, C.; Pittelkow, C.M.; Stringer, L.C.; Kudzala, M.; Shackelford, G.E. The adaptive capacity of maize-based conservation agriculture systems to climate stress in tropical and subtropical environments: A meta-regression of yields. *Agric. Ecosyst. Environ.* **2018**, *251*, 194–202. [[CrossRef](#)]
15. Thierfelder, C.; Cheesman, S.; Rusinamhodzi, L. A comparative analysis of conservation agriculture systems: Benefits and challenges of rotations and intercropping in Zimbabwe. *Field Crops Res.* **2012**, *137*, 237–250. [[CrossRef](#)]
16. Valbuena, D.; Erenstein, O.; Homann-Kee Tui, S.; Abdoulaye, T.; Claessens, L.; Duncan, A.J.; Gérard, B.; Rufino, M.C.; Teufel, N.; van Rooyen, A.; et al. Conservation Agriculture in mixed crop-livestock systems: Scoping crop residue trade-offs in Sub-Saharan Africa and South Asia. *Field Crops Res.* **2012**, *132*, 175–184. [[CrossRef](#)]
17. Khah, E.M.; Ellis, R.H.; Roberts, E.H. Effects of laboratory germination, soil temperature and moisture content on the emergence of spring wheat. *J. Agric. Sci.* **1986**, *107*, 431. [[CrossRef](#)]
18. Araus, J.L.; Cairns, J.E. Field high-throughput phenotyping: The new crop breeding frontier. *Trends Plant Sci.* **2014**, *19*, 52–61. [[CrossRef](#)] [[PubMed](#)]
19. Fiorani, F.; Schurr, U. Future scenarios for plant phenotyping. *Annu. Rev. Plant Biol.* **2013**, *64*, 267–291. [[CrossRef](#)] [[PubMed](#)]
20. Casadesús, J.; Kaya, Y.; Bort, J.; Nachit, M.M.; Araus, J.L.; Amor, S.; Ferrazzano, G.; Maalouf, F.; Maccaferri, M.; Martos, V.; et al. Using vegetation indices derived from conventional digital cameras as selection criteria for wheat breeding in water-limited environments. *Ann. Appl. Biol.* **2007**, *150*, 227–236. [[CrossRef](#)]
21. Hunt, E.R.; Hively, W.D.; Daughtry, C.S.T.; Mccarty, G.W.; Fujikawa, S.J.; Ng, T.L.; Tranchitella, M.; Linden, D.S.; Yoel, D.W. Remote Sensing of Crop Leaf Area Index Using Unmanned Airborne Vehicles. In Proceedings of the Pecora 17 Symposium, Beltsville, MD, USA, 18 November 2008; pp. 18–20.
22. Jin, X.; Liu, S.; Baret, F.; Hemerlé, M.; Comar, A. Estimates of plant density of wheat crops at emergence from very low altitude UAV imagery. *Remote Sens. Environ.* **2017**, *198*, 105–114. [[CrossRef](#)]
23. Verger, A.; Vigneau, N.; Cheron, C.; Gilliot, J.M.; Comar, A.; Baret, F. Green area index from an unmanned aerial system over wheat and rapeseed crops. *Remote Sens. Environ.* **2014**, *152*, 654–664. [[CrossRef](#)]
24. Zarco-Tejada, P.J.; Guillén-Climent, M.L.; Hernández-Clemente, R.; Catalina, A.; González, M.R.; Martín, P. Estimating leaf carotenoid content in vineyards using high resolution hyperspectral imagery acquired from an unmanned aerial vehicle (UAV). *Agric. For. Meteorol.* **2013**, *171–172*, 281–294. [[CrossRef](#)]
25. Jones, H.G.; Serraj, R.; Loveys, B.R.; Xiong, L.; Wheaton, A.; Price, A.H. Thermal infrared imaging of crop canopies for the remote diagnosis and quantification of plant responses to water stress in the field. *Funct. Plant Biol.* **2009**, *36*, 978–989. [[CrossRef](#)]
26. Yousfi, S.; Kellas, N.; Saidi, L.; Benlakehal, Z.; Chaou, L.; Siad, D.; Herda, F.; Karrou, M.; Vergara, O.; Gracia, A.; et al. Comparative performance of remote sensing methods in assessing wheat performance under Mediterranean conditions. *Agric. Water Manag.* **2016**, *164*, 137–147. [[CrossRef](#)]

27. Monneveux, P.; Sheshshayee, M.S.; Akhter, J.; Ribaut, J. Using carbon isotope discrimination to select maize (*Zea mays* L.) inbred lines and hybrids for drought tolerance. *Plant Sci.* **2007**, *173*, 390–396. [[CrossRef](#)]
28. Vogel, H. The Need for Integrated Weed Management Systems in Smallholder Conservation Farming in Zimbabwe. *Tropenlandwirt* **1995**, *96*, 35–56.
29. Muoni, T.; Rusinamhodzi, L.; Thierfelder, C. Weed control in conservation agriculture systems of Zimbabwe: Identifying economical best strategies. *Crop Prot.* **2013**, *53*, 23–28. [[CrossRef](#)]
30. Mugandani, R.; Wuta, M.; Makarau, A.; Chipindu, B.; Gweru, S.R.; Pleasant, M.; Mugandani, R.; Wuta, M.; Makarau, C.B. Re-Classification of the Agro-Ecological Regions of Zimbabwe in Conformity With Climate Variability and Change. *Afr. Crop Sci. J.* **2012**, *20*, 361–369.
31. Zaman-Allah, M.; Vergara, O.; Araus, J.L.; Tarekegne, A.; Magorokosho, C.; Zarco-Tejada, P.J.; Hornero, A.; Albà, A.H.; Das, B.; Craufurd, P.; et al. Unmanned aerial platform-based multi-spectral imaging for field phenotyping of maize. *Plant Met.* **2015**, *11*, 35. [[CrossRef](#)] [[PubMed](#)]
32. Pointer, M.R. A comparison of the CIE 1976 colour spaces. *Color Res. Appl.* **1981**, *6*, 108–118. [[CrossRef](#)]
33. Kefauver, S.C.; Vicente, R.; Vergara-Díaz, O.; Fernandez-Gallego, J.A.; Kerfal, S.; Lopez, A.; Melichar, J.P.E.; Serret Molins, M.D.; Araus, J.L. Comparative UAV and Field Phenotyping to Assess Yield and Nitrogen Use Efficiency in Hybrid and Conventional Barley. *Front. Plant Sci.* **2017**, *8*, 1–15. [[CrossRef](#)] [[PubMed](#)]
34. Bendig, J.; Bolten, A.; Bennertz, S.; Broscheit, J.; Eichfuss, S.; Bareth, G. Estimating biomass of barley using crop surface models (CSMs) derived from UAV-based RGB imaging. *Remote Sens.* **2014**, *6*, 10395–10412. [[CrossRef](#)]
35. Rouse, J.W.; Hass, R.H.; Schell, J.A.; Deering, D.W. Monitoring vegetation systems in the great plains with ERTS. In Proceedings of the Third Earth Resources Technology Satellite (ERTS) Symposium, Houston, TX, USA, 1 January 1973; pp. 309–317.
36. Huete, A.R. A soil-adjusted vegetation index (SAVI). *Remote Sens. Environ.* **1988**, *25*, 295–309. [[CrossRef](#)]
37. Rondeaux, G.; Steven, M.; Baret, F. Optimization of soil-adjusted vegetation indices. *Remote Sens. Environ.* **1996**, *55*, 95–107. [[CrossRef](#)]
38. Roujean, J.-L.; Breon, F.-M. Estimating PAR absorbed by vegetation from bidirectional reflectance measurements. *Remote Sens. Environ.* **1995**, *51*, 375–384. [[CrossRef](#)]
39. Huete, A.; Didan, K.; Miura, T.; Rodriguez, E.P.; Gao, X.; Ferreira, L.G. Overview of the radiometric and biophysical performance of the MODIS vegetation indices. *Remote Sens. Environ.* **2002**, *83*, 195–213. [[CrossRef](#)]
40. Gamon, J.A.; Serrano, L.; Surfus, J.S. The photochemical reflectance index: An optical indicator of photosynthetic radiation use efficiency across species, functional types, and nutrient levels. *Oecologia* **1997**, *112*, 492–501. [[CrossRef](#)] [[PubMed](#)]
41. Daughtry, C. Estimating Corn Leaf Chlorophyll Concentration from Leaf and Canopy Reflectance. *Remote Sens. Environ.* **2000**, *74*, 229–239. [[CrossRef](#)]
42. Gamon, J.A.; Huemmrich, K.F.; Wong, C.Y.S.; Ensminger, I.; Garrity, S.; Hollinger, D.Y.; Noormets, A.; Peñuelas, J. A remotely sensed pigment index reveals photosynthetic phenology in evergreen conifers. *Proc. Natl. Acad. Sci. USA* **2016**, *113*, 13087–13092. [[CrossRef](#)] [[PubMed](#)]
43. Haboudane, D.; Miller, J.R.; Tremblay, N.; Zarco-Tejada, P.J.; Dextraze, L. Integrated narrow-band vegetation indices for prediction of crop chlorophyll content for application to precision agriculture. *Remote Sens. Environ.* **2002**, *81*, 416–426. [[CrossRef](#)]
44. Gitelson, A.A.; Merzlyak, M.N.; Chivkunova, O.B. Optical Properties and Nondestructive Estimation of Anthocyanin Content in Plant Leaves. *Photochem. Photobiol.* **2001**, *74*, 38–45. [[CrossRef](#)]
45. Gitelson, A.A.; Zur, Y.; Chivkunova, O.B.; Merzlyak, M.N. Assessing carotenoid content in plant leaves with reflectance spectroscopy. *Photochem. Photobiol.* **2002**, *75*, 272–281. [[CrossRef](#)]
46. Peñuelas, J.; Filella, I.; Biel, C.; Serrano, L.; Savé, R. The reflectance at the 950–970 nm region as an indicator of plant water status. *Int. J. Remote Sens.* **1993**, *14*, 1887–1905. [[CrossRef](#)]
47. Coplen, T.B.; Zhu, X.K. Explanatory Glossary of Terms Used in Expression of Relative Isotope Ratios and Gas Ratios. Available online: http://old.iupac.org/reports/provisional/abstract08/coplen_prs.pdf (accessed on 1 February 2018).
48. Friedrich, T.; Derpsch, R.; Kassam, A. Overview OD the global spread of conservation agriculture. *Field Act. Sci. Rep.* **2012**, *6*, 1–7.

49. Thierfelder, C.; Matemba-Mutasa, R.; Rusinamhodzi, L. Yield response of maize (*Zea mays* L.) to conservation agriculture cropping system in Southern Africa. *Soil Tillage Res.* **2015**, *146*, 230–242. [[CrossRef](#)]
50. Mupangwa, W.; Twomlow, S.; Walker, S. The influence of conservation tillage methods on soil water regimes in semi-arid southern Zimbabwe. *Phys. Chem. Earth* **2008**, *33*, 762–767. [[CrossRef](#)]
51. Thierfelder, C.; Wall, P.C. Effects of conservation agriculture techniques on infiltration and soil water content in Zambia and Zimbabwe. *Soil Tillage Res.* **2009**, *105*, 217–227. [[CrossRef](#)]
52. Duiker, S.W.; Haldeman, J.F.J.; Johnson, D.H. Tillage x Maize Hybrid Interactions. *Agron. J.* **2006**, *98*, 436–442. [[CrossRef](#)]
53. Hlatywayo, R.; Mhlanga, B.; Mazarura, U.; Mupangwa, W.; Thierfelder, C. Response of Maize (*Zea mays* L.) Secondary Growth Parameters to Conservation Agriculture and Conventional Tillage Systems in Zimbabwe. *J. Agric. Sci.* **2016**, *8*, 112. [[CrossRef](#)]
54. Zamir, M.S.I.; Ahmad, A.; Javeed, H.M.R. Comparative performance of various wheat (*Triticum aestivum* L.) cultivars to different tillage practices under tropical conditions. *Afr. J. Agric. Sci.* **2010**, *5*, 1799–1803.
55. Mahmood, T.; Trethowan, R. Crop Breeding for Conservation Agriculture. In *Conservation Agriculture*; Farooq, M., Siddique, K.H.M., Eds.; Springer International Publishing: Cham, Switzerland, 2015; pp. 159–179.
56. Herrera, J.M.; Verhulst, N.; Trethowan, R.M.; Stamp, P.; Govaerts, B. Insights into genotype × tillage interaction effects on the grain yield of wheat and maize. *Crop Sci.* **2013**, *53*, 1845–1859. [[CrossRef](#)]
57. Gracia-Romero, A.; Kefauver, S.C.; Vergara-Diaz, O.; Zaman-Allah, M.A.; Prasanna, B.M.; Cairns, J.E.; Araus, J.L. Comparative performance of ground versus aerially assessed RGB and multispectral indices for early-growth evaluation of maize performance under phosphorus fertilization. *Front. Plant Sci.* **2017**, *8*, 1–13. [[CrossRef](#)] [[PubMed](#)]
58. Garbulsky, M.F.; Peñuelas, J.; Gamon, J.; Inoue, Y.; Filella, I. The photochemical reflectance index (PRI) and the remote sensing of leaf, canopy and ecosystem radiation use efficiencies. A review and meta-analysis. *Remote Sens. Environ.* **2011**, *115*, 281–297. [[CrossRef](#)]
59. Genty, B.; Briantais, J.-M.; Baker, N.R. The relationship between the quantum yield of photosynthetic electron transport and quenching of chlorophyll fluorescence. *Biochim. Biophys. Acta (BBA) Gen. Subj.* **1989**, *990*, 87–92. [[CrossRef](#)]
60. Tambussi, E.A.; Casadesus, J.; Munn-Bosch, S.; Araus, J.L. Photoprotection in water-stressed plants of durum wheat (*Triticum turgidum* var. durum): Changes in chlorophyll fluorescence, spectral signature and photosynthetic pigments. *Funct. Plant Biol.* **2002**, *29*, 35–44. [[CrossRef](#)]
61. Kosmowski, F.; Stevenson, J.; Campbell, J.; Ambel, A.; Haile Tsegay, A. On the Ground or in the Air? A Methodological Experiment on Crop Residue Cover Measurement in Ethiopia. *Environ. Manag.* **2017**, *60*, 705–716. [[CrossRef](#)] [[PubMed](#)]
62. Thorp, K.R.; Tian, L.F. A review on remote sensing of weeds in agriculture. *Prec. Agric.* **2004**, *5*, 477–508. [[CrossRef](#)]



© 2018 by the authors. Licensee MDPI, Basel, Switzerland. This article is an open access article distributed under the terms and conditions of the Creative Commons Attribution (CC BY) license (<http://creativecommons.org/licenses/by/4.0/>).



CHAPTER 3



UAV and Ground Image-Based Phenotyping: A Proof of Concept with Durum Wheat

Adrian Gracia-Romero, Shawn C. Kefauver, Jose A. Fernandez-Gallego, Omar Vergara-Díaz, María Teresa Nieto-Taladriz and José L. Araus

Published in:
Remote Sensing (2019), 11, 1244

Article

UAV and Ground Image-Based Phenotyping: A Proof of Concept with Durum Wheat

Adrian Gracia-Romero ^{1,2}, Shawn C. Kefauver ^{1,2}, Jose A. Fernandez-Gallego ^{1,2},
Omar Vergara-Díaz ^{1,2}, María Teresa Nieto-Taladriz ³ and José L. Araus ^{1,2,*}

¹ Integrative Crop Ecophysiology Group, Plant Physiology Section, Faculty of Biology, University of Barcelona, 08028 Barcelona, Spain; adriangraciaromero@hotmail.com (A.G.-R.); sckefauver@ub.edu (S.C.K.); fernandezgallego@gmail.com (J.A.F.-G.); omarvergaradiaz@gmail.com (O.V.-D.)

² AGROTECNIO (Center for Research in Agrotechnology), Av. Rovira Roure 191, 25198 Lleida, Spain

³ Instituto Nacional de Investigación y Tecnología Agraria y Alimentaria (INIA), Ctra. de la Coruña Km. 7.5, 28040 Madrid, Spain; mt Nieto@inia.es

* Correspondence: jaraus@ub.edu; Tel.: +34-608-644-144

Received: 14 March 2019; Accepted: 22 May 2019; Published: 25 May 2019



Abstract: Climate change is one of the primary culprits behind the restraint in the increase of cereal crop yields. In order to address its effects, effort has been focused on understanding the interaction between genotypic performance and the environment. Recent advances in unmanned aerial vehicles (UAV) have enabled the assembly of imaging sensors into precision aerial phenotyping platforms, so that a large number of plots can be screened effectively and rapidly. However, ground evaluations may still be an alternative in terms of cost and resolution. We compared the performance of red–green–blue (RGB), multispectral, and thermal data of individual plots captured from the ground and taken from a UAV, to assess genotypic differences in yield. Our results showed that crop vigor, together with the quantity and duration of green biomass that contributed to grain filling, were critical phenotypic traits for the selection of germplasm that is better adapted to present and future Mediterranean conditions. In this sense, the use of RGB images is presented as a powerful and low-cost approach for assessing crop performance. For example, broad sense heritability for some RGB indices was clearly higher than that of grain yield in the support irrigation (four times), rainfed (by 50%), and late planting (10%). Moreover, there wasn't any significant effect from platform proximity (distance between the sensor and crop canopy) on the vegetation indexes, and both ground and aerial measurements performed similarly in assessing yield.

Keywords: wheat; grain yield; High-Throughput Plant Phenotyping; UAV; RGB; multispectral; canopy temperature

1. Introduction

Projected changes in temperature and precipitation patterns in the coming decades are positioning the Mediterranean Basin as one of the most prominent climate change hotspots [1], where severe impacts on agriculture are expected [2]. Of particular concern for the Iberian Peninsula is an increase in the frequency and severity of droughts associated with a decrease in precipitation and coupled with an increase in evapotranspiration, caused by rising temperatures [3]. Yields of small-grain cereals, such as wheat, will be largely influenced by these scenarios, especially in the rainfed regions that represent nearly 90% of the land under wheat cultivation (MAPAMA <https://www.mapama.gob.es/>, 2017), and which are already characterized by low and irregular precipitation events during late spring and summer. Hence, improving crop yield under drought and/or high temperature conditions is the

principal goal for breeders. Durum wheat is, by extension, the main cereal cultivated on the southern and eastern shores of the Mediterranean Basin and one of the main cereals in southern Europe [4].

Yield is a phenotypically complicated trait, not only because of its genetic complexity [5], but also due to the relative magnitude of gene–environment interactions [6,7], and it is one of the most integrative traits influenced by known and unknown factors. Thus, genotype evaluations in multi-environment trials are needed, at least in the advanced (generations) stages of selection. However, the major point at issue is that high-throughput plant phenotyping (HTPP) may still represent a bottleneck in breeding programs [7], owing to the need to increase the accuracy, precision, and throughput of the methodologies used, while reducing costs and minimizing labor [8,9]. Furthermore, HTPP approaches should allow multi-temporal trait-specific measurements to evaluate the yield components at different phenological moments.

Nowadays, and almost by definition, HTPP implies the use of non-invasive remote sensing approaches of different nature [5,10], given the possibility of screening larger populations faster than conventional phenotyping procedures. Moreover, recent progress and advances in the technology of aeronautics and sensors have allowed the adoption of unmanned aerial vehicle (UAV) platforms, capable of precisely screening hundreds of plots in a short period of time [7,11]. Further benefits of the simultaneous characterization of many plots are found by minimizing the effect of the changing environmental conditions associated with time-consuming ground measurements. This is evident especially when measuring the canopy temperature [12], which greatly varies throughout the day. In recent years, a considerable bulk of the literature has clearly demonstrated the potential of unmanned airborne platforms for large-scale crop monitoring, mainly due to the high spatial and spectral resolution of the sensors [13,14]. So far, the implementation of aerial platforms in HTPP programs has been extensive and successful in assessing crop performance under different management conditions. As a counterpart, even if potentially of lower throughput, ground-based phenotyping on single plots using cameras or sensors held by hand [15–17] or a pole [18] represent low-cost alternatives to aerial assessments. In addition, shorter distances between sensors and plant targets increase the data spatial resolution [19].

The formulation of different wavelength indexes derived from multispectral and hyperspectral sensors and cameras is well established, and their applications to phenotyping range from measurements of biomass (e.g., normalized difference vegetation index, NDVI [20]) or water content (e.g., water band index, WBI [21]), to assessments of pigment composition (e.g., modified chlorophyll absorption ratio index, MCARI [22]). Canopy temperature measurements are used for the detection of changes in stomatal conductance and transpiration rates, as a response to the water status of the plant [23,24]. At present, the use of red–green–blue (RGB) images may represent a low-cost alternative to the expensive tools just mentioned [25]. The implementation of visible imaging has been extensive and successful for providing a wide range of phenomic data to assess aspects related to the architecture and the color of the plant [26].

All these remote sensing HTPP methodologies are amenable to high-throughput phenotyping in multi-environment trials. Identifying and monitoring plant parameters critical to assessing crop production at key developmental stages will be of great assistance to model and predict yields. The novelty of this study, with respect to recently published work, is that it compares the performance of different UAV remote sensing technologies (RGB, multispectral, and thermal) measured at four different phenological stages for assessing the genotypic performance of durum wheat under a wide range of growing conditions (supplementary irrigation, rainfed, or late-planting). For the processing of this large amount of data we also present the MosaicTool software, for high-throughput data extraction and processing of UAV phenotyping data. The final objective is to provide guidance as to the appropriate RGB, multispectral, and thermal image indexes (i.e., appropriate traits) for the identification of high-yielding as well as resilient varieties. Besides studying phenotypic correlations, the heritability of these traits and their genetic correlations with grain yield have been analyzed. Moreover, the benefits and disadvantages of the use of phenotyping platforms in terms of aerial versus

ground positioning will be evaluated for their potential to discriminate between cultivars and also regarding their throughput capacity and cost.

2. Materials and Methods

2.1. Plant Material, Site Description and Growing Conditions

Twenty-three semi-dwarf varieties of durum wheat (*Triticum turgidum* L. subsp. durum (Desf) Husn.) marketed in Spain during the last four decades (Mexa, Vitron, Simeto, Gallareta, Pedroso, Regallo, Arcobaleno, Claudio, Burgos, Dorondon, Avispa, Amilcar, Saragolla, Solea, Euroduro, Don Ricardo, Core, Kiko Nick, Sculpur, Athoris, Don Norman, Olivadur, and Iberus) were evaluated at the experimental station of the Instituto Nacional de Investigación y Tecnología Agraria y Alimentaria (INIA) of Colmenar de Oreja (41°42′44.99″N, 4°41′47.70″O, 590 masl), situated at 40 km south of Madrid (Spain). Climatic data from 2017 was recorded through the Spanish platform SIAR (Servicio de Información Agroclimática para el Regadío, www.siar.es) from meteorological stations next to the field. Monthly temperature and rainfall averages are plotted in Figure 1. Colmenar de Oreja presented high temperatures accompanied with low precipitation during the reproductive period (April, May, and the first half of June).

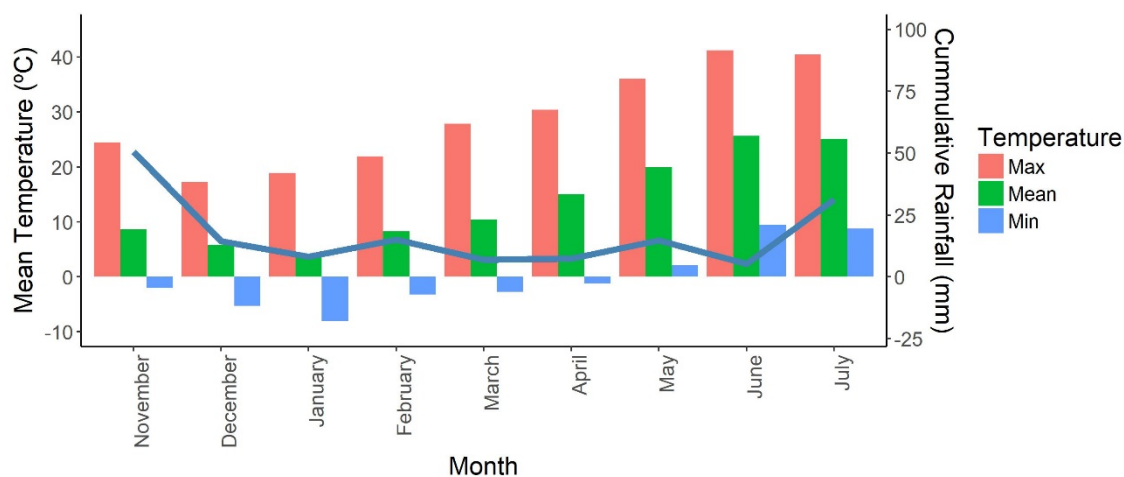


Figure 1. Cumulative monthly rainfall (blue line) and maximum, minimum, and mean temperature (bars) in Colmenar de Oreja for the 2016–2017 crop cycle.

The panel was grown under three different growing treatments: a supplementary irrigation trial, to simulate optimal growing conditions; a rainfed trial without supplementary irrigation, to implement drought stress; and a late-planting trial, leading to higher-than-optimal temperatures throughout the entire crop development period, in order to induce heat stress. The experimental set up consisted of an alpha-lattice design with three replicates in 6 m long and 1.5 m wide plots (a total of 69 plots of 9 m²), where seeds were planted with a sowing density of 250 seeds m⁻² in 6 rows per plot on 22 December 2016 for the normal planting trials and on 1 March 2017 for the late-planting. Before sowing, the field was fertilized with 400 kg ha⁻¹ of 15:15:15 N:P:K fertilizer (15% N + 15% P₂O₅ + 15% K₂O) and a second application of 150 kg ha⁻¹ of urea in a 46% dilution was applied before stem elongation. The rainfed conditions were only provided with one emergency irrigation of 60 mm in order to ensure full plant emergence. Both the supplementary irrigation and late-planting trials were watered every two weeks with irrigations of 60 mm. For all three trials, the crop was harvested on 19 July 2017. Grain yield (GY) (Mg ha⁻¹) was determined for the entire plot, using a harvester. The water content in the grains was between 9.2% and 10.7%.

Aerial and ground phenotyping measurements and sampling were performed during four different visits, planned for assessing crops at the specific development phases of interest (Table 1). At each visit, Zadocks scale values [27] were determined visually for each plot. Moreover, days

after sowing (DAS) and growing degree days (GDD) were counted. GDD was calculated as follows (Equation (1)):

$$GDD = \sum \left(\frac{T_{max} + T_{min}}{2} \right) - T_{base}, \quad (1)$$

where T_{max} corresponds to the highest daily temperature, T_{min} to the lowest, and the T_{base} used was 0 °C.

Table 1. Phenology information of the crop across the measuring/sampling visits, presented as days after sowing (DAS), the growing degree days (GDD), and the developmental period of the crops, expressed with the Zadocks growth scale and the phenological stage.

	Sampling	Date	DAS	GDD	Zadocks Scale	Phen. Stage
Supplementary Irrigation	1 st	26/04/2017	125	2224.05	55–59	Heading
	2 nd	04/05/2017	133	2399.68	61	Anthesis
	3 rd	18/05/2017	147	2767.24	75	Milk Grain Filling
	4 th	06/06/2017	166	3377.17	87	Senescence
Rainfed	1 st	26/04/2017	125	2224.05	55–57	Heading
	2 nd	04/05/2017	133	2399.68	61–65	Anthesis
	3 rd	18/05/2017	147	2767.24	77–79	Late Grain Filling
	4 th	06/06/2017	166	3377.17	90–99	Senescence
Late-Planting	1 st	26/04/2017	56	1270.57	30–32	Stem Elongation
	2 nd	04/05/2017	64	1446.21	45–47	Booting
	3 rd	18/05/2017	78	1813.76	58–59	Heading
	4 th	06/06/2017	97	2423.69	75–79	Milk Grain Filling

2.2. Aerial Platform Description and Orthomosaic Reconstruction Procedure

The aerial UAV system, also commonly known as a drone, was an eight rotor Mikrokoopter Oktokopter 6S12 XL (HiSystems GmbH, Moomerland, Germany). Flights were performed under clear sky conditions, with image data captured at an altitude of 50 m. The payload configuration allowed the measurements to be gathered in two flights per trial: the first included the red–green–blue (RGB) cameras, and the second one with both multispectral and thermal cameras that were mounted at the same time. An active two servo gimbal was used to correct for the effect of pitch and roll movements during the flight. Pre-processed aerial images from each sensor were combined to obtain an accurate orthomosaic (Figure 2) by producing a 3D reconstruction with Agisoft PhotoScan Professional software (Agisoft LLC, St. Petersburg, Russia, www.agisoft.com) [28]. To that end, images with at least 80% overlap were used (Table 2). Then, regions of interest corresponding to each plot were segmented and exported using the MosaicTool (Shawn C. Kefauver, <https://integrativecropecophysiology.com/software-development/mosaictool/>, <https://gitlab.com/sckefauver/MosaicTool>, University of Barcelona, Barcelona, Spain) integrated as a plugin for the open source image analysis platform FIJI (Fiji is Just Image); <http://fiji.sc/Fiji>).

Table 2. Number of images comprising each orthomosaic. *, the values refer to the flights conducted over the late-planting trial.

Date of Sampling	RGB	Multispectral	Thermal
26/04/2017	133	24 *	543 *
04/05/2017	184	61	605
18/05/2017	182	71	804
06/06/2017	97 *	36 *	585 *

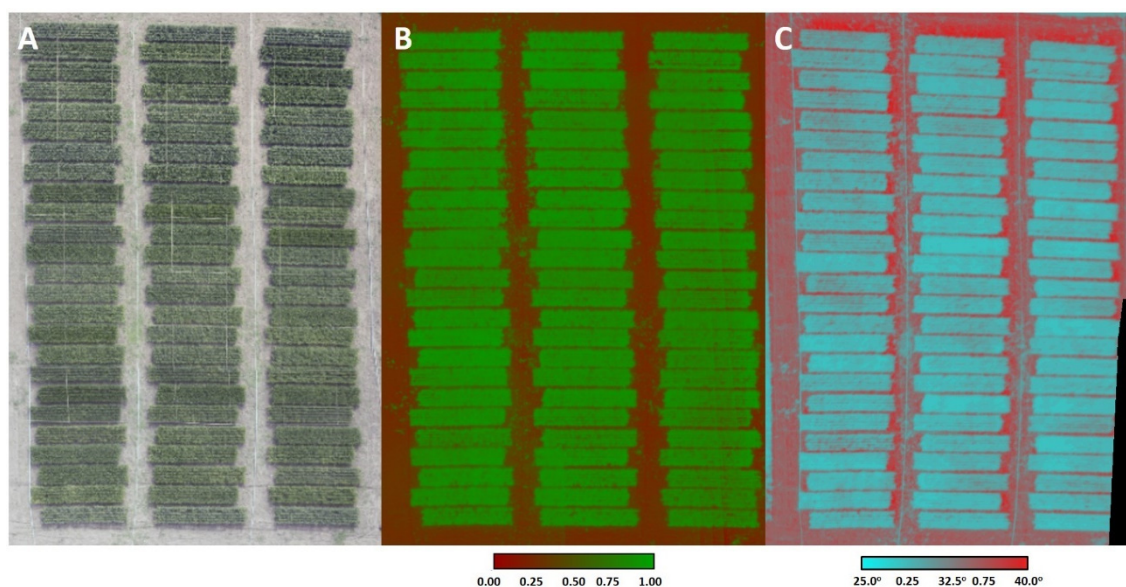


Figure 2. Red–green–blue (RGB) (A), false-color normalized difference vegetation index (NDVI) (B), and false-color thermal (C) orthomosaic examples corresponding to the late-planting trial during the heading stage at the third sampling visit. Both the multispectral and thermal mosaics have been given false colors: in the former, low NDVI values have been colored red and high values colored green, in the latter, warmer temperature values have been colored red and the colder values colored blue.

2.3. RGB Vegetation Indexes

Vegetation indexes derived from RGB images were evaluated for each plot, from the ground and aerially. At ground level, one picture was taken per plot, holding the camera at 80 cm above the plant canopy, in a zenithal plane and focusing near the center of each plot between 11:00 and 13:00 h. To facilitate the procedure, the camera was attached to a monopod Sony Monopod VCTMP1 (Sony Corporation, Minato, Japan) to adjust and to stabilize the distance between the camera and the top of the canopy to 1 m (Table 3). The conventional digital camera used was a 20.1-megapixel Sony ILCE-QX1 (Sony Corporation, Minato, Japan), with images saved in JPEG format at a resolution of 4608×3072 pixels. Aerial RGB images were obtained using a 16-megapixel Lumix GX7 (Panasonic, Osaka, Japan) and saved in JPEG format at a resolution of 4592×3448 pixels. According to the used camera, the ground sample distance (GSD) for a flight of 50 m altitude was 0.941 cm/pixel. The color calibration of both cameras with the ColorChecker Passport Photo (X-Rite, Inc., USA) reported correlations R^2 between 0.88 and 0.94 for all the RGB parameters (data not shown).

Segmented ground and aerial images were subsequently analyzed using the MosaicTool plugin. This software includes a JAVA8 version of Breedpix 2.0 (Jaume Casadesús, <https://bio-protocol.org/e1488>, IRTA, Lleida, Spain) that enables the extraction of RGB indexes in relation to different color properties of potential interest [29]. Derived from the HIS (hue–intensity–saturation) color space, average values from all the pixels of the image were determined for hue, referring to the color tint; saturation, an indication of how much the pure color is diluted with white color; and intensity, as an achromatic measurement of the reflected light. In addition, the portion of pixels with hue classified as green was determined with the green area (GA) and greener area (GGA) indexes. GA is the percentage of pixels in the image with a hue range from 60° to 180° , including yellow to bluish-green color values. Meanwhile, GGA is more restrictive, because it reduces the range from 80° to 180° , thus excluding the yellowish-green tones. Both indexes are also used for the formulation of the crop senescence index (CSI) [30], which provides a scaled ratio between yellow and green pixels to assess the percentage of senescent vegetation. From the CIELab and the CIELuv color space models (recommended by the International Commission on Illumination (CIE) for improved color chromaticity compared to HIS color space), dimension L^* represents lightness and is very similar to intensity from the HIS color

space, whereas a^* and u^* represent the red–green spectrum of chromaticity, and b^* and v^* represent the yellow–blue color spectrum [31]. Besides the Breedpix indexes mentioned, two other indexes were measured with digital values of the red, green, and blue bands derived from the RGB color model. The normalized green–red difference index (NGRDI) is similar to the NDVI, but uses green instead of near-infrared (NIR) bands [32]. The triangular greenness index (TGI) estimates chlorophyll content based on the area of a triangle with the three points corresponding to the red, green, and blue bands [33].

Table 3. Sensors and cameras used during this experiment and their major specifications.

Measure	Sensor/Camera and Approximated Cost	Image	Major Specifications
RGB indexes	Sony ILCE-QX1 <500 €		20.1 Megapixel. Sensor size: 23.20 × 15.40 mm. Focal length: 35 mm. Triggered and exposure time. programed in automatic mode.
	Panasonic Lumix GX7 <500 €		16 Megapixels. Sensor size: 17.3 × 13.0 mm. Focal length: 35 mm. Triggered and exposure time programed in automatic mode.
Multispect. indexes	Tetracam micro-MCA12 <25,000 €		Incident Light Sensor (ILS). 15.6 Megapixels. Sensor size: 6.66 × 5.32 mm. Wavelength range: 450 to 950 nm.
	Trimble GreenSeeker Handheld Crop Sensor <500 €		Wavelength range: 670 and 840 nm. Field of view: 25 cm (1 m from the canopy).
Canopy temperature	Raytek PhotoTemp™ MXSTM TD infrared thermometer <300 €		Temperature range: −30 to 900 °C. Wavelength range: 8 to 14 μm.
	FLIR Tau2 640 thermal imaging camera < 8000 €		With a VOx uncooled microbolometer equipped with a TeAx Thermal Capture 2.0. Temperature range: −55 to 95 °C. Wavelength range: 7.5 to 13.5 μm.
Pigment content	Dualex Force-A <4000 €		Measured area: 5 mm in diameter Sample thickness: 1 mm maximum Light sources: 5 LED; 1 UV-A, 1 red and 2 near NIR (near-infrared)

2.4. Multispectral Vegetation Indexes

The normalized difference index was determined first at ground level (NDVI.g) for each plot using a portable active sensor, the GreenSeeker handheld crop sensor (Trimble, Sunnyvale, CA, USA), by passing the sensor over the middle of each plot at a constant height of 0.5 m above and perpendicular to

the canopy, between 11:00 to 13:00 h. Alongside this, a Tetracam micro-MCA (Multiple Camera Array) 12 (Tetracam Inc., Chatsworth, CA, USA) was used for assessment of the aerial multispectral data. The camera consists of twelve independent image sensors and optics, each with user configurable filters of center wavelengths and full-width half-max bandwidths (450 ± 40 , 550 ± 10 , 570 ± 10 , 670 ± 10 , 700 ± 10 , 720 ± 10 , 780 ± 10 , 840 ± 10 , 860 ± 10 , 900 ± 20 , 950 ± 40 nm). The images captured were passed to twelve separate flash memory cards. Moreover, it has one camera sensor dedicated to ILS (incident light sensor) facing upwards, that uses micro-filters to provide an accurate band-by-band reflectance calibration in real-time. The flights with the multispectral camera were performed at noon (between 12:00 and 14:00 h). After flights for data acquisition, the multispectral images from each band were aligned and calibrated to reflectance using PixelWrench II version 1.2.2.2 (Tetracam, Chatsworth, CA, USA). A suite of multispectral indexes was calculated from the different bands using custom code developed in FIJI and integrated within the MosaicTool software. The formulation of both the RGB and multispectral indexes is detailed in Table 4.

Table 4. Indexes derived from the RGB and multispectral cameras. The wavelengths used in the formulation of the multispectral indexes have been adapted slightly based on the multispectral micro-MCA Tetracam camera. * Note that for the PRI index, B550 is used instead of the original B531 by the cited reference study.

Target Group	Index	Formula	Type; Bands	Ref
Vegetation cover	Green Area (GA)	$60^\circ < Hue < 180^\circ$	RGB; HIS color model	[29]
	Greener Area (GGA)	$80^\circ < Hue < 180^\circ$	RGB; HIS color model	[29]
Greenness	Crop Senescence Index (CSI)	$\frac{(GA-GGA)}{GA}$	RGB; HIS color model	[30]
	a*; b*		RGB; CIElab color model	[29]
	u*; v*		RGB; CIEluv color model	[29]
	Normalized Green-Red Difference Index (NGRDI)	$\frac{(Green\ DN-Red\ DN)}{(Green\ DN+Red\ DN)}$	RGB; Red and Green bands	[33]
	Triangular Greenness Index (TGI)	$-0.5 \cdot [190 \cdot (Red\ DN - Green\ DN) - 120 \cdot (Red\ DN - Blue\ DN)]$	RGB; Red, Green and Blue bands	[33]
	Normalized Difference Vegetation Index (NDVI)	$\frac{(B840-B670)}{(B840+B670)}$	Multispectral; Red, NIR	[34]
	Soil Adjusted Vegetation Index (SAVI)	$\frac{(1+L) \cdot (B840-B670)}{(B840+B670+L)}$ Intermediate vegetation, L = 0.5	Multispectral; Red, NIR	[35]
	Optimized soil-adjusted vegetation index (OSAVI)	$\frac{(B780-B670)}{(B780+B670+0.16)}$	Multispectral; Red, NIR	[36]
	Renormalized Difference Vegetation Index (RDVI)	$\frac{(B840-B670)}{\sqrt{(B840+B670)}}$	Multispectral; Red, NIR	[37]
	Enhanced Vegetation Index (EVI)	$\frac{2.5 \cdot (B840-B670)}{(B840+(6 \cdot B670)-(7.5 \cdot B45))}$	Multispectral; Blue, Red, NIR	[38]

Table 4. Cont.

Target Group	Index	Formula	Type; Bands	Ref
Leaf Pigments	Modified Chlorophyll Absorption Ratio Index (MCARI)	$(B700 - B670) - 0.2 \cdot (B700 - B550) \cdot \left(\frac{B700}{B670}\right)$	Multispectral; Green, Red, NIR	[22]
	Transformed Chlorophyll Absorption Index (TCARI)	$3 \cdot (B700 - B670) - 0.2 \cdot (B700 - B550) \cdot \left(\frac{B700}{B670}\right)$	Multispectral; Green, Red, NIR	[39]
	TCARI/OSAVI ratio	$\frac{TCARI}{OSAVI}$	Multispectral; Green, Red, NIR	[39]
	Anthocyanin Reflectance Index 2 (ARI2)	$B840 \cdot \left(\frac{1}{B550} - \frac{1}{B700}\right)$	Multispectral; Blue, Red, NIR	[40]
	Carotenoid Reflectance Index 2 (CRI2)	$\left(\frac{1}{B550} - \frac{1}{B700}\right)$	Multispectral; Blue, Red	[41]
Photosynthetic Activity	Photochemical Reflectance Index (PRI)*	$\frac{(B550 - B570)}{(B550 + B570)}$	Multispectral; Green	[42]
	Chlorophyll Carotenoid Index (CCI)	$\frac{(B550 - B670)}{(B550 + B670)}$	Multispectral; Green, NIR	[43]
Water content	Water Band Index (WBI)	$\frac{(B970)}{(B900)}$	Multispectral; NIR	[21]

2.5. Canopy Temperature

Canopy temperature (CT) was measured at noon (12:00–14:00 h) from ground level and aerially. For the ground measurements, a PhotoTemp™ MXSTM TD infrared thermometer (Raytek, Santa Cruz, USA) was used, pointing towards the canopy at a distance of about 1 m and in the opposite direction to the sun. Simultaneously, air temperature was measured across the plots using a thermos-hygrometer (Testo 177-H1 Logger, Lenzkirch, Germany). The difference between the ambient and the canopy temperature, known as the canopy temperature depression (CTD) [44], was calculated as follows (Equation (2)):

$$CTD = AT - CT. \quad (2)$$

For the aerial measurements, the canopy temperature was measured using a FLIR Tau2 640 thermal imaging camera (FLIR Systems, Nashua, NH, USA) with a VOx uncooled microbolometer equipped with a TeAx Thermal Capture 2.0 (TeAx Technology, Wilnsdorf, Germany), for recording full resolution thermal video (640 × 520 pixels at 20 frames per second). This camera included a thermal couple sensor that measured the actual temperature of the camera sensor, which was used to correct for temperature fluctuations of the VOx sensor during the flight. The thermal images were first exported using TeAx ThermoViewer v1.3.12 software (TeAx Technology, Wilnsdorf, Germany) in raw 16-bit TIFF format as Kelvin × 10,000, and converted to 32-bit temperatures in celsius using a custom batch processing macro function in FIJI [45], also integrated within the MosaicTool software. CT aerial measurements corresponded to average temperature over all the pixels of the plot images. CTD was also calculated using the UAV CT data using the same formula as in Equation (2).

2.6. Leaf Pigment Assessment

Leaf pigment contents were measured using a leaf-clip portable sensor Dualex Force-A (Dualex, Orsay, France) that measured chlorophyll non-destructively, and flavonoids and anthocyanins, as

unitless indexes [46]. In addition, it calculated the nitrogen balance index (NBI), which is the chlorophyll/flavonoids ratio related to the nitrogen and carbon allocation [47]. The Dualex operated with a UV excitation beam at 357 nm, corresponding to the maximum absorption for flavonoids; another LED that operated in the green band for anthocyanins; a red reference beam at 650 nm, corresponding to the absorption for chlorophyll; and two other references in the near-infrared. For each plot, five flag leaves were selected randomly, and the values were averaged. The measurements were done at the adaxial leaf side and in a middle position of the blade between the leaf base and the apex. Dualex measurements were carried out from 10:00 to 12:00 h.

2.7. Statistical Analysis

Data was analyzed statistically using the open source software R [48] and RStudio 1.0.44 [49] (R Foundation for Statistical Computing, Vienna, Austria). Means and standard errors of the GY and all the measurements and indexes were calculated. The effects of growing conditions (water regime and late-planting), genotypes, and their interaction with GY and the remote sensing measurements were determined through a two-factor analysis of variance (ANOVA) for each sample. Differences were considered significant at p -value ≤ 0.05 . Fisher's LSD (Least significant difference) test was used to determine post hoc differences at each growing condition between the cultivars. To analyze the relationship between the measurements and GY, bivariate Pearson correlation coefficients were calculated. For a further dissection of the genotypic effect on these correlations, broad-sense heritabilities (H^2) and genetic correlations (r_g) were computed using Meta-R (Multi-Environment Trial Analysis with R for Windows), version 6.01 [50]. Genetic variance components were computed across the genotypes for each growing condition as the ratio of the square root of the among genotype variance to the mean value of the corresponding GY or measurement across all genotypes and across the interaction of genotypes and replicates. The broad-sense heritability was calculated as follows (Equation (3)):

$$H^2 = \frac{\sigma_g^2}{\sigma_g^2 + \sigma_{g*Rep}^2 + \frac{\sigma_e^2}{n_{Rep}}}, \quad (3)$$

where σ_g^2 , σ_{g*Rep}^2 , and σ_e^2 are the genotype, genotype*replicate, and error variance components, and n_{Rep} is the number of replicates. Genetic correlations (r_g) between remote sensing indices and GY were calculated as follows (Equation (4)):

$$r_g = \frac{COV_{Index*GY}}{\sqrt{\sigma_{Index}^2 + \sigma_{GY}^2}}, \quad (4)$$

where $COV_{index*GY}$ is the covariance between the index and the GY, σ_{index}^2 is the variance component of the index, and σ_{gy}^2 is the variance component of GY.

3. Results

3.1. Effects of the Growing Conditions on Yield

Significant differences in grain yield were reported in relation to the growing conditions and the genotypes used (Table 5). The highest-yielding conditions were found under normal planting supported with irrigation—lack of irrigation reduced the yield by almost half. The heat stress effect caused by late-planting also reduced the yields of all the genotypes in comparison to the normal planting with supplementary irrigation conditions.

Table 5. Grain yield (Mg/ha) of the set of modern (semi dwarf) durum wheat cultivars across the imposed growing conditions. Cultivars are ordered from the highest-yielding to the lowest. Values are mean \pm standard error of three replicates per cultivar. Different letters (a, b, c, d) indicate significant differences between cultivars within each growing condition according to Fisher's LSD test. Significance levels of the ANOVAs: ** $P < 0.01$; *** $P < 0.001$.

Supplementary Irrigation		Rainfed		Late-Planting	
Olivadur	6.03 \pm 0.18 a	Olivadur	3.58 \pm 0.13 a	Euroduro	5.06 \pm 0.07 a
Burgos	5.67 \pm 0.23 ab	Athoris	3.28 \pm 0.08 ab	Burgos	4.87 \pm 0.12 ab
Sculpur	5.34 \pm 0.03 abc	Claudio	3.22 \pm 0.10 ab	Claudio	4.62 \pm 0.08 abc
Euroduro	5.31 \pm 0.12 abc	Kiko Nick	3.14 \pm 0.14 ab	Olivadur	4.44 \pm 0.09 abcd
Iberus	5.21 \pm 0.06 abc	Avispa	3.08 \pm 0.17 ab	Sculpur	4.31 \pm 0.05 abcd
Claudio	5.19 \pm 0.07 abc	Burgos	3.06 \pm 0.11 ab	Iberus	4.21 \pm 0.13 bcde
Vitron	5.14 \pm 0.12 abc	Amilcar	3.06 \pm 0.06 ab	Athoris	4.19 \pm 0.04 bcde
Athoris	5.08 \pm 0.22 abc	Dorondon	3.04 \pm 0.07 ab	Solea	4.01 \pm 0.12 cdef
Kiko Nick	5.07 \pm 0.19 abc	Sculpur	2.88 \pm 0.05 abc	D. Norman	3.98 \pm 0.03 cdef
Regallo	5.02 \pm 0.14 abc	Regallo	2.83 \pm 0.15 abc	Regallo	3.89 \pm 0.11 cdefg
Dorondon	4.96 \pm 0.16 abcd	Vitron	2.81 \pm 0.08 abc	Vitron	3.78 \pm 0.02 cdefg
Pedroso	4.92 \pm 0.22 abcd	Iberus	2.73 \pm 0.15 abcd	Saragolla	3.74 \pm 0.17 defgh
Amilcar	4.80 \pm 0.11 abcd	D. Ricardo	2.72 \pm 0.14 abcd	D. Ricardo	3.69 \pm 0.11 defghi
Avispa	4.76 \pm 0.16 abcd	Euroduro	2.65 \pm 0.10 abcd	Dorondon	3.50 \pm 0.10 efghi
Saragolla	4.74 \pm 0.17 abcd	D. Norman	2.63 \pm 0.12 abcd	Kiko Nick	3.45 \pm 0.10 efghi
Gallareta	4.71 \pm 0.25 abcd	Simeto	2.59 \pm 0.20 abcd	Gallareta	3.43 \pm 0.11 efghi
Mexa	4.59 \pm 0.13 abcd	Gallareta	2.57 \pm 0.06 abcd	Avispa	3.24 \pm 0.05 fghi
Sole	4.55 \pm 0.17 abcd	Mexa	2.52 \pm 0.12 abcd	Amilcar	3.18 \pm 0.06 ghi
D. Ricardo	4.48 \pm 0.06 bcd	Pedroso	2.50 \pm 0.11 abcd	Mexa	3.08 \pm 0.13 hi
Simeto	4.11 \pm 0.14 cd	Arcobaleno	2.34 \pm 0.15 bcd	Arcobaleno	3.08 \pm 0.05 hi
D. Norman	4.10 \pm 0.09 cd	Saragolla	2.27 \pm 0.14 bcd	Pedroso	3.06 \pm 0.07 hi
Arcobaleno	4.05 \pm 0.11 cd	Solea	1.82 \pm 0.06 cd	Simeto	2.95 \pm 0.08 i
Core	3.46 \pm 0.04 d	Core	1.61 \pm 0.08 d	Core	3.05 \pm 0.18 hi
Mean	4.84 \pm 0.04	Mean	2.74 \pm 0.04	Mean	3.78 \pm 0.04
ANOVA	0.003 **	ANOVA	0.002 **	ANOVA	0.000 ***

3.2. Phenotypic Variability of the Vegetation Indexes, Canopy Temperature, and Pigment Measurements Assessing GY Differences

Over the growing season, large amounts of phenotypic data were generated from each of the experimental conditions (Supplementary Tables S1–S5). The performance of the remote sensing indexes varied considerably across the growing conditions. Differences in the relationships of the indexes with yield underlay the variation in phenology (Figure 3). For most of the indexes calculated there was a genotypic growing effect, particularly for the RGB and multispectral measurements. Genotypic differences in the thermal approximations were clearly found at the beginning of heading in the rainfed trial. For the rest of the conditions, genotypic differences in the CT were only revealed for the aerial measurements.

Under the high-yielding conditions corresponding to the support irrigation plots, all of the measured indexes presented significant correlations to yield before anthesis. GA was the RGB index measured from ground that best correlated with GY during anthesis ($r = 0.545$), increasing in strength at grain filling ($r = 0.684$) and decreasing again with maturity ($r = 0.435$). In terms of multispectral measurements, during anthesis the correlations obtained were very low but increased during grain filling (Figure 4), with the best GY assessments being achieved by the NDVI ($r = 0.639$ measured from the ground, and $r = 0.545$ aerially) and its reformulations, the soil adjusted vegetation index (SAVI, $r = 0.651$) and the renormalized difference vegetation index (RDVI, $r = 0.647$). The thermal measurements showed a negative correlation with GY but the correlation coefficients were low. Finally, no significant correlations were reported from the pigment measurements derived from the Dualex (Supplementary Table S6).

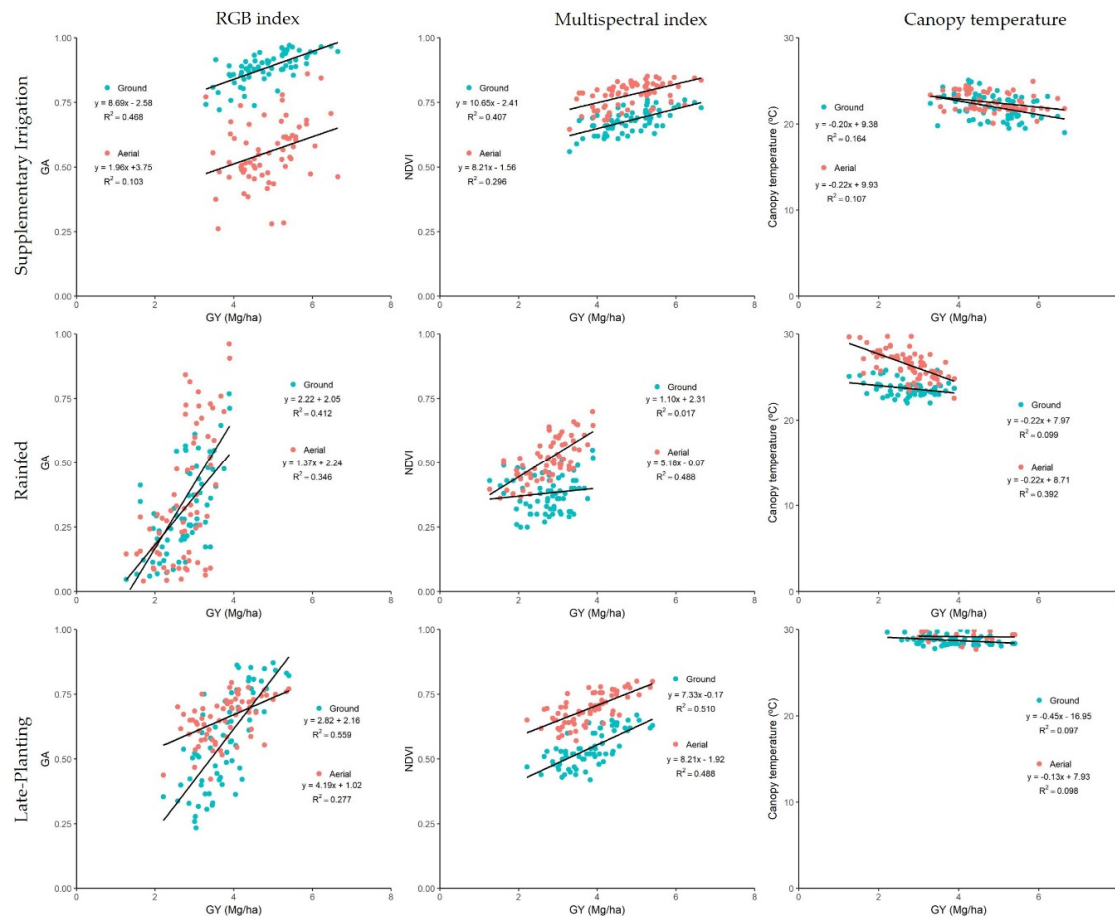


Figure 4. Relationships between grain yield with the RGB index green area (GA) (left), the multispectral index NDVI (middle) and the canopy temperature (right), measured from the ground level (red points) and from the aerial level (blue points) during grain filling for the supplementary irrigation (top), the rainfed (middle), and the late-planting (bottom) growing conditions. Correlations were studied across the 72 plots from each growing condition.

3.3. Evaluation of GY and Remote Sensing Traits Heritability

To characterize the impact of the genetic diversity on GY and the remote sensing measurements, broad-sense heritability was estimated. The GY heritability calculated for the stressed conditions corresponding to rainfed conditions ($H^2 = 0.620$) and late-planting ($H^2 = 0.855$) was much higher than the GY heritability calculated for the supplementary irrigation condition ($H^2 = 0.206$). Besides this, to validate the strength of the indexes as predictors of GY differences between genotypes, the products between the broad-sense heritability and the determination coefficient of the genetic correlations ($r_g \times H^2$) were calculated for a selection of measurements that correlated highly to yield (Figure 5). For the support irrigation trial, most of the values of that product exceeded the H^2 of GY, whereas in the case of rainfed conditions, the product values were generally lower than the H^2 of GY, although some were still higher. Regarding late-planting conditions, the indexes during anthesis had lower H^2 and $r_g \times H^2$ products than the H^2 of GY, but both approximations overtook during grain filling.

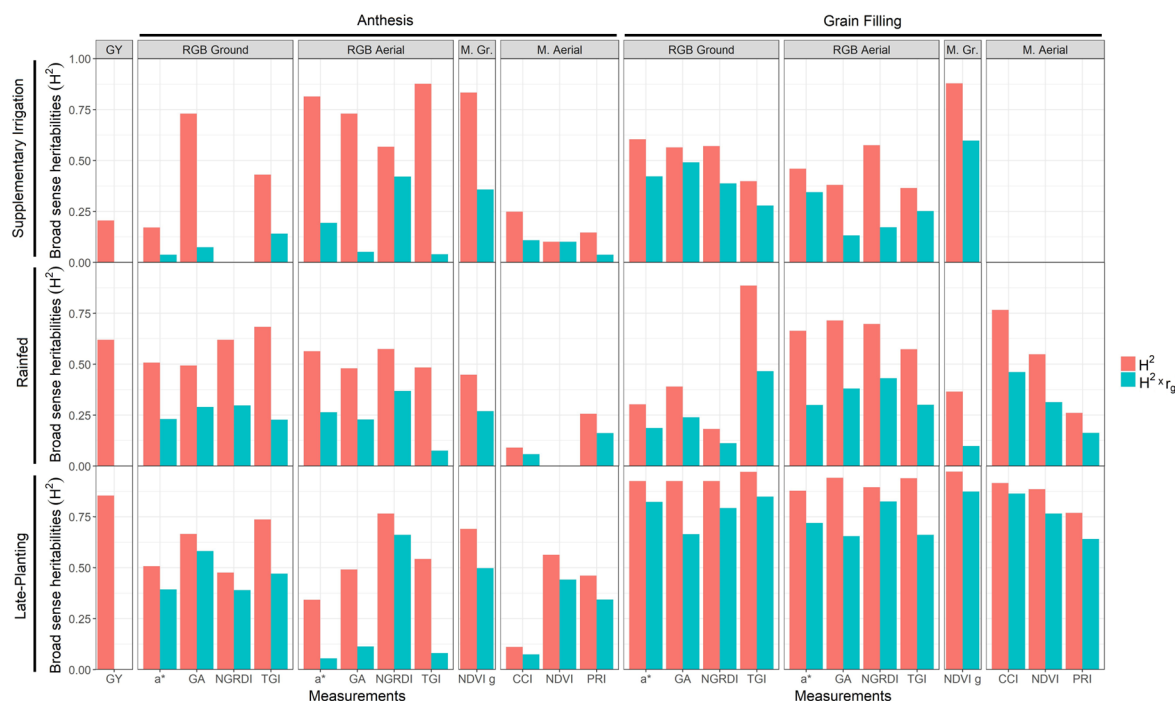


Figure 5. Bar graph comparison of the grain yield and the H^2 (orange) and $H^2 \times r_g$ (blue) indexes of a selection of indexes.

3.4. GY Predictive Models

Using these indexes, which presented the highest correlations with GY at every phenological stage, step-wise linear regression models were calculated in order to generate GY prediction models (Table 6). The results indicated that grain filling was the optimal stage for predicting GY in this study, particularly in the late-planting conditions, where the models explained more than 50% of the yield variability. Additionally, a stepwise analysis was performed within each growing condition, with GY as a dependent variable and the full set of RGB, multispectral, and thermal indexes and measurements from all the sampling dates as independent variables. For the irrigation trial, the equation combined the NGRDI from anthesis, the PRI from grain filling, and the hue from late grain filling. For the rainfed trial, the connection between assessment of the NGRDI at heading, the CT during anthesis, and the NDVI at grain filling far outperformed any of the previous regressions. In the case of late-planting, the combined equation was also a better predictor of GY, using the ground vegetation cover measurement via GGA, the SAVI during anthesis, and the CCI at grain filling.

Finally, for the purpose of testing how accurately the prediction models were, the success rate of prediction for the five highest yielding varieties with each equation was calculated. Most of the equations were correct 60% of the time. Unexpectedly, the equation derived from the CT measurement during anthesis under rainfed conditions, which was the equation explaining most the GY variation, only managed to predict two of the five highest-yielding cultivars correctly. The only equation that achieved a 100% success rate was the one using the CCI during grain filling under late-planting conditions.

Table 6. Multilinear regression (stepwise) of grain yield (GY) as a dependent variable and the remote sensing traits (RGB and multispectral indexes and the thermal measurements) measured both from the ground and aerially as independent variables. Regressions were studied across plots (n = 72) within each growing condition (supplementary irrigation, rainfed, and late-planting). The strength in the prediction of the five highest-yielding cultivars was determined (PS%). R², determination coefficient; RSE, residual standard error; A, anthesis; GF, grain filling; LGF, late grain filling; H, heading.

Trial	Phenological Stage	Equation	R ²	RSE	p-Value	PS%	
Supplementary Irrigation	Anthesis	GY = 64.84 NGRDI + 1.68	0.254	0.652	0.000	60	
	Grain Filling	GY = 8.69 GA - 2.85	0.468	0.551	0.000	60	
		GY = 0.00096 TGI - 2.00	0.270	0.645	0.000	40	
		GY = 12.19 SAVI - 1.83	0.423	0.573	0.000	80	
		GY = 26.29 PRI - 0.32	0.287	0.637	0.000	60	
	Senescence	GY = 0.07 Hue + 1.98	0.361	0.603	0.000	60	
		GY = -0.14 a* + 2.43	0.201	0.675	0.000	60	
	Combination	GY = 33.64 NGRDI.A + 11.72 PRI.LGF + 0.04 Hue.LGF - 0.92	0.421	0.583	0.000	80	
	Rainfed	Heading	GY = 0.0009 TGI + 2.00	0.270	0.645	0.000	80
			GY = -0.466 u* - 0.63	0.371	0.478	0.000	40
GY = 63.80 NGRDI + 0.29			0.468	0.440	0.000	60	
Anthesis		GY = -0.08 u* + 1.83	0.340	0.490	0.000	60	
		GY = 4.06 GA - 0.28	0.442	0.450	0.000	60	
		GY = 42.97 NGRDI + 1.59	0.453	0.446	0.000	60	
		GY = 7.95 NDVI - 3.56	0.440	0.451	0.000	60	
		GY = -0.36 CT + 11.71	0.581	0.390	0.000	40	
Grain Filling		GY = -0.10 a* + 2.40	0.413	0.462	0.000	60	
		GY = 2.22 GA + 2.02	0.413	0.462	0.000	60	
		GY = 7.79 NGRDI + 3.12	0.386	0.472	0.000	60	
		GY = 5.18 NDVI + 0.07	0.489	0.431	0.000	60	
		GY = 28.12 PRI - 1.67	0.438	0.452	0.000	60	
		GY = 8.88 CCI + 1.76	0.433	0.454	0.000	60	
Combination		GY = -2.94 TCARIO/SAVI + 4.45	0.488	0.431	0.000	80	
		GY = 22.09 NGRDI.A - 0.28 CT.GF - 0.57 NDVI.GF + 9.45	0.632	0.371	0.000	60	
Late-Planting		Heading	GY = -0.11 u* + 1.88	0.366	0.555	0.000	60
			GY = 5.90 GGA - 0.63	0.376	0.551	0.000	60
	GY = 9.19 NGRDI + 1.95		0.349	0.563	0.000	60	
	Anthesis	GY = 7.16 GA - 2.38	0.434	0.524	0.000	60	
		GY = 64.79 NGRDI + 0.43	0.398	0.541	0.000	80	
		GY = 11.52 SAVI - 2.27	0.406	0.537	0.000	80	
GY = -0.43 CT + 15.46		0.414	0.533	0.000	60		
Grain Filling	GY = -0.15 a* + 2.46	0.588	0.447	0.000	80		
	GY = 2.82 GA + 2.16	0.559	0.463	0.000	80		
	GY = 0.0009 TGI + 1.80	0.533	0.476	0.000	80		
	GY = 9.29 SAVI - 0.19	0.563	0.461	0.000	80		
	GY = 13.89 CCI + 0.56	0.568	0.458	0.000	100		
	GY = -1.08 CRI2 + 6.45	0.488	0.499	0.000	80		
Combination	GY = 1.13 GGA.H + 4.03 SAVI.A + 10.05 CCI.GF - 1.51	0.625	0.433	0.000	80		

4. Discussion

4.1. Implications of Growing Conditions on Final GY

Drought (understood as the combination of water stress and heat) and heat stress alone are among the most limiting environmental factors that impact wheat development, inducing many biochemical, molecular, and physiological changes that affect crop yield [51]. In this study, stressed conditions

(rainfed and late-planting) reduced yield substantially in contrast to optimal conditions (supplementary irrigation at the normal planting date), with drought being the most restrictive factor that affected yield. The delay in the sowing date exposed cultivars to increased temperatures during the entire growth cycle, but particularly during the reproductive stages. Meanwhile, grain filling occurred during May in the normal planting trials, with the mean temperature for this month being 19.95 °C; this development stage in the late planting trials took place during late May and the first half of June, and the temperatures rose to 25.62 °C. The temperature established as optimal for the phases of grain filling is around 22 °C and exposure to higher temperatures can significantly decrease GY due to the reduction in the time to capture resources [52]. Moreover, an increase in temperature also results in increases in respiration losses, including dark respiration [53,54] and photorespiration [55], therefore affecting yield negatively. Previous studies have concluded that the response of the crop to shifting the planting date is a region-specific adaptation strongly influenced by climate conditions [56–58]. The loss of yield reported in this study agrees with the model-predicted winter wheat yields in semi-arid regions [59].

4.2. Ability of the Remote Sensing Measurements to Assess Genotypic Differences in Yield under Different Growing Conditions

Given their versatility, remote sensing techniques are currently the most commonly used approaches in HTPP [9], leading to the possibility of generating large amounts of data, as can be observed in this study. The considerable variation in the range of management practices used has greatly influenced wheat cultivar performance, proving that finding the most suitable timing of growth stages to measure remote sensing indexes remains entirely dependent on the target environment [60]. The measurements were performed at critical growth stages for the prediction of yield, as previously reported by Fernandez-Gallego et al. [61]. Post-analysis of this information indicates how crop development can be visualized through the evolution of the indexes and, thus, these trends can be related to crop parameters. Therefore, it is necessary to dissect all these data to determine what needs to be measured, when it needs to be measured, and how it should be measured in relation to our purpose, which in this instance is forecasting yield.

During the phases of ear emergence and flowering, the highest correlations with GY (for the three conditions) were obtained with indexes that were associated with the assessment of vegetation cover. Heading and anthesis are two critical growing stages because an appropriate heading and flowering time will help cultivars maximize their yield potential [62]. As most of the carbohydrates for grain filling are formed after heading [63], a larger leaf area is positively correlated with GY, determining the future number of grains and their weight [64,65]. Derived from the RGB images, the GA and GGA indexes are reliable estimations of the crop coverage of the soil, because they represent the percentage of green pixel values per plot [29,66]. Besides this, vegetation cover can also be determined by assessing how green the plot is on average, such as the a^* and u^* measurements from the CIElab and the CIEluv color spaces, where the values go from high negative values (green) to low negative or even positive values (lack of green), or the NGRDI index, which is the normalized difference between green and red reflectance. Alongside this, the multispectral indexes use the difference between the NIR and red bands, because this difference is larger for green vegetation and declines to near 0 for soil, making the NDVI suitable for vegetation coverage [67]. The NDVI correlations were improved through the index's reformulations as SAVI and OSAVI, which include parameters for reduction of the brightness effect of the soil [35,36]. In accordance with Duan et al. [68], who dynamically monitored NDVI during a growing season for contrasting wheat cultivars and growing conditions, we also reported a higher correlation with GY during the anthesis period. In most cases, the spectral-resolution precision of the multispectral indexes provides benefits in assessing genotypic differences in GY, but when canopies were found to be very dense (for example under support irrigation during most of the reproductive period), the vegetation indexes reported values near their saturation point. In these cases, the much higher spatial resolution offered by the RGB images allowed indexes like the NGRDI or TGI to perform close to or even surpass the multispectral indexes. However, the values of these

indexes responded greatly to stress applications, with drought and heat stress decreasing the index values notably, exhibiting a wider range of values corresponding to the genotypic performance of the cultivars under each treatment and reporting more robust correlations.

Moving on to grain filling, the total photosynthetically active area (i.e., the green vegetation area) during this stage has been reported as being very closely related to the final GY [69]. The decrease in canopy greenness due to the ripening process was markedly synchronized with the values of the vegetation indexes. Therefore, as senescence varies considerably depending on genotype [70], stay-green and early senescence phenotypes can be easily identified, for example, with the NDVI [71,72]. This is of importance for selecting genotypes with an extended duration of active photosynthesis, particularly under conditions that tend to accelerate senescence [73]. With regard to the assessment of genotypic differences in GY, our results showed that the most suitable phenological stage for conducting measurements was around the last stages of grain filling, detecting genotypic differences in canopy greenness and, thus, stay-green, similar to previous studies monitoring wheat trials repeatedly over the entire growing season [74]. Stay-green has been principally associated with extended periods of photosynthetic activity and maintaining the supply of assimilated carbon in order to ensure that grain mass is maximized. Thus, a longer duration of flag leaf greenness through GF has been associated with an increased yield wheat [75]. Moreover, Christopher et al. [72] also concluded that, for wheat, the high correlations between NDVI and yield obtained during GF were due to the fact that this was the key phenological stage for assessing genotypic differences in senescence dynamics. However, some studies in bread wheat, such as Kichey et al. [76] and Derkx et al. [77] have reported a lack of yield increase while retaining green leaf area for longer during GF. To overcome these inconsistencies may require examining plant biomass, additional information about pigment content, and the regulatory processes of photosynthesis, which could help to further understand the genetic differences in yield.

Indeed, assessing differences in the photosynthetic capacity, independently of the green biomass, can be of a great importance. For instance, changes in photosynthesis nearly parallel changes in chlorophyll content. The chlorophyll-related indices measured (chlorophyll from the leaf sensor, and the TGI, transformed chlorophyll absorption index (TCARI), MCARI, and CCI assessed at the canopy level) showed how the pigment content increased until anthesis, and then started decreasing during grain filling. Regarding its performance in assessing yield, on one side, the leaf relative chlorophyll content measured with the leaf sensor did not correlate well with GY. These readings provide useful information for diagnosing plant N status and, by the time N is a limiting factor, it may work efficiently as a GY predictor [78]. However, without nutrient restrictions, the leaf chlorophyll content–GY relationship is not so clear. Moreover, it is only measured in the flag leaf, not across the canopy. Based on similar results, Monostori et al. [79] concluded that relative chlorophyll content values should be calibrated according to the cultivars used and depending on their performance. On the other hand, chlorophyll measurements derived from the RGB and multispectral images did show some significant correlations with GY. Taking into account that, while pigment-meters like the Dualex estimate the chlorophyll concentration using the last developed leaves and thus the last to senesce, the HTPP reflectance indexes related to pigment content are assessed at the canopy level. Thus, while still being sensitive to chlorophyll content, any differences present in green biomass may also influence the pigment measurements and the indexes will measure the total physical volume of chlorophyll at the canopy.

Apart from chlorophyll assessments, the actual photosynthetic capacity can be determined with the CCI and PRI indexes. Both indexes use narrowband reflectance at 531 nm, located between two broad bands of strong pigment absorption related to chlorophylls a and b, and they help to separate more steady-state photosynthetic pigments from those related to photosynthetic stress and efficiency. The photochemical reflection index (PRI) was formulated to assess how efficiently radiation is used by plants during photosynthesis [80], as it is highly sensitive to changes in the short-term xanthophyll cycle [81]. Distinct from the PRI, the chlorophyll carotenoid index (CCI) also includes information from red reflectance, indicating changes in the chlorophyll to carotenoid ratio [43]. Therefore, these

indexes are suitable measurements for estimation of the photosynthetic variability induced by heat and drought. The best performance of these indexes occurred with measurements made during the grain filling stage, owing to their potential to detect the photoprotective response to excess light [82]. Because radiation is available in excess in the Mediterranean Basin [83], photo-protection mechanisms are needed to prevent cell damage and to ensure that plant metabolism continues normally [42], so radiation use efficiency is a key trait under such conditions [84].

Stomatal regulation is a key determinant of plant photosynthesis and is highly influenced by the surrounding environment. As an alternative to the direct assessment of leaf stomatal conductance, measuring the canopy temperature (CT) provides an instantaneous proxy of plant water status [85]. Stomatal closure induced by environmental stress will cause an increase in leaf temperature. Thus, negative correlations were reported between the canopy temperature and GY. Assuming that the normal season planting and the support-irrigated trial represented close to optimal growing conditions, there should have been no disturbances affecting stomatal conductance. Still, considering the low correlations observed, the pattern observed can be related to the capability of genotypes to be more or less photosynthetically active. Under non-water-limited conditions, a cooler CT has been associated with genetic gains in wheat yield due to higher stomatal conductance and greater maximum photosynthetic rates [86]. On the other hand, the CT correlation with grain yield for the stressed conditions (rainfed and late-planting) was clearly stronger than in the supplemental irrigation trial, which reported negative correlations. The genotypes that produced the lowest GY presented elevated CT during the anthesis and grain filling periods, and vice versa. Hence, genotypes with a higher resistance to drought and heat can be identified as plants with cooler leaves [87]. Therefore, CT measurements characterize the crop physiologically and in a way that is complimentary to assessing plant density or greenness.

To effectively utilize the remote sensing measurements to assess GY, predictive models were calculated using step-wise regressions. Most of the best grain yield predictors obtained were formulated using traits measured during grain filling. Even so, models combining various measurements taken at different phenological stages greatly improved the prediction capacity. The potential yield of a crop is given by the interception of irradiance of the canopy, but it is also determined by the conversion of that irradiance into chemical energy [88]. The incorporation of high-throughput monitoring into prediction models enables more accurate selection of superior breeding lines [89,90]. The models developed here incorporated a vegetation cover measurement during the pre-anthesis and anthesis phases to assess crop density, an approximation of the rate of photosynthesis applied to the estimation of the light use efficiency (PRI, CCI) or the stomatal conductance (CT) during grain filling, and finally a measurement of the delay in senescence of the plants. In accordance with our findings, Crain et al. [74] concluded that NDVI and CT could be used for indirect selection for GY under heat and drought, based on their results of trait heritability and correlation to GY.

4.3. Comparative Performance of Ground Versus Aerially Assessed Indexes

The main benefit of incorporating imaging methodologies into aerial-based platforms is that researchers are then able to cover larger experimental areas in less time, thus minimizing the effects of diurnal variation in environmental variables, like changes in radiation and temperature, or the occurrence of clouds [44]. The aerial indexes worked very similarly to the ground measurements, reinforcing their usefulness for high-throughput plant phenotyping in the field.

As counterbalance to the high-throughput capacity of aerial imaging, the platform distance from the canopy led to a loss in image resolution. In the case of RGB measurements, even though the sensor size of the cameras used was very similar (23.20×15.40 mm for the Sony QX1 and 17.3×13 mm for the Olympus OM-D), the distance between the crop and the camera reduced the resolution of the resulting plot level images when they were captured from the aerial HTPP. As an illustration, while the aerial plot images had a resolution of 473×129 pixels, the resolution of the images taken from the ground was 5456×3632 pixels. Despite this restriction, aerial indexes were still highly correlated with

grain yield, especially at grain filling. The reduction in the number of pixels had a greater effect on the assessments related to fractional vegetation cover, such as the indexes derived from the HIS color model, including information of both vegetation and bare soil [91], so the yield prediction capacities of the GA, GGA, and CSI were generally lower when measured from the aerial platform. The other RGB indexes seemed to be less sensitive to this loss in spatial resolution and were better at maintaining the correlation coefficients across platforms. Besides this, it is also important to take into consideration the fact that aerial images are able to assess the whole plot (therefore overcoming canopy heterogeneity), while the ground-based approaches only allow for assessment of less than a tenth of the total plot, and for this reason more than one measurement may be needed. A similar trend was observed with the NDVI assessments, with the GreenSeeker measurements on the ground being slightly better correlated than the aerial measures derived from the multispectral images. This is because this hand-held sensor produces data covering almost the whole plot, with the final value corresponding to the average of 10–20 measurements captured while walking across the plot. When comparing the performance of CT measured from the ground and aurally for GY, a clear difference was found between the two approaches, with CT measured from the UAV showing better results. Traditionally, hand-held infrared thermometers have been used but they can be problematic in large field studies due to the temporal changes during the time required to measure all plots [12]. Because temperature can fluctuate quickly, it is of profound importance to screen the whole trial as quickly as possible, in order to have comparable data across all the plots. The use of UAVs permits the acquisition of thermal images of a large number of plots in a short time, overcoming this environmental variability restriction.

In that sense, aerial remote sensing platforms are an effective way to rapidly monitor crops, particularly in large fields. However, even when UAVs have reached comparatively affordable prices, the associated cost entailed in their employment still makes them a relatively expensive approach in some cases. Besides the price of the platform and the sensors, it is compulsory to pay for vehicle insurance, and a certified pilot and trained operator must be engaged to carry out the flights. Thus, the implementation of an aerial platform in a phenotyping study might demand a considerable initial investment, but later savings in manpower will compensate for the initial investment because there will be fewer employees to pay. Another aspect to consider is the sizeable technical capacity necessary for data processing, from radiometric calibration of the images and the creation of a georeferenced ortho-mosaic to ensure effective and efficient data extraction and analysis. For these reasons, ground-based or hand-held methodologies might be more feasible alternatives in certain circumstances due to their low cost and ease of management. In addition, most ground-based sensors generate measurements with no need for extra time for data processing and index calculation. As proposed by Araus and Kefauver [9] and applied in this study, an innovative option could be the attachment of a camera to a “pheno-pole”. The camera is controlled remotely with a smartphone by Wi-Fi, so it is possible for the pole to be as high as 4 m, allowing measurements of tall crops, like maize or fruit trees. Using ground-based phenotyping methodologies requires more time for data acquisition, but the staff require fewer technical skills, and as indicated above, the post-image treatment is minimal and frequently the software needed for extracting vegetation indices from the images is open access. The RGB indices are clear examples where a range of open access software is already available (<https://integrativecropecophysiology.com/software-development/>). One last point is that drones as objects in airspace are still under discussion within regulatory frameworks and UAV-related laws are in a constant evolutionary progress [92], thus their full implementation in many countries is limited. For these reasons, users need to take stock of the strengths, opportunities, and limitations associated with each sensor and platform and make a choice depending on their objectives. Future improvements will make these technologies more user-friendly and available for all types of end-users [93], and smartphones may play a central role in these solutions.

The time spent on fieldwork in the current study using the aerial platform for RGB imaging was approximately 10 min, including five minutes for pre-flight preparation procedures and five minutes for the flight itself. Before conducting any flight, it is essential to complete certain pre-flight checklist

tasks to ensure that the flight will perform correctly without any technical incidents. The alignment of the raw images onto georeferenced orthomosaics took 15 min. Finally, the semi-automatic extraction and processing of the data took another 15 min. In contrast, the time required for capturing images manually from the ground or using a hand-held sensor, such as the GreenSeeker or a thermal gun, was around 12 min, and the RGB data processing only took five minutes. Nonetheless, leaf clamp meters like the Dualex require longer periods of time because the estimated time per plot is around one minute to capture at least six individual measurements. In small field trials, the throughput differences between the two approaches might seem small, but in large studies the time/cost differences become much greater. Considering this task's calculated time for aerial images acquisition as a reference, we have simulated how long it would take to measure a larger field of 300 plots. Without changing the plot dimensions, a 300-plot field would cover more or less an area of 0.4 Ha. However, the time would not increase much and in less than 10 min the whole field would be screened. Similarly, the pre-processing would also be increased only a bit.

4.4. Repeatability and Applicability of Remote Sensing Measurements for Assessing GY

Success in collecting accurate phenotyping data is intimately connected with heritability of the trait [94]. Broad-sense heritability is a reflection of both the genetic variance and the level of precision that can be achieved within and across trials [95], and sometimes it is termed as repeatability. The heritability metrics assess the quality of the measurements, and these are a key element for implementing such new technologies in breeding programs, because they will help plant breeders to forecast the grain yield behavior of the succeeding generation. The possibility of being able to promptly evaluate the improvement target, in this case grain yield, with an index would permit breeders to make well-informed decisions about the cultivars. According to the results obtained, the most robust measurements were made in the rainfed and the late-planting trial, during grain filling, increasing the confidence of using such measurements for selection under suboptimal growing conditions. Traditional and time-consuming manual measurements of plant height have been used as selection traits for yield improvement. The high estimates of H^2 reported in our results suggest the possibility of using remote sensing measurements to forecast the grain yield behavior of the succeeding generation.

5. Conclusions

It is particularly important to evaluate the response of the remote sensing indexes to the crop genotypic performance in order to implement correctly those methodologies in phenotyping. Knowing which are the remote sensing parameters that best predict genotypic variability in yield and when to measure them will help to develop accurate yield prediction models for phenotyping, which may help to accelerate the selection process in breeding programs. Moreover, a better understanding of the strengths and limitations of these indices may help to forecast production or to improve crop monitoring associated with management practices. In our study, the performance of the set of vegetation indexes studied varied widely across the growing conditions and the phenological stages. Measurements related to the greenness of the canopy were the best for assessing genotypic differences in GY according to the phenotypic and genotypic correlations and heritabilities calculated, regardless of the nature of the data collected (RGB or multispectral). Furthermore, our results proved that grain filling was the best phenological stage to forecast GY among those evaluated. At the beginning of grain filling, vegetation indexes can assess the amount of biomass present, and thus the photosynthetically active area that contributes to the filling of the grain. Moreover, at the end of the stage, we can evaluate the length of this period and see which cultivars stay green (i.e., photosynthetically active) for longer, with their concomitant delay in senescence. Therefore, the RGB-derived vegetation indexes are presented as the most suitable traits to be measured, because despite being a low-cost tool, this set of indexes performed as well as, and sometimes better than, indexes derived from more expensive devices (i.e., multispectral and thermal indexes). Besides this, when studying crop and genotype responses to drought and heat,

canopy temperature assessed from an aerial platform has proven to be a useful addition to the other two categories of remote sensing techniques.

As has been proven in this work, the ground and aerial measurements performed very similarly in terms of assessing GY. For this reason, when scaling to large scale studies, the selection of the platform may depend not only on its cost, but also the time and skill required to conduct the measurements properly. The only exception is canopy temperature, where the simultaneous evaluation of all the plots from the UAV (T.a) performed much better than the temperature measured sequentially from the ground (T.g) in individual plots.

Supplementary Materials: The following are available online at <http://www.mdpi.com/2072-4292/11/10/1244/s1>, Table S1: Effect of growing conditions across phenological stages for the RGB indexes assessed from the ground level, Table S2: Effect of growing conditions across phenological stages for the RGB indexes assessed aeri ally, Table S3: Effect of growing conditions across phenological stages for the multispectral indexes assessed aeri ally, Table S4: Effect of the growing conditions across phenological stages for the thermal measurements, Table S5: Effect of growing conditions across phenological stages for the Dualex measurements, Table S6: Correlation coefficients of the relationships between the pigment measurements with the Dualex and the GY.

Author Contributions: A.G.-R., S.C.K. and J.L.A. conceived and designed the experiment. M.T.N.-T. managed and directed the wheat trials at the experimental station of Colmenar de Oreja (Aranjuez). A.G.-R., J.A.F.-G., O.V.-D. and J.L.A. conducted the field measurements. SCK carried out the flights for the obtainment of the aerial measurements. A.G.-R. processed and analyzed the images, did the statistical analysis and wrote the paper under the supervision of J.L.A. and S.C.K. and the contributions from all the other authors. J.L.A. is the head of the Integrative Crop Ecophysiology research group and Principal Investigator of the MINECO project which funds this research.

Funding: This study was supported by the Spanish project AGL2016-76527-R “Fenotipeado En Trigo Duro: Bases Fisiológicas, Criterios De Selección Y Plataformas De Evaluación”, from the Ministerio Economía y Competitividad of the Spanish Government. A.G.-R. is a recipient of a FPI doctoral fellowship from the same institution. We also acknowledge the support from the Institut de Recerca de l’Aigua and the Universitat de Barcelona. J.L.A. acknowledges the funding support from ICREA, Generalitat de Catalunya, Spain.

Acknowledgments: The authors of this research thank the personnel from the experimental station of INIA at Colmenar de Oreja (Aranjuez) for their continued support of our research. We thank the Integrative Crop Ecophysiology Group members their assistance during the collection of phenotic data during the study. Finally, we thank Jaume Casadesus for providing the Breedpix software.

Conflicts of Interest: The authors declare no conflict of interest.

Abbreviations

MAPAMA	Ministerio de Agricultura y Pesca Alimentación y Medio Ambiente
UAV	Unmanned Aerial Vehicle
RGB	Red-Green-Blue
NDVI	Normalized Difference Vegetation Index
GA	Green Area
CCI	Chlorophyll Content Index
TGI	Triangular Greenness Index
GY	Grain Yield
HTPP	High-Throughput Plant Phenotyping
MET	Multi-Environment Trials
INIA	Instituto Nacional de Investigación y Tecnología Agraria y Alimentaria
SIAR	Servicio de Información Agroclimática para el Regadío
NBI	Nitrogen Balance Index
CT	Canopy Temperature
CTD	Canopy Temperature Depression
ANOVA	Analysis of Variance
H ²	Heritability

r_g	Genetic Correlations
σ_g^2	Genotype Variance
σ_g^2	Genotype Variance
σ_e^2	Error variance
n	Number of Replicates

References

1. Diffenbaugh, N.S.; Giorgi, F. Climate change hotspots in the CMIP5 global climate model ensemble. *Clim. Chang.* **2012**, *114*, 813–822. [[CrossRef](#)]
2. Asseng, S.; Ewert, F.; Martre, P.; Rötter, R.P.; Lobell, D.B.; Cammarano, D.; Kimball, B.A.; Ottman, M.J.; Wall, G.W.; White, J.W.; et al. Rising temperatures reduce global wheat production. *Nat. Clim. Chang.* **2015**, *5*, 143–147. [[CrossRef](#)]
3. Vicente-Serrano, S.M.; Lopez-Moreno, J.I.; Beguería, S.; Lorenzo-Lacruz, J.; Sanchez-Lorenzo, A.; García-Ruiz, J.M.; Azorin-Molina, C.; Morán-Tejada, E.; Revuelto, J.; Trigo, R.; et al. Evidence of increasing drought severity caused by temperature rise in southern Europe. *Environ. Res. Lett.* **2014**, *9*, 1–9. [[CrossRef](#)]
4. Royo, C.; Soriano, J.M.; Alvaro, F. Wheat: A Crop in the Bottom of the Mediterranean Diet Pyramid. In *Mediterranean Identities—Environment, Society, Culture*; IntechOpen: London, UK, 2017. [[CrossRef](#)]
5. Reynolds, M.; Langridge, P. Physiological breeding. *Curr. Opin. Plant Biol.* **2016**, *31*, 162–171. [[CrossRef](#)] [[PubMed](#)]
6. Quintero, A.; Molero, G.; Reynolds, M.P.; Calderini, D.F. Trade-off between grain weight and grain number in wheat depends on G×E interaction: A case study of an elite CIMMYT panel (CIMCOG). *Eur. J. Agron.* **2018**, *92*, 17–29. [[CrossRef](#)]
7. Araus, J.L.; Cairns, J.E. Field high-throughput phenotyping: The new crop breeding frontier. *Trends Plant Sci.* **2014**, *19*, 52–61. [[CrossRef](#)] [[PubMed](#)]
8. Cobb, J.N.; DeClerck, G.; Greenberg, A.; Clark, R.; McCouch, S. Next-generation phenotyping: Requirements and strategies for enhancing our understanding of genotype-phenotype relationships and its relevance to crop improvement. *Theor. Appl. Genet.* **2013**, *126*, 867–887. [[CrossRef](#)]
9. Araus, L.; Kefauver, S.C. Breeding to adapt agriculture to climate change: Affordable phenotyping solutions. *Curr. Opin. Plant Biol.* **2018**, *45*, 237–247. [[CrossRef](#)] [[PubMed](#)]
10. Atzberger, C. Advances in Remote Sensing of Agriculture: Context Description, Existing Operational Monitoring Systems and Major Information Needs. *Remote Sens.* **2013**, *5*, 949–981. [[CrossRef](#)]
11. Araus, J.L.; Kefauver, S.C.; Zaman-allah, M.; Olsen, M.S.; Cairns, J.E. Translating High-Throughput Phenotyping into Genetic Gain. *Trends Plant Sci.* **2018**, *23*, 451–466. [[CrossRef](#)]
12. Deery, D.M.; Rebetzke, G.J.; Jimenez-Berni, J.A.; James, R.A.; Condon, A.G.; Bovill, W.D.; Hutchinson, P.; Scarrow, J.; Davy, R.; Furbank, R.T. Methodology for High-Throughput Field Phenotyping of Canopy Temperature Using Airborne Thermography. *Front. Plant Sci.* **2016**, *7*, 1808. [[CrossRef](#)]
13. Yang, G.; Liu, J.; Zhao, C.; Li, Z.; Huang, Y. Unmanned Aerial Vehicle Remote Sensing for Field-Based Crop Phenotyping: Current Status and Perspectives. *Front. Plant Sci.* **2017**, *8*, 1111. [[CrossRef](#)]
14. Berni, J.A.J.; Member, S.; Zarco-tejada, P.J.; Suárez, L.; Fereres, E. Thermal and Narrowband Multispectral Remote Sensing for Vegetation Monitoring From an Unmanned Aerial Vehicle. *IEEE Trans. Geosci. Remote Sens.* **2009**, *47*, 1–17. [[CrossRef](#)]
15. Yousfi, S.; Kellas, N.; Saidi, L.; Benlakehal, Z.; Chaou, L.; Siad, D.; Herda, F.; Karrou, M.; Vergara, O.; Gracia, A.; et al. Comparative performance of remote sensing methods in assessing wheat performance under Mediterranean conditions. *Agric. Water Manag.* **2016**, *164*, 137–147. [[CrossRef](#)]
16. Vergara-Díaz, O.; Zaman-allah, M.A.; Masuka, B.; Hornero, A.; Zarco-Tejada, P.; Prasanna, B.M.; Cairns, J.E.; Araus, J.L. A Novel Remote Sensing Approach for Prediction of Maize Yield Under Different Conditions of Nitrogen Fertilization. *Front. Plant Sci.* **2016**, *7*, 1–13. [[CrossRef](#)] [[PubMed](#)]
17. Vergara-Díaz, O.; Kefauver, S.C.; Elazab, A.; Nieto-Taladriz, M.T.; Araus, J.L. Grain yield losses in yellow-rusted durum wheat estimated using digital and conventional parameters under field conditions. *Crop J.* **2015**, *3*, 200–210. [[CrossRef](#)]

18. Fernandez-Gallego, J.A.; Kefauver, S.C.; Gutiérrez, N.A.; Nieto-Taladriz, M.T.; Araus, J.L. Wheat ear counting in-field conditions: High throughput and low-cost approach using RGB images. *Plant Methods* **2018**, *14*, 22. [[CrossRef](#)] [[PubMed](#)]
19. Condorelli, G.E.; Maccaferri, M.; Newcomb, M.; Andrade-Sanchez, P.; White, J.W.; French, A.N.; Sciara, G.; Ward, R.; Tuberosa, R. Comparative Aerial and Ground Based High Throughput Phenotyping for the Genetic Dissection of NDVI as a Proxy for Drought Adaptive Traits in Durum Wheat. *Front. Plant Sci.* **2018**, *9*, 1–17. [[CrossRef](#)]
20. Tucker, C.J. Red and photographic infrared linear combinations for monitoring vegetation. *Remote Sens. Environ.* **1979**, *8*, 127–150. [[CrossRef](#)]
21. Peñuelas, J.; Filella, I.; Biel, C.; Serrano, L.; Savé, R. The reflectance at the 950–970 nm region as an indicator of plant water status. *Int. J. Remote Sens.* **1993**, *14*, 1887–1905. [[CrossRef](#)]
22. Daughtry, C.; Walthall, C.L.; Kim, M.S.; Brown de Colstoun, E.; McMurtrey, J.E. Estimating Corn Leaf Chlorophyll Concentration from Leaf and Canopy Reflectance. *Remote Sens. Environ.* **2000**, *74*, 229–239. [[CrossRef](#)]
23. Jackson, R.D.; Reginato, R.J.; Idso, S.B. Wheat canopy temperature: A practical tool for evaluating water requirements. *Water Resour. Res.* **1988**, *13*, 651–656. [[CrossRef](#)]
24. Moran, M.S.; Clarke, T.R.; Inoue, Y.; Vidal, A. Estimating crop water deficit using the relation between surface-air temperature and spectral vegetation index. *Remote Sens. Environ.* **1994**, *49*, 246–263. [[CrossRef](#)]
25. Casadesús, J.; Villegas, D. Conventional Digital Cameras as a Tool for Assessing LAI and Biomass for Cereal Breeding. *New Technol.* **2013**, *56*, 1–27.
26. Gracia-Romero, A.; Kefauver, S.C.; Vergara-Díaz, O.; Zaman-Allah, M.A.; Prasanna, B.M.; Cairns, J.E.; Araus, J.L. Comparative Performance of Ground vs. Aerially Assessed RGB and Multispectral Indices for Early-Growth Evaluation of Maize Performance under Phosphorus Fertilization. *Front. Plant Sci.* **2017**, *8*, 2004. [[CrossRef](#)]
27. Zadoks, J.C.; Chang, T.T.; Konzak, C.F. A decimal code for the growth stages of cereals. *Weed Res.* **1974**, *14*, 415–421. [[CrossRef](#)]
28. Bendig, J.; Bolten, A.; Bennertz, S.; Broscheit, J.; Eichfuss, S.; Bareth, G. Estimating biomass of barley using crop surface models (CSMs) derived from UAV-based RGB imaging. *Remote Sens.* **2014**, *6*, 10395–10412. [[CrossRef](#)]
29. Casadesus, J.; Kaya, Y.; Bort, J.; Nachit, M.M.; Araus, J.L.; Amor, S.; Ferrazzano, G.; Maalouf, F. Using vegetation indices derived from conventional digital cameras as selection criteria for wheat breeding in water-limited environments. *Ann. Appl. Biol.* **2007**, *150*, 227–236. [[CrossRef](#)]
30. Zaman-Allah, M.; Vergara, O.; Araus, J.L.; Tarekgegne, A.; Magorokosho, C.; Zarco-Tejada, P.J.; Hornero, A.; Albà, A.H.; Das, B.; Craufurd, P.; et al. Unmanned aerial platform-based multi-spectral imaging for field phenotyping of maize. *Plant Methods* **2015**, *11*, 35. [[CrossRef](#)] [[PubMed](#)]
31. Pointer, M.R. A comparison of the CIE 1976 colour spaces. *Color Res. Appl.* **1981**, *6*, 108–118. [[CrossRef](#)]
32. Hunt, R.; Cavigelli, M.; Daughtry, C.; McMurtrey, J.E.; Walthall, C.L. Evaluation of Digital Photography from Model Aircraft for Remote Sensing of Crop Biomass and Nitrogen Status. *Precis. Agric.* **2005**, *6*, 359–378. [[CrossRef](#)]
33. Hunt, E.R.; Doraiswamy, P.C.; McMurtrey, J.E.; Daughtry, C.S.T.; Perry, E.M.; Akhmedov, B. A visible band index for remote sensing leaf chlorophyll content at the canopy scale. *Int. J. Appl. Earth Obser. Geoinf.* **2013**, *21*, 103–112. [[CrossRef](#)]
34. Rouse, J.W.; Hass, R.H.; Schell, J.A.; Deering, D.W. Monitoring vegetation systems in the great plains with ERTS. In Proceedings of the Third Earth Resources Technology Satellite (ERTS) Symposium, Washington, DC, USA, 10–14 December 1973; Volume 1, pp. 309–317.
35. Huete, A. A soil-adjusted vegetation index (SAVI). *Remote Sens. Environ.* **1988**, *25*, 295–309. [[CrossRef](#)]
36. Rondeaux, G.; Steven, M.; Baret, F. Optimization of soil-adjusted vegetation indices. *Remote Sens. Environ.* **1996**, *55*, 95–107. [[CrossRef](#)]
37. Roujean, J.-L.; Breon, F.-M. Estimating PAR absorbed by vegetation from bidirectional reflectance measurements. *Remote Sens. Environ.* **1995**, *51*, 375–384. [[CrossRef](#)]
38. Huete, A.; Didan, K.; Miura, T.; Rodriguez, E.P.; Gao, X.; Ferreira, L.G. Overview of the radiometric and biophysical performance of the MODIS vegetation indices. *Remote Sens. Environ.* **2002**, *83*, 195–213. [[CrossRef](#)]

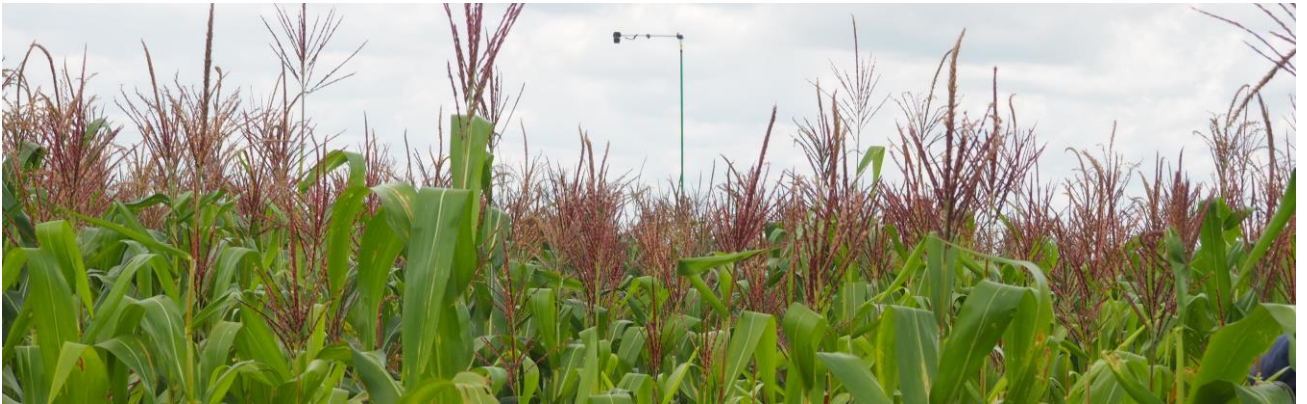
39. Haboudane, D.; Miller, J.R.; Tremblay, N.; Zarco-Tejada, P.J.; Dextraze, L. Integrated narrow-band vegetation indices for prediction of crop chlorophyll content for application to precision agriculture. *Remote Sens. Environ.* **2002**, *81*, 416–426. [[CrossRef](#)]
40. Gitelson, A.A.; Merzlyak, M.N.; Chivkunova, O.B. Optical Properties and Nondestructive Estimation of Anthocyanin Content in Plant Leaves. *Photochem. Photobiol.* **2001**, *74*, 38–45. [[CrossRef](#)]
41. Gitelson, A.A.; Zur, Y.; Chivkunova, O.B.; Merzlyak, M.N. Assessing carotenoid content in plant leaves with reflectance spectroscopy. *Photochem. Photobiol.* **2002**, *75*, 272–281. [[CrossRef](#)]
42. Gamon, J.A.; Peñuelas, J.; Field, C.B. A narrow-waveband spectral index that tracks diurnal changes in photosynthetic efficiency. *Remote Sens. Environ.* **1992**, *41*, 35–44. [[CrossRef](#)]
43. Gamon, J.A.; Huemmrich, K.F.; Wong, C.Y.S.; Ensminger, I.; Garrity, S.; Hollinger, D.Y.; Noormets, A.; Peñuelas, J. A remotely sensed pigment index reveals photosynthetic phenology in evergreen conifers. *Proc. Natl. Acad. Sci. USA* **2016**, *113*, 13087–13092. [[CrossRef](#)]
44. Costa, J.M.; Grant, O.M.; Chaves, M.M. Thermography to explore plant-environment interactions. *J. Exp. Bot.* **2013**, *64*, 3937–3949. [[CrossRef](#)]
45. Kefauver, S.C.; Vicente, R.; Vergara-Díaz, O.; Fernandez-Gallego, J.A.; Kerfal, S.; Lopez, A.; Melichar, J.P.E.; Serret Molins, M.D.; Araus, J.L. Comparative UAV and Field Phenotyping to Assess Yield and Nitrogen Use Efficiency in Hybrid and Conventional Barley. *Front. Plant Sci.* **2017**, *8*, 1–15. [[CrossRef](#)]
46. Cerovic, Z.G.; Masdoumier, G.; Ghozlen, N.B.; Latouche, G. A new optical leaf-clip meter for simultaneous non-destructive assessment of leaf chlorophyll and epidermal flavonoids. *Physiol. Plant.* **2012**, *146*, 251–260. [[CrossRef](#)]
47. Cerovic, Z.G.; Ghozlen, N.B.; Milhade, C.; Obert, M.; Debusson, S.; Le Moigne, M. Nondestructive Diagnostic Test for Nitrogen Nutrition of Grapevine (*Vitis vinifera* L.) Based on Dualex Leaf-Clip Measurements in the Field. *J. Agric. Food Chem.* **2015**, *63*, 3669–3680. [[CrossRef](#)]
48. RStudio Team. *RStudio: Integrated Development for R*; RStudio, Inc.: Boston, MA, USA; Available online: <http://www.rstudio.com/> (accessed on 12 September 2018).
49. *R Core Team R: A Language and Environment for Statistical Computing*; R Foundation for Statistical Computing: Vienna, Austria, 2017.
50. Alvarado, G.; López, M.; Vargas, M.; Pacheco, Á.; Rodríguez, F.; Burgueño, J.; Crossa, J. META-R (Multi Environment Trial Analysis with R for Windows) Version 6.01. 2017. Available online: <https://data.cimmyt.org/dataset.xhtml?persistentId=hdl:11529/10201/> (accessed on 16 December 2018).
51. Prasad, P.V.V.; Staggenborg, S. Impacts of drought and/or heat stress on physiological, developmental, growth, and yield processes of crop plants. In *Response of Crops to Limited Water: Understanding and Modeling Water Stress Effects on Plant Growth Processes Response of Crops*; American Society of Agronomy: Madison, WI, USA, 2008; pp. 301–355.
52. Farooq, M.; Bramley, H.; Palta, J.A.; Siddique, K.H.M. Heat Stress in Wheat during Reproductive and Grain-Filling Phases. *Crit. Rev. Plant Sci.* **2011**, *30*, 491–507. [[CrossRef](#)]
53. Pinto, R.S.; Molero, G.; Reynolds, M.P. Identification of heat tolerant wheat lines showing genetic variation in leaf respiration and other physiological traits. *Euphytica* **2017**, *213*, 1–15. [[CrossRef](#)]
54. Rashid, M.A.; Andersen, M.N.; Wollenweber, B.; Kørup, K.; Zhang, X.; Olesen, J.E. Impact of heat-wave at high and low VPD on photosynthetic components of wheat and their recovery. *Environ. Exp. Bot.* **2018**, *147*, 138–146. [[CrossRef](#)]
55. Long, S.P.; Ort, D.R. More than taking the heat: Crops and global change. *Curr. Opin. Plant Biol.* **2010**, *13*, 241–248. [[CrossRef](#)]
56. Torriani, D.S.; Calanca, P.; Schmid, S.; Beniston, M.; Fuhrer, J. Potential effects of changes in mean climate and climate variability on the yield of winter and spring crops in Switzerland. *Clim. Chang.* **2007**, *34*, 59–69. [[CrossRef](#)]
57. Ghahramani, A.; Kocic, P.N.; Moore, A.D.; Zheng, B.; Chapman, S.C.; Howden, M.S.; Crimp, S.J. The Value of Adapting to Climate Change in Australian Wheat Farm Systems: Farm to Cross-Regional Scale. *Agric. Ecosyst. Environ.* **2015**, *211*, 112–125.
58. Nouri, M.; Homaeae, M.; Bannayan, M.; Hoogenboom, G. Towards shifting planting date as an adaptation practice for rainfed wheat response to climate change. *Agric. Water Manag.* **2017**, *186*, 108–119. [[CrossRef](#)]
59. Weiss, A.; Hays, C.J.; Won, J. Assessing winter wheat responses to climate change scenarios: A simulation study in the U.S. *Great Plains.* **2003**, *58*, 119–147.

60. Altenbach, S.B.; DuPont, F.M.; Kothari, K.M.; Chan, R.; Johnson, E.L.; Lieu, D. Temperature, water and fertilizer influence the timing of key events during grain development in a US spring wheat. *J. Cereal Sci.* **2003**, *37*, 9–20. [[CrossRef](#)]
61. Fernandez-gallego, J.A.; Kefauver, S.C.; Vatter, T. Low-cost assessment of grain yield in durum wheat using RGB images. *Eur. J. Agron.* **2019**, *105*, 146–156. [[CrossRef](#)]
62. Snape, J.W.; Butterworth, K.; Whitechurch, E.; Worland, A.J. Waiting for fine times: Genetics of flowering time in wheat. *Euphytica* **2001**, *119*, 185–190. [[CrossRef](#)]
63. Asana, R.D.; Mani, V.S. Studies in Physiological Analysis of Yield. II. Further Observations on Varietal Differences in Photosynthesis in the Leaf, Stem and Ear of Wheat. *Physiol. Plant.* **1955**, *8*, 8–19. [[CrossRef](#)]
64. Ugarte, C.; Calderini, D.F.; Slafer, G.A. Grain weight and grain number responsiveness to pre-anthesis temperature in wheat, barley and triticale. *Field Crops Res.* **2007**, *100*, 240–248. [[CrossRef](#)]
65. González, F.G.; Slafer, G.A.; Miralles, D.J. Grain and floret number in response to photoperiod during stem elongation in fully and slightly vernalized wheats. *Field Crops Res.* **2003**, *81*, 17–27. [[CrossRef](#)]
66. Lukina, E.V.; Stone, M.L.; Raun, W.R. Estimating vegetation coverage in wheat using digital images. *J. Plant Nut.* **1999**, *22*, 341–350. [[CrossRef](#)]
67. Cabrera-Bosquet, L.; Molero, G.; Stellacci, A.M.; Bort, J.; Nogues, S.; Araus, J.L. NDVI as a potential tool for predicting biomass, plant nitrogen content and growth in wheat genotypes subjected to different water and nitrogen conditions. *Cereal Res. Commun.* **2011**, *39*, 147–159. [[CrossRef](#)]
68. Duan, T.; Chapman, S.C.; Guo, Y.; Zheng, B. Field Crops Research Dynamic monitoring of NDVI in wheat agronomy and breeding trials using an unmanned aerial vehicle. *Field Crops Res.* **2017**, *210*, 71–80. [[CrossRef](#)]
69. Gregersen, P.L.; Culetic, A.; Boschian, L.; Krupinska, K. Plant senescence and crop productivity. *Plant Mol. Biol.* **2013**, *82*, 603–622. [[CrossRef](#)] [[PubMed](#)]
70. Thomas, H.; Ougham, H. The stay-green trait. *J. Exp. Bot.* **2014**, *65*, 3889–3900. [[CrossRef](#)]
71. Christopher, J.; Veyradier, M.; Borrell, A.; Harvey, G.; Fletcher, S.; Chenu, K. Phenotyping novel stay-green traits to capture genetic variation in senescence dynamics. *Funct. Plant Biol.* **2014**, *41*, 1035–1048. [[CrossRef](#)]
72. Christopher, J.T.; Christopher, M.J.; Borrell, A.K.; Fletcher, S.; Chenu, K. Stay-green traits to improve wheat adaptation in well-watered and water-limited environments. *J. Exp. Bot.* **2016**, *67*, 5159–5172. [[CrossRef](#)]
73. Spano, G.; Di Fonzo, N.; Perrotta, C.; Platani, C.; Ronga, G.; Lawlor, D.W.; Napier, J.A. Physiological characterization of stay green mutants in durum wheat. *J. Exp. Bot.* **2003**, *54*, 1415–1420. [[CrossRef](#)] [[PubMed](#)]
74. Crain, J.; Reynolds, M.; Poland, J. Utilizing High-Throughput Phenotypic Data for Improved Phenotypic Selection of Stress-Adaptive Traits in Wheat. *Crop Sci.* **2017**, *659*, 648–659. [[CrossRef](#)]
75. Lopes, M.S.; Reynolds, M.P. Stay-green In Posidonia in oceanica spring wheat cadmium can be induces determined changes by in spectral DNA reflectance methylation measurements and chromatin (normalized patterning difference vegetation index) independently from phenology. *J. Exp. Bot.* **2012**, *63*, 3789–3798. [[CrossRef](#)] [[PubMed](#)]
76. Kichey, T.; Hirel, B.; Heumez, E. In winter wheat (*Triticum aestivum* L.), post-anthesis nitrogen uptake and remobilisation to the grain correlates with agronomic traits and nitrogen physiological markers. *Field Crop Res.* **2007**, *102*, 22–32. [[CrossRef](#)]
77. Derkx, A.P.; Orford, S.; Griffiths, S.; Foulkes, M.J.; Hawkesford, M.J. Identification of Differentially Senescing Mutants of Wheat and Impacts on Yield, Biomass and Nitrogen. *J. Integr. Plant Biol.* **2012**, *54*, 555–566. [[CrossRef](#)]
78. Buchailot, M.L.; Gracia-Romero, A.; Vergara-Diaz, O.; Zaman-Allah, M.A.; Tarekegne, A.; Cairns, J.E.; Prasanna, B.M.; Araus, J.L.; Kefauver, S.C. Evaluating Maize Genotype Performance under Low Nitrogen Conditions Using RGB UAV Phenotyping Techniques. *Sensor* **2019**, *19*, 1815. [[CrossRef](#)] [[PubMed](#)]
79. Monostori, I.; Árendás, T.; Hoffman, B.; Galiba, G.; Gierczik, K.; Szira, F.; Vágújfalvi, A. Relationship between SPAD value and grain yield can be affected by cultivar, environment and soil nitrogen content in wheat. *Euphytica* **2016**, *211*, 103–112. [[CrossRef](#)]
80. Gamon, J.A.; Serrano, L.; Surfus, J.S. The photochemical reflectance index: An optical indicator of photosynthetic radiation use efficiency across species, functional types, and nutrient levels. *Oecologia* **1997**, *112*, 492. [[CrossRef](#)] [[PubMed](#)]
81. Peñuelas, J.; Garbulsky, M.F.; Filella, I. Photochemical reflectance index (PRI) and remote sensing of plant CO₂ uptake. *New Phytol.* **2011**, *191*, 596–599. [[CrossRef](#)] [[PubMed](#)]

82. Magney, T.S.; Vierling, L.A.; Eitel, J.U.H.; Huggins, D.R.; Garrity, S.R. Response of high frequency Photochemical Reflectance Index (PRI) measurements to environmental conditions in wheat. *Remote Sens. Environ.* **2016**, *173*, 84–97. [[CrossRef](#)]
83. Loss, S.P.; Siddique, K.H.M. *Morphological and Physiological Traits Associated with Wheat Yield Increases in Mediterranean Environments*; Sparks, D.L., Ed.; Academic Press: Boston, MA, USA, 1994; Volume 52, pp. 229–276.
84. Villegas, D.; Aparicio, N.; Royo, C. Assessment of durum wheat yield and carbon isotope discrimination by reflectance indices WI and PRI. In *Cereal Science and Technology for Feeding Ten Billion People: Genomics Era and beyond*; Options Méditerranéennes: Série A. Séminaires Méditerranéens: Zaragoza, Spain, 2008; Volume 81, pp. 403–405.
85. Araus, J.L.; Bort, J.; Steduto, P.; Villegas, D.; Royo, C. Breeding cereals for Mediterranean conditions: Ecophysiological clues for biotechnology application. *Ann. Appl. Biol.* **2003**, *142*, 129–141. [[CrossRef](#)]
86. Fischer, R.A.; Rees, D.; Sayre, K.D.; Lu, Z.-M.; Condon, A.G.; Saavedra, A.L. Wheat Yield Progress Associated with Higher Stomatal Conductance and Photosynthetic Rate, and Cooler Canopies. *Crop Sci.* **1998**, *38*, 1467–1475. [[CrossRef](#)]
87. Berger, B.; Parent, B.; Tester, M. High-throughput shoot imaging to study drought responses. *J. Exp. Bot.* **2010**, *61*, 3519–3528. [[CrossRef](#)]
88. Aparicio, N.; Villegas, D.; Casadesus, J.; Araus, J.L.; Royo, C. Spectral vegetation indices as nondestructive tools for determining durum wheat yield. *Agron. J.* **2000**, *92*, 83–91. [[CrossRef](#)]
89. Crain, J.; Mondal, S.; Rutkoski, J.; Singh, R.P.; Poland, J. Combining High-Throughput Phenotyping and Genomic Information to Increase Prediction and Selection Accuracy in Wheat Breeding. *Plant Genome* **2018**, *11*, 1–14. [[CrossRef](#)]
90. Petersen, L.K. Real-Time Prediction of Crop Yields From MODIS Relative Vegetation Health: A Continent-Wide Analysis of Africa. *Remote Sens.* **2018**, *10*, 1726. [[CrossRef](#)]
91. Torres-Sánchez, J.; Peña, J.M.; Castro, A.I. Multi-temporal mapping of the vegetation fraction in early-season wheat fields using images from UAV. *Comput. Electron. Agric.* **2014**, *103*, 104–113. [[CrossRef](#)]
92. Stöcker, C.; Bennett, R.; Nex, F.; Gerke, M.; Zevenbergen, J. Review of the current state of UAV regulations. *Remote Sens.* **2017**, *9*, 459. [[CrossRef](#)]
93. Gago, J.; Douthe, C.; Coopman, R.E.; Gallego, P.P.; Ribas-Carbo, M.; Flexas, J.; Escalona, J.; Medrano, H. UAVs challenge to assess water stress for sustainable agriculture. *Agric. Water Manag.* **2015**, *153*, 9–19. [[CrossRef](#)]
94. Sudhakar, P.; Latha, P.; Reddy, P.V. *Phenotyping Crop Plants for Physiological and Biochemical Traits*; Academic Press: Boston, MA, USA, 2016.
95. Piepho, H.P.; Möhring, J. Computing heritability and selection response from unbalanced plant breeding trials. *Genetics* **2007**, *177*, 1881–1888. [[CrossRef](#)]



© 2019 by the authors. Licensee MDPI, Basel, Switzerland. This article is an open access article distributed under the terms and conditions of the Creative Commons Attribution (CC BY) license (<http://creativecommons.org/licenses/by/4.0/>).



CHAPTER 4

Leaf versus whole-canopy remote sensing methodologies for crop monitoring under conservation agriculture: a case of study with maize in Zimbabwe

Adrian Gracia-Romero, Shawn C. Kefauver, Omar Vergara-Díaz, Esnath Hamadziripi, Mainassara A. Zaman-Allah, Christian Thierfelder, Boddupalli M. Prassana³, Jill E. Cairns and José L. Araus

Published in:
Scientific Reports (2020) 10:16008



OPEN

Leaf versus whole-canopy remote sensing methodologies for crop monitoring under conservation agriculture: a case of study with maize in Zimbabwe

Adrian Gracia-Romero^{1,2}, Shawn C. Kefauver^{1,2}, Omar Vergara-Díaz^{1,2}, Esnath Hamadziripi³, Mainassara A. Zaman-Allah³, Christian Thierfelder³, Boddupalli M. Prassana³, Jill E. Cairns³ & José L. Araus^{1,2}✉

Enhancing nitrogen fertilization efficiency for improving yield is a major challenge for smallholder farming systems. Rapid and cost-effective methodologies with the capability to assess the effects of fertilization are required to facilitate smallholder farm management. This study compares maize leaf and canopy-based approaches for assessing N fertilization performance under different tillage, residue coverage and top-dressing conditions in Zimbabwe. Among the measurements made on individual leaves, chlorophyll readings were the best indicators for both N content in leaves ($R < 0.700$) and grain yield (GY) ($R < 0.800$). Canopy indices reported even higher correlation coefficients when assessing GY, especially those based on the measurements of the vegetation density as the green area indices ($R < 0.850$). Canopy measurements from both ground and aerial platforms performed very similar, but indices assessed from the UAV performed best in capturing the most relevant information from the whole plot and correlations with GY and leaf N content were slightly higher. Leaf-based measurements demonstrated utility in monitoring N leaf content, though canopy measurements outperformed the leaf readings in assessing GY parameters, while providing the additional value derived from the affordability and easiness of using a pheno-pole system or the high-throughput capacities of the UAVs.

Currently, Sub-Saharan Africa (SSA) has one of the lowest cereal self-sufficiency ratios of the world while also having one of the greatest projected increases in population¹. By 2050, the population in SSA is expected to grow 2.5-fold, requiring a tripling of the actual cereal production in order to meet demand². The staple crop in SSA is maize, but its production is being limited by a decline in soil fertility. Particularly, Zimbabwe has been considered a hotspot for both nutrient and water limitation in agricultural production³. Traditional practices of monoculture and soil tillage have led to a decline in soil fertility⁴, causing the use of N fertilizers to become essential. Yet, this situation cannot be considered sustainable given the economic and environmental impact associated with high fertilization rates⁵.

In this context, reducing N fertilizer rates without implicating major losses in grain yield (GY) is a way of preserving natural resources and the environment without compromising food security while facing the projected changes in temperature and precipitation patterns. To that end, apart from breeding for improved plant varieties, changes in agricultural management must be considered, too. Conservation agriculture (CA), characterized by minimum soil disturbance, permanent soil cover and diversified crop rotations, has been promoted as a pragmatic solution for increasing yields while conserving natural resources. Conventional tillage (CT) practices (i.e.

¹Integrative Crop Ecophysiology Group, Plant Physiology Section, Faculty of Biology, University of Barcelona, Barcelona, Spain. ²AGROTECNIO (Center for Research in Agrotechnology), Av. Rovira Roure 191, 25198 Lleida, Spain. ³International Maize and Wheat Improvement Center, CIMMYT Southern Africa Regional Office, Harare, Zimbabwe. ✉email: jaraus@ub.edu

conventional plough-based practices) improves the aeration of the soil but may result in detrimental effects to the environment and hence lead to yield decreases in long term⁶. Soil compaction is managed by deep tillage, but this mechanical disturbance has also been shown to lead to long-term declines in organic matter, an increase in water loss by runoff, and soil erosion⁴. Reducing or avoidance of soil erosion helps to retain soil moisture and reduces the use of fossil fuels, thus lowering costs and chances of total crop loss due to drought⁷. On the other hand, the application of plant residues usually leads to an increase in crop yields due to its benefits to water retention and improved soil fertility, but its success relies on the amount and quality of the residues and the initial fertility status of the soil⁷. The application of residue resources, such as crop stover, in combination with mineral fertilizers is being increasingly implemented to address declines in soil fertility⁸. However, an important drawback of the promotion of CA practices is the competing uses of crop residues (e.g. livestock feed, as fuel or for construction) that act against their use in CA mulch applications^{9–12}. Also, poorer farmers often sell their residues to livestock keepers¹³. A better understanding of the minimum crop residue mulching thresholds that are required in order to provide CA benefits to farmers would allow farmers the flexibility to remove biomass for other purposes. Moreover, improvements in crop residue management practices may produce relevant changes towards enhancing the potential sequestration of organic carbon by farmlands, as an option for mitigation of greenhouse emissions.

Still, an appropriate N fertilizer use regimen under CA is crucial to promote microbiological activity¹⁴. For this reason, N management programs must be critically evaluated, including application rate and timing as well as the type of the N fertilizer used. On-field, fast and non-destructive indicators of crop nutritional status, such as leaf chlorophyll meters have been used for N fertilization monitoring, as chlorophyll concentration is strongly related to the N status of the plant¹⁵. The most often used leaf-clip device is the SPAD-502 from Minolta-Konica that assesses Chl concentration from leaf transmittance¹⁶. A newer alternative is the three-in-one instrument Dualex from Force-A, that, besides chlorophylls (Chl a + b), also measures leaf epidermal flavonoids (Flav) and anthocyanins (Anth)¹⁷. However, the main limitation of the leaf-clip-type instruments for large-scale studies is that these techniques are time consuming. One potential solution is the use of remote sensing methodologies for data collection at the canopy level, which have become valuable tools for precision agriculture and high-throughput plant phenotyping¹⁸. Besides multispectral sensors and imagers, further opportunities are found in the use of conventional digital Red–Green–Blue (RGB) cameras as low-cost tools for crop monitoring. Images are used to produce RGB indexes based on the color properties of the canopy, which have become very useful in forecasting yield and assessing crop variability¹⁹. The assessment of the photosynthetic area of the canopy as well as the stay-green capacity during the crop cycle are important factors for determining grain yield²⁰. The successful implementation of aerial platforms with the assembly of imaging sensors has been extensive for assessing crop performance under different growing conditions, permitting the screening of a large number of plots precisely and efficiently. In terms of monitoring/phenotyping platforms, the use of unmanned aerial vehicles (UAVs, a.k.a. drones) represents an increasingly common option, particularly considering the popularization of drones²¹. Nevertheless, the adoption of drone technology can be limited by both lack of economic resources and restrictive laws associated with the use of aerial vehicles (manned and unmanned). In such cases, an innovative option for canopy assessments of tall crops like maize or fruit trees is the attachment of a camera to a pole that may reach several meters above the crop. This alternative might require more time for data acquisition compared to UAV measurements, but less technical skills are required by the staff for image acquisition and further processing, in terms of the image alignment in orthomosaics, the posterior extraction of the individual plots or other image processing that may be required when using UAVs. Thus, for example in the case of CA and maize, increases in the performance of vegetation indices for assessing crop yield has been reported when the images were subject to pre-processing, such as applying a soil cover mask for segregating the crop biomass from the soil residue cover²².

Besides remote sensing evaluations, laboratory (i.e. analytical) traits, may be also deployed for crop phenotyping and monitoring²³. The stable carbon ($\delta^{13}\text{C}$) and nitrogen ($\delta^{15}\text{N}$) isotope compositions, when analyzed in plant matter, inform on the water regimen and nitrogen metabolism conditions, respectively, of the plant^{24,25}. Even in the case of a C4 species like maize, $\delta^{13}\text{C}$ may still differentiate between water growing conditions²⁶. In fact, both isotopic signatures have been used before in maize for assessing the effect of tillage practices²² and nitrogen fertilization²⁵ on the water and nitrogen growing conditions of the crop, even when treatments differences for both traits were only found when comparing different N fertilization levels within a common tillage system²⁵.

The main focus of this study is to compare the performance of a set of single-leaf and canopy-based remote sensing indices for assessing the influence of the top-dressing levels and the combination of tillage and residue levels on maize yield and N leaf content. Two different specialized portable leaf pigment-meters, as well as leaf scans for measuring the color of the leaves were used to assess the leaf N content. Concerning the canopy scale assessments, RGB images were taken at the ground level from a height of 4 m a.g.l. (above the ground level) using a pheno-pole and from the aerial level at a height of 30 m a.g.l. using a UAV. As a complementary selection strategy, carbon and nitrogen isotope signatures were analyzed in the leaves, as a potential tool for evaluating water and nitrogen status or differences in N assimilation.

Results

Crop yield response to tillage, the residues and top-dressing application and the associated interactions. Tillage, residue application and the top-dressing levels effects on the grain yield (GY) were evaluated (Fig. 1). The factor residue application did not report significant effects on GY (p value = 0.657), but no-tillage plots responded with increasing yield to the residue application up to 6 Mg ha⁻¹, but GY decreased when the residue application was increased to 8 Mg ha⁻¹. Within each residue treatment, the increase of top-dressing applications resulted in a significant yield improvement (p value = 0.000***), except for in the application of 2 Mg ha⁻¹ of residues, where the plots without N fertilization were still outperformed in terms of yield by

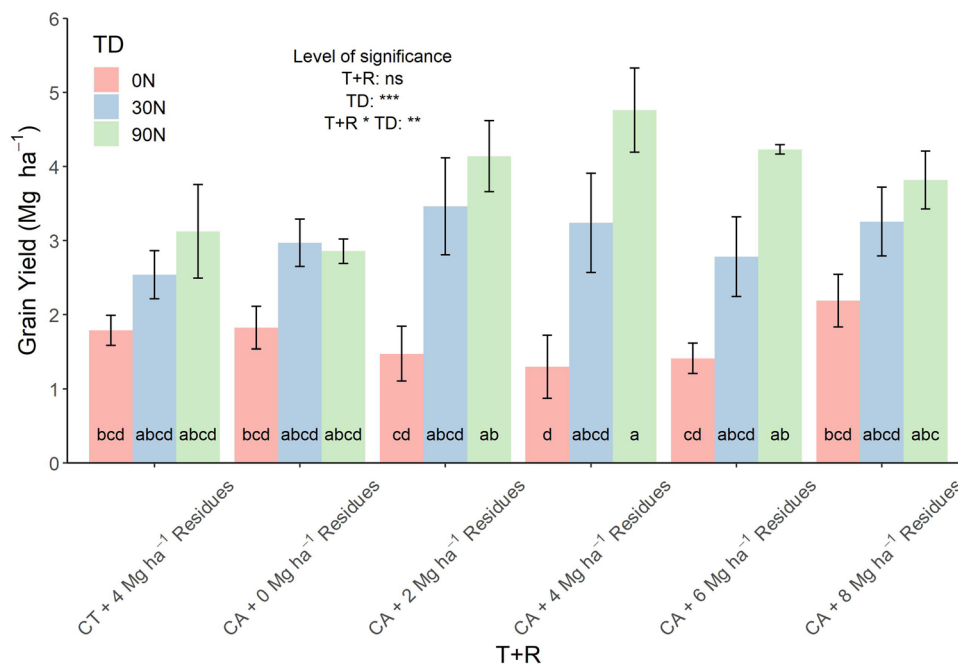


Figure 1. Average maize grain yield across the growing conditions. CA corresponds to plots grown under conservation agriculture management and CT to conventional tillage plots. T + R corresponds to the levels of the combination effect of tillage and residue application, TD to the Top-dressing levels and T + R * TD to the interaction of both factors. The error bars show the standard error of the five replicates. Different letters (a, b, c, d) indicate significant differences between the residue and top-dressing treatments according to Fisher's LSD test. Significance levels of the ANOVAs: $p < 0.05$; $**p < 0.01$; $***p < 0.001$; ns no significant.

those plots with 4 or 6 kg ha⁻¹ AN in the top-dressing. The interaction of both, treatment and sub-treatments, which had a significant effect on GY (p value = 0.007**) was grouped in four homogeneous groups. Of these, the treatment combining the application of 6 Mg ha⁻¹ of residues together with the highest top-dressing level was clearly identified alone as the highest-yielding condition (4.76 Mg ha⁻¹ of GY). The lowest yield was achieved under the application of 6 Mg ha⁻¹ of residues but without N fertilizer (1.29 Mg ha⁻¹ of GY). When the levels of N were null or low at the top-dressing treats, the CT produced higher yields than the no-tillage (with the exception of the 30N conditions). However, the application of fertilizers with elevated N fertilization levels increased yields in the conditions with 4, 6 and 8 Mg ha⁻¹ of residues in comparison to the CT conditions. The higher the residue application was, the higher the positive effect of the top-dressing N treatment on grain yield.

Effects of growing conditions on leaf total nitrogen content and carbon and nitrogen stable isotope compositions. Tillage and residue treatment as well as the top-dressing fertilization had a significant effect on the total N leaf content (Fig. 2A) and its isotope signature composition (Fig. 2B). The main differences in the leaf N content were caused by the top-dressing ($p < 0.000***$), with the highest values at 90N (2.83%) in comparison to the other two sub-treatments (1.17% for 0N and 1.98% for 30N) (Supplemental Table 1). Comparing the soil preparation conditions, when the residue application was the same, conventional tillage plots showed higher N content in their leaves. The leaf N content decreased significantly ($p = 0.044^*$) across the residue application, with the highest values at 0 Mg ha⁻¹ and the lowest at 8 Mg ha⁻¹. A strong positive correlation between the N leaf content and the GY was found. The CT treatment presented higher values of $\delta^{15}\text{N}$ than the no-tillage treatments at the same residue conditions. In contrast to the N content, the correlation of the $\delta^{15}\text{N}$ with GY was weaker and negative. On the other hand, the $\delta^{13}\text{C}$ exhibited significant differences across the application of top-dressing reporting more negative values with the increase of AN fertilizer, but no significant differences were attributed to the residue levels (Fig. 2C). More negative $\delta^{13}\text{C}$ values corresponded to higher GY, reporting higher correlations.

Implications of growing conditions on the leaf pigments readings and the RGB index derived from the scans. The conditions derived from both residue and the top-dressing applications significantly influenced the leaf pigment readings (Table 1). The variance analysis showed there were significant differences in the effects of growing conditions on all the leaf pigments. The chlorophyll values, from both devices, were clearly benefited by the top-dressing applications ($p < 0.001***$), reporting the highest values in the plots grown under 90N conditions (SPAD: 48.31 and Dualex: 38.27) (Supplemental Table 1). Regarding the differences between the two devices, the SPAD readings were slightly higher than the measurements with the Dualex, whereas the value difference between both sensors moved by the same percentage through the experimental conditions (Supplemental Figure 1).

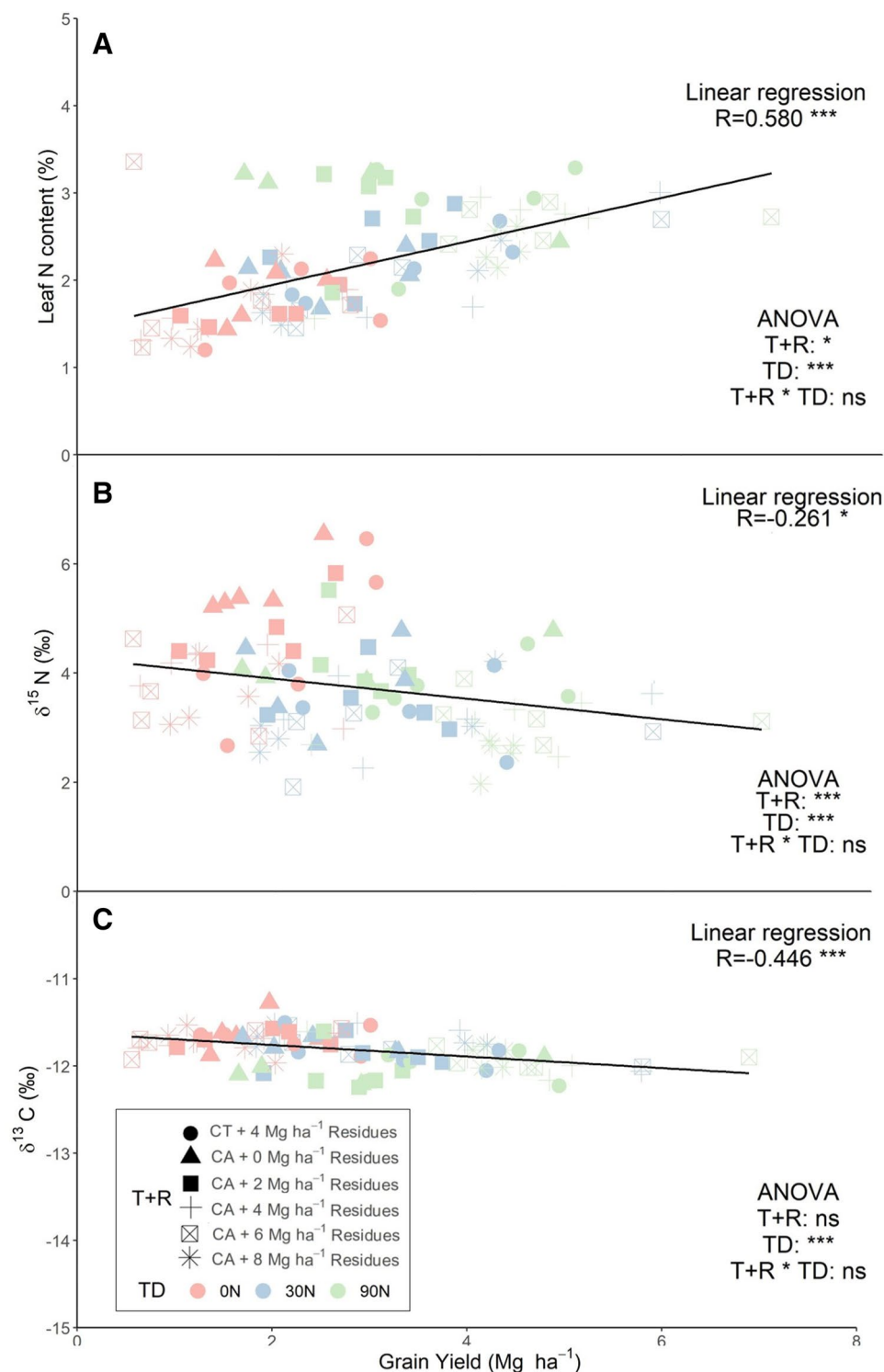


Figure 2. Relationship between the leaf N content (A), the N (B) and the C isotope (C) composition with grain yield. Correlations were studied across the 90 plots from all the growing conditions. CA corresponds to plots grown under conservation agriculture management and CT to conventional tillage plots. T + R corresponds to the levels of the combination effect of tillage and residue application, TD to the Top-dressing levels and T + R * TD to the interaction of both factors. Significance levels of the correlations and ANOVAs: ns, $p > 0.05$; * $p < 0.05$; ** $p < 0.01$; *** $p < 0.001$.

	T + R	TD	T R * TD
Dualex			
SPAD	ns	1.017e-13***	ns
Chl	ns	1.426e-11***	ns
Flav	ns	4.384e-06***	ns
Anth	ns	1.241e-11***	ns
NBI	ns	2.612e-09***	ns

Table 1. Effect of the combination of the tillage and residue application (T + R), the top-dressing (TD) and the combination of both factors (T + R * TD) on the leaf pigment readings. Significance levels of the ANOVAs: no significant (ns), $p > 0.05$; * $p < 0.05$; ** $p < 0.01$; *** $p < 0.001$.

	RGB scans			RGB ground			RGB aerial		
	T + RL	TD	T + RL * TD	T + RL	TD	T + RL * TD	T + RL	TD	T + RL * TD
Hue	ns	2.249e-07***	ns	0.02878*	5.304e-15***	ns	ns	1.878e-15***	ns
Intensity	ns	6.742e-11***	ns	ns	ns	ns	6.958e-05***	2.685e-16***	ns
Saturation	ns	3.308e-11***	ns	0.01413*	4.244e-12***	ns	0.033*	2e-16***	ns
GA	0.033*	0.0002957***	ns	ns	2e-16***	ns	ns	2e-16***	ns
GGA	ns	8.792e-08***	ns	ns	2e-16***	ns	ns	2.2e-16***	0.008**
CSI	ns	9.696e-08***	ns	0.044*	2.85e-11***	ns	ns	2e-16***	0.019*
Lightness	ns	9.798e-12***	ns	ns	ns	ns	1.337e-06***	2.2e-16***	ns
a*	ns	3.99e-11***	ns	0.039*	1.652e-15***	ns	ns	6.981e-09***	ns
b*	ns	3.504e-12***	ns	0.005**	4.472e-09***	ns	9.912e-05***	2.2e-16***	ns
u*	ns	2.268e-09***	ns	0.041*	5.324e-15***	ns	ns	3.996e-14***	ns
v*	ns	3.915e-12***	ns	0.004**	2.634e-05***	ns	5.568e-06***	2.2e-16***	ns
NGRDI	ns	ns	ns	ns	2e-16***	ns	ns	1.658e-14***	0.010*
TGI	ns	ns	ns	0.001**	3.825e-08***	0.006**	0.0001***	1.56e-06***	ns

Table 2. Effect of the combined effect of the tillage conditions with the residue applications levels (T + RL) and the top-dressing (TD) on the RGB indices derived from the leaf scans, and the plot images taken from the ground and the aerial level. These indices are defined in the “Methods” section. Significance levels of the correlations and ANOVAs: no significant (ns), $p > 0.05$; * $p < 0.05$; ** $p < 0.01$; *** $p < 0.001$.

By contrast, the measurements of the Flav and Anth content responded significantly to top-dressing, showing a reduction with increasing N top-dressing (negative correlation). Finally, the Chl/Flav ratio represented as the NBI index increased with the nitrogen top-dressing (Supplemental Figure 1).

Leaf scan images were processed to measure different indices describing color parameters (Supplemental Table 2). Indices related to the greenness of the image (Hue, a*, u*, GA, GGA and NGRDI) were very close to their saturation limits (Table 2), but an increase in the green parameters pairing with the increase of the residue application could still be noticed in Hue, a* and v* indices. Conversely, most of the calculated indices reported significant differences across the top-dressing levels, except for the indices derived from the combination of the reflectance of the R, G and B bands, NGRDI and TGI. Darker shades of green could be observed at the scans of leaves grown under 90N conditions (Supplemental table 2) through the Hue ($90.09^\circ \pm 0.43$) or the a* values (-20.67 ± 0.43), in comparison with the shades of green reported under the 0 N conditions (Hue: $86.23^\circ \pm 0.54$ and a*: -25.54 ± 0.39). The only index that responded significantly for both treatments and their interactive effect was Saturation. Saturation values increased with the residue application ($p = 0.016^*$) but decreased with the top-dressing application ($p < 0.000^{***}$). The indices GA and GGA were completely saturated showing values at their highest ranges beyond 0.95.

Effects of growing conditions on the whole-canopy RGB indices measured from the ground and from the air.

With regard to the ground RGB evaluation (Supplemental Table 3), all the indices coincided in informing that the treatment of conventional tillage with the application of 4 Mg ha⁻¹ of residues exhibited the greenest canopies (Hue: $77.66^\circ \pm 3.22$ and a*: -13.49 ± 0.94). Concerning the indices derived from the aerial images, however, the greenest plots were reported under the no-tillage conditions with 6 Mg ha⁻¹ of residues (Hue: $64.94 \pm 2.57^\circ$ and a*: -10.83 ± 0.62). For both levels (ground and aerial) of measurement, the values of the indices that estimated the greenness of the canopy under CA increased with the application of residues till 6 Mg ha⁻¹ and started to decrease with 8 Mg ha⁻¹. Contrarily to the RGB indices derived from the scans on single leaves, the greenness measurements at canopy level decreased significantly as the top-dressing levels diminished, presenting the lowest values at the 0N conditions (from the ground level = Hue: $60.35^\circ \pm 1.62$ and a*: -8.16 ± 0.62 ; from the aerial level = Hue: $56.97^\circ \pm 1.77$ and a*: -8.53 ± 0.39). Besides, the shades of yel-

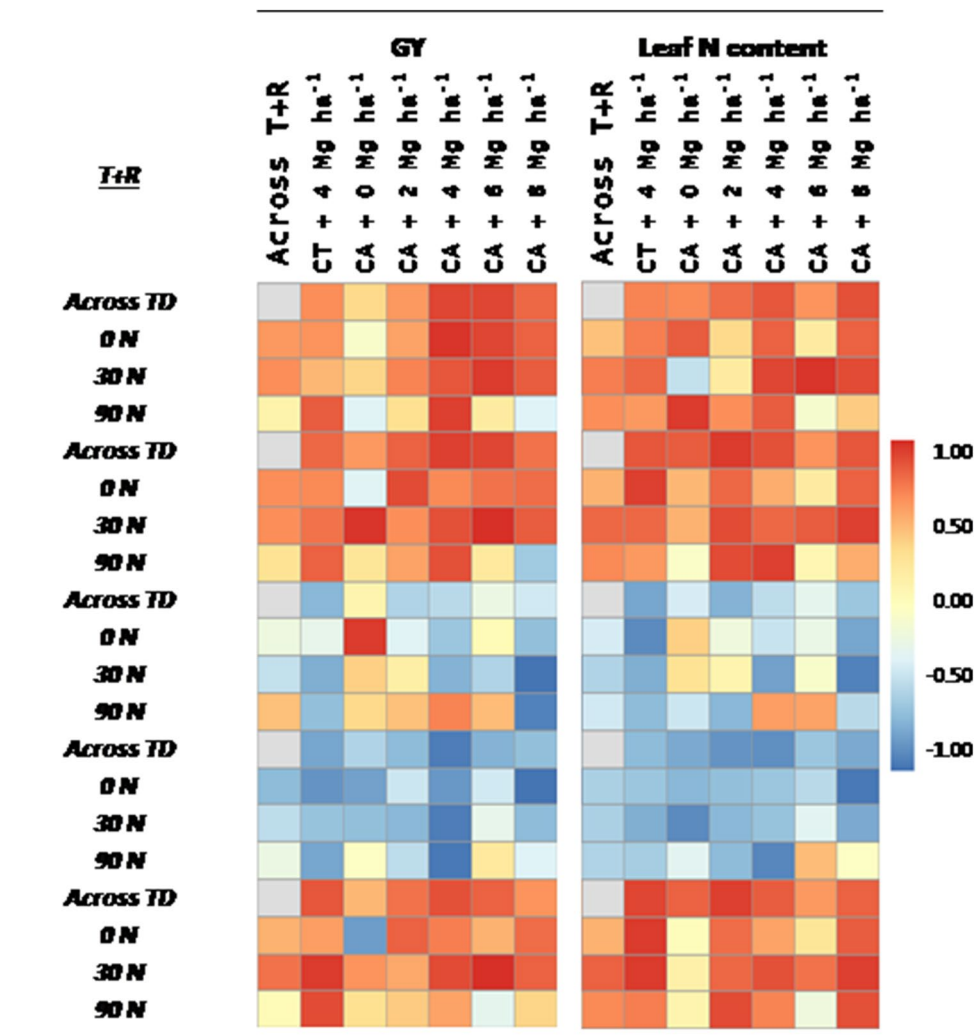


Figure 3. Heat map of Pearson correlation coefficients (R values) between the leaf-clip sensor readings with the grain yield (GY) and the N leaf content inside each growing condition, across treatments (Across T) and across the combination of residue levels and treatments (Across R+T). CA corresponds to plots grown under conservation agriculture management and CT to conventional tillage plots. Correlations colors are scaled according to the key above.

low, expressed by the b^* component, increased significantly with the residue application but were significantly reduced with the increment of the top-dressing level, for both levels (ground and aerial) of measurement.

Performance of the leaf and canopy-based measurements monitoring N and predicting GY.

To assess the accuracy of the leaf and canopy-based measurements for the assessment of the leaf N content and the GY prediction, the determination coefficients across the growing conditions were performed (Fig. 3). Chlorophyll readings, regardless the leaf clip used, showed very similar behavior as the leaf N content, reporting high and positive correlations between them. The correlations between chlorophyll measurements and GY were slightly lower, but still strong and significant. Nevertheless, the chlorophyll measurements derived from the Dualex were slightly better correlated to the N content and GY than the SPAD readings. Flav and Anth readings correlated negatively to N content, but only Anth correlated negatively to GY. The NBI reading highly correlated positively with both N content and GY.

Correlation coefficients for the relationships of the leaf N content and GY with the RGB indices derived from the leaf scans and the ground and aerial canopy images are presented in Fig. 4. According to the RGB leaf scans, greenness measures corresponding to Hue, a^* and u^* indices correlated positively to N content. The measures more related to the yellow color of the leaf, as the b^* and the v^* , and the Intensity, Saturation and Lightness reported negative correlations against GY. Regardless of the platform (from the ground or from the UAV), GA and GGA were the best correlated with the leaf N content, followed by Hue and NGRDI. Besides, CSI, a^* and u^* also correlated well, but negatively, against leaf N content. Except for the CSI, the prediction of the N content was slightly higher when measured from the ground. With reference to predicting GY, the performance of the indices was stronger than in estimating leaf N content and for most of the indices, excluding the a^* and the NGRDI

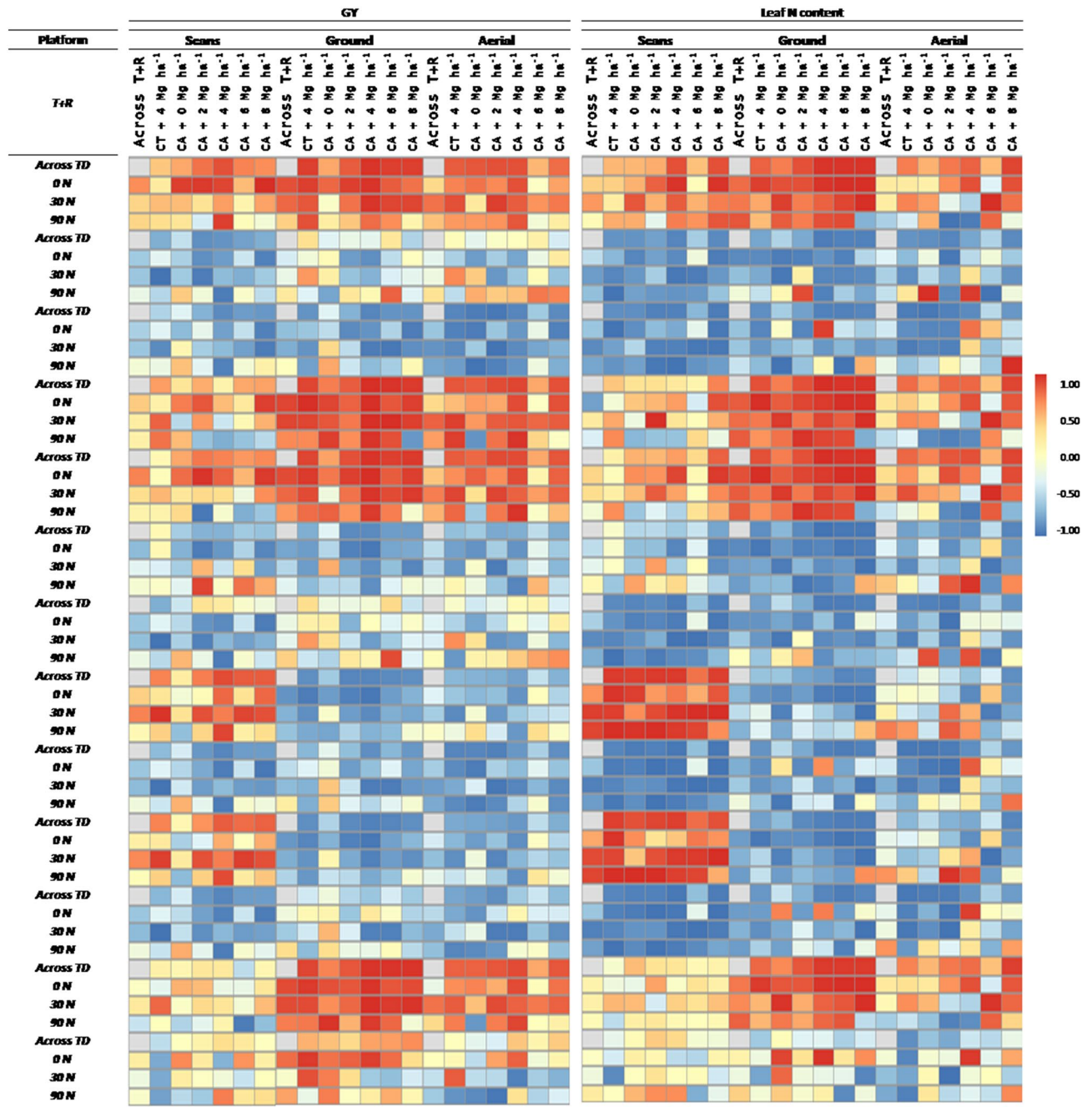


Figure 4. Heat map of Pearson correlation coefficients (R values) between the RGB indices derived from leaf scans, and from the ground and aerial canopy images against the GY and the leaf N content inside each growing condition, across treatments (Across T) and across the combination of residue levels and treatments (Across R + T). CA corresponds to plots grown under conservation agriculture management and CT to conventional tillage plots. Correlations colors are scaled according to the key above.

indices, the aerial assessments outperformed the ground measurements. Among all, the best correlated indices measured at ground level were the GA and the NGRDI. On the other hand, the best GY predictors measured from the aerial level were all the indices derived from the HSI color model (the Hue, the GA, the GGA and the CSI). For both (ground and aerial) platforms, the index that performed the worst in terms of assessing GY was the TGI. The canopy greenness-related indices derived from the HSI, RGB CIELab* and CIELuv* color systems presented a very similar capacity for assessing GY differences across the residue and top-dressing treatments. Moreover, almost all the correlation coefficients calculated were very high and consistent for both ground and aerial platform levels but being generally slightly higher at aerial level. The highest correlations were achieved at the no-tillage conditions with a residue application between 4 and 6 Mg ha⁻¹. Besides, the lowest correlations were achieved at the no-tillage plots without any residue applications and under 90N top-dressing conditions.

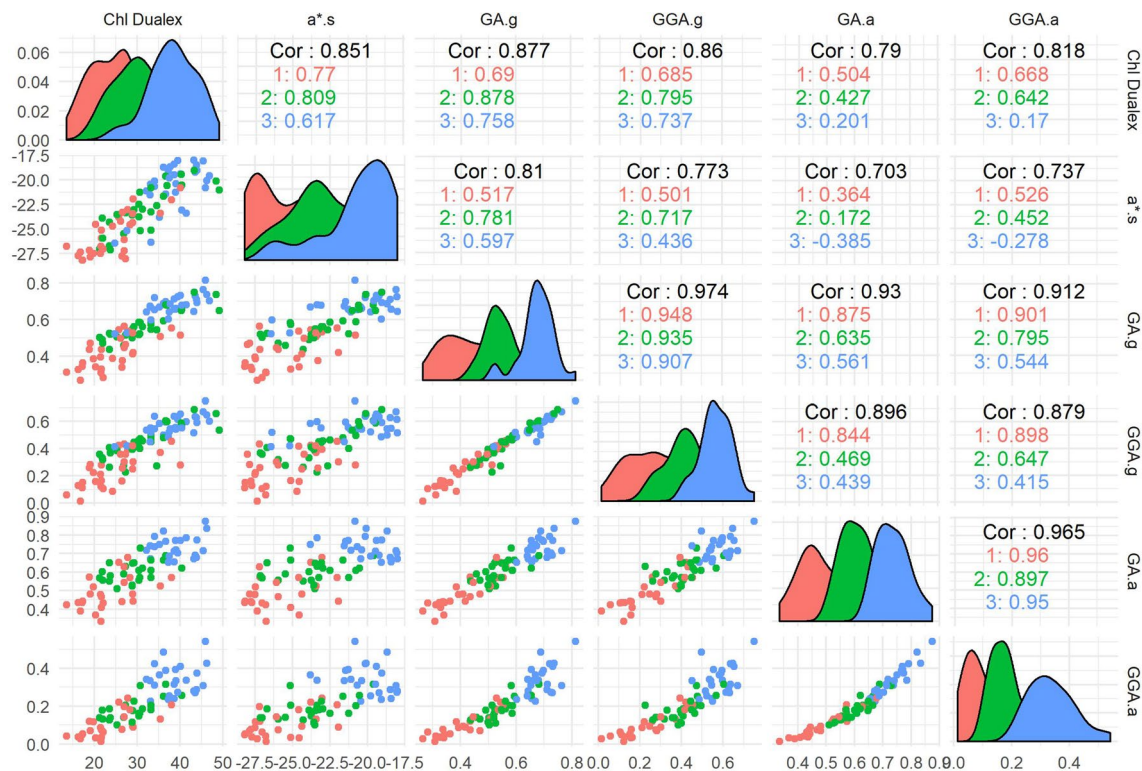


Figure 5. Diagnostic panel of each variable by itself and their relationship to each other categorized according to the top-dressing treatments: 0N in red, 30N in green and 90N in blue. Bottom-left charts represent the scatter plot correlations and the upper-right represent the correlation coefficients. The Cor value corresponds the correlation across all treatments, the value 1 to the correlation inside the 0N plots, the value 2 to the correlation inside the 30N plots and the value 3 to the correlation inside the 90N plots. The diagonal shows a smoothed-out histogram of the values of the measures.

Leaf, canopy and aerial measurement calibrations. In order to validate the relationship between the parameters measured at different scales (leaf vs canopy) and placements (ground vs aerial) a pairwise comparison was performed (Fig. 5). The parameters selected were those measurements that best correlated to N leaf content and GY. The chlorophyll content measured with the Dualex was highly correlated to the greenness of the leaf derived from the a^* index measured from the scans. When the GA and GGA canopy measurements were used, the correlations against Chl were still strong, regardless the observation height level (ground vs aerial). However, the relationship against the aerial measurements of GA and GGA were much weaker. The greenness indices of the leaf derived from the leaf scans paralleled the corresponding indices measured at canopy level; thus, strong correlations were found, particularly for the measurements at ground level, while for the aerial measurements the correlations inside each top-dressing treatment were low. Finally, the comparison between the canopy GA and GGA indices from the ground and aerial images resulted in very high correlation coefficients. Along with the scatter plot charts and correlation coefficients, density plots to assess the measurements distribution are also provided in the same panel.

Discussion

Influence of tillage, crop residues and top-dressing with non maize yield. Top-dressing with N fertilizer induced the most notable effect on the parameters assessed: GY, leaf N content, signature of stable C and N isotopes, leaf pigment content and the different vegetation indices measures at single leaf and canopy levels. Nitrogen is a major nutrient for crop production and our results showed a positive yield response to N application (Fig. 1). Albeit the effect of the residue level alone did not improve yield, the combination of top dressing with N resulted in a significant yield increase. Among the plots fertilized with the higher amounts of N, increasing the residue level had a positive effect on yield, reaching the top at 6 Mg ha^{-1} but decreasing with 8 Mg ha^{-1} . Permanent residue soil cover helps to ensure better rainfall infiltration while reducing evaporative water losses²⁷, therefore improving yields in low rainfall areas²⁸. Moreover, the use of cereal stover increased short-term immobilization of N, having a potential positive effect on crop nutrient response²⁹. However, an excess of residues can also be detrimental to crop emergence given the physical obstacles for seedlings or may provide a favorable habitat for plant pathogens³⁰. Besides, the application of residues may also decrease, at least temporary, the availability of N for the plant, since it is used by microorganisms that decompose the residues into organic matter³¹ and thus limit GY. Fonte et al.³² presented similar results from the combination of fertilizer and residue effects on yield and also reported that the addition of N had the most consistent effect of increasing yield.

Differences in leaf N content and N and C isotopic signatures. The top-dressing fertilizer rate increase resulted in an increase in the leaf N content, where the maximum leaf N content was obtained under the no-tillage conditions without residue application and the 90N fertilizer treatment (Fig. 2A). Once the leaves reach a threshold in N concentration, the plant aims to increase the biomass rather promoting the increase of the N concentration of the leaves, while the N concentration in the leaves further increase when the plant achieves its maximum growth³³. The decrease reported in the N content of the leaves across the residue levels might be related to an increase of the microbiological activity at the top layers of the soil³¹. The nitrogen isotope composition has been used to study the dynamics of N in soil–plant systems³⁴. Depending on the N source used as a N fertilizer the $\delta^{15}\text{N}$ will vary, reporting values closer to zero when the origin of the N-fertilizer is synthetic³⁵. As the top-dressing rate of N fertilization increased, the $\delta^{15}\text{N}$ reported lower values, proving that $\delta^{15}\text{N}$ can be used to characterize the level of N fertilization³⁶. The decrease of the $\delta^{15}\text{N}$ due the increase of the residue levels might be explained by the discrimination of the microorganism with the remaining soil N being impoverished in ^{15}N ³⁷. The carbon isotope composition ($\delta^{13}\text{C}$) is an indicator of the water status of the plant; in the case of C4 species usually decreasing in response to water stress^{26,38–40}. Even if at a much lesser extent than in C3 species, $\delta^{13}\text{C}$ in the plant matter of C4 plants also depends on the intercellular to the atmospheric CO_2 concentration of the leaf, which is affected by differences in water regime or in intrinsic photosynthetic capacity²⁶. The lack of differences in $\delta^{13}\text{C}$ discarded any improvement effect on the water status of the plants due to the residue level coverage. However, our results showed how a higher N concentration in leaves caused a decrease in $\delta^{13}\text{C}$. These results agree with Vergara-Díaz et al.²⁵ This effect may be attributed to a boost in the photosynthetic capacity due to the increase of N concentration or alternatively to a greater associated transpiration area, causing some degree of water stress and a decrease in stomatal conductance. Both factors may lower the ratio of intercellular to atmospheric CO_2 , which, in the case of a C4 plant like maize, may cause a small decrease in $\delta^{13}\text{C}$ ⁴¹.

Evaluation of leaf-based and whole-canopy measurements for monitoring leaf N content and predicting GY. Chlorophyll measurements exhibited the same trend as the leaf N content. Changes in leaf N content resulted in changes in the photosynthetic proteins, that represents a large portion of the total leaf N⁴². The close positive relationships between leaf chlorophyll values and N content demonstrated the potential to estimate in-season leaf N content of leaf tissues based on the SPAD or Dualex readings. As leaf chlorophyll content is very sensitive to variations in N supply, this parameter can be used for a quick detection of N deficiency^{43,44}. Conversely, the response of Flav and Anth to leaf N content was negative (Fig. 3). Similar findings were presented in Zhang et al.⁴⁵ where Flav and Anth were found to be particularly sensitive and consistent indicators of N fertilization conditions.

Grain yield comparisons to the leaf pigment readings also resulted in significant correlations. This agreed with the results presented in Cairns et al.⁴⁶ where SPAD readings were significantly correlated with GY during grain filling. However, the potential of the relative leaf chlorophyll readings for predicting GY in maize could vary depending on the phenological stage when measurements are taken. Buchailot et al.⁴⁷ studied the variations in SPAD measures in assessing GY differences over two phenological stages before grain filling and reported higher correlations during the vegetative stage rather than during flowering. Monneveux et al.⁴⁸ reported no significant correlations between SPAD and GY during neither middle nor late grain filling. Thus, it is very important to consider the timing of the measurement of leaf pigment contents for performing reliable GY predictions.

Because the color of the maize leaves is mainly determined by their content in chlorophylls and carotenoids⁴⁹, digital color analysis might be also considered as a potential method for evaluating foliar nutrition. The leaf scans showed how the more N fertilizer was added, the greener the leaves were and the correlations of RGB indices (Hue, a^* and u^*) against N and chlorophyll were very high. The color tendency across the residue levels was lighter green tones (yellowish) as the amount of residue is increased. This is consistent with the above results, as the darker is the leaf's green, higher is the amount of chlorophylls and the nitrogen content^{50,51}. This can be clearly seen through the indices derived from the RGB scans. The CIE a^* and u^* components establish the color position between the red/magenta and the green, with negative values indicating green⁵², where inside this green range, more negative values indicate lighter green while less negative values indicate darker green. On the opposite way, the b^* and v^* positive values represent the yellow color spectrum⁵² and thus, the correlation of these indices against N content and GY is negative. Concerning the HSI parameters, lower Hue degrees correspond to more yellowish colors, and higher degrees correspond to darker green tones. The other two HSI parameters, Intensity and Saturation, inform about the brightness of the color^{53,54} and a decrease of their values matched with darker leaves (i.e. with higher chlorophyll contents and higher N content). Concerning the GA, GGA or CSI indices, while they are frequently used as good predictors of GY in field canopy measurements, which was confirmed in our study, they correlated poorly against GY when these indices were assessed at the single leaf level through the image scans. Similarly, the NGRDI and the TGI indices, as estimations of image greenness and indices formulated for canopy images, have been successfully applied for assessing GY at the canopy level^{55,56} but failed here at the leaf level due to saturated values.

Canopy color related indices acquired from both the ground level and aerially performed worse for examining leaf N content than the single leaf-based indices, but, in terms of predicting GY, the canopy measurements performed better than those same indices at the leaf level. Conversely, at the canopy level, leaf color differences are less relevant and thus, the estimation of N content or chlorophylls resulted a bit more problematic (Fig. 6). However, considering that RGB canopy derived indices are known as effective measurements of green biomass, the strong correlations reported with the leaf N content might be more related to the N fertilization effects on growth rather than the leaf N content itself. Gracia-Romero et al.⁵⁷ came to the same conclusion while studying the performance of RGB and multispectral indices assessing leaf phosphorous content in a maize trial. Nevertheless, one of the main benefits of the canopy images is to enable assessing the heterogeneity of the plot as a

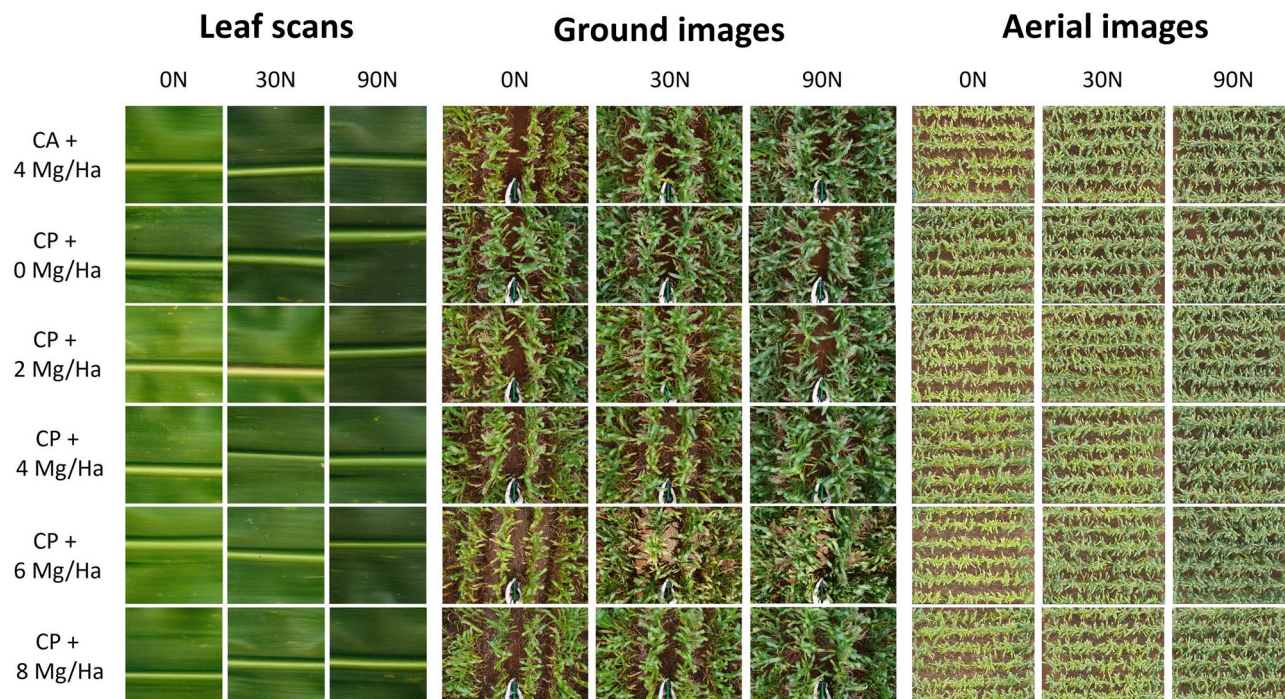


Figure 6. RGB leaf scans and canopy images taken from the ground and aerial level.

whole. Thus, canopy measurements have the potential to minimize the influences of the sampling location of the leaf better than the leaf-clip sensors, where the averaged values of 5–10 leaves and a sampling area of solely 6 mm² (for both Dualex and SPAD) is assumed to be a representative measure of the plot. Attempts to improve the representativity of the single-leaf measurements, imply measuring always the same kind of leaves (flag leaves, top leaves...), while paying attention that leaves are fully intact, clean and free of signs of disease or damage⁵⁸. However, the variability within the canopy is assumed to be captured with few measurements of individual leaves.

The indices that performed better assessing differences in GY were the ones related to vegetation cover, as the GA and the GGA. Both indices quantify the portion of green pixels, being GGA more restrictive by excluding the yellowish green fraction of vegetation, and therefore are considered reliable estimators of vegetation cover⁵⁹. Another biomass-assessment index is the NGRDI, which is formulated similarly to the well-known Normalized Difference Vegetation Index (NDVI), but instead of using information from the near-infrared reflection bands, it incorporates information from the green band and thus it can be calculated with images from conventional RGB cameras⁵⁶. The strength in assessing GY in the indices capturing green tonalities values (like the Hue or the a*) has a different explanation. Although these indices are not strict vegetation-density indicators as the GA or the GGA, the differences in crop cover between plots were the main source of variability rather than the canopy color itself. The measurements derived from those indices are indicators of the greenness of the image derived from the combination of effects of the chlorophyll concentration, the canopy green leaf area and the canopy architecture⁶⁰. Otherwise, the Crop Senescence Index (CSI), as it is formulated from the combination of GA and GGA indices⁶¹, provides truthful information about the variation of the canopy color derived from the development of leaf senescence caused by growing conditions. The CSI reported a wide change across the growing conditions and highly correlated to GY. Earlier senescence due to low N fertilization conditions resulted in elevated CSI values, providing efficacy in plant stress detection. In fact, RGB canopy indices have been proven to perform far better in predicting GY than the NDVI or other multispectral indices in other maize and wheat studies^{22,57,62}.

Comparison of measurements scales (leaf vs canopy based, and ground vs aerial) in assessing maize performance. The canopy remote sensing methodologies, when applied from aerial platforms, can be considered as robust approaches for rapidly assessing a large number of plots, particularly for large scale field-based studies. In this study, the ground level images taken with a 4 m pole only permitted coverage of a portion of the plot and therefore did not account for the possible heterogeneity of the plot; the time spent on fieldwork to cover the 90 plots was approximately one hour. On the other hand, the aerial images permitted assessing the totality of the plot area and the flight duration for covering the whole trial was less than 10 min (including the pre-flight procedures). However, aerial images require preparation before image processing, including building the image mosaics and segmenting the plots, compared to the ground images, which can be processed directly. In terms of accuracy, ground evaluation images had a much higher spatial resolution (5456 × 3632 pixels), while aerial images had much lower resolution (478 × 379 pixels for a flight at 30 m a.g.l.). Despite these differences, the RGB indices from both platforms were highly correlated and their precision in assessing leaf N content was very similar and for GY prediction even higher in the case of the aerial measurements. Thus, UAV imagery is

presented as a very promising methodology for mapping stress detection in crops. Nevertheless, the cost of the aerial platform and the requirement of qualified operators (or the existence of legal restrictions) might limit the adoption of these methodologies in development countries. For this reason, using ground-based approaches like attaching a camera to a pheno-pole might be considered a good alternative.

Conclusions

Proper nitrogen management is crucial to conservation agriculture as evidenced by the significant yield increase recorded when the application of residues is combined with N fertilizer application as top-dressing. Quantifying the optimal quantity of stover that can be incorporated as a residue cover will benefit yield and will be of economic importance for the small holder farmers. This study demonstrated the potential of remote sensing tools at leaf and canopy scale to predict GY and assess leaf N content. This would enable the adjustment of N fertilizer inputs for optimizing GY, therefore making the N fertilizer applications more efficient.

In this study, leaf-based measurements proved to be good indicators of leaf N content, mostly because chlorophylls are tightly associated with leaf proteins, and thus to the N concentration. This is also reported as leaf color changes in the RGB scans. Despite performing robustly for leaf N content monitoring, operating at the leaf scale is time-consuming and its application in large scale studies and in assessing GY is limited. The other limitation to consider is that the selection of the leaves to be assessed can be subjective. On the other hand, canopy based RGB indices were shown to be effective measurements of crop density, as a direct effect of the soil N availability in the plot. As a low-cost tool in comparison to the more specialized leaf-clip sensors, digital photography is a promising approach for precision agriculture and crop management. Regarding the comparison between the ground and aerial platform-based measurements, both performed very similarly in terms of assessing leaf N content and GY. The selection of the platform would depend on its costs and the skills required, but with the use of drones there is certainly an improved high-throughput capacity. Stable nitrogen isotope composition, and, despite the C4 nature of the crop, carbon isotope composition, provided relevant information of the effect of crop management conditions in maize.

Methods

Site description and plant material. The experiment was located at the Southern Africa Regional Office of CIMMYT (International Maize and Wheat Improvement Center) located in Harare (17° 43' 32" S, 31° 00' 59" E, at an altitude of 1498 m above sea level), during the crop season 2016/2017 (Fig. 7). The soil type at the field site is characterized by a pH slightly below 6. The previously sown crop was maize with no tillage and without residue application and fertilized using compound D with 200 kg ha⁻¹ ammonium nitrate (AN). The plant material used in this experiment was the commercial maize variety “PGSG3”.

Experimental design and crop management. The experiment was arranged in a split-plot design with five replications. Maize residue management in combination with two tillage treatments and nitrogen levels were two factors of interest. The maize residue treatments were randomly assigned to main plots and nitrogen levels treatments were randomly assigned to sub-plots. Overall, 90 plots were studied (6 main treatments × 3 sub-treatments × 5 replicates). The plot size was 6 rows × 0.9 m × 6 m long (5.4 m × 6 m = 32 m²). No tillage was employed during the experiment, except for the first treatment plots, that were managed using conventional tillage and the application of 4 Mg ha⁻¹ of residue. The other five treatments were managed without soil tillage and an increase of the residue application from 0 to 8 Mg ha⁻¹ (0 Mg ha⁻¹, 2 Mg ha⁻¹, 4 Mg ha⁻¹, 6 Mg ha⁻¹, 8 Mg ha⁻¹). Maize stover treatments produced by the previous crop was weighed using a hanging scale KERN® (Kern, Balingen, Germany), spread (flat) uniformly over the soil surface immediately after harvest in June at the respective rates. Three different fertilization regimens were established in order to generate a range of N soil levels in the growing conditions (Table 3).

Split application of top dressing was done using ammonium nitrate (AN) (34.5%N), first applied at 4 weeks after planting (WAP) and second at 7 WAP. Post emergence herbicides and hand pulling was used to control weeds. Complementary irrigation was provided when necessary to avoid unwanted drought stress.

The planting was done during the summer season 2016–2017 after receiving sufficient rainfall (20 mm received within two consecutive days). A ripper was used to open planting rows followed by hand planting. Seeds of PGS 63 were sown two seeds per station on 17th November 2016 and thinned to 1 plant per station at V3 targeting 44,444 plants ha⁻¹.

Data collection. The date of emergence was recorded when 50% of the crop emerged. At harvest maize grain and stover yield were recorded from final harvest area of 4 rows × 4 m in the middle of each plot. Maize cobs were removed manually from the stalks and weighed. Sub-samples of ten cobs were randomly selected from each plot and weighed, air-dried and shelled; moisture content was determined using a Dickey–John mini GAC moisture tester (Döschner Microwave Systems GmbH, Rellingen, Germany) and then dry weight determined (at 0.1 g precision). Maize grain yield was calculated, converted to mass ha⁻¹ at 125 g kg⁻¹ moisture content. Total maize stalks and leaves of each sample was weighed using a hanging scale KERN®. A sub-sample of three plants (stalks) were randomly selected from each sample and grinded using mulcher into small pieces and a representative sub-sample of approximately 500 g was collected and weighed immediately to obtain field weight then air dried. Stalk sub-sample was re-weighed after drying to determine dry weight (at 0.1 g precision).

The field data measurements with different methodologies and sensors were taken during the 5th February 2017. The crop was between the R1–R2 phenological stages.

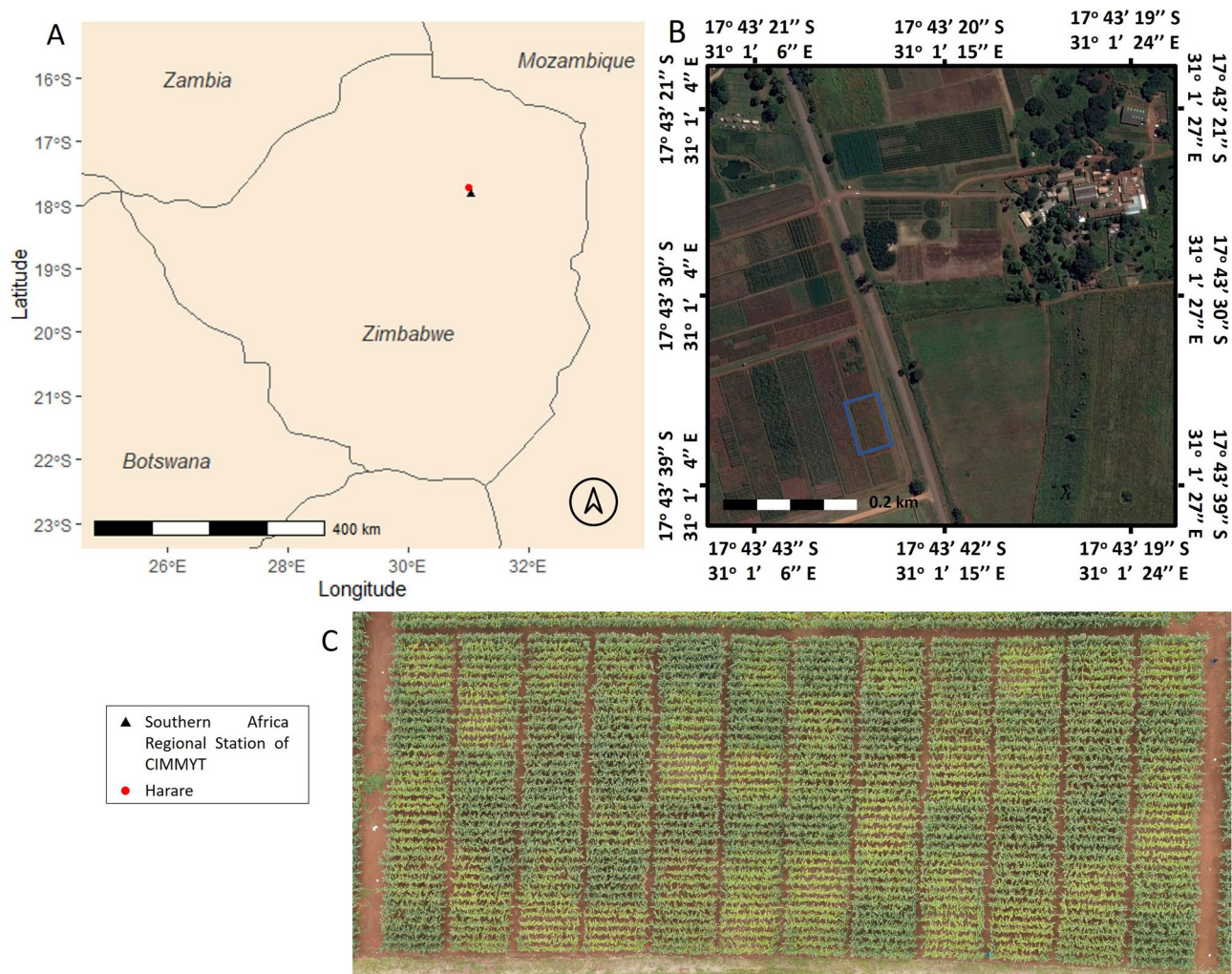


Figure 7. (A) Map of Zimbabwe with the location of Harare and the Southern Africa Regional Station of CIMMYT. (B) Landsat-8 satellite image of the study area acquired from DigitalGlobe using Google Earth Pro on the 28th of March 2017. (C) Aerial image Red–Green–Blue (RGB) orthomosaic at 30 m of the trial.

Subtreatments	Top-dressing fertilizer
0N	28 kg ha ⁻¹ P ₂ O ₅ and 14 kg ha ⁻¹ K ₂ O
30N	200 kg ha ⁻¹ Compound D (7:14:7) and 46 kg ha ⁻¹ AN
90N	200 kg ha ⁻¹ Compound D (7:14:7) and 220 kg ha ⁻¹ AN

Table 3. Top-dressing fertilizer treatments.

Leaf-clip sensors. Two different clip sensors were used in order to estimate the chlorophyll content. On the one hand, the SPAD-502 chlorophyll meter (Konica Minolta Inc., Japan) that measures the light transmitted by the plant leaf when the sensor provide light from a red LED (650 nm) and an infrared LED (940 nm). On the other, the Dualex Scientific (Force-A, Orsay, France) sensor operates with a red reference beam at 650 nm and a UV light at 375 nm. This latter sensor, besides chlorophylls a + b (Chl), it also produces relative measures of flavonoids (Flav) and anthocyanin (Anth) content and the nitrogen balance index (NBI), which is the ratio Chl/Flav related to the nitrogen and carbon allocation^{17,63}. The plot measurements derived from both sensors correspond to the average of five measurements of five different leaves from five different plants. The measurements were taken from the middle portion of the leaves, a mix between the upper and the lower leaves around the cob.

RGB images and RGB indices calculation. RGB indices were formulated from images taken at three different scales. On one side, the central part of the leaf placed just below the ear of six different plants per plot were scanned using a flatbed scanner CanonScan Lide 120 (Canon, Tokyo, Japan). At the ground level, one picture was taken per plot, holding the camera at 4 m above the plant canopy in a zenithal plane and focusing



Figure 8. Ground level RGB canopy images system using the pheno-pole.

near the center of each plot using a “pheno-pole” (camera extension pole) Megaview Lite (Megaview Photomast Systems, Twello, Netherlands) made of glass fiber (Fig. 8). The conventional digital camera used was a 20.1-megapixel Sony ILCE-QX1 (Sony Corporation, Minato, Japan) with images saved in JPEG format at a resolution of 5456×3632 pixels. The camera was controlled remotely using a smartphone. At the aerial level, an eight rotor Mikrokopter Oktokopter XL 4S (HiSystems GmbH, Moomerland, Germany) equipped with a 16-megapixel Lumix GX7 (Panasonic, Osaka, Japan) was used and images were taken at 30 m above the ground level. Images were saved in JPEG format at a resolution of 4592×3448 pixels. In order to correct the effect of pitch and roll movements of the drone during the flight, an active two-servo gimbal was used to steady the camera.

The scanned images were cropped semi-automatically using the open source image analysis platform FIJI (Fiji is Just Image); <https://fiji.sc/Fiji>) into six different images of 1176×1286 pixels corresponding to each section of the six leaves from six different plants. The measurements were taken from the middle portion of the leaves. For the orthomosaic reconstruction procedure with the aerial images, a 3D reconstruction model was produced using the Agisoft PhotoScan Professional software (Agisoft LLC, St. Petersburg, Russia, www.agisoft.com)⁶⁴ by using aerial images with at least 80% overlap. Then, regions of interest corresponding to each plot were segmented and exported using the MosaicTool (Shawn C. Kefauver, <https://integrativecropcophysiology.com/software-development/mosaictool/>, <https://gitlab.com/sckefauver/MosaicTool>, University of Barcelona, Barcelona, Spain) integrated as a plugin for FIJI. Finally, segmented scans, ground images and segmented aerial images were subsequently analyzed using also the MosaicTool plugin⁶², that enables the extraction of RGB indices in relation to different color properties of potential interest⁵⁹. Derived from the HSI (Hue–Saturation–Intensity) color space, the parameters Hue, referring to the color tint; Saturation, an indication of how much the pure color is diluted with white color; and Intensity, as an achromatic measurement of the reflected light, were extracted. In addition, the portion of pixels classified as green by their Hue values was determined by the Green Area (GA) and the Greener Area (GGA) indices. The GA corresponds to the percentage of pixels that have a Hue value between 60° and 180° . Meanwhile, the GGA is more restrictive, because it reduces the range from 80° to 180° , thus excluding the yellowish-green tones. Both indices are also used for the formulation of the crop senescence index (CSI)⁶¹, which provides a scaled ratio between yellow and green pixels to assess the percentage of senescent vegetation. The CSI index was calculated as follows:

$$CSI = \frac{(GA - GGA)}{GA} \times 100 \quad (1)$$

From the CIELab and the CIELuv color space models (recommended by the International Commission on Illumination—CIE—for improved color chromaticity compared to HSI color space), the following parameters

were calculated: L^* , that represents lightness and is very similar than the intensity from the HSI color; the a^* and u^* , that represent the red green spectrum of chromaticity; and the b^* and v^* represent the yellow–blue color spectrum⁵². Further, besides those indices calculated with the Breedpix software, two additional indices derived from the RGB color model were calculated using the digital numbers (DN) of the red, green and blue bands. One, the normalized green–red difference index (NGRDI) is formulated very similarly than the well-known normalized difference vegetation index (NDVI), but instead of using the near-infrared information, it uses the information from the red and green bands⁵⁵. It is formulated as follows:

$$NGRDI = \frac{(Green\ DN - Red\ DN)}{(Green\ DN + Red\ DN)} \quad (2)$$

The other index is the triangular greenness index (TGI), that estimates chlorophyll content based on the area of a triangle with the three points corresponding to the red, green, and blue bands⁵⁶, and it is formulated as follows:

$$TGI = -0.5 \cdot [190 \cdot (Red\ DN - Green\ DN) - 120 \cdot (Red\ DN - Blue\ DN)] \quad (3)$$

Therefore, this set of indices was calculated at three different scales: scan, ground and aerial.

Total nitrogen content and nitrogen and carbon stable isotope compositions. The same maize leaves scanned and used for leaf clip sensor measurements were oven dried at 70 °C for 24 h and were grounded to a fine powder using a ball mill. Then, samples of approximately 0.7 mg of dry matter were weighed into tin capsules, sealed, and then loaded into an elemental analyzer (Flash 1112 EA; ThermoFinnigan, Schwerte, Germany) coupled with an isotope ratio mass spectrometer (Delta C IRMS, ThermoFinnigan), operating in continuous flow mode. Measurements were carried out at the Scientific Facilities of the University of Barcelona. The $^{13}C/^{12}C$ ratios of plant material were expressed in composition ($\delta^{13}C$) notation⁶⁵ as follows:

$$\delta^{13}C(\text{‰}) = \left[\left(\frac{R_{\text{sample}}}{R_{\text{standard}}} \right) - 1 \right] \times 1000 \quad (4)$$

in which R_{sample} refers to plant material and R_{standard} to Pee Dee Belemnite (PDB) calcium carbonate. International isotope secondary standards of a known $^{13}C/^{12}C$ ratio (IAEA CH7, polyethylene foil, IAEA CH6 sucrose and USGS 40 l-glutamic acid) were calibrated against Vienna Pee Dee Belemnite calcium carbonate (VPDB) with an analytical precision of 0.1‰. The $^{15}N/^{14}N$ ratios of plant material were also expressed in δ notation ($\delta^{15}N$) using international secondary standards of known $^{15}N/^{14}N$ ratios (IAEA N1 and IAEA N2 ammonium sulfate and IAEA NO₃ potassium nitrate), with analytical precision of about 0.2‰.

During the same process, nitrogen content was determined through the combustion of dry matter. Nitrogen was expressed as a concentration per unit dry weight.

Statistical analysis. Statistical analyses were conducted using the open source software, R and RStudio 1.0.44 (R Foundation for Statistical Computing, Vienna, Austria). Means and standard errors were calculated using the summarySE() function from the “Rmisc” package. Tukey’s HSD test was used to determine post hoc differences at each growing condition using the HSD.test() function from the “agricolae” package. Data for the set of physiological traits were subjected to factorial completely randomized analyses of variance (ANOVAs). To test the effects of growing conditions on the different traits studied using the anova() function with a linear model. A two-ways linear model ANOVA was used to examine the influence of the top-dressing levels (0, 30 and 90N) and the combination of tillage and residue level (CA + 4 Mg/Ha Residues and CP + 0, 2, 4, 6 and 8 Mg/Ha Residues). Differences were considered significant at p value ≤ 0.05 . A bivariate correlation procedure was used to calculate the Pearson correlation coefficients of the different remote sensing indices against GY and leaf N content using the cor.test() function. All the chart figures were designed using the package “ggplot2”.

Received: 17 January 2020; Accepted: 10 September 2020

Published online: 29 September 2020

References

1. Sulser, T. B., Mason-D’Croz, D., Robinson, S., Wiebe, K. & Rosegrant, M. W. Africa in the global agricultural economy in 2030 and 2050. In *ReSAKSS Annual Trends and Outlook report 2014* (eds Badiane, O. & Makombe, T.). International Food Policy Research Institute (IFPRI). (2015).
2. Van Ittersum, M. K. *et al.* Can sub-Saharan Africa feed itself?. *Proc. Natl. Acad. Sci. U.S.A.* **113**, 14964–14969 (2016).
3. Mueller, N. D. *et al.* Closing yield gaps through nutrient and water management. *Nature* **490**, 254–257 (2012).
4. Thierfelder, C., Matemba-Mutasa, R. & Rusinamhodzi, L. Yield response of maize (*Zea mays* L.) to conservation agriculture cropping system in Southern Africa. *Soil Till. Res.* **146**, 230–242 (2015).
5. Good, A. G. & Beatty, P. H. Fertilizing nature: a tragedy of excess in the commons. *PLoS Biol.* **9**, e1001124 (2011).
6. Geocosky, D. C., Sauer, T. J. & Hatfi, J. L. Challenging balance between productivity and environmental quality: tillage impacts. In *Soil Management: Building a Stable Base for Agriculture* Vol. 1373 (eds Hatfield, J. L. & Sauer, T. J.) 13–37 (ASA and SSSA, Madison, 2011).
7. Thierfelder, C., Rusinamhodzi, L., Setimela, P., Walker, F. & Eash, N. S. Conservation agriculture and drought-tolerant germplasm: reaping the benefits of climate-smart agriculture technologies in central Mozambique. *Renew. Agric. Food Syst.* **31**, 414–428 (2016).

8. Vanlauwe, B. *et al.* Agronomic use efficiency of N fertilizer in maize-based systems in sub-Saharan Africa within the context of integrated soil fertility management. *Plant Soil* **339**, 35–50 (2011).
9. Giller, K. E. *et al.* A research agenda to explore the role of conservation agriculture in African smallholder farming systems. *Field Crops Res.* **124**, 468–472 (2011).
10. Jaleta, M., Kassie, M. & Shiferaw, B. Tradeoffs in crop residue utilization in mixed crop–livestock systems and implications for conservation agriculture. *Agric. Syst.* **121**, 96–105 (2013).
11. Baudron, F., Delmotte, S., Corbeels, M., Herrera, J. M. & Titttonell, P. Multi-scale trade-off analysis of cereal residue use for livestock feeding vs. soil mulching in the Mid-Zambezi Valley, Zimbabwe. *Agric. Syst.* **134**, 97–106 (2015).
12. Valbuena, D. *et al.* Conservation agriculture in mixed crop–livestock systems: scoping crop residue trade-offs in Sub-Saharan Africa and South Asia. *Field Crop Res.* **132**, 175–184 (2012).
13. Guto, S. N. Chakula bila kulima? Trade-offs concerning soil and water conservation in heterogeneous smallholder farms of Central Kenya. Ph.D. Thesis (2011).
14. Chivenge, P., Vanlauwe, B. & Six, J. Does the combined application of organic and mineral nutrient sources influence maize productivity? A meta-analysis. *Plant Soil* **342**, 1–30 (2011).
15. Bullock, D. G. & Anderson, D. S. Evaluation of the Minolta SPAD-502 chlorophyll meter for nitrogen management in corn. *J. Plant Nutr.* **21**, 741–755 (1998).
16. Markwell, J., Osterman, J. C. & Mitchell, J. L. Calibration of the Minolta SPAD-502 leaf chlorophyll meter. *Photosynth. Res.* **46**, 467–472 (1995).
17. Cerovic, Z. G., Masdoumier, G., Ghozlen, N. B. & Latouche, G. A new optical leaf-clip meter for simultaneous non-destructive assessment of leaf chlorophyll and epidermal flavonoids. *Physiol. Plantarum.* **146**, 251–260 (2012).
18. Atzberger, C. Advances in remote sensing of agriculture: Context description, existing operational monitoring systems and major information needs. *Remote Sens.* **5**, 949–981 (2013).
19. Sakamoto, T. *et al.* An alternative method using digital cameras for continuous monitoring of crop status. *Agric. For. Meteorol.* **113**, 154–155 (2012).
20. Fernandez-Gallego, J. A. *et al.* Low-cost assessment of grain yield in durum wheat using RGB images. *Eur. J. Agron.* **105**, 146–156 (2019).
21. Araus, J. L. & Kafauver, S. C. Breeding to adapt agriculture to climate change: affordable phenotyping solutions. *Curr. Opin. Plant Biol.* **45**, 237–247 (2018).
22. Gracia-Romero, A. *et al.* Phenotyping conservation agriculture management effects on ground and aerial remote sensing assessments of maize hybrids performance in Zimbabwe. *Remote Sens.* **10**(2), 349 (2018).
23. Araus, J. L. & Cairns, J. E. Field high-throughput phenotyping: the new crop breeding frontier. *Trends Plant Sci.* **19**, 52–61 (2014).
24. Yousefi, S., Serret, M. D., Marquez A. J., Voltas, J. & Araus, J. L. Combined use of $\delta^{13}\text{C}$, $\delta^{18}\text{O}$ and $\delta^{15}\text{N}$ tracks nitrogen metabolism and genotypic adaptation of durum wheat to salinity and water deficit. *New Phytol.* **194**, 230–244 (2012).
25. Vergara-Díaz, O. *et al.* A novel remote sensing approach for prediction of Maize yield under different conditions of nitrogen fertilization. *Front. Plant Sci.* **7**, 1–13 (2016).
26. Araus, L., Sánchez, C. & Cabrera-Bosquet, L. Is heterosis in maize mediated through better water use?. *New Phytol.* **187**(2), 392–406 (2010).
27. Thierfelder, C. & Wall, P. C. Investigating conservation agriculture (CA) systems in Zambia and Zimbabwe to mitigate future effects of climate change. *J. Crop Improv.* **24**, 113–121 (2010).
28. Rusinamhodzi, L. *et al.* A meta-analysis of long-term effects of conservation agriculture on maize grain yield under rain-fed conditions. *Agron. Sustain. Dev.* **31**, 657–673 (2011).
29. Kafesu, N. *et al.* Comparative fertilization effects on maize productivity under conservation and conventional tillage on sandy soils in a smallholder cropping system in Zimbabwe. *Field Crops Res.* **218**, 106–114 (2018).
30. Arvidsson, J., Etana, A. & Rydberg, T. Crop yield in Swedish experiments with shallow tillage and no-tillage 1983–2012. *Eur. J. Agron.* **52**, 307–315 (2014).
31. Habig, J. & Swanepoel, C. Effects of conservation agriculture and fertilization on soil microbial diversity and activity. *Environmental* **2**, 358–384 (2015).
32. Fonte, S. J., Quansah, G. W. & Six, J. Fertilizer and residue quality effects on organic matter stabilization in soil aggregates. *Soil Biol. Biochem.* **73**(3), 961–966 (2009).
33. Gabriel, J. L. *et al.* Airborne and ground level sensors for monitoring nitrogen status in a maize crop. *Biosyst. Eng.* **160**, 124–133 (2017).
34. Choi, W.-J., Lee, S.-M., Ro, H.-M., Kim, K.-C. & Yoo, S.-H. Natural ^{15}N abundances of maize and soil amended with urea and composted pig manure. *Plant Soil* **245**, 223–232 (2002).
35. Bateman, A. S., Kelly, S. D. & Jickells, T. D. Nitrogen isotope relationships between crops and fertilizer: implications for using nitrogen isotope analysis as an indicator of agricultural regime. *J. Agric. Food Chem.* **53**, 5760–5765 (2005).
36. Serret, M. D., Ortiz-Monasterio, I., Pardo, A. & Araus, J. L. The effects of urea fertilization and genotype on yield, nitrogen use efficiency, $\delta^{15}\text{N}$ and $\delta^{13}\text{C}$ in wheat. *Ann. Appl. Biol.* **153**, 243–257 (2008).
37. Amundson, R. *et al.* Global patterns of the isotopic composition of soil and plant nitrogen. *Glob. Biogeochem. Cycles* <https://doi.org/10.1029/2002GB001903> (2003).
38. Farquhar, G. D., Ehleringer, R. & Hubick, K. T. Carbon isotope discrimination and photosynthesis. *Annu. Rev. Plant Physiol. Plant Mol. Biol.* **40**, 503–537 (1989).
39. Monneveux, P., Sheshshayee, M. S., Akhter, J. & Ribaut, J. M. Using carbon isotope discrimination to select maize (*Zea mays* L.) inbred lines and hybrids for drought tolerance. *Plant Sci.* **173**, 390–396 (2007).
40. Cabrera-Bosquet, L., Molerio, G., Nogués, S. & Araus, J. L. Water and nitrogen conditions affect the relationships of $\Delta^{13}\text{C}$ and $\Delta^{18}\text{O}$ to gas exchange and growth in durum wheat. *J. Exp. Bot.* **60**, 1633–1644 (2009).
41. Farquhar, G. D. On the nature of carbon isotope discrimination in C4 species. *Aust. J. Plant Physiol.* **10**, 205 (1983).
42. Evans, J. R. Nitrogen and photosynthesis in the flag leaf of wheat (*Triticum aestivum* L.). *Plant Phys.* **5**, 297–302 (1983).
43. Szabó, É. Effect of some physiological properties on the quality parameters of different winter wheat varieties in a long-term experiment. *Cereal Res. Commun.* **42**, 126–138 (2013).
44. Giunta, F., Motzo, R. & Deidda, M. SPAD readings and associated leaf traits in durum wheat, barley and triticale cultivars. *Euphytica* **125**, 197–205 (2002).
45. Zhang, Y., Tremblay, N. & Zhu, J. Evaluation of the Multiplex[®] fluorescence sensor for the assessment of corn nitrogen status. *J. Food Agric. Environ.* **10**(1), 1008–1016 (2012).
46. Cairns, J. E., Sanchez, C., Vargas, M., Ordoñez, R. & Araus, J. L. Dissecting maize productivity: ideotypes associated with grain yield under drought stress and well-watered conditions. *J. Integr. Plant Biol.* **54**, 1007–1020 (2012).
47. Buchailot, M. L. *et al.* Evaluating maize genotype performance under low nitrogen conditions using RGB UAV phenotyping techniques. *Sensors* **19**(8), 1815 (2019).
48. Monneveux, P., Sanchez, C. & Tiessen, A. Future progress in drought tolerance in maize needs new secondary traits and cross combinations. *J. Agric. Sci.* **146**, 287–300 (2008).

49. Hu, H. *et al.* Assessment of chlorophyll content based on image color analysis, comparison with SPAD-502. In *2nd International Conference on Information Engineering and Computer Science—Proceedings, ICIECS 2010* (2010).
50. Sevik, H., Belkaylai, N. & Aktar, G. Change of chlorophyll amount in some landscape plants. *J. Biotech. Sci.* **2**(1), 10–16 (2014).
51. Sevik, H., Karakas, H. & Karaca, U. Color—chlorophyll relationship of some indoor ornamental plants. *Int. J. Eng. Sci. Res. Technol.* **2**, 1706–1712 (2013).
52. Pointer, M. R. A comparison of the CIE 1976 colour spaces. *Color Res. App.* **6**, 108–118 (2009).
53. Cooper, F. G. *Munsell Manual of Color* (Munsell Color Company Inc, Boston, 1929).
54. Carper, W. J., Lillesand, T. M. & Kiefer, R. W. The use of intensity-hue-saturation transformations for merging SPOT panchromatic and multispectral image data. *Photogram. Eng. Remote Sens.* **56**(4), 459–467 (1990).
55. Hunt, E. R. Jr., Cavigelli, M., Daughtry, C. S. T., McMurtrey Iii, J. & Walthall, C. L. Evaluation of digital photography from model aircraft for remote sensing of crop biomass and nitrogen status. *Precis. Agric.* **6**, 359–378 (2005).
56. Hunt, R. & Perry, E. M. A visible band index for remote sensing leaf chlorophyll content at the canopy scale. *Int. J. Appl. Earth Obs. Geoinf.* **21**, 103–112 (2013).
57. Gracia-Romero, A. *et al.* Comparative performance of ground vs. Aerially assessed rgb and multispectral indices for early-growth evaluation of maize performance under phosphorus fertilization. *Front. Plant Sci.* **8**, 2004 (2017).
58. Süß, A. *et al.* Measuring leaf chlorophyll content with the Konica Minolta SPAD-502Plus—theory, measurement, problems, interpretation. *EnMAP Field Guides Technical Report, GFZ Data Services* (2015).
59. Casadesus, J. *et al.* Using vegetation indices derived from conventional digital cameras as selection criteria for wheat breeding in water-limited environments. *Ann. App. Biol.* **150**, 227–236 (2007).
60. Erdle, K., Mistele, B. & Schmidhalter, U. Comparison of active and passive spectral sensors in discriminating biomass parameters and nitrogen status in wheat cultivars. *Field Crops Res.* **124**, 74–84 (2011).
61. Zaman-Allah, M. *et al.* Unmanned aerial platform-based multi-spectral imaging for field phenotyping of maize. *Plant Methods* **11**, 35 (2015).
62. Gracia-Romero, A., Kefauver, S. C., Fernandez-Gallego, J. A., Vergara-Díaz, O. & Araus, J. L. UAV and ground image-based phenotyping: a proof of concept with Durum wheat. *Remote Sens.* **11**(10), 1244 (2019).
63. Cerovic, Z. G. *et al.* Nondestructive diagnostic test for nitrogen nutrition of grapevine (*Vitis vinifera* L.) based on dual leaf-clip measurements in the field. *J. Agric. Food Chem.* **63**, 3669–3680 (2015).
64. Bendig, J. *et al.* Estimating biomass of barley using crop surface models (CSMs) derived from UAV-based RGB imaging. *Remote Sens.* **6**, 10395–10412 (2014).
65. Coplen, T. B. & Zhu, X. K. Explanatory glossary of terms used in expression of relative isotope ratios and gas ratios. IUPAC Recommendations 1–27 (2008).

Acknowledgements

The authors of this research thank the personnel from CIMMYT Southern Africa Regional Office at Harare for their support during the field measurements and sampling, and their continued support of our research. Finally, we thank Jaume Casadesus for providing the Breedpix software. The authors of this research thank the personnel from CIMMYT Southern Africa Regional Office at Harare for their support during the field measurements and sampling, and their continued support of our research. Finally, we thank Jaume Casadesus for providing the Breedpix software.

Author contributions

C.T. designed the trial and conducted all the crop management steps at the Southern African Regional Office of CIMMYT in Harare with the help of CIMMYT technicians. M.Z.-A., B.P. and J.C. directed the research questions and analysis. M.Z.-A. carried out the UAV flights for the obtainment of aerial measurements. A.G.-R., S.C.K., O.V.-D., J.L.A. and E.H. conducted the field measurements and the collection of samples. A.G.-R. processed and analyzed the images, analyzed the leaf samples at the laboratory and wrote the paper under the supervision of J.A. and S.K. and with the contributions from all the other authors.

Funding

This work was supported by the Bill & Melinda Gates Foundation and USAID funded project Stress Tolerant Maize for Africa (STMA) (grant number OPP1134248) and the CGIAR Research Program on Maize (MAIZE). The CGIAR Research Program MAIZE receives W1&W2 support from the Governments of Australia, Belgium, Canada, China, France, India, Japan, Korea, Mexico, Netherlands, New Zealand, Norway, Sweden, Switzerland, U.K., U.S., and the World Bank. A.G.-R. is a recipient of a FPI doctoral fellowship from the AGL2016-76527-R Project from the Ministerio de Economía y Competitividad of the Spanish Government. We also acknowledge the support from the Institut de Recerca de l'Aigua and the Universitat de Barcelona. J.L.A. acknowledges the funding support from ICREA, Generalitat de Catalunya, Spain.

Competing interests

The authors declare no competing interests.

Additional information

Supplementary information is available for this paper at <https://doi.org/10.1038/s41598-020-73110-3>.

Correspondence and requests for materials should be addressed to J.L.A.

Reprints and permissions information is available at www.nature.com/reprints.

Publisher's note Springer Nature remains neutral with regard to jurisdictional claims in published maps and institutional affiliations.



Open Access This article is licensed under a Creative Commons Attribution 4.0 International License, which permits use, sharing, adaptation, distribution and reproduction in any medium or format, as long as you give appropriate credit to the original author(s) and the source, provide a link to the Creative Commons licence, and indicate if changes were made. The images or other third party material in this article are included in the article's Creative Commons licence, unless indicated otherwise in a credit line to the material. If material is not included in the article's Creative Commons licence and your intended use is not permitted by statutory regulation or exceeds the permitted use, you will need to obtain permission directly from the copyright holder. To view a copy of this licence, visit <http://creativecommons.org/licenses/by/4.0/>.

© The Author(s) 2020



CHAPTER 5

High-throughput phenotyping to define of durum wheat ideotypes adapted to Mediterranean environments

Adrian Gracia-Romero, Thomas Vatter, Shawn C. Kefauver, Fatima Z. Rezzouk, Joel Segarra, María Teresa Nieto-Taladriz, Nieves Aparicio and José L. Araus

Submitted to:
The Plant Journal

High-throughput phenotyping to define of durum wheat ideotypes adapted to Mediterranean environments

Adrian Gracia-Romero¹, Thomas Vatter¹, Shawn C. Kefauver¹, Fatima Z. Rezzouk¹, Joel Segarra¹, María Teresa Nieto-Taladriz², Nieves Aparicio³ and José L. Araus¹

¹Integrative Crop Ecophysiology Group, Plant Physiology Section, Faculty of Biology, University of Barcelona, Barcelona, Spain and AGROTECNIO (Center for Research in Agrotechnology), Av. Rovira Roure 191, 25198 Lleida, Spain

²Instituto Nacional de Investigación y Tecnología Agraria y Alimentaria (INIA), Ctra. de la Coruña Km. 7.5, 28040 Madrid, Spain

³Agro-technological Institute of Castilla y León (ITACyL), Ctra de Burgos 119, 47071, Valladolid, Spain

Abstract

Durum wheat is one of the main staple crops in the Mediterranean, where abiotic stresses such as water stress, high temperature and soil fertility are main factors limiting productivity. Understanding the complex interactions between the genotypic, environmental and agronomic management factors (G x E x M) is crucial for the success of yield improvement programs. Plant breeders seek to define ideotypes understood as selection criteria based on a combination of physiological and morphological traits that may help crops to perform optimally within a given agro-climatic context. The present study aims to define ideotypes specific for different Mediterranean agroclimatic conditions. A set of 24 modern cultivars of durum wheat were grown over three consecutive crop seasons (from 2016 to 2019), at three different sites located across a wide range of latitudes in Spain (Coria del Rio, Aranjuez and Valladolid) and grown under different management conditions (support irrigation, rainfed, low-nitrogen and late planting) and a wide range of productivity. Phenology (heading time) was assessed. In addition, different remote sensing methodologies including canopy temperature (CT) and vegetation indices (Vis) derived from RGB (Red-Green-Blue) and multispectral images taken at ground and aerial levels and pigment content at single leaf level. Measurements were performed during the reproductive stage (heading to grain filling). At maturity grain yield (GY) and the stable C ($\delta^{13}\text{C}$) and N isotope composition and total N content of mature grains analyzed. A feature selection based on a detection rate over 100 cross-

validation runs of LASSO regression was performed across all the measurements along the phenology to assess which traits were more critical predicting GY. In general terms, indicator of a higher biomass, such as plant height or canopy green biomass inferred from VIs, together with indicators of better water status, such as lower CT and $\delta^{13}\text{C}$, were the most incorporated traits of the GY models. Under water-limited environments, best cultivars also exhibited higher levels of protective pigments (during anthesis and the delay of canopy senescence. For the late-planting conditions, exposed to higher temperatures, a higher photosynthetic efficiency, inferred from the photosynthesis reflectance index was also involved. However, phenology was not chosen in any case. We conclude that the idiotypic traits identified and the high throughput methods to phenotype them may be useful for identifying high performing wheat cultivars under a wide range of Mediterranean conditions.

Introduction

Resilience of staple food crops as wheat to the variability of climatic and field conditions plays a vital role to ensure food security. This is particularly evident for durum wheat one of the main herbaceous crops in the Mediterranean, frequently submitted to abiotic stresses such as water stress and high temperature and other unfavorable conditions which limit its productivity. As crop performance gets disturbed through different mechanisms, a diversity of responses to growing conditions can be considered as key determinant for boosting yield and stability in breeding programs (Kahiluoto *et al.*, 2019). The susceptibility of wheat to stress caused by climatic variability is dependent on the degree of adaptation of a cultivar to the local growing conditions (B. *et al.*, 2003). Understanding the complex interactions between the genotype, the environment conditions and the specific agronomic management (G x E x M) is crucial for the success of crop improvement programs. This includes not only to characterize the target trait, usually the grain yield, but eventually also phenotypic traits of diverse nature, such as phenology and other morphophysiological traits putatively associated with the yield.

The definition of a combination of morphological and physiological traits which theoretically optimize crop performance under a particular environmental condition is known as crop ideotype. The first wheat ideotype was proposed by (Donald, 1968) for non-limiting agronomical conditions and defined as plants of short stature, strong stem, low tillering capacity and large and erect ears. According to this approach, the breeding of new cultivars resulted in an improvement of lodging prevention, amenable for high

nitrogen fertilization inputs, and a boost of harvest index (Hamblin, 1993). When focus on Mediterranean conditions phenological adjustment, including earlier heading, anthesis and maturity, and to a lesser extent early vigor, have been recurrent traits when designing “Mediterranean ecotypes” (Loss and Siddique, 1994; Sadras and Richards, 2014). However, the benefits accounted by shorter crop cycles appear as a nearly exploded (Chairi *et al.*, 2018), so other traits conferring adaptation to Mediterranean conditions have to be explored.

The concept of crop ideotype allow breeders to focus their selection process on specific trait-based model, rather than just the traditional empirical method of selection for yield. However, the concept of ideotype has to move a step ahead, from the empirical enumeration of potential traits putatively associated with crop performance, by beneficiating of the current developments on high throughput phenotyping, including statistical models (Paleari *et al.*, 2020). Modern breeding strategies are moving from the development of high-plasticity genotypes to improve performance under a wide range of environments, to model the specified set of characteristics of a genotype for a particular environmental growing condition (Jaradat, 2018). Therefore, a more modern definition of the concept of ideotype can be referred to the seeking of the best crop phenotype to grow in a given environment, with a defined cropping system (Martre *et al.*, 2015).

Ideotype design for a target environment implies a concrete guideline of traits determining yield through the crop cycle. To that end, the main objective of crop phenotyping in support of the ideotypic characterization is to measure a key set of traits, informing on crop growth and agronomic performance, and that will determine yield. Hence, the phenotyping process seek the identification of which traits should be measured and how to measure them (Watt *et al.*, 2020). Plant phenotyping pursues the non-invasive characterization of genotypes interacting with the environment, and studies are focusing in developing high-throughput plant phenotyping (HTPP) methodologies at affordable costs, issue often regarded as a major bottleneck in the breeding process (Araus and Cairns, 2014). Broadly, high-throughput phenotyping is currently mostly based in non-destructive (mainly of remote sensing nature) evaluations at different levels, from measurements on single leaves, such as for example their pigment content, or their chlorophyll fluorescence, to the more and more frequent evaluation at the canopy level using sensors and imagers of different nature, either from ground or placed in aerial platforms (Gracia-Romero *et al.*, 2019). The formulation of vegetation indices (VIs)

based, for example, on the combination of different spectral bands is well established assessing morphological and physiological plant aspects at both, canopy and single-leaf levels. Currently, the implementation of low-cost conventional cameras to formulate vegetation indices derived from red-green-blue image (i.e., information from the visible range) is increasingly successful as Vis in studying aspects related to the above-canopy architecture and color (Jose A. Fernandez-Gallego *et al.*, 2019). Moreover, canopy temperature (CT) has been related to water-use and yield formation in crops, since transpiration is the main factor reducing leaf's temperature (Jackson *et al.*, 1988; González-Dugo *et al.*, 2006). However, phenotyping is not necessarily restricted to the use of a panoply of different remote sensing techniques, but also some analytical (i.e. lab) traits may be very useful. Thus, the analysis of stable isotopes, when performed on plant dry matter, constitutes an integrative indicator of plant status over the crop cycle. The stable carbon ($\delta^{13}\text{C}$) and nitrogen ($\delta^{15}\text{N}$) isotope compositions, when analyzed in plant matter, inform on the water regimen (Farquhara and Richardsb, 1984) and nitrogen metabolism (Yousfi *et al.*, 2012) of the plant.

At the present, one of the major challenges, related with the successful implementation of HTPP defining ideotypes, lies on unlocking the potential of the huge amounts of data generated by the high-through phenotyping platforms (Coppens *et al.*, 2017). The interpretation of data and the extraction of useful information relies on the development of algorithms. Conventionally, these statistical models are based on response functions between yield and some input variables, estimating production reasonably well (Filippi *et al.*, 2019). New insights in machine learning (ML) aim the interpretation of data by the development of algorithms built from training sets (van Klompenburg *et al.*, 2020) and are increasingly being used for agricultural applications (Liakos *et al.*, 2018). Least absolute shrinkage and selection operator (LASSO) is a regression analysis method that choose models that both fit well and minimize the number of predictors by performing a variable selection (Tibshirani, 1996). This approach is being presented as an effective strategy to selecting relevant measured features to build a GY prediction model.

This study aimed the evaluation of the performance of a set of wheat cultivars grown in a wide range of Spanish latitudes for three consecutive crop seasons, with very diverse climatic conditions, and in trials under different growing conditions (well-irrigated, rainfed, late-planting and low-nitrogen). Apart from the GY, the evaluation was carried out through leaf pigments readings and canopy field evaluation using RGB (Red-Green-

Blue) and multispectral vegetation indices and thermal measurements evaluated from ground and using a unmanned aerial vehicle- Measurements were performed at different phenological stages during the reproductive part of the crop, since Mediterranean agro-environments are characterized by the occurrence of terminal (i.e. during the last part of the crop cycle) stresses, such as drought and heat. Thereafter, variables measured were used to perform GY prediction models within environments using the LASSO model and the detection rate across 100 validations was used to the design of wheat ideotypes.

2. Materials and Methods

2.1. Experimental design and varieties

Experiments were carried out under field conditions in three experimental stations located across a wide range of latitudes in Spain (Figure 1): two belonging to the Spanish “Instituto Nacional de Investigación y Tecnología Agraria y Alimentaria” (INIA) and placed in Coria del Rio, Seville ($37^{\circ}14'N$, $06^{\circ}03'W$, 5 masl) and Colmenar de Oreja – Aranjuez, Madrid ($40^{\circ}04'N$, $3^{\circ}31'W$, 590 masl), and one at the headquarters of the “Instituto Tecnológico Agrario de Castilla y León” (ITACyL) in Zamadueñas, Valladolid ($41^{\circ}41'N$, $04^{\circ}42'W$, 700 masl) during three consecutive crop seasons between 2016 and 2019.

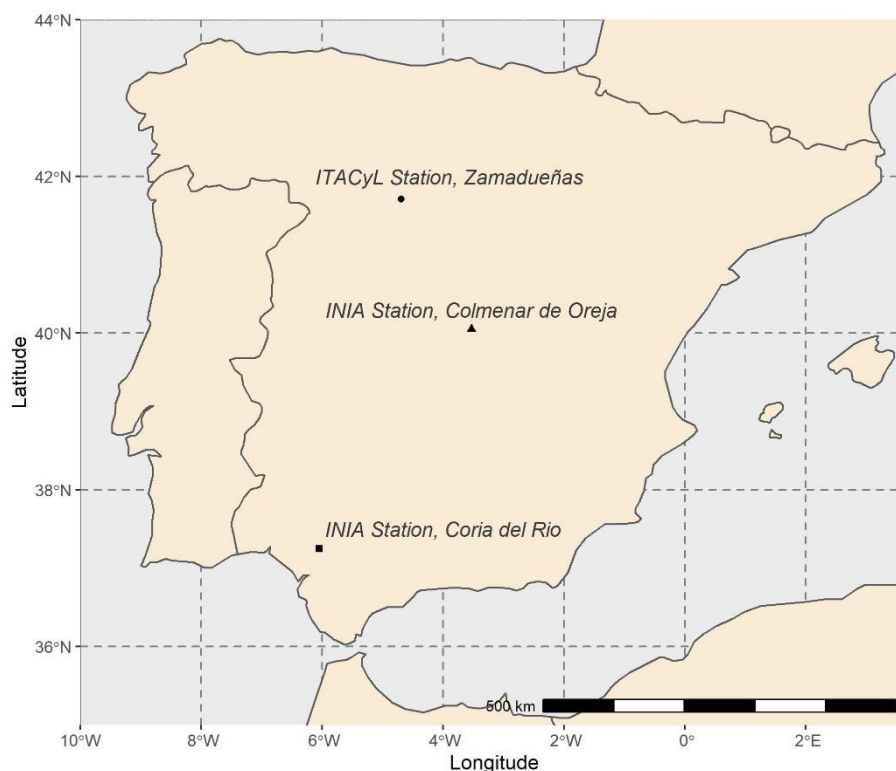


Figure 1. Map of Spain with the location of the experimental stations.

Climatic data from the different crop seasons at each experimental station was recorded through the Spanish platform SIAR (Servicio de Informacion Agroclimática para el Regadio, www.siar.es) from meteorological stations next to the fields. Monthly temperature and rainfall averages are plotted in Figure 2. The trial of Coria del Rio recorded an average temperature of 14.5, 13.1 and 14.4 °C, an accumulated precipitation of 188.2, 380.6 and 134.6 mm and a potential evapotranspiration of 660.6, 561.3 and 700.9 mm from sowing to physiological maturity for each growing season. The trials in Aranjuez achieved an average temperature of 11.4, 9.5 and 10.4°C, an accumulated precipitation of 86.4, 300.7 and 89.8 mm and a potential evapotranspiration of 595.8, 512.4 and 588.3 mm for each growing season. Finally, the fields of Valladolid recorded 11.7, 9.6 and 10.1°C, an accumulated precipitation of 107.3, 420.5 and 103.3 mm and a potential evapotranspiration of 580.3, 459.5 and 537.9 mm.

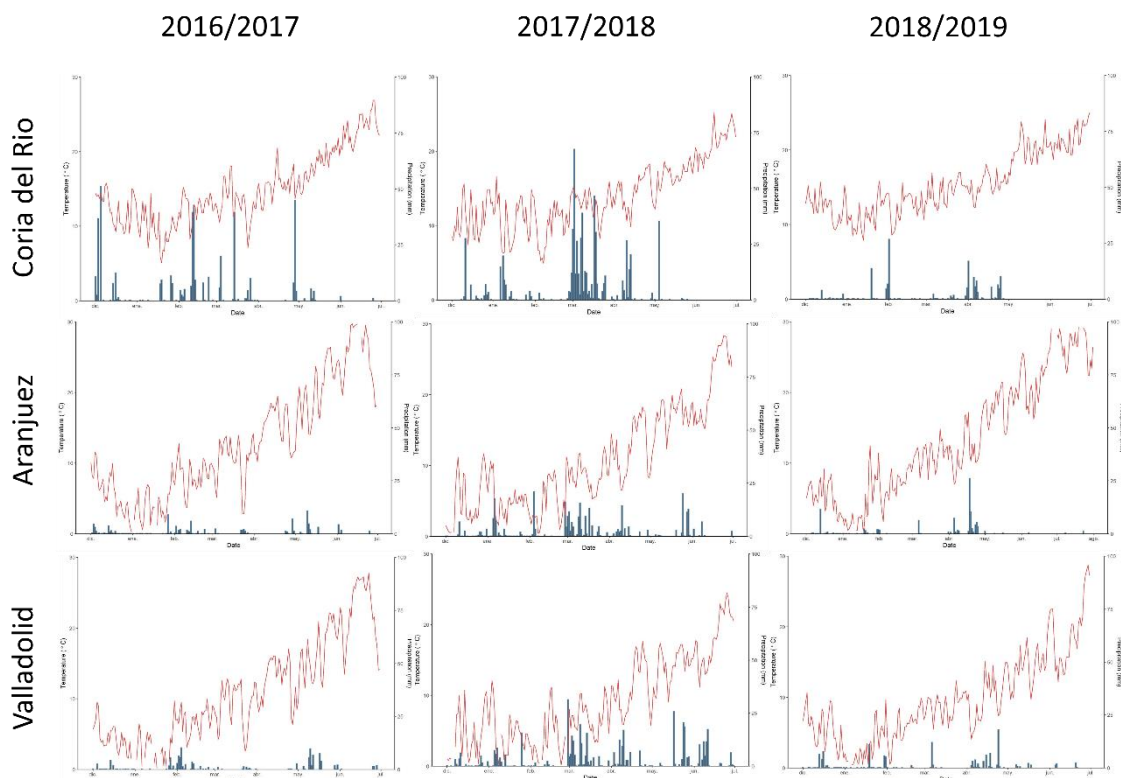


Figure 2. Mean temperature (red) and rainfall (blue) in Coria del Rio, Aranjuez and Valladolid for the crop seasons 2016/2017, 2017/2018 and 2018/2019.

A panel of 24 semi-dwarf varieties of durum wheat marketed in Spain, France and Italy during the last four decades was grown at each experimental station (Table 1), sown in a randomized blocks design with three replicates.

Table 1. Set of modern semi-dwarf durum wheat cultivars tested in this study with year of release, country of origin and available information on provenance and/or pedigree.

Genotype	Year of release	Country	Provenance/Pedigree
Mexa	1980	Spain	GERARDO-VZ-469/3/JORI(SIB)//ND-61-130/LEEDS
Vitron	1983	Spain	TURCHIA-77/3/JORI-69(SIB)/(SIB)ANHINGA//(SIB)FLAMINGO
Simeto	1988	Italy	CAPEITI-8/VALNOVA[1620][1622][1623][1625][1666]
Gallareta	1994	Spain	RUFF/FLAMINGO//MEXICALI-75/3/SHEARWATER
Pedroso	1993	Spain	Battle seeds
Regallo	1990	Spain	Diputación General de Aragón
Arcobaleno	1996	Spain	Chen/Altar84
Claudio	1998	Italy	SEL.CIMMYT-35/DURANGO//ISEA-1938/GRAZIA
Burgos	1999	Spain	SUDDEUTSCHE SAATZ
Dorondon	1990	Spain	Genética y Gestión,S.C.
Avispa	2001	Italy	Limagrain-CIMMYT
Amilcar	2002	Spain	ZEGZAG-1/LUNDE-5//GREENSHANK-32
Saragolla	2004	Italy	Iride/0114
Solea	2005	Spain	Monsanto Agriculture Spain
Euroduro	2007	Spain	IRTA
Don Ricardo	2008	Spain	Agrovegetal-CIMMYT
Core	2009	Spain	Eurogen, PROSEME seeds
Kiko Nick	2009	Spain	SEL.CIMMYT-35/DURANGO//ISEA-1938/GRAZIA
Sculptur	2011	France	RAGT Semence
Athoris	2011	Italy	Limagrain Europe
Don Norman	2012	Spain	Agrovegetal - CIMMYT
Olivadur	2013	Spain	RAGT 2N SAS seeds
Iberus	2014	Spain	Agromonegros
Haristide	2015	France	Caussade Semences S.A.

Supplemental irrigation, rainfed and late-planting conditions were imposed in the fields of Aranjuez and Valladolid, while in Coria del Rio, due to the presence of a shallow water caused by proximity to the Guadalquivir River, genotypes were evaluated under rainfed conditions. Additionally, a low nitrogen and rainfed conditions were also imposed in Valladolid during the last two cropping seasons. Field management information of each growing conditions at each field station is presented in Table 2.

Table 2. Agronomic information for each study site during each growing season. L, Location; T, Trial; Y, Year.

L	T	Y	Sowing date	Harvest date	Irrigation (mm)	Precip. (mm)	Water received (mm)	Basic dressing (8-15-15 NPK kg ha ⁻¹)	Top dressing (46% Urea kg ha ⁻¹)
Coria	Rainfed	2016/17	14/12/16	12/06/17	0	188.2	188.2	450 _(12/12/16)	227 _(15/03/17)
		2017/18	20/12/17	19/06/18	0	380.6	380.6	450 _(18/12/17)	227 _(13/03/18)
		2018/19	18/12/19	18/06/19	0	134.6	134.6	450 _(14/12/18)	227 _(14/03/19)
Aranjuez	Irrigation	2016/17	14/12/16	19/07/17	395	595.8	990.8	450 _(16/12/16)	227 _(15/03/17)
		2017/18	28/11/17	04/07/18	140	512.4	652.4	450 _(23/11/17)	185 _(28/02/19)
		2018/19	29/11/18	28/06/19	540	588.3	1128.3	450 _(23/11/17)	230 _(27/02/18)
	Rainfed	2016/17	14/12/16	19/07/17	0	595.8	595.8	450 _(16/12/16)	227 _(15/03/17)
		2017/18	28/11/17	04/07/18	0	512.4	512.4	450 _(26/02/18)	185 _(28/02/19)
		2018/19	29/11/18	28/06/19	0	588.3	588.3	450 _(26/11/18)	230 _(27/02/18)
	Late	2016/17	01/03/17	19/07/17	425	595.8	1020.8	450 _(16/12/16)	227 _(15/03/17)
		2017/18	26/02/18	10/07/18	220	512.4	732.4	450 _(26/11/18)	185 _(16/04/19)
		2018/19	27/02/19	05/07/19	680	588.3	1268.3	450 _(23/02/19)	230 _(23/04/18)
Valladolid	Irrigation	2016/17	29/11/16	06/07/17	155	107.3	262.3	300 _(07/11/16)	150 _(17/02/17) + 150 _(21/03/17)
		2017/18	13/11/17	25/07/18	109.8	420.5	420.5	300 _(12/11/17)	150 _(20/02/18) + 150 _(17/04/18)
		2018/19	03/12/18	15/07/19	152.7	103.3	103.3	300 _(16/11/18)	150 _(28/02/19) + 150 _(12/04/19)
	Rainfed	2016/17	29/11/16	06/07/17	55	107.3	162.3	300 _(07/11/2016)	150 _(17/02/17) + 150 _(21/03/17)
		2017/18	23/11/17	20/07/18	0	420.5	420.5	300 _(12/11/17)	150 _(20/02/18) + 150 _(17/04/18)
		2018/19	03/12/18	03/07/19	0	103.3	103.3	300 _(16/11/18)	150 _(28/02/19) + 150 _(12/04/19)
	Late	2016/17	09/02/17	20/07/17	155	107.3	107.3	300 _(07/11/16)	150 _(21/03/17)
	Low-N	2017/18	23/11/17	20/07/18	0	420.5	420.5	0	0
		2018/19	03/12/18	03/07/19	0	103.3	103.3	0	0

2.2 Data collection

Phenology information, plant height and remote sensing measurements were recorded during various sampling visits at each site along the crop seasons in order to assess wheat performance at different growing stages (Table 3). The development of cultivars was determined by using Zadoks scale values (Zadoks *et al.*, 1974), as well as the counting of days after sowing (DAS) and growing degree days (GDD). GDD was calculated as follows (Equation (1)):

$$GDD = \sum \left(\frac{T_{max} + T_{min}}{2} \right) - T_{base} \quad (1)$$

where T_{max} corresponds to the highest daily temperature, T_{min} to the lowest, and the T_{base} used was 0 °C. Days to heading (DTH) were determined when approximately 50 % of ears had emerged. Plant height (PH) was measured using a ruler placed zenithally in the central rows of each selected plot, and values were taken by observing the whole canopy and averaging the distance from the ground to the overall tip of the ears, excluding the awns. Grain yield (GY) ($Mg\ ha^{-1}$) was determined for the entire plot, using a harvester. The set of sensors and cameras used will be described in the following sections.

Table 3. Dates of the sampling visits to the field and the approximate phenological stages (across the set of 24 genotypes), the count of days after sowing (DAS) and accumulated growing degree days (GDD) of the crops. L, Location; T, Trial; Y, Year.

L	T	Y	Sampling date	Phenological Stage	DAS	GDD	
Coria	Rainfed	2016/17	05/04/17	Heading	112	1360.12	
			25/04/17	Grain filling	132	1680.20	
			18/04/18	Anthesis	119	1440.45	
		2017/18		Late grain filling	146	1884.88	
			2018/19	04/04/19	Anthesis	107	1425.84
				02/05/19	Grain filling	135	1863.46
Aranjuez	Irrigation	2016/17	26/04/17	Heading	125	2224.05	
			04/05/17	Anthesis	133	2399.68	
				Milk grain filling	147	2767.24	
			06/06/17	Senescence Stem	166	3377.17	
		2017/18	20/04/18	elongation	143	990.67	
			16/05/18	Anthesis	169	1387.76	
				Milk development	181	1622.30	
			28/05/18				

			Medium		
		11/06/18	dought	195	1864.20
		13/05/19	Anthesis	165	1511.91
	2018/19	27/05/19	Grain filling	179	1769.29
		11/06/19	Senescence	194	2070.86
		26/04/17	Heading	125	2224.05
	2016/17	04/05/17	Anthesis	133	2399.68
			Late grain		
		18/05/17	filling	147	2767.24
		06/06/17	Senescence	166	3377.17
			Stem		
	Rainfed	20/04/18	elongation	143	990.67
		16/05/18	Anthesis	169	1387.76
	2017/18		Milk		
		28/05/18	development	181	1622.30
			Medium		
		11/06/18	dought	195	1864.20
		13/05/19	Anthesis	165	1511.91
	2018/19	27/05/19	Grain filling	179	1769.29
		11/06/19	Senescence	194	2070.86
			Stem		
		26/04/17	Elongation	56	1270.57
	2016/17	04/05/17	Booting	64	1446.21
		18/05/17	Heading	78	1813.76
			Milk Grain		
		06/06/17	Filling	97	2423.69
			Stem		
	Late	20/04/18	Elongation	53	990.67
		16/05/18	Heading	79	1387.76
	2017/18	28/05/18	Pre-anthesis	91	1622.30
		11/06/18	Soft dought	105	1864.20
			Stem		
		13/05/19	Elongation	75	1511.91
	2018/19	27/05/19	Anthesis	89	1769.29
			Milk Grain		
		11/06/19	Filling	104	2070.86
			Stem		
		16/05/17	Anthesis	168	1382.38
	2016/17	07/06/17	Grain filling	190	1794.34
		17/05/18	Pre-anthesis	185	1176.57
			Milk		
	2017/18	30/05/18	development	198	1385.46
		13/06/18	Late Milk	212	1599.35
		15/05/19	Pre-anthesis	163	1274.48
			Milk		
	2018/19	29/05/19	development	177	1473.95
			Late grain		
		12/06/19	filling	191	1708.50
		16/05/17	Anthesis	168	1382.38
	2016/17	07/06/17	Grain filling	190	1794.34
		17/05/18	Pre-anthesis	534	1176.57
	2017/18				

			Milk		
		30/05/18	development	198	1385.46
		13/06/20			
		18	Late Milk	212	1599.35
		15/05/19	Pre-anthesis	163	1274.48
	2018/19		Milk		
		29/05/19	development	177	1473.95
		12/06/19	Late Milk	191	1708.50
Late	2016/17	16/05/17	Heading	96	1382.38
		07/06/17	Anthesis	118	1794.34
		17/05/18	Pre-anthesis	185	1176.57
	2017/18		Milk		
		30/05/18	development	198	1385.46
		13/06/18	Mid Milk	212	1599.35
Low-N		15/05/19	Pre-anthesis	163	1274.48
	2018/19		Milk		
		29/05/19	development	177	1473.95
		12/06/19	Late Milk	191	1708.50

2.3 Leaf pigments

The content of different leaf pigments was assessed using the Dualex Scientific (Force-A, Orsay, France), a sensor that operates with a red reference beam at 650 nm and a UV light at 375 nm (Cerovic *et al.*, 2012). This sensor produces relative measures of chlorophylls a + b (Chl), flavonoids (Flav) and anthocyanin (Anth) content, and also calculates the nitrogen balance index (NBI), which is the ratio Chl/Flav related to the nitrogen and carbon allocation. For each visit and plot five measurements of five different leaves from five different plants were performed. The measurements were taken from the middle portion of the leaves.

2.4 RGB images and derived vegetation indices

Vegetation indices derived from RGB images were evaluated for each plot from the ground and aerial levels. Ground evaluations were conducted using a 20.1-megapixel Sony ILCE-QX1 (Sony Corporation, Minato, Japan) attached to a Sony Monopod VCTMP1 (Sony Corporation, Minato, Japan) and the distance to the crop canopy adjusted to 1 m. Aerial RGB images during the three consecutive crop seasons were captured with a 16-megapixel Lumix GX7 (Panasonic, Osaka, Japan) with the ground sample distance (GSD) for a flight of 50 m altitude as 0.941 cm/pixel. During the crop seasons 2018/2019, aerial images were captured using a DJI Mavic 2 Pro (DJI Corporation, Shenzhen, China) with a 20-megapixel camera with the GSD for a flight of 50 m altitude as 0.201 cm/pixel.

The color calibration of both cameras with the ColorChecker Passport Photo (X-Rite, Inc., USA) reported correlations (R^2) between 0.88 and 0.94 for all the RGB parameters (data not shown).

The processing of the RGB images for the calculation of the vegetation indices in relation to different color properties of potential interest was performed with the MosaicTool (<https://gitlab.com/sckefauver/MosaicTool/>). University of Barcelona, Barcelona, Spain) integrated as a plugin for FIJI (Fiji is Just ImageJ; <https://fiji.sc/Fiji/>) (Gracia-Romero *et al.*, 2019). Derived from the HSI (Hue–Saturation–Intensity) color space, the parameters Hue, referring to the color tint; Saturation, an indication of how much the pure color is diluted with white color; and Intensity, as an achromatic measurement of the reflected light, were extracted (Table 4). In addition, the portion of pixels classified as green by their Hue values was determined by the Green Area (GA) and the Greener Area (GGA) indices (Casadesús *et al.*, 2007). The GA corresponds to the percentage of pixels that have a Hue value between 60° and 180° . Meanwhile, the GGA is more restrictive, because it reduces the range from 80° to 180° , thus excluding the yellowish-green tones. Both indices were also used for the formulation of the crop senescence index (CSI) (Zaman-Allah *et al.*, 2015), which provides a scaled ratio between yellow and green pixels to assess the percentage of senescent vegetation. From the CIELab and the CIELuv color space models (recommended by the International Commission on Illumination—CIE—for improved color chromaticity compared to HSI color space), the following parameters were calculated: L^* , that represents lightness and is very similar than the intensity from the HSI color; the a^* and u^* , that represent the red–green spectrum of chromaticity; and the b^* and v^* that represent the yellow–blue color spectrum (Pointer, 2009). Further, besides those indices calculated with the Breedpix software, two additional indices, derived from the RGB color space, were calculated using the digital numbers (DN) of the red, green and blue bands. One, the normalized green–red difference index (NGRDI) is formulated very similarly than the well-known normalized difference vegetation index (NDVI), but instead of using the near-infrared information, it uses the information from the red and green bands (Hunt *et al.*, 2005). The other index is the triangular greenness index (TGI), that estimates chlorophyll content based on the area of a triangle with the three points corresponding to the red, green, and blue bands (Hunt *et al.*, 2012).

2.5 Multispectral Vegetation Indices

Ground-based multispectral sensing was conducted through measurements of the GreenSeeker (Trimble, Sunnyvale, CA, USA), by passing the sensor over the middle of each plot at a constant height of 0.5 m above and perpendicular to the canopy calculates NDVI. For the aerial assessments, a Tetracam micro-MCA (Multiple Camera Array) 12 (Tetracam Inc., Chatsworth, CA, USA) consisting of twelve independent image sensors and optics, each with user configurable filters (450 ± 40 , 550 ± 10 , 570 ± 10 , 670 ± 10 , 700 ± 10 , 720 ± 10 , 780 ± 10 , 840 ± 10 , 860 ± 10 , 900 ± 20 , 950 ± 40 nm) was used. The twelfth sensor is dedicated to ILS (incident light sensor) facing upwards and uses micro-filters to provide an accurate band-by-band reflectance calibration in real-time. PixelWrench II version 1.2.2.2 (Tetracam, Chatsworth, CA, USA) was used to pre-process the multispectral images by aligning and calibrating each band. A suite of multispectral indexes was calculated from the different bands using custom code developed in FIJI and integrated within the MosaicTool software (Table 4).

2.6 Canopy Temperature

Ground-based canopy temperature (CT) assessments were performed using the infrared thermometer PhotoTempTMMXSTMTD (Raytek, Santa Cruz, USA), pointing towards the canopy at a distance of about 1 m and in the opposite direction to the sun. Simultaneously, air temperature was measured across the plots using a thermohygrometer (Testo 177-H1 Logger, Lenzkirch, Germany). The difference between the ambient and the canopy temperature, known as the canopy temperature depression (CTD). The CT measurements from the UAV system were performed using the FLIR Tau2 640 thermal imaging camera (FLIR Systems, Nashua, NH, USA) with a VOx uncooled microbolometer equipped with a TeAx Thermal Capture 2.0 (TeAx Technology, Wilnsdorf, Germany), that records thermal couple sensor readings of the actual temperature of the camera sensor and has a resolution thermal video of 640×520 pixels at 20 frames per second. This camera included a correct for temperature fluctuations of the VOx sensor during the flight. The thermal images were first exported using TeAx ThermoViewer v1.3.12 software (TeAx Technology, Wilnsdorf, Germany) in raw 16-bit TIFF format as Kelvin $\times 10000$ and converted to 32-bit temperatures in celsius using a custom batch processing macro function in FIJI (Kefauver *et al.*, 2017), also integrated within the MosaicTool software. CT aerial measurements corresponded to

average temperature over all the pixels of the plot images. CTD was also calculated using the UAV CT data.

Table 4. Indices derived from the RGB, multispectral and thermal cameras with their targeted trait, the spectral information used and their formulations. The wavelengths used in the formulation of the multispectral indexes have been adapted slightly based on the multispectral micro-MCA Tetracam camera. * Note that for the PRI index, B550 is used instead of the original B531 by the cited reference study.

Target trait	Spectral information	Index name	Abbev.	Formula	Reference
Vegetation cover, Canopy greenness	RGB; HIS color model, CIElab color model	Green Area	GA	$60^\circ < \text{Hue} < 180^\circ$	(Casadesús <i>et al.</i> , 2007)
		Greener Area	GGA	$80^\circ < \text{Hue} < 180^\circ$	
		Crop Senescence Index	CSI	$(\text{GA} - \text{GGA})/100$	(Zaman-Allah <i>et al.</i> , 2015)
	Multispectral Indices based on RGB values	Hue	-	-	(Pointer, 2009)
		a*	-	-	
		u*	-	-	
	Multispectral Indices based on RGB values	Normalized Green Red Difference Index	NGRDI	$(\text{Green DN} - \text{Red DN})/(\text{Green DN} + \text{Red DN})$	(Hunt <i>et al.</i> , 2005)
		Triangular Greenness Index	TGI	$-0.5 \cdot [190 \cdot (\text{Red DN} - \text{Green DN}) - 120 \cdot (\text{Red DN} - \text{Blue DN})]$	(Hunt <i>et al.</i> , 2012)
		Normalized Difference Vegetation Index	NDVI	$(\text{B}840 - \text{B}670)/(\text{B}840 + \text{B}670)$	(Rouse, J. W. <i>et al.</i> , 1976)
	Multispectral Indices	Soil Adjusted Vegetation Index	SAVI	$(1+L) \cdot (\text{B}840 - \text{B}670)/(\text{B}840 + \text{B}670 + L)$	(Huete, 1988)
		Optimized soil-adjusted vegetation index	OSAVI	$(\text{B}780 - \text{B}670)/(\text{B}780 + \text{B}670 + 0.16)$	(Rondeaux <i>et al.</i> , 1996)
		Renormalized Difference Vegetation Index	RDVI	$(\text{B}840 - \text{B}670)/\sqrt{(\text{B}840 + \text{B}670)}$	(Roujean and Breon, 1995)
	Multispectral Indices	Enhanced Vegetation Index	EVI	$2.5 \cdot (\text{B}840 - \text{B}670)/(\text{B}840 + (6 \cdot \text{B}670) - (7.5 \cdot \text{B}45))$	(Huete <i>et al.</i> , n.d.)

Photosynthetic capacity	Multispectral Indices	Modified Chlorophyll Absorption Ratio Index	MCARI I	$(B700-B670) - 0.2 \cdot (B700-B550) \cdot (B700/B670)$	(Daughtry <i>et al.</i> , 2000)
		Transformed Chlorophyll Absorption Index	TCARI	$3 \cdot (B700-B670) - 0.2 \cdot (B700-B550) \cdot (B700/B670)$	(Haboudane <i>et al.</i> , 2002)
		TCARI/OSAVI ratio	TCARI/OSAVI I	TCARI/OSAVI	
		Anthocyanin Reflectance Index 2	ARI2	$B840 \cdot (1/B550 - 1/B700)$	(Gitelson <i>et al.</i> , 2001)
		Carotenoid Reflectance Index 2	CRI2	$(1/B550 - 1/B700)$	(Gitelson <i>et al.</i> , 2002)
		Photochemical Reflectance Index*	PRI	$(B550-B570)/(B550+B570)$	(Gamon <i>et al.</i> , 1992)
Water status	Multispectral Indices	Chlorophyll Carotenoid Index	CCI	$(B550-B670)/(B550+B670)$	(Gamon <i>et al.</i> , 2016)
		Water Band Index	WBI	$B970/B900$	(Penuelas <i>et al.</i> , 1993)
	Thermal information	Canopy temperature	CT	-	(Costa <i>et al.</i> , 2013)
		Canopy Temperature Depression	CTD	-	

2.3 Aerial platforms description and orthomosaic reconstruction procedure

Two different unmanned aerial vehicles (drones) were used: the oktokofter 6S12 XL (HiSystems GmbH, Moomerland, Germany) and the compact quadcopter Mavic 2 Pro (DJI Corporation, Shenzhen, China). Flights were performed under clear sky conditions, with image data captured at an altitude of 50 m. The payload configuration of the Mikrokofter Oktokofter allowed the measurements to be gathered in two flights per trial: the first included the red–green–blue (RGB) cameras, and the second one with both multispectral and thermal cameras that were mounted at the same time. Meanwhile, the Mavic 2 Pro only was configured with the RGB camera. Both UAVs have an active two servo gimbal was used to correct for the effect of pitch and roll movements during the flight. Pre-processed aerial images from each sensor were combined to obtain an accurate orthomosaic by producing a 3D reconstruction with Agisoft PhotoScan Professional

software (Agisoft LLC, St. Petersburg, Russia, <http://www.agisoft.com>) (Bendig *et al.*, 2014). To that end, images with at least 80% overlap were used. Then, regions of interest corresponding to each plot were segmented and exported using the MosaicTool.

2.7 Stable carbon and nitrogen isotope composition and total C and N contents

Mature grains collected at harvest were dried 60 °C for a minimum of 48h and pulverized to a fine powder, from which 1 mg was enclosed in tin capsules, and analysed using an elemental analyser (Flash 1112 EA; ThermoFinnigan, Schwerte, Germany) coupled with an isotope ratio mass spectrometer (Delta C IRMS, ThermoFinnigan), operating in continuous flow mode at the Scientific and Technical facilities of the University of Barcelona (Centres Científics i Tecnològics de la Universitat de Barcelona, CCIUB). The $^{13}\text{C}/^{12}\text{C}$ ratios of plant material were expressed in δ notation as stable carbon isotope composition ($\delta^{13}\text{C}$) as follows (Equation (2)):

$$\delta^{13}\text{C} = \left[\left(\frac{R_{\text{sample}}}{R_{\text{standard}}} \right) - 1 \right] \times 1000 \quad (2)$$

where R_{sample} refers to plant material and R_{standard} to Pee Dee Belemnite (PDB) calcium carbonate. International isotope secondary standards of a known $^{13}\text{C}/^{12}\text{C}$ ratio (IAEA CH7, polyethylene foil, IAEA CH6 sucrose and USGS 40 l-glutamic acid) were calibrated against Vienna Pee Dee Belemnite calcium carbonate (VPDB) with an analytical precision of 0.1‰. The $^{15}\text{N}/^{14}\text{N}$ ratios of plant material were also expressed in δ notation ($\delta^{15}\text{N}$) using international secondary standards of known $^{15}\text{N}/^{14}\text{N}$ ratios (IAEA N1 and IAEA N2 ammonium sulfate and IAEA NO_3 potassium nitrate), with analytical precision of about 0.2‰. During the same process, total nitrogen and carbon contents were determined through the combustion of dry matter, expressed as a concentration per unit dry weight.

2.8 Statistical Analysis

The statistical analysis was performed using the open-source software R and RStudio 1.0.44 (R Development Core Team., 2010)(R Foundation for Statistical Computing, Vienna, Austria). Means and standard errors of the agronomic data were calculated. The effects of managing conditions, growing seasons, genotypes, and their interaction with GY and the remote sensing measurements were determined through a two-factor analysis of variance (ANOVA) for each sample. Differences were considered significant at $p\text{-value} \leq 0.05$. To analyze the relationship between the measurements and GY, bivariate

Pearson correlation coefficients were calculated. Grain yield predictive models were developed by using the least absolute shrinkage and selection operator (LASSO) regression (Figure 3). In a first step the data was randomly separated into a training set containing 80% of genotypes and a hold-out test set comprised of the remaining 20% of genotypes. Optimal lambda to be used in the regression model was obtained using 10 times 10-fold cross-validation on the training set. The prediction variables included in the final model were extracted. To determine the predictive ability of the full model for grain yield, the trained model was applied to the independent test set. The predictive ability was defined to be the squared Pearson product-moment correlation between predicted and observed phenotypic values of the test set. As a measure of accuracy, the root mean square error (RMSE) was calculated. To enable easy comparison a normalized RMSE obtained by dividing the RMSE by the mean of the grain yield observed in the test set was computed. Given the limited size of the available data set, to avoid potential bias introduced by the splitting of the full data set into training and test set, the described workflow was repeated 100 times. The final RMSE and r-squared value were defined to be the mean of these measures across all 100 data splits. To obtain a measure of the importance of each predictive variable, the count of each prediction variable over all 100 trained models was recorded. The most sixth used variables across the 100 trained models were selected and used to create a reduced set of highly important prediction variables.

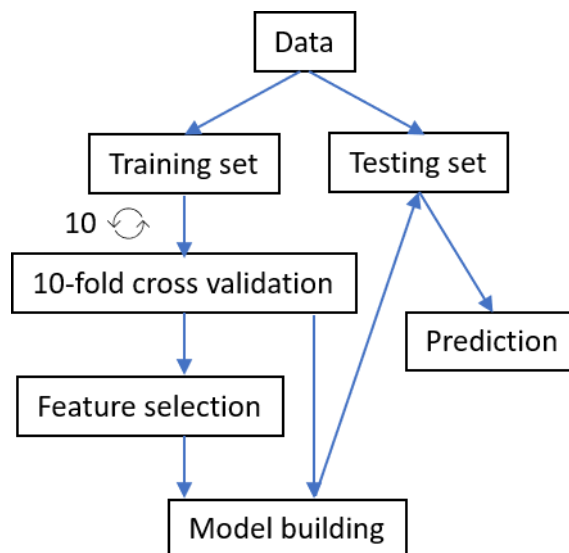


Figure 3. The experimental workflow of model development and validation

3 Results

3.1 Genotype x Environment interaction on GY

The combined analysis of variance across years, locations, management treatments and genotypes revealed that mean squares were significant for grain yield (Table 5). Considering all the experiments between the crop seasons 2016/2017 to 2018/2019, most of the variance was caused by the growing conditions due the difference management trials, followed by the factor year and location. For each individual crop season, also the management was the factor that most contributed to GY, with the exception of the cropping season 2017/2018 when the highest influence on GY was due the Location*Trial interaction. The genotype factor accounted a low but significant effect on GY.

Table 5. Analysis of variance for grain yield based on the set of cultivars across locations and management trials between each individual and the conjunction of crop seasons. Values presented are the mean square values, the P-values and the calculation of percentage contribution to total variation (CTV). Significance levels: ns, no significant; *, P<0.05; **, P<0.01; ***, P<0.001.

Source of variation	2016/17-2018/19			2016/2017			2017/2018			2018/2019		
	MS	Pv	CTV	MS	Pv	CTV	MS	Pv	CTV	MS	Pv	CTV
Y	506.34	***	28.62									
L	262.85	***	14.86	289.09	***	42.94	113.518	***	20.83	14.94	***	3.315
T	635.17	***	35.90	338.93	***	50.34	121.015	***	22.20	420.36	***	93.28
G	4.29	***	0.24	3.77	***	0.56	1.836	***	0.337	1.94	***	0.43
LxT	9.24	***	0.52	37.73	***	5.604	303.998	***	55.78	9.24	***	2.05
LxG	2.09	***	0.11	1.68	***	0.25	2.512	***	0.461	0.82	*	0.182
TxG	1.17	***	0.06	0.95	ns	0.141	0.513	ns	0.094	1.11	***	0.246
LxTxG	1.16	***	0.06	0.46	ns	0.068	1.016	*	0.186	1.7	***	0.377
LxYxG	183.95	***	10.40									
LxYxT	1.35	***	0.07									
LxY	87.72	***	4.95									
YxT	70.3	***	3.97									
YxG	1.47	***	0.08									
YxTxG	0.68	ns	0.03									
LxYxTxG	0.73	ns	0.04									
Residuals	0.61		0.03	0.7		0.104	0.594		0.109	0.55		0.122

In Table 6, the ANOVA comparison between all genotypes for each testing experimental trial is presented with the ranking of the highest and lowest yielding genotypes. Significant differences in GY were reported in all trials, except with the irrigation and

rainfed conditions in Valladolid 2016/2017, the rainfed conditions of Aranjuez 2017/2018, the rainfed and low-nitrogen conditions of Valladolid 2017/2018. The irrigation trials were the most yielding environments in each location, achieving the highest yields in Valladolid during the crop seasons 2018/2019 (Olivadur, 9.06 ± 0.66 Mg ha⁻¹ as the top genotype) and 2019/2020 (Avispa, 9.02 ± 0.30 Mg ha⁻¹ as the top genotype). The next highest yielding conditions were in Coria, despite growing under rainfed conditions, during 2016/2017 (Don Ricardo, 8.52 ± 0.51 Mg ha⁻¹ as the top genotype) and after that, the irrigation trial in Aranjuez during 2017/2018 (Mexa, 8.28 ± 0.38 Mg ha⁻¹ as the top genotype). On the other side, the lowest yielding trials were those grown under rainfed conditions. Particularly, the lowest yields were achieved in the rainfed trails in Aranjuez during 2018/2019 (Simeto, 0.80 ± 0.06 Mg ha⁻¹ as the top genotype). To a lesser extent than the rainfed environments, the late-planting and the low-nitrogen trials also contributed to reduce yields in comparison to the well irrigated trials at the same locations. However, and despite representing both irrigation and fertilization limitations, low-N plots reported higher yields than the rainfed trials in Valladolid.

Table 6. Grain yield (Mg ha⁻¹) and phenology (days from planting to heading) \pm standard error of the top three highest yielding genotypes and the top 3 lowest yielding genotypes for each of the 21 environments tested. P-values inform about the ANOVA analysis of the effect of the genotypes tested on grain yield and days to heading.

L	T	Y	Highest yielding genotype		Lowest yielding genotype		p-value
Coria	Rainfed	2016/2017	<i>DRicardo</i>	8.52 ± 0.51	<i>Simeto</i>	5.83 ± 0.24	***
			<i>Amilcar</i>	8.26 ± 0.04	<i>Core</i>	5.07 ± 0.26	
			<i>Euroduro</i>	8.22 ± 0.32	<i>Pedroso</i>	4.74 ± 0.26	
	Rainfed	2017/2018	<i>Olivadur</i>	6.65 ± 0.05	<i>Pedroso</i>	4.16 ± 0.05	***
			<i>KikoNick</i>	6.46 ± 0.28	<i>Gallareta</i>	4.58 ± 0.38	
			<i>Athoris</i>	6.46 ± 0.25	<i>Vitron</i>	4.95 ± 0.03	
	Rainfed	2018/2019	<i>Athoris</i>	5.08 ± 0.07	<i>Arcobaleno</i>	3.41 ± 0.59	*
			<i>Iberus</i>	4.80 ± 0.33	<i>Saragolla</i>	3.37 ± 0.43	
			<i>KikoNick</i>	4.73 ± 0.39	<i>Pedroso</i>	3.08 ± 0.25	
Aranjuez	Irrigation	2016/2017	<i>Olivadur</i>	6.03 ± 0.42	<i>DNorman</i>	4.10 ± 0.22	**
			<i>Burgos</i>	5.67 ± 0.53	<i>Arcobaleno</i>	4.05 ± 0.26	
			<i>Sculptur</i>	5.34 ± 0.08	<i>Core</i>	3.46 ± 0.10	
	Irrigation	2017/2018	<i>Mexa</i>	8.28 ± 0.38	<i>Pedroso</i>	5.93 ± 0.68	**
			<i>Amilcar</i>	8.25 ± 0.29	<i>Olivadur</i>	5.51 ± 0.78	
			<i>Vitron</i>	7.97 ± 0.21	<i>Haristide</i>	3.83 ± 1.17	
	Irrigation	2018/2019	<i>Amilcar</i>	5.75 ± 0.22	<i>Haristide</i>	3.52 ± 0.43	***
			<i>Dorondon</i>	5.38 ± 0.71	<i>Sculpdur</i>	3.50 ± 0.28	
			<i>Euroduro</i>	5.34 ± 0.31	<i>Pedroso</i>	3.48 ± 0.18	
Rainfed	2016/2017	<i>Olivadur</i>	3.58 ± 0.30	<i>Saragolla</i>	2.27 ± 0.32	**	

		<i>Athoris</i>	3.28 ± 0.20	<i>Solea</i>	1.82 ± 0.14		
		<i>Claudio</i>	3.22 ± 0.24	<i>Core</i>	1.61 ± 0.20		
	2017/2018	<i>KikoNick</i>	4.19 ± 0.15	<i>Solea</i>	2.97 ± 0.43		
		<i>Avispa</i>	3.93 ± 0.43	<i>Saragolla</i>	2.65 ± 0.53	ns	
		<i>Claudio</i>	3.91 ± 0.14	<i>Haristide</i>	2.49 ± 0.38		
	2018/2019	<i>Solea</i>	1.65 ± 0.07	<i>Regallo</i>	0.87 ± 0.06		
		<i>Olivadur</i>	1.63 ± 0.05	<i>Pedroso</i>	0.87 ± 0.22	**	
		<i>Amilcar</i>	1.62 ± 0.09	<i>Simeto</i>	0.80 ± 0.06		
	2016/2017	<i>Euroduro</i>	5.06 ± 0.16	<i>Pedroso</i>	3.06 ± 0.17		
		<i>Burgos</i>	4.87 ± 0.27	<i>Simeto</i>	3.05 ± 0.42	***	
		<i>Claudio</i>	4.62 ± 0.19	<i>Core</i>	2.95 ± 0.19		
Late	2017/2018	<i>Core</i>	4.98 ± 0.12	<i>Sculpdur</i>	2.76 ± 0.24		
		<i>KikoNick</i>	4.75 ± 0.22	<i>Haristide</i>	2.57 ± 0.38	***	
		<i>Athoris</i>	4.63 ± 0.26	<i>Olivadur</i>	2.27 ± 0.16		
	2018/2019	<i>Euroduro</i>	5.65 ± 0.36	<i>Haristide</i>	3.34 ± 0.27		
		<i>Solea</i>	5.02 ± 0.14	<i>Pedroso</i>	3.14 ± 0.26	***	
		<i>KikoNick</i>	4.62 ± 0.36	<i>Simeto</i>	2.99 ± 0.12		
Irrigation	2016/2017	<i>Arcobaleno</i>	7.81 ± 0.05	<i>Amilcar</i>	6.23 ± 0.59		
		<i>Olivadur</i>	7.81 ± 0.53	<i>Core</i>	6.23 ± 0.64	ns	
		<i>Mexa</i>	7.53 ± 0.53	<i>Pedroso</i>	5.92 ± 0.25		
	2017/2018	<i>Haristide</i>	7.82 ± 0.52	<i>Saragolla</i>	5.77 ± 0.25		
		<i>Olivadur</i>	7.20 ± 0.30	<i>Pedroso</i>	5.74 ± 0.52	*	
		<i>Claudio</i>	6.94 ± 0.13	<i>Simeto</i>	5.50 ± 0.15		
2018/2019	<i>Olivadur</i>	9.06 ± 0.66	<i>DRicardo</i>	5.01 ± 1.39			
	<i>Athorix</i>	8.07 ± 0.77	<i>Vitron</i>	4.91 ± 0.44	***		
	<i>Avispa</i>	7.88 ± 0.92	<i>Sculptur</i>	4.21 ± 0.26			
Valladolid	Rainfed	2016/2017	<i>Arcobaleno</i>	3.79 ± 0.66	<i>Euroduro</i>	1.94 ± 0.33	
			<i>Dorondon</i>	3.66 ± 0.28	<i>Pedroso</i>	1.75 ± 1.40	ns
			<i>Claudio</i>	3.57 ± 0.08	<i>Iberus</i>	1.71 ± 0.70	
		2017/2018	<i>Amilcar</i>	8.41 ± 0.19	<i>Pedroso</i>	6.03 ± 0.31	
			<i>Burgos</i>	7.86 ± 0.68	<i>Simeto</i>	5.85 ± 0.81	ns
			<i>Sculpdur</i>	7.85 ± 0.59	<i>Saragolla</i>	5.23 ± 0.85	
	2018/2019	<i>DRicardo</i>	2.90 ± 0.48	<i>Haristide</i>	1.46 ± 0.16		
		<i>Arcobaleno</i>	2.73 ± 0.07	<i>Euroduro</i>	1.42 ± 0.12	ns	
		<i>Solea</i>	2.52 ± 0.46	<i>Olivadur</i>	1.40 ± 0.21		
	Late	2016/2017	<i>Athoris</i>	6.93 ± 0.59	<i>Gallareta</i>	4.12 ± 0.76	
			<i>Olivadur</i>	6.54 ± 0.41	<i>Pedroso</i>	4.09 ± 0.32	***
			<i>Euroduro</i>	6.19 ± 0.36	<i>Simeto</i>	4.09 ± 0.55	
Low-N	2017/2018	<i>KikoNick</i>	4.23 ± 0.44	<i>Sculpdur</i>	5.90 ± 0.31		
		<i>Regallo</i>	4.48 ± 0.34	<i>Amilcar</i>	6.48 ± 0.47	ns	
		<i>Gallareta</i>	4.51 ± 0.83	<i>Haristide</i>	6.48 ± 0.29		
	2018/2019	<i>Saragolla</i>	3.33 ± 0.46	<i>Simeto</i>	1.54 ± 0.60		
		<i>Amilcar</i>	3.16 ± 0.87	<i>Haristide</i>	1.53 ± 0.49	ns	
		<i>Dorondon</i>	2.83 ± 0.40	<i>DNorman</i>	1.43 ± 0.36		

3.2 Climatic data description during the experimental seasons

The experiment sites covered a wide range of Spanish latitudes and thus, the climatic conditions were very diverse during the different crop seasons. The location-agronomical conditions- year combinations were considered as 21 different environments for the expression of the genotypes tested. Such differences represented by daily mean temperatures and water inputs (precipitation and irrigation). In the case of Coria, the crop cycles were characterized by high temperatures during the first development stages (January-April) and abundant precipitations during the 2016/2017 and 2017/2018 cycles, but more reduced in the 2018/2019 cycle. The environmental conditions of the trials in Aranjuez were constant for the three years studied in terms of temperature characterized as a semi-arid climate, with cold temperatures during winter and with low precipitations during the whole cycle. The Valladolid environments are the coldest with also low precipitations. The 2018/2019 was the season with the highest values of accumulated rainfall concentrated in spring.

3.3 Crop phenology

In terms of crop phenology, differences in crop behavior as consequence of climatic variance and the imposition of management trials became apparent by the relation between the accumulation of DAS and GDD achieved at each phenological stage. Overall, the late-planting trials reported the shortest crop cycles, reporting higher GDD in less DAS during the reproductive and grain filling phenological stages in comparison with the normal-planting trials of the same locations during the same crop seasons. Beside the late-planting trials, higher mean temperatures during the cycles of Coria reported the achievement of the phenological stages earlier in terms of DAS but with similar GDD than the normal-planting trials in Aranjuez. Finally, the irrigation, rainfed and low-N trials in Valladolid showed a higher accumulation of both DAS and GDD when achieving anthesis and grain filling stages.

3.4 Phenotypic data analysis and variable selection for the GY prediction

The performance of the proposed approaches as phenotyping methodologies for yield prediction varied significantly across environments. In order to assess which combination of variables and for what particular environment were more critical to predict yield, the set of vegetation indices (VIs) and other measurements were ranked using the feature selection strategy described in the Materials and Methods section 2.8 and the top 6

variables with the highest detection rate (DR) are shown in Table 7. The LASSO variable selection was calculated using the training data set and revealed a wide variation across the environments. The most repeated variables across the environments were plot greenness indices (NGRDI, NDVI and GA) measured at heading, anthesis and grain filling stages. CT measures together with the multispectral indices WBI and PRI also had a stable performance across the environments particularly when measured during anthesis and early stages of grain filling. In addition, leaf-based pigment content measures showed highest importance to the GY models under the limiting growing conditions. Out of all the phenological moments measured, measures in anthesis and grain filling were the more times reported in the GY models. The highest correlations against individual traits against GY were reported with measurements related to plot greenness in grain filling stages.

Table 7. Top 6 indices selected by the LASSO algorithms showing the highest detection rates (DR) in yield prediction models based on 100 cross-validation runs, correlation coefficient (r) against yield and the ANOVA test between genotypes. L, Location; T, Trial; Y, Year.

L	T	Y	Phenological		DR	r	anova
			Variable	Stage			
Coria	Rainfed	2016/2017	CSI	Heading	100	-0.153	0.3185
			WBI	Heading	100	0.369	**
			NGRDI	Grain filling	99	0.236	***
			PRI	Heading	99	0.143	ns
			NGRDI	Heading	98	-0.089	***
			PRI	Grain filling	94	0.215	ns
		2017/2018	GA.a	Late grain filling	100	0.477 ***	ns
			EVI	Late grain filling	95	0.331 **	ns
			EVI	Anthesis	92	-0.053	ns
			Height	Anthesis	92	0.207	ns
			Anth	Late grain filling	90	0.018	ns
			Zadocks	Late grain filling	87	0.129	***
	2018/2019	Carbon	Maturity	100	0.069	***	
		$\delta^{13}C$	Maturity	100	-0.483 ***	***	
		Height	Grain filling	100	0.092	***	
		Anth	Anthesis	98	0.383 **	**	
		Height	Anthesis	96	0.367 **	***	
		CT.g	Anthesis	96	-0.310 **	ns	
Aranjuez	Irrigation	2016/2017	Chl	Grain filling	100	-0.074	***
			CSI.a	Grain filling	99	-0.630 ***	***
			NDVI.g	Grain filling	99	0.452 ***	***
			CTD.g	Heading	92	-0.142	ns
			T.g	Anthesis	90	-0.405 ***	ns

		v.g	Grain filling	90	0.377 **	***
	2017/2018	CRI2	Pre-anthesis	93	0.481 ***	ns
		WBI	Pre-anthesis	91	0.23	ns
		CSI.a	Pre-anthesis	90	-0.307 **	ns
		v.g	Anthesis	87	-0.035	ns
		WBI	Grain filling	85	0.417	**
		Anth	Anthesis	83	-0.101	**
	2018/2019	Flav	Anthesis	100	0.293 *	***
		Height	Anthesis	100	0.194	***
		Carbon	Maturity	99	-0.061	ns
		Flav	Milk development	99	-0.109	**
		CSI.g	Milk development	96	-0.335 **	ns
		NDVI.g	Anthesis	91	-0.109	**
	2016/2017	CTD.a	Anthesis	92	0.674 ***	ns
		NDVI.g	Heading	89	0.628 ***	***
		R780	Anthesis	89	0.576 ***	***
		Anth	Heading	82	0.004	***
		GGA.a	Anthesis	82	0.564 ***	**
		GGA.g	Grain filling	75	0.584 ***	ns
Rainfed	2017/2018	PRI	Anthesis	98	-0.380 ***	ns
		NDVI.g	Milk development	92	0.553 ***	ns
		NGRDI.a	Pre-anthesis	92	0.429 ***	ns
		Zadocks	Milk development	92	-0.151	ns
		WBI	Anthesis	91	0.643 ***	ns
		Anth	Anthesis	86	-0.400 ***	***
	2018/2019	Carbon	Maturity	100	-0.028	ns
		Chl	Anthesis	100	0.024	ns
		CSI	Grain filling	100	-0.181	ns
		CTD.g	Anthesis	100	0.111	ns
		CTD.g	Grain filling	100	0.136	ns
		$\delta^{13}C$	Maturity	100	-0.265 *	NS
Late	2016/2017	EVI	Anthesis	99	-0.253 *	ns
		u.a	Heading	99	-0.334 **	*
		PRI	Heading	97	0.395 *	ns
		Flav	Anthesis	91	-0.019	***
		R720	Heading	90	-0.273 *	ns
		ARI2	Heading	83	0.175	ns
	2017/2018	Flav	Milk development	100	0.517 ***	ns
		TGI.g	Pre-anthesis	100	0.034	***
		PRI	Milk development	94	0.082	ns
		WBI	Milk development	88	0.029	ns

		Carbon	Maturity	88	0.137	ns
		CSI.a	Stem elongation	88	0.029	ns
2018/2019		Anth	Anthesis	100	-0.255 *	ns
		Flav	Grain filling	100	-0.256 *	ns
		Anth	Grain filling	99	-0.001	ns
		Chl	Anthesis	98	0.027	*
		Height	Anthesis	98	0.311 **	*
		v.a	Anthesis	98	0.019	***
2016/2017		Anth	Anthesis	100	-0.124	**
		T.a	Grain filling	100	-0.587 ***	ns
		Hue.a	Anthesis	97	0.289 *	***
		Flav	Anthesis	96	0.274 *	**
		NGRDI.g	Anthesis	96	0.247 *	*
2017/2018		CSI.g	Anthesis	93	0.354 **	ns
		CSI.g	Anthesis	99	-0.314 **	ns
		$\delta^{15}\text{N}$	Maturity	92	-0.181	ns
		NGRDI.a	Pre-anthesis	90	0.500 ***	***
		$\delta^{13}\text{C}$	Maturity	88	-0.085	***
		CTD.g	Late Milk	87	0.013	ns
2018/2019		PH	Late Milk	86	0.132	ns
		T.g	Late Milk	99	-0.370 ***	ns
		GGA.g	Late Milk	95	0.392 ***	ns
		$\delta^{13}\text{C}$	Maturity	94	-0.407 ***	*
		TGI.a	Late Milk	91	0.135	ns
		CTD.g	Late Milk	88	0.301	ns
	NGRDI.a	Pre-anthesis	88	0.052	ns	
2016/2017		Flav	Anthesis	100	0.393 ***	ns
		NBI	Anthesis	100	0.036	ns
		PRI	Grain filling	100	0.301 *	ns
		T.g	Grain filling	100	-0.640 ***	ns
		NDVI	Grain filling	99	-0.063	*
		T.a	Grain filling	99	-0.270 *	ns
2017/2018		Anth	Pre-anthesis	100	-0.275 *	ns
		CSI.g	Anthesis	98	-0.415 ***	*
		Chl	Anthesis	96	0.245 *	**
		WBI	Pre-anthesis	95	0.330 **	ns
		$\delta^{13}\text{C}$	Maturity	93	-0.280 *	ns
		GA.g	Anthesis	93	0.758 ***	*
2018/2019		Anth	Pre-anthesis	100	-0.313 **	**
		Anth	Milk development	99	0.387 **	ns
		NGRDI.a	Late Milk	98	0.114	ns
		Nitrogen	Maturity	97	-0.541 ***	ns
		$\delta^{15}\text{N}$	Maturity	94	0.307 **	ns
	PH	Pre-anthesis	89	0.714 ***	ns	
Late	2016/2017	Date heading	Heading	100	-0.026	ns

	EVI_plot	Anthesis	99	0.644 ***	ns
	u.a	Anthesis	98	-0.802 ***	ns
	PRI_plot	Anthesis	95	0.759 ***	ns
	Flav	Anthesis	91	-0.182	ns
	u.a	Heading	91	0.624 ***	ns
		Milk			
	WBI	development	99	0.269 **	ns
	Carbon	Maturity	98	0.330 **	ns
2017/2018	CTD.g	Pre-anthesis	98	0.351 **	ns
	$\delta^{13}\text{C}$	Maturity	98	0.019	***
	$\delta^{15}\text{N}$	Maturity	98	0.102	ns
	NDVI.g	Pre-anthesis	98	0.533 ***	ns
	NGRDI.g	Late Milk	100	0.146	***
	Nitrogen	Maturity	100	-0.297 *	ns
		Milk			
2018/2019	Flav	development	97	0.161	ns
	Flav	Pre-anthesis	96	0.068	**
	Carbon	Maturity	95	-0.295 *	ns
	$\delta^{13}\text{C}$	Maturity	93	-0.141	ns

In Coria, the models highlighted the importance of cultivars with both dense and photosynthetically active crop cover across the seasons (from heading to late phases of grain filling). Higher correlations against GY were reported with the GA aerial calculations during late grain filling stage in 2017/2018 ($r=0.477^{***}$) and $\delta^{13}\text{C}$ during 20218/2019 ($r=-0.483^{***}$).

In the environments studied in Aranjuez, the models did not focus on crop cover during heading and anthesis, instead indices more sensitive to stress response were selected. Thus, during the crop season of 2016/2017, when the precipitations were low and the accumulated potential evapotranspiration were high, CT assessments during the reproductive stages reported high correlations against yield in both irrigation ($r=-0.405^{***}$) and rainfed trials ($r=0.674^{***}$). Instead, during the following crop seasons, the best correlations were achieved with the measurements of stress protective pigments, but those correlations were positive in the irrigation trials (CRI2 in 2017/2018, $r=0.481^{***}$; Flav in 2018/2019, $r=0.293^*$) and negative in the rainfed trials (Anth in 2017/2018, $r=-0.400$). Likewise, in the rainfed trials of Aranjuez of 2017/2018, high correlations against GY were reported during anthesis with the PRI ($r=-0.380^{***}$) and WBI ($r=0.643^{***}$). For both irrigation and rainfed trials in Aranjuez, indices that assessed cultivars with delay senescence reported the best correlations against GY during grain filling, like the CSI assessed aerially during 2016/2017 in the irrigation trial ($r=-0.630^{***}$) or the NDVI

assessed at ground level during 2017/2018 in the rainfed trial ($r=0.533^{***}$). During 2018/2019, despite most of the indices measured in the rainfed trials reported weak correlations, the best correlations against GY were reported from $\delta^{13}\text{C}$ values calculated from the grains ($r=-0.265^*$). Under the late-planting conditions of Aranjuez, assessments performed during anthesis of crop biomass, through the u^* index from the UAV RGB images in 2016/2017 ($r=-0.334^{**}$) and plant height measurements in 2018/2019 ($r=0.311^{**}$) were among the best predictors of GY. However, the selection and performance of some of the indices under the late-planting conditions in Aranjuez were also dependent on the climatic variability across the different years studied; while Flav measurements during 2017/2018 were correlated positively to yield ($r=0.417^{***}$), in 2018/2019 Anth measurements correlated negatively ($r=-0.255^*$).

Finally, the calculated models highlighted the importance of values of high biomass during the reproductive stages of all the trials in Valladolid across the crop seasons. Specially, very high correlations were reported during anthesis in the rainfed trials. This is the case of GA assessed at ground level during 2017/2018 ($r=0.758^{***}$), and in the late-planting trial, with u^* assessed at aerial level during 2016/2017 ($r=-0.802^{***}$). Regarding the leaf readings of photoprotective pigments during anthesis, results were dependent on the environmental conditions. Under rainfed conditions, when there was a limited access to water Anth readings correlated positively with GY like in 2016/2017 ($r=0.393^{***}$), while the relation was negative when the drought stress was less severe like in 2017/2018 ($r=-0.275^*$) and 2018/2019 ($r=-0.313^{**}$). Nevertheless, Flav readings recorded during anthesis under the irrigation trials responded positively to GY ($r=0.274^*$). Furthermore, measurements during anthesis under the late-planting trial reported a very high correlation between PRI and GY ($r=0.759^{***}$). About the measurements performed during the grain filling, under both irrigation and rainfed trials of Valladolid, CT assessments were the best correlated measurements against GY, as it was shown in the irrigation trials 2016/2017 with CT assessed aerially ($r=-0.587^{***}$) and in 2018/2019 with CT assessed at ground level ($r=-0.370^{***}$) or in the rainfed trials with CT values at ground level in 2016/2017 ($r=-0.640^{***}$). The water status of the cultivars across the crop seasons was also reflected on the $\delta^{13}\text{C}$ values of the grains, reporting high correlations with GY during 2018/2019 in the irrigation ($r=-0.407^{***}$) and rainfed conditions ($r=-0.280^*$), but also on WBI values of low-N conditions of 2017/2018 ($r=0.269^{***}$). Results of nitrogen content in grains reported high correlations to GY,

negative in rainfed trials in 2018/2019 ($r=-0.541^{***}$) but positive in low-N trials in same season ($r=-0.295^*$).

3.5 Model performance and accuracy predicting GY

Prior to the evaluation of the parameter's importance, GY predictive models were described using all the available variables for each field. Then, the sixth best-performing features were iteratively added into ML models to their accuracy predicting GY. The test accuracies obtained are shown in Table 8 and widely varied across environments. In comparison to the models using all the variables available, predictions using the selected features performed slightly better, except in few cases. Thus, the best prediction model was reported using all the variables under the irrigation conditions of Valladolid during 2016/2017 ($R^2= 0.759$, $RMSE=0.445$). Overall, the best yield predictions were achieved under the rainfed conditions of Valladolid, where models with feature selection explained 63.2, 54,9 and 59,5% of GY variability, respectively for each crop season. In the same location, GY predictions were also high in 2016/2017 under the late-planting conditions ($R^2= 0.657$, $RMSE=0.564$) and in 2018/2019 under the low-N conditions ($R^2= 0.595$, $RMSE=0.384$). Regarding to the environments of Aranjuez, high predictions were only achieved in 2016/2017 under the irrigation ($R^2= 0.561$, $RMSE=0.383$) and rainfed conditions ($R^2= 0.703$, $RMSE=2.152$).

Table 8. Least absolute shrinkage and selection operator (LASSO) regression models for the prediction of grain yield. Two regression models were performed for each environment: one using the full set of measurements across the sampling visits and an another only using the six most selected variables. The statistics represent the mean across the 100 cross-validation runs. RMSE, root mean square error; R^2 , coefficient of determination; MAE, mean absolute error.

L	T	Y	All the indices			Selected indices		
			RMSE	R2	MAE	RMSE	R2	MAE
Coria	Rainfed	2016/2017	1.390	0.238	0.984	0.931	0.244	0.748
		2017/2018	1.609	0.164	0.941	0.689	0.230	0.533
		2018/2019	0.743	0.252	0.620	0.639	0.287	0.506
Aranjuez	Irrigation	2016/2017	0.622	0.425	0.493	0.480	0.561	0.383
		2017/2018	1.000	0.456	0.804	0.905	0.438	0.746
		2018/2019	1.249	0.170	0.838	0.864	0.152	0.703
	Rainfed	2016/2017	128.742	0.673	33.496	7.482	0.703	2.152
		2017/2018	0.505	0.484	0.407	0.486	0.473	0.399
		2018/2019	0.587	0.111	0.453	0.463	0.098	0.347
	Late	2016/2017	0.878	0.457	0.531	0.556	0.396	0.448
		2017/2018	0.876	0.193	0.709	0.685	0.236	0.551
		2018/2019	1.063	0.158	0.774	0.768	0.153	0.628
Valladolid	Irrigation	2016/2017	0.551	0.759	0.445	0.613	0.675	0.468
		2017/2018	0.845	0.276	0.649	0.738	0.267	0.561
		2018/2019	2.045	0.157	1.640	1.391	0.254	1.072
	Rainfed	2016/2017	0.690	0.657	0.564	0.677	0.632	0.535
		2017/2018	0.742	0.576	0.560	0.724	0.549	0.561
		2018/2019	0.630	0.419	0.489	0.480	0.595	0.384
	Late	2016/2017	0.581	0.543	0.410	0.690	0.657	0.564
		2017/2018	1.148	0.229	0.848	0.955	0.282	0.729
	Low-N	2018/2019	0.754	0.473	0.602	0.480	0.595	0.384

4. Discussion

The complex and interactive effects on yield of the wheat genotypes and the specific environment where they grow hampers the correct selection of phenotypic traits to define specific ideotypes. In our study, the environment effect was understood as the combination of location, year and the managing conditions, and the results obtained reported significant differences on the genotypic performance in terms of GY and the capacity of phenotypical (morphological and physiological) traits to predict yield. The aim of the present study was to determine guidelines for plant phenotyping of well adapted genotypes based on the analysis a set of remote sensing traits measured during

the reproductive stage together with stable isotope signature in mature kernels. Final objective was to understand which specific traits are the most critical to develop GY-prediction models in a wide range of environmental growing conditions. For that, a set of 24 commercial semidwarf (i.e., post Green Revolution) cultivars of durum wheat cultivated in Spain during the past four decades were tested.

4.1 Environment effect on genotypic performance of GY and traits

The wide range of growing conditions provided for the different environments tested in this study allowed an extensive evaluation of the yield performance of the set of wheat genotypes and for the identification of the physiological traits involved. The growing conditions set as management trials had the highest impact on yield, accounting for 88.10% of the total variation, when all crop seasons were considered. Under Mediterranean conditions, water regime and temperature have been described as the factors that explain a major portion of GY variation in cereals (Voltas *et al.*, 2002) (. The drought stress imposed by the rainfed trials highly reduced GY in comparison to the well-irrigated trials of the same locations. Whereas, year-to-year variation in weather has a great impact on the GY of rainfed trials (other than that of Coria, which reaches the water table from the Guadalquivir river), as quantity and distribution of rainfall along the three cropping seasons was different. Climatic variability, in precipitation and temperature, is known as responsible of affecting crop yields and phenology. The delay in the planting date implies higher temperatures during all the crop cycle and particularly during the reproductive and grain filling phases of wheat (Farooq *et al.*, 2011), which reduces the duration of crop cycle, increases respiration rates and eventually the occurrence of heat stress, overall decreasing GY in comparison to the normal planting with supplementary irrigation conditions. Meanwhile, the combination of lower N-fertilizer without irrigation conditions in Valladolid reported higher yields than the rainfed trials across the years (except for the 2017/2018 season). This could be explained by the lack of fertilizer reducing vegetative biomass, and potential transpiration losses, therefore making less severe the drought stress during the reproductive stage. Since the average GY under stressed conditions was reduced in comparison to the well-watered irrigation conditions, the importance of breeding for resilience to these stresses is emphasized (Juliana *et al.*, 2019).

4.2 Significance of biomass, stay-green, photosynthetic efficiency, water status and leaf pigments monitoring for GY prediction

The present study aimed to prove the applicability of a set of phenotypic traits to predict GY throughout the growing seasons. Our findings showed a wide variability in terms of phenotypic traits chosen within each growing conditions. The year-to-year variation in weather not only modify the degree of stress experienced by crops but also its timing. Therefore, for each specific condition, it is necessary to dissect what traits need to be measured, when they need to be measured, and how they should be measured in relation to the breeding target, which in this instance is forecasting yield.

Before than any disturbance of photosynthetic performance, an abiotic stress such as water stress affects leaf expansion and crop growth. Above ground biomass, as a measure of crop development, have been used as a useful selection trait for yield improvement in wheat, particularly under stressing conditions (Jose A Fernandez-Gallego *et al.*, 2019) (Fernandez-Gallego *et al.* 2019). Both multispectral and RGB indices generated measures of canopy cover that reported high correlations to GY. The NDVI is one of the most used indices due to its combination of the characteristic low reflectance in the visible region of the spectrum (400 – 700nm) and the high reflectance in the near-infrared (NIR) (700-1100nm) region (Hassan *et al.*, 2019), which permits the effectively assessment of vegetative cover and vigor. The NDVI together with some of its reformulations based on slight modifications decrease the effect of soil or the problem of saturation with dense canopies, were repeatedly selected in the GY prediction models. Further, the calculation of RGB indices based on the color properties of the canopy as the NGRDI also were reported as great predictors of GY. Therefore, cultivars exhibiting lower values of leaf area growth, as measured through Vis, indicated poorer genotypic performance in terms of GY. Oppositely, cultivars with higher aboveground biomass may be related to a better water and nutrient availability, and consequently to a higher GY. Moreover, those VIs, when measured during grain filling, monitor leaf/canopy photosynthesis duration and become a critical approach to detect cultivars with delayed senescence (Gracia-Romero *et al.*, 2019). In fact, under terminal stress conditions, stay-green attitude is generally associated with lower yields (Sadras and Richards, 2014; Gregersen *et al.*, 2013). To this end, VIs derived from the RGB cameras performed very well as the elevated image resolution permits the assessment of stay-green in a very precise manner (Fernandez-Gallego *et al.* 2019). GA, GGA and CSI, as representations of the percentage of green

pixels, when measured at the plot level, are the most frequently chosen indices with higher detection rates in the LASSO models across the environments, particularly when measured during grain filling (Gracia-Romero *et al.*, 2019). Moreover, these indices presented the highest correlations against GY. However, under environments without major growth limitations, corresponding to the conditions of the years with more precipitations in Coria or the well irrigated trials of Aranjuez and Valladolid, those VIs related to the above biomass were not reported as the most critical for the GY models. VIs, when measured during the grain filling phases of the crop, may also capture differences in stay green being very useful to identify cultivars retaining leaves greener longer after anthesis. Our results reported this as a common trait of the high-yielding phenotypes among the environments assessed. Delaying the ripening process and maintaining the canopy greenness has been reported as being very closely related to the final GY (Gregersen *et al.*, 2013). But only functional stay-green is of interest for crop improvement, meaning that photosynthesis and accumulation of assimilates to harvested tissues are prolonged (Christopher *et al.*, 2016). Canopy-based indices were selected over the chlorophyll assessments at leaf level. Hence, early senescence phenotypes were easily identified using indices evaluated at the plot level such as GA or NDVI. The GY models developed in the environments under suboptimal conditions, as the rainfed and the late-planting trials, highlight the importance of selecting genotypes with extended duration of active photosynthesis.

Besides the assessment of green plant biomass, our results highlighted the importance of detecting the actual plant photosynthetic capacity for predicting yield. The actual carbon fluxes were analyzed through two approaches. On one side, multispectral indices more targeted towards the photosynthetic capacity of the crop canopy such as PRI, CRI2 or ARI2 were measurements selected repeatedly in the GY predictive models. Thus under the heat stress conditions induced by the late-planting trials of both Valladolid and Aranjuez, our results reported the estimation of the photosynthetic variability by the index PRI as a good indicator of higher yielding cultivars. Other mechanisms that inform how active are the plants is measuring the water status. Our results reported the turgor of the leaves assessed with the water band index (WBI) as one of the most selected indices particularly under the rainfed and late-planting trials showing positive correlations against GY. Another proxy of water status is CT, that provides an instantaneous proxy of crop water conditions and any stress that induces a stomatal closure will be translated into an

increase of leaves temperature. Significant and negative correlations of CT measurements against GY were reported across all the environments studied. Thus, CT measurements are reported as an effective tool to assess genotypic response to stress and then, a good predictor of yield (Araus *et al.*, 2002).

The evaluation of pigment concentration using hand-held portable devices is one of the more common measurements, especially chlorophyll readings are considered very useful to diagnosticate environmental stress as indicators of leaf senescence (Xiong *et al.*, 2015; Neufeld *et al.*, 2006) or lack of nitrogen (Buchailot *et al.*, 2019).. However, our results reported that the leaf chlorophyll content–GY relationship only worked efficiently as indicator of stay-green. The behavior of the Flav and Anth leaf readings against GY varied across the environments measured. Flavonoids and anthocyanins are polyphenolic secondary metabolic compounds with various functions in growth, development, reproduction, and stress defense (Ma *et al.*, 2014b). Several studies have reported flavonoids accumulation after drought treatment, which were similar to the results of Ma *et al.*, (2014a), supporting a protective role when plants are exposed to drought. According to this, our results showed a positive relation between Flav and Anth readings during the anthesis and early grain filling stages with GY, indicating those cultivars more capable to confront the stress exhibit higher content of these protective pigments. However, when leaf pigments were measured before anthesis, elevated Flav and Anth values were reported on those cultivars more affected by stress and then lower yields were expected. This was the case of the rainfed and late-planting conditions of Aranjuez during 2017/2018. Another example is the rainfed conditions of Valladolid during 2017/2018, where Anth correlation against GY was negative during pre-anthesis ($r=-0.313^{**}$) and positive during the milk development ($r=0.387^{**}$).

Carbon isotope composition, when analyzed in mature kernels, is proposed as an integrative indicator of cultivars water status along the crop cycle (Araus *et al.*, 2013). Negative correlations reported between $\delta^{13}\text{C}$ and GY are associated to the better water status of the higher-yielding cultivars, exhibiting lower $\delta^{13}\text{C}$, being capable to maintain higher stomatal conductance and then, fixing more CO_2 and yielding more.

In the case of nitrogen, its mature grain concentration together with its isotope compositions as $\delta^{15}\text{N}$ are used to study the dynamics of N in the soil-plant system informing also about the N source used (Serret *et al.* 2008) and the nitrogen metabolism of the plant as affected by growing conditions (Yousfi *et al.* 2012). Positive correlations

between $\delta^{15}\text{N}$ and GY have been reported for durum wheat have been reported, particularly under the irrigation environments, showing the ability of cultivars to access better to soil resources (Yousfi et al. 2009; Araus et al. 2013).

4.3 GY prediction models for specific environment ideotype description

Development of precise crop yield prediction models is a major challenge of the modern agriculture as it provides timely information for optimum agronomical practices application and management decisions but also allows market prices to be modelled (Kumar, 2016; Peng *et al.*, 2015). Crop models can also be practical for exploring the opportunities of different cultivars on specific cultivation areas, as the assessment of the phenotypic profile will help to understanding the interactive effects of genotypes with the agronomic and environmental factors on crop performance and then, final yield. Therefore, the proposed methodology consisted in the phenotypic characterization of traits involved with tolerance/resistance to the environmental conditions to design the ideotypes. Previous characterization of phenotypic profile by a set of remote sensing traits to define an ideotypes can be found in (Palaia *et al.*, 2020). Results indicated that algorithms with a selection of variables performed similar to the algorithms based on the full set of measurements. Overall, the feature variable selection according to LASSO incorporated to the GY-prediction models (i) measurements of canopy size during the pre-anthesis and anthesis phases, as approximation to the potential crop photosynthesis, (ii) the estimation of the light use efficiency (PRI, CCI) and (iii) or the transpiration (CT, $\delta^{13}\text{C}$ of mature kernels) during grain filling, and finally a measurement of the delay in senescence of the plants (NDVI, GA). These findings are in the line with the component analysis proposed by (Passioura, 1977; Passioura, 1996) about the traits to select for increasing yield: (1) the capacity to capture more water; (2) the efficiency for producing dry matter per unit of absorbed water; and (3) the ability to allocate an increased proportion of the biomass into grains.

Reproductive period embracing from heading to physiological maturity is critical to maximize yield under Mediterranean conditions, which are frequently characterized by the occurrence of terminal abiotic stresses such as drought, when most of the carbohydrates for grain filling are formed (Snape *et al.*, 2001). In agreement with that traits assessing vegetation cover during these stages were selected in the majority of the environments. Cultivars with larger canopies were determinant to GY, especially on those environments were drought stress affected the grain filling, whereas for well-watered

trials it was less important Genotypes with larger canopy at anthesis or beginning of grain filling are those able to use more of the available water and therefore potentially better suited to yield more (Condorelli *et al.*, 2018). During anthesis, leaf pigment measurements indicating stress protection also were reported to be significant to GY. Along the cropping season with less precipitation, and thus less water supply to the rainfed trials, higher Flav readings marked the cultivars with higher tolerance to the growing conditions. Moreover, these cultivars exhibited lower CT, which means are able to maintain higher rates of transpiration which suggest they use more water. In fact, during grain filling, the estimation of the photosynthetic variability became an important predictor in the GY models. Thus, the indices with highest detection rate in the GY models were indicators of photosynthetic capacity and water status, such as the multispectral indices PRI or WBI, together with CT.

4.4 Formulation of ideotype recommendation for each agro-environment based on the measurements performed

After the evaluation of the performance assessing GY of all the measurements under each environmental condition, the most relevant traits were used for defining the best yielding ideotypes for each of the eight specific combinations of location-and management conditions (Table 9).

Table 9. Summary of potential traits contributing to the development of well adapted wheat ideotypes under the eight different environmental conditions, understood as the combinations of location and management practices. Except for late-planting conditions in Valladolid, for each of these combinations data of three consecutive crop seasons has been used. Environments are presented from the most (left column) to the less yielding (far right column).

	Valladolid Irrigation	Aranjuez Irrigation	Coria Rainfed	Valladolid Late	Aranjuez Late	Valladolid Nitrogen	Valladolid Rainfed	Aranjuez Rainfed
<i>Heading/ Pre-anthesis</i>	NGRDI ↑	NDVI ↑		u.a	u* PRI ↑	CT ↓ NDVI ↑	Anth PH ↑	NDVI ↑
<i>Anthesis</i>	NGRDI ↑	CT ↓	PH ↑ Anth ↑ CT ↓	EVI ↑ PRI ↑	Anth PH ↑		Anth ↑ GA ↑ Chl ↑	CT ↓ GGA ↑
<i>Grain filling</i>	CT ↓ GGA ↑	NDVI ↑ CSI ↓	GA ↑		Flav PRI ↑	CT ↓	PRI ↑ CT ↓ Anth ↑	GGA ↑
<i>Maturity</i>	$\delta^{13}\text{C}$ ↓		$\delta^{13}\text{C}$ ↓		Carbon ↑	Nitrogen ↓ Carbon ↓	$\delta^{13}\text{C}$ ↓ $\delta^{15}\text{N}$ ↑ Nitrogen ↑	$\delta^{13}\text{C}$ ↓

Under the support irrigation conditions in Valladolid, the most productive genotypes exhibited enhanced crop cover (higher NGRDI or GGA) through the reproductive cycle in synchrony with a better water status (lower CT and $\delta^{13}\text{C}$ in mature grains). Cultivars with higher yields under the irrigation conditions provided by the irrigation trials of Aranjuez exhibited enhanced growth (higher NDVI) with a better water status (lower CT) during anthesis, but especially the grain filling periods were reported to be longer in relation to the stay-green VIs (lower CSI). Results obtained across the crop seasons in Coria, suggests that high-yielding ideotypes would be represented by cultivars with higher biomass (higher PH) values that present better water status (lower CT and $\delta^{13}\text{C}$) together with the development of photoprotective pigments (higher Anth) during the anthesis stages and the ability of delaying senescence (higher GA) during grain filling. Therefore, those genotypes able to use more water were the most productive.

In the late-planting conditions, elevated temperatures expected around anthesis induces grain sterility and thus, lower GY (John and Megan, 1999). From the only season assessed for the late-planting conditions in Valladolid, best cultivars exhibited enhanced crop biomass and canopy greenness (higher EVI) with better photosynthetic activity during anthesis (higher PRI). The ideotypes suggested for late-planting trials in Aranjuez were

characterized for having larger biomass (higher NDVI and PH) through all the reproductive periods. Here, the development of protection pigments plays an important role (higher Anth), defining those cultivars better prepared to confront the heat stress while the photosynthetic capacity is maintained elevated (higher PRI).

Wheat genotypes with better nitrogen use efficiency will help to reduce the need for N fertilizers (Frels *et al.*, 2018). Among the cultivars studied in the low-N trials in Valladolid, the main difference of the high-yielding cultivars, apart from the improved biomass and water status, were associated to the C and N content of the grains.

In relation to the rainfed conditions of Valladolid, besides improved crop biomass (higher PH and lower CSI) and water status measures (lower CT and $\delta^{13}\text{C}$) along the season, the changes in protection pigments played an important role on the definition of the high-yielding ideotypes decreasing before (lower Anth) and increasing during anthesis (higher Anth). Regarding to the rainfed conditions in Aranjuez, higher-yielding ideotypes were cultivars capable to produce more dense and greener canopies (higher NDVI and GGA values) while ensuring higher photosynthetic rates (lower CT at anthesis and lower $\delta^{13}\text{C}$ of mature kernels), while delaying senescence (higher GGA during grain filling).

5. Conclusions

The results of the present study showed that environmental conditions caused a significant influence on the agronomical performance of wheat cultivars and GY highly varied between years, locations and treatments. The reported phenotypic plasticity of the cultivars studied highlighted the importance selecting genotypes with specific ideotypic characteristics for each environment. This is in spite the fact that some common characteristics emerged as a key phenotypic traits across a wide range of growing conditions. This is the case for example of higher biomass, better water status, stay green or a better photosynthetic efficiency. In the context of cultivars recommendations, crop models based on high-throughput phenotyping data have an important role assessing the integration G x E x M interactions. The assessment of different physiological traits via remote sensing approaches and the isotopic signature of the mature grain served to describe ideotypes of durum wheat for specific Mediterranean conditions varying in water availability and growing temperature. The LASSO approach permitted the selection of the most critical remote sensing indices to the definition of specific agroclimatic ideotypes based on the phenotypic profile of the cultivars. In this sense, higher values of

indices informing about crop cover and canopy greenness through the growing cycle together with the assessment of a water status indicator as low CT during anthesis were common traits critical to GY across the environments studied. When drought was a limiting factor, the most productive cultivars reported higher stay-green indicator and hence, exhibited longer grain filling periods. High Ant and Flav readings also were reported critical to GY, anticipating the cultivars response to drought and their ability to deal with it. Although higher temperatures during the cycles of late-planting trials reduced GY, as water was not a limited factor, ideotype designed highlighted elevated rates of photosynthesis activity, using indices like PRI. The results obtained in this study represent the successful use of UAV-derived data with leaf-based pigment readings and PH as an effective methodology to evaluate wheat cultivars under water and heat stress. LASSO models showed the importance of the combined use VIs, even derived from an RGB camera, with CT assessments during reproductive stages of the crop on accurate GY predictions. Moreover, and for a wide range of growing conditions, lower $\delta^{13}\text{C}$ were associated to higher-yielding cultivars as integrates the performance through the whole cycle, and particularly during the reproductive stages and supported the definition of more precise ideotypes.

Author contributions

A.G.-R., S.C.K. and J.L.A. conceived and designed the experiment. M.T.N.-T. managed and directed the wheat trials at the INIA experimental stations of Aranjuez and Coria del Rio; and N.A. the ITACyL experimental station in Valladolid. A.G.-R., T. V., F.Z.R., J.S., S.C.K. and J.L.A. conducted the field measurements. A.G.-R. and S.C.K. carried out the flights for the obtainment of the aerial measurements. F.Z.R. conducted the stable isotope composition of the mature grains. A.G.-R. processed and analyzed the images. T.V. developed the R code for the LASSO analysis. A.G.-R. did the statistical analysis and wrote the paper under the supervision of J.L.A. and S.C.K. and the contributions from all the other authors. J.L.A. is the head of the Integrative Crop Ecophysiology research group and Principal Investigator of the MINECO project which funds this research.

Funding

We acknowledge the support of the Spanish project PID2019-106650RB-C21 from the Ministerio de Ciencia e Innovación. A.G.-R. is a recipient of a FPI doctoral fellowship from the same institution. We also acknowledge the support from the Institut de Recerca

de l'Aigua and the Universitat de Barcelona. J.L.A. acknowledges support from the Institució Catalana de Investigació i Estudis Avançats (ICREA) Academia, Generalitat de Catalunya, Spain.

Acknowledgments

The authors of this research thank the personnel from the experimental stations of INIA in Coria and Aranjuez and ITACyL in Valladolid for their continued support of our research. We thank the Integrative Crop Ecophysiology Group members their assistance during the collection of phenotypic data during the study. Finally, we thank Jaume Casadesús for providing the Breedpix software.

References

- Araus, J.L., Cabrera-Bosquet, L., Serret, M.D., Bort, J. and Nieto-Taladriz, M.T.** (2013) Comparative performance of $\delta^{13}\text{C}$, $\delta^{18}\text{O}$ and $\delta^{15}\text{N}$ for phenotyping durum wheat adaptation to a dryland environment. *Funct. Plant Biol.*, **40**, 595–608. Available at: <https://doi.org/10.1071/FP12254>.
- Araus, J.L. and Cairns, J.E.** (2014) Field high-throughput phenotyping: The new crop breeding frontier. *Trends Plant Sci.*, **19**, 52–61.
- Araus, J.L., Slafer, G.A., Reynolds, M.P. and Royo, C.** (2002) Plant breeding and drought in C3 cereals: What should we breed for? *Ann. Bot.*, **89**, 925–940.
- B., W., J.R., P. and J., S.** (2003) Lack of interaction between extreme high-temperature events at vegetative and reproductive growth stages in wheat. *J. Agron. Crop Sci.*, **189**, 142–150.
- Bendig, J., Bolten, A., Bennertz, S., Broscheit, J., Eichfuss, S. and Bareth, G.** (2014) Estimating biomass of barley using crop surface models (CSMs) derived from UAV-based RGB imaging. *Remote Sens.*, **6**, 10395–10412.
- Buchailot, M.L., Gracia-Romero, A., Vergara-Diaz, O., Zaman-Allah, M.A., Tarekegne, A., Cairns, J.E., Prasanna, B.M., Araus, J.L. and Kefauver, S.C.** (2019) Evaluating maize genotype performance under low nitrogen conditions using RGB UAV phenotyping techniques. *Sensors (Switzerland)*, **19**.
- Casadesús, J., Kaya, Y., Bort, J., et al.** (2007) Using vegetation indices derived from conventional digital cameras as selection criteria for wheat breeding in water-limited environments. *Ann. Appl. Biol.*, **150**, 227–236.
- Cerovic, Z.G., Masdoumier, G., Ghozlen, N. Ben and Latouche, G.** (2012) A new optical leaf-clip meter for simultaneous non-destructive assessment of leaf chlorophyll and epidermal flavonoids. *Physiol. Plant.*, **146**, 251–260.
- Chairi, F., Vergara-Diaz, O., Vatter, T., Aparicio, N., Nieto-Taladriz, M.T., Kefauver, S.C., Bort, J., Serret, M.D. and Araus, J.L.** (2018) Post-green revolution genetic advance in durum wheat: The case of Spain. *F. Crop. Res.*, **228**, 158–169.

- Christopher, J.T., Christopher, M.J., Borrell, A.K., Fletcher, S. and Chenu, K.** (2016) Stay-green traits to improve wheat adaptation in well-watered and water-limited environments. *J. Exp. Bot.*, **67**, 5159–5172.
- Condorelli, G.E., Maccaferri, M., Newcomb, M., Andrade-Sanchez, P., White, J.W., French, A.N., Sciara, G., Ward, R. and Tuberosa, R.** (2018) Comparative aerial and ground based high throughput phenotyping for the genetic dissection of NDVI as a proxy for drought adaptive traits in durum wheat. *Front. Plant Sci.*, **9**.
- Coppens, F., Wuyts, N., Inzé, D. and Dhondt, S.** (2017) Unlocking the potential of plant phenotyping data through integration and data-driven approaches. *Curr. Opin. Syst. Biol.*, **4**, 58–63.
- Costa, J.M., Grant, O.M. and Chaves, M.M.** (2013) Thermography to explore plant-environment interactions. *J. Exp. Bot.*, **64**, 3937–3949.
- Daughtry, C.S.T., Walthall, C.L., Kim, M.S., Colstoun, E.B. de and McMurtrey, J.E.** (2000) Estimating Corn Leaf Chlorophyll Concentration from Leaf and Canopy Reflectance. *Remote Sens. Environ.*, **74**, 229–239. Available at: <https://www.sciencedirect.com/science/article/pii/S0034425700001139>.
- Donald, C.M.** (1968) The breeding of crop ideotypes. *Euphytica*, **17**, 385–403. Available at: <https://doi.org/10.1007/BF00056241>.
- Farooq, M., Bramley, H., Palta, J.A. and Siddique, K.H.M.** (2011) Heat stress in wheat during reproductive and grain-filling phases. *CRC. Crit. Rev. Plant Sci.*, **30**, 491–507.
- Farquhara, G.D. and Richardsb, R.A.** (1984) *Isotopic Composition of Plant Carbon Correlates with Water-use Efficiency of Wheat Genotypes.*
- Fernandez-Gallego, Jose A, Kefauver, S.C. and Vatter, T.** (2019) Low-cost assessment of grain yield in durum wheat using RGB images. *Eur. J. Agron.*, **105**, 146–156.
- Fernandez-Gallego, Jose A., Kefauver, S.C., Vatter, T., Aparicio Gutiérrez, N., Nieto-Taladriz, M.T. and Araus, J.L.** (2019) Low-cost assessment of grain yield in durum wheat using RGB images. *Eur. J. Agron.*, **105**, 146–156.
- Filippi, P., Jones, E.J., Wimalathunge, N.S., et al.** (2019) An approach to forecast grain crop yield using multi-layered, multi-farm data sets and machine learning. *Precis. Agric.*, **20**, 1015–1029.
- Frels, K., Guttieri, M., Joyce, B., Leavitt, B. and Baenziger, P.S.** (2018) Evaluating canopy spectral reflectance vegetation indices to estimate nitrogen use traits in hard winter wheat. *F. Crop. Res.*, **217**, 82–92. Available at: <https://doi.org/10.1016/j.fcr.2017.12.004>.
- Gamon, J.A., Huemmrich, K.F., Wong, C.Y.S., Ensminger, I., Garrity, S., Hollinger, D.Y., Noormets, A. and Peñuelask, J.** (2016) A remotely sensed pigment index reveals photosynthetic phenology in evergreen conifers. *Proc. Natl. Acad. Sci. U. S. A.*, **113**, 13087–13092.
- Gamon, J.A., Peñuelas, J. and Field, C.B.** (1992) A narrow-waveband spectral index that tracks diurnal changes in photosynthetic efficiency. *Remote Sens. Environ.*, **41**, 35–44. Available at:

<https://www.sciencedirect.com/science/article/pii/003442579290059S>.

- Gitelson, A.A., Merzlyak, M.N. and Chivkunova, O.B.** (2001) Optical Properties and Nondestructive Estimation of Anthocyanin Content in Plant Leaves. *Photochem. Photobiol.*, **74**, 38.
- Gitelson, A.A., Zur, Y., Chivkunova, O.B. and Merzlyak, M.N.** (2002) Assessing Carotenoid Content in Plant Leaves with Reflectance Spectroscopy¶. *Photochem. Photobiol.*, **75**, 272.
- González-Dugo, M.P., Moran, M.S., Mateos, L. and Bryant, R.** (2006) Canopy temperature variability as an indicator of crop water stress severity. *Irrig. Sci.*, 1–8.
- Gracia-Romero, A., Kefauver, S.C., Fernandez-Gallego, J.A., Vergara-Díaz, O., Nieto-Taladriz, M.T. and Araus, J.L.** (2019) UAV and ground image-based phenotyping: A proof of concept with durum wheat. *Remote Sens.*, **11**.
- Gregersen, P.L., Culetic, A., Boschian, L. and Krupinska, K.** (2013) Plant senescence and crop productivity. *Plant Mol. Biol.*, **82**, 603–622.
- Haboudane, D., Miller, J.R., Tremblay, N., Zarco-Tejada, P.J. and Dextraze, L.** (2002) Integrated narrow-band vegetation indices for prediction of crop chlorophyll content for application to precision agriculture. *Remote Sens. Environ.*, **81**, 416–426. Available at: <https://www.sciencedirect.com/science/article/pii/S0034425702000184>.
- Hamblin, J.** (1993) Chapter 77 The Ideotype Concept : Useful or Outdated ?
- Hassan, M.A., Yang, M., Rasheed, A., Yang, G., Reynolds, M., Xia, X., Xiao, Y. and He, Z.** (2019) A rapid monitoring of NDVI across the wheat growth cycle for grain yield prediction using a multi-spectral UAV platform. *Plant Sci.*, **282**, 95–103. Available at: <https://doi.org/10.1016/j.plantsci.2018.10.022>.
- Huete, A., Didan, K., Miura, T., Rodriguez, E.P., Gao, X. and Ferreira, L.G.** *Overview of the radiometric and biophysical performance of the MODIS vegetation indices*, Available at: www.elsevier.com/locate/rse.
- Huete, A.R.** (1988) A soil-adjusted vegetation index (SAVI). *Remote Sens. Environ.*, **25**, 295–309. Available at: <https://www.sciencedirect.com/science/article/pii/003442578890106X>.
- Hunt, E.R., Cavigelli, M., Daughtry, C.S.T., McMurtrey, J.E. and Walthall, C.L.** (2005) Evaluation of digital photography from model aircraft for remote sensing of crop biomass and nitrogen status. *Precis. Agric.*, **6**, 359–378.
- Hunt, E.R., Doraiswamy, P.C., McMurtrey, J.E., Daughtry, C.S.T., Perry, E.M. and Akhmedov, B.** (2012) A visible band index for remote sensing leaf chlorophyll content at the Canopy scale. *Int. J. Appl. Earth Obs. Geoinf.*, **21**, 103–112.
- Jackson, R.D., Reginato, R.J. and Idso, S.B.** (1988) Wheat canopy temperature: A practical tool for evaluating water requirements. *Water Resour. Res.*, **13**, 651–656. Available at: <https://doi.org/10.1029/WR013i003p00651>.
- Jaradat, A.A.** (2018) Statistical Modeling of Phenotypic Plasticity under Abiotic Stress in *Triticum durum* L. and *Triticum aestivum* L. Genotypes. *Agron.*, **8**.
- John, R.P. and Megan, G.** (1999) Temperatures and the growth and development of

wheat: a review. *Eur. J. Agron.*, **10**, 23–36. Available at: %5C%5CGRAEFE%5CJournals%5CEuropean_Journal_of_Agronomy%5C_3.pdf

- Juliana, P., Montesinos-López, O.A., Crossa, J., et al.** (2019) Integrating genomic-enabled prediction and high-throughput phenotyping in breeding for climate-resilient bread wheat. *Theor. Appl. Genet.*, **132**, 177–194. Available at: <https://doi.org/10.1007/s00122-018-3206-3>.
- Kahiluoto, H., Kaseva, J., Balek, J., et al.** (2019) Decline in climate resilience of European wheat. *Proc. Natl. Acad. Sci. U. S. A.*, **116**, 123–128.
- Kefauver, S.C., Vicente, R., Vergara-Díaz, O., Fernandez-Gallego, J.A., Kerfal, S., Lopez, A., Melichar, J.P.E., Serret Molins, M.D. and Araus, J.L.** (2017) Comparative UAV and field phenotyping to assess yield and nitrogen use efficiency in hybrid and conventional barley. *Front. Plant Sci.*, **8**.
- Klompenburg, T. van, Kassahun, A. and Catal, C.** (2020) Crop yield prediction using machine learning: A systematic literature review. *Comput. Electron. Agric.*, **177**, 105709. Available at: <https://doi.org/10.1016/j.compag.2020.105709>.
- Kumar, M.** (2016) Impact of climate change on crop yield and role of model for achieving food security. *Environ. Monit. Assess.*, **188**. Available at: <http://dx.doi.org/10.1007/s10661-016-5472-3>.
- Liakos, K.G., Busato, P., Moshou, D., Pearson, S. and Bochtis, D.** (2018) Machine Learning in Agriculture: A Review. *Sensors*, **18**.
- Loss, S.P. and Siddique, K.H.M.** (1994) Morphological and Physiological Traits Associated with Wheat Yield Increases in Mediterranean Environments. *Adv. Agron.*, **52**, 229–276.
- Ma, D., Sun, D., Wang, C., Li, Y. and Guo, T.** (2014a) Expression of flavonoid biosynthesis genes and accumulation of flavonoid in wheat leaves in response to drought stress. *Plant Physiol. Biochem.*, **80**, 60–66. Available at: <https://www.sciencedirect.com/science/article/pii/S0981942814001120>.
- Ma, D., Sun, D., Wang, C., Li, Y. and Guo, T.** (2014b) Plant Physiology and Biochemistry Expression of flavonoid biosynthesis genes and accumulation of flavonoid in wheat leaves in response to drought stress. *Plant Physiol. Biochem.*, **80**, 60–66. Available at: <http://dx.doi.org/10.1016/j.plaphy.2014.03.024>.
- Martre, P., Quilot-Turion, B., Luquet, D., Memmah, M.-M.O.-S., Chenu, K. and Debaeke, P.** (2015) Chapter 14 - Model-assisted phenotyping and ideotype design. In V. O. Sadras and D. F. B. T.-C. P. (Second E. Calderini, eds. San Diego: Academic Press, pp. 349–373. Available at: <https://www.sciencedirect.com/science/article/pii/B9780124171046000145>.
- Neufeld, H.S., Chappelka, A.H., Somers, G.L., Burkey, K.O., Davison, A.W. and Finkelstein, P.L.** (2006) Visible foliar injury caused by ozone alters the relationship between SPAD meter readings and chlorophyll concentrations in cutleaf coneflower. *Photosynth. Res.*, **87**, 281–286.
- Paleari, L., Vesely, F.M., Ravasi, R.A., Movedi, E., Tartarini, S., Invernizzi, M. and Confalonieri, R.** (2020) Analysis of the Similarity between in Silico Ideotypes and

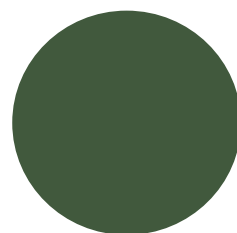
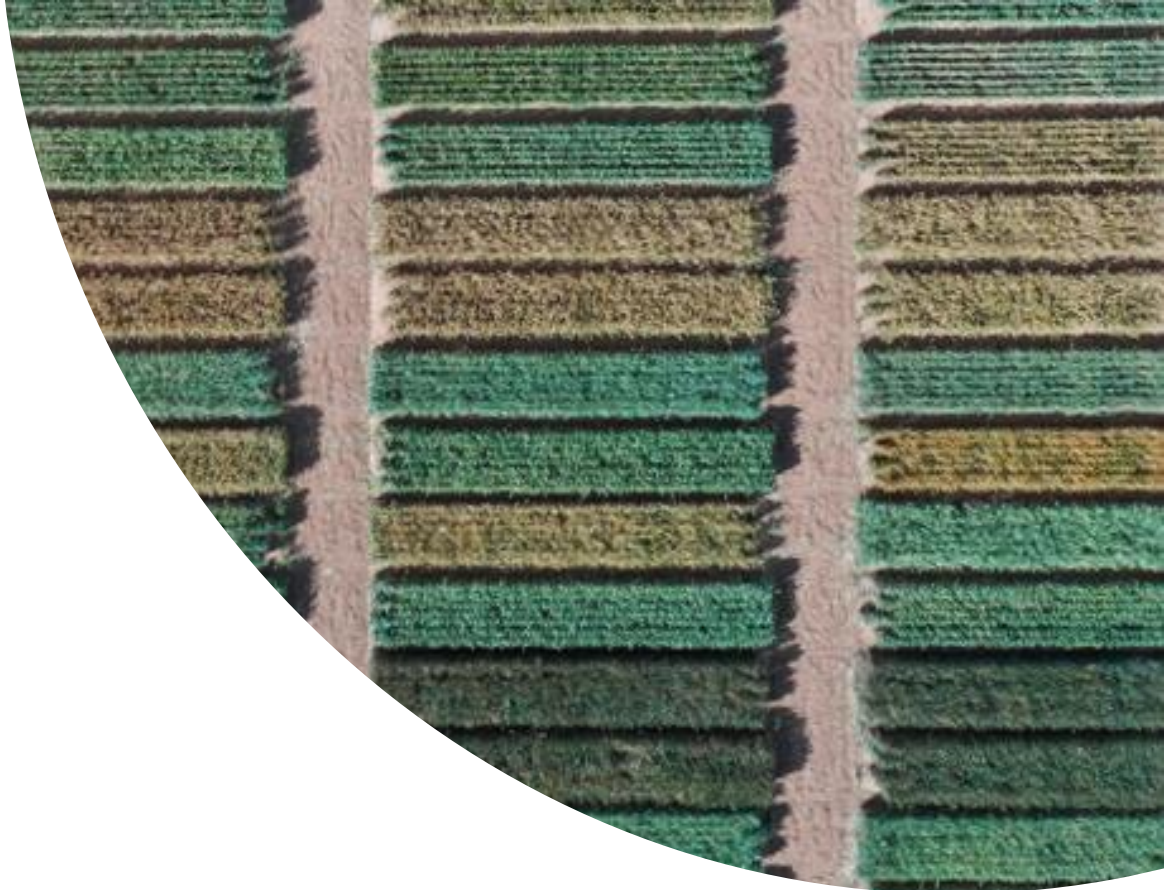
- Phenotypic Profiles to Support Cultivar Recommendation—A Case Study on *Phaseolus vulgaris* L. *Agronomy*, **10**, 1733.
- Passioura, J.B.** (1977) 1977passiouraJAIAS. *J. Aust. Inst. tagricultural Sci.*, **43**, 117–120.
- Passioura, J.B.** (1996) Drought and drought tolerance. *Plant Growth Regul.*, **20**, 79–83. Available at: <https://doi.org/10.1007/BF00024003>.
- Peng, Y., Hsu, C. and Huang, P.** (2015) Developing Crop Price Forecasting Service Using Open Data from Taiwan Markets. , 172–175.
- Penuelas, J., Filella, I., Biel, C., Serrano, L. and Save, R.** (1993) The reflectance at the 950-970 nm region as an indicator of plant water status. *Int. J. Remote Sens.*, **14**, 1887–1905.
- Pointer, M.R.** (2009) A comparison of the CIE 1976 colour spaces. *Color Res. Appl.*, **6**, 108–118. Available at: <http://doi.wiley.com/10.1002/col.5080060212> [Accessed December 15, 2017].
- R Development Core Team.** (2010) *R a language and environment for statistical computing : reference index*, R Foundation for Statistical Computing.
- Rondeaux, G., Steven, M. and Baret, F.** (1996) Optimization of soil-adjusted vegetation indices. *Remote Sens. Environ.*, **55**, 95–107. Available at: <https://www.sciencedirect.com/science/article/pii/0034425795001867>.
- Roujean, J.-L. and Breon, F.-M.** (1995) Estimating PAR absorbed by vegetation from bidirectional reflectance measurements. *Remote Sens. Environ.*, **51**, 375–384. Available at: <https://www.sciencedirect.com/science/article/pii/0034425794001143>.
- Rouse, J. W., J., Haas, R.H., Schell, J.A. and Deering, D.W.** (1976) Monitoring vegetation systems in the Great Plains with ERTS. In *NASA. Goddard Space Flight Center 3d ERTS-1 Symp., Vol. 1, Sect. A*. pp. 24–26.
- Sadras, V.O. and Richards, R.A.** (2014) Improvement of crop yield in dry environments: Benchmarks, levels of organisation and the role of nitrogen. *J. Exp. Bot.*, **65**, 1981–1995.
- Snape, J.W., Butterworth, K., Whitechurch, E. and Worland, A.J.** (2001) *Waiting for fine times: genetics of flowering time in wheat.*
- Tibshirani, R.** (1996) Regression Shrinkage and Selection Via the Lasso. *J. R. Stat. Soc. Ser. B*, **58**, 267–288. Available at: <https://doi.org/10.1111/j.2517-6161.1996.tb02080.x>.
- Voltas, J., Eeuwijk, F. a van, Igartua, E., García Del Moral, L.F., Molina-cano, J.L. and Romagosa, I.** (2002) Genotype by environment interaction and adaptation in barley breeding: Basic concepts and methods of analysis. *Barley Sci. Recent Adv. from Molecular Biol. to Agron. Yield Qual.*, 205–241.
- Watt, M., Fiorani, F., Usadel, B., Rascher, U., Muller, O. and Schurr, U.** (2020) Phenotyping: New Windows into the Plant for Breeders. *Annu. Rev. Plant Biol.*, **71**, 689–712.
- Xiong, D., Chen, J., Yu, T., Gao, W., Ling, X., Li, Y., Peng, S. and Huang, J.** (2015)

SPAD-based leaf nitrogen estimation is impacted by environmental factors and crop leaf characteristics. *Sci. Rep.*, **5**, 1–12.

Yousfi, S., Serret, M.D., Márquez, A.J., Voltas, J. and Araus, J.L. (2012) Combined use of δ 13C, δ 18O and δ 15N tracks nitrogen metabolism and genotypic adaptation of durum wheat to salinity and water deficit. *New Phytol.*, **194**, 230–244.

Zadoks, J.C., Chang, T.T. and Konzak, C.F. (1974) A decimal code for the growth stages of cereals. *Weed Res.*, **14**, 415–421.

Zaman-Allah, M., Vergara, O., Araus, J.L., et al. (2015) Unmanned aerial platform-based multi-spectral imaging for field phenotyping of maize. *Plant Methods*, **11**, 35.



DISCUSSION

DISCUSSION

Advances in high-throughput phenotyping will enable the screening, of a large number of lines in a fast, accurate and inexpensive manner, and thus, will help accelerating the advancement of the rate of genetic improvement of the breeding process. Phenotyping platforms based on unmanned aerial vehicles (UAVs) with a variety are becoming widely used to monitor genotype performance. The current thesis represents the practical implementation of a set of phenotyping procedures to assess their capabilities to predict genotypic differences regarding yield and the physiological response maize and wheat cultivars to environmental conditions involving water and nutrient deficiencies and management techniques.

Breeding for yield, a phenotypically complex trait

The magnitude of the gene-environment-management interactions makes yield a phenotypically complex trait (Araus & Cairns, 2014; Quintero et al., 2018), resulting from the integration of multiple morphological and physiological processes and their integration through the crop cycle. The substantial need of increasing yield to meet the expectations of food demand face the additional challenge of climate change with drought, extreme temperature events, nutrient deficiencies and land degradation among the main abiotic stresses with major impacts on crop yield. In the field, crops are usually subjected to a combination of different abiotic stresses that may cause extensive production losses. Those abiotic stresses cause limiting conditions for achieving the yield potential, arising the importance of understanding the implications between cultivars, agronomic conditions and the environment in order to design future breeding strategies. The results presented in this thesis demonstrated the high levels of influence of environmental conditions, agricultural management practices and genotype used on the yield performance of the maize and wheat studies. The presented work demonstrated that

the relative performance of a genotype varies with the environmental conditions and with crop management.

Studies of maize were performed in the Sub-Saharan Africa (SSA) research station of the International Maize and Wheat Improvement Center (CIMMYT). Together with increasing threats of climate change, the loss of soil fertility is critical for agricultural production in SSA as the limited availability of fertilizers is a leading factor that contributes to low yields. Low levels of soil phosphorous (P) and nitrogen (N), are the main constraints to crop growth in these areas (Buerkert et al., 2001). In Chapters 1, 2 and 4, the deficit of P and N significantly reduced the maize yield in comparison with the control conditions. Phosphorous and nitrogen are essential nutrients for plant growth and development, and their deficiency reduces photosynthetic capacity and thus yield. Since the use of fertilizers cannot be considered always a sustainable practice, given the economic and environmental costs (Good & Beatty, 2011), the genotypic differences reported suggest that changes in the cultivars used may contribute to enhancing yield potential.

Under these conditions where fertilizers become essential, field management can contribute greatly to crop yield growth. Efforts to decrease overuse of inputs by agricultural management strategies could increase the cereal production while minimizing the environmental impacts of intensification. In Chapters 2 and 4, in light of soil degradation, conservation agriculture (CA) practices have been proposed as alternatives to tillage-based agriculture in SSA as a pragmatic solution to increasing production while conserving the natural resource base. CA consists of a set of core principles, including minimum soil disturbance, permanent soil cover, and diversified crop rotations supported by integrated soil, crop, and water management, which aims to reduce and/or revert many negative effects of conventional farming practices. In this

sense, remote sensing techniques similar to those used for phenotyping may be also deployed to monitoring the performance of crop management techniques such as CA. In addition, as CA is more and more widely used, crop breeding under these specific conditions become a priority. However, phenotyping performance using remote sensing techniques may be affected by the specific conditions of residue cover. Our work in maize showed the benefits of CA as a potential system to increase yield, where the combination of minimal tillage with residue coverage produces higher yields compared to the plots grown under conventional conditions. The effect of the CA conditions was also shown in the VIs measured as more dense/green canopies. One of these benefits is attributed to the water-harvesting effects of minimum-tillage practices (Mupangwa et al., 2008; Thierfelder & Wall, 2009), but even any direct measurement of water status was reported in none of the studies.

In the case of study in the Chapter 4, the combined effects of tillage, the amount of residue cover and N fertilizer on grain yield was evaluated as the success of the CA practices relies on the amount and quality of the residues and the initial fertility status of the soil (Thierfelder et al., 2016). The appropriate use of N top-dressing fertilizers to promote soil microbiota activity (Chivenge et al., 2011) and the competing use of crop residues (Giller et al., 2011; Jaleta et al., 2013) might be drawbacks for the promotion of CA practices. Our results reported that a proper combination of N-fertilizer with an optimal quantity of stover incorporated as residue cover resulted in a significant yield increase.

Moving to the wheat experiments, trials were conducted in a wide range of Spanish latitudes for several consecutive crop seasons (with very diverse climatic conditions) and in trials under different growing conditions (well-irrigated, rainfed, late-planting and low-nitrogen). Agriculture in Spain is particularly sensitive to climate

because of the low average precipitation level and its marked interannual variability. Therefore, the combination of location, management conditions and year were considered as different environments that provided a wide range of climatic conditions for the phenotypic expression of the genotypes tested. Under Mediterranean conditions, water regime and temperature have been described as the main factors that explain a major portion of GY variation in cereals (Voltas et al., 2002). The drought stress imposed by the rainfed trials greatly reduced GY in comparison to the well-irrigated trials of the same locations, while yield reductions related to the heat stress imposed by the late planting treatments were less severe. Regarding to the combination of low N-fertilizer and without irrigation conditions in Valladolid, the studies concluded that the lack of fertilizer reduced the plot biomass and then the drought stress was not that much severe during grain filling.

Remote sensing ability to assess genotypic differences in yield under different growing conditions

Remote sensing approaches have become fundamental methodologies for agricultural monitoring and to improve precision and throughput in phenotyping. Remote sensing methods enable detailed non-invasive information to be captured throughout the plant life cycle. This is proved by the growing body of literature demonstrating the usefulness of remote sensing for a wide range of applications in agriculture: growth monitoring, yield prediction, stress detection, nutrient deficiency diagnosis, and control of plant diseases (Fiorani & Schurr, 2013). Moreover, the results presented reported that all these remote sensing methodologies are amenable to high-throughput phenotyping under different conditions.

According to the FAO definition, the soil surface of crops under CA must be covered at least by 30% of stover (Kosmowski et al., 2017). This characteristic makes use

of these remote sensing techniques for monitoring CA as a particular case, as the crop residue coverage add noise to the measures. The results shown in Chapter 2 reported an accuracy decrease of the VIs assessing yield under CA conditions in comparison to the conventional ploughing conditions. The main reason that explains this limitation is the difficulty in segregating what is biomass from the plants and what is the coverage. To solve this constraint, the application of a vegetation mask using a NDVI threshold on the VIs helped to avoid the soil background reflectance and then the performance assessing yield improved.

Multispectral VIs performance determining differences in grain yield

Traditionally, the use of multispectral sensors for the development of VIs associated with vegetation parameters such as above-ground biomass, water and nutrient deficiency, has been involved for phenotyping purposes. In our work, the normalized difference vegetation index (NDVI) performed among the best GY predictors for both wheat and maize studies. The strong contrast between the near infrared (NIR) and red bands make such index good measurement of canopy greenness and canopy cover (Tucker, 1979). The effect of the abiotic stresses studied produced reduction in leaf expansion and crop growth, and thus, above ground biomass, which estimated with NDVI and its reformulations (soil adjusted vegetation index, SAVI; optimized soil adjusted vegetation index, OSAVI; enhanced vegetation index, EVI) performed well determining genotypic differences in growth and yield among the wheat and maize cultivars studied. Besides the assessment of green plant biomass, the use of specific narrow bands from 510 to 550 nm that are very sensitive to changes in the de-epoxidation of the xanthophyll cycle permitted the assessment of the photosynthetic capacity of the cultivars. Thus, our work also highlighted the performance of indices like the photochemical reflectance index (PRI) and chlorophyll carotenoid index (CCI) as indicators of photosynthetic efficiency.

Particularly, high and positive correlations were reported in Chapter 2 between PRI and GY, indicating that low PRI values reflected a lower light use efficiency of PSII that will finally be translated in a yield loss. Finally, the assessment of NIR wavelengths permitted the calculation of the water band index (WBI) as an indicator of the turgor of the leaves. The feature selection performed in Chapter 5 reported WBI as a good yield indicator under arid environments.

RGB Indices performance determining differences in grain yield

The use of information derived from conventional digital RGB (of red, green, blue) images may represent a low-cost alternative to the use of multispectral or hyperspectral information for formulating vegetation indices. The studies presented in this PhD thesis emphasize the capabilities of RGB vegetation indices as phenotypic traits for predicting both maize and wheat performance under different field conditions. Particularly, indices that performed better in assessing differences in yield were the ones more related to canopy greenness (such as a^* or GGA) and thus to vegetation cover. Green area (GA) and greener area (GGA) indices quantify the portion of green pixels being a reliable estimator of vegetation cover (Lukina et al., 1999). In our work with maize, the indices that performed better assessing differences in GY were the ones related to vegetation cover, as the GA and the GGA, as the crop cover was main source of variability rather than the canopy color itself. In Chapters 1 and 2, as measurements were performed in seedlings, RGB indices were reported as good indicators initial vigor at early growing stages as response to the lack of phosphorus (Chapter 1) and to the CA management (Chapter 2). Whereas in the Chapter 4, maize was in a reproductive stage, then RGB were estimating differences in biomass. Regarding to the wheat studies, RGB indices performed as a good indicators of plot biomass during the stage of anthesis, but specially indices performed well as early-senescence indicators during grain filling.

Lastly, in Chapter 4, RGB indices calculated from maize leaves scans were reported as a potential method for evaluating foliar nutrition. Results reported how the leaf colors tended to be in darker green tonalities as the more N fertilizer was added to the plot. Hence, more yellowish tones measured as low NGRDI values for example, were related to N deficiency.

Canopy Temperature performance determining differences in grain yield

The assessment of canopy temperature (CT) holds a great promise for and indirect selection of maize and wheat cultivars with optimized water status. CT measurements in maize studies were only assessed at seedling stage in Chapter 2, and results did not report any benefits of CA on the soil moisture. Meanwhile, the results presented with wheat reported greater transpiration measured as cooler canopies, as a major driver leading to higher yields. Particularly under the more stressed conditions, high and negative correlations between CT and GY can be related to the capability of genotypes to be more photosynthetically active by keeping higher stomatal conductance and lower canopy temperature. Hence, genotypes with a higher resistance to drought and heat can be identified as plants with cooler leaves (Berger et al., 2010).

Comparative Performance of Ground Versus Aerially Assessed Indexes

Considering that time has been one of the largest limitations to phenotyping under field conditions, the possibility to incorporate remote sensing methodologies onto UAVs enabled the characterization of a larger number of plots, precisely and efficiently, while helping to minimize the effect of the changing environmental conditions during the sampling (Araus & Cairns, 2014). The successful implementation of aerial platforms with the assembly of imaging sensors has been extensive for assessing crop performance under different growing conditions, for phenotyping and precision agriculture purposes.

In all of our studies, ground and aerial measurements were taken at the same time on the same day in order to reduce the most the variation in the environmental factors such as light intensity. Though, main differences are due to the resolution of the images: even using cameras with the same sensor size, the distance between the camera and the crop canopy will affect the spatial resolution of the image. This might be relevant because as higher is the image resolution the plants in the image are better defined, while in low resolution images the boundaries between soil and vegetation could be diffuse (Torres-Sánchez et al., 2014). When indices of vegetation cover are calculated, as GA or GGA, the reduction in the number of total pixels in the image could negatively affect the identification of differences in vegetation color.

In our results with maize studies, particularly in Chapters 1 and 2 when the measurements were taken in early stages, these limitations are underlined since the densities of the canopies were low, more soil background was captured in the images and accurate plant cover are more important. In terms of spatial resolution, the performance of RGB indices measured at ground level was better than that of the same VIs assessed from aerial platforms. Nevertheless, advances in digital photography allow new sensors with higher resolutions which may overcome the inherent problem of a low resolution when images are acquired from aerial platforms. Another important issue is that aerial photographs facilitate the coverage of the whole plot and therefore overcoming canopy heterogeneity, while this is usually not possible for the images taken at ground level, and then the whole variability of the plot might not be captured in just one image. In Chapter 4, and together with the RGB images, NDVI was assessed from both levels (aerial and ground). The ground measurements with the GreenSeeker performed slightly better than the NDVI derived from the aerial images. Despite those methodological differences, both approaches offered essentially similar kinds of information as indicated the correlation

coefficients calculated between the same indices measured at ground and aerial level in both maize and wheat studies. However, in the case of tall crops such as maize, ground evaluations might result difficult in advanced phenological stages. In Chapter 4, an innovative option has been proposed by the attachment of a camera to a very long “pheno-pole”. However, it only permitted coverage of a portion of the plot and therefore did not account for the possible heterogeneity of the plot.

In the case of CT, measurements performed clearly much better as GY predictors when were assessed at aerial level than at ground level, arising the benefits of UAV platforms overcoming environmental variability restriction by the characterization of a large number of plots faster. Because temperature can fluctuate quickly due to miscellaneous factors (e.g., sun illumination angle, wind, occurrence of clouds), it is of profound importance to screen the whole trial as quickly as possible, in order to have comparable data across all the plots. Manual evaluations at ground level, even taken in short time intervals, can be affected by the constant changes in the environmental conditions. Thus, hand-held infrared thermometers can be problematic in large field studies due to the temporal changes during the time required to measure all plots (Deery et al., 2016).

For the implementation of the phenotyping platform, apart from the accuracy of the measurements, there are other methodological approaches to consider. Firstly, despite UAVs have reached comparatively affordable prices, the associated cost entailed in their employment (the cost of the aerial platform and the requirement of qualified operators) still makes them a relatively expensive approach in some cases. Moreover, the existence of legal restrictions limits the adoption of these methodologies in some countries, particularly their deployment from aerial platforms. Another aspect to consider is the sizeable technical capacity necessary for data processing, from radiometric calibration of

the images and the creation of a georeferenced ortho-mosaic to ensure effective data extraction and analysis. For these reasons, ground-based or hand-held methodologies might be more feasible alternatives in certain circumstances due to their low cost and easy management. To overcome the limitations of segmentation the aerial images, in this thesis the MosaicTool software was developed for a semi-automatic segmentation of the complete field images and to formulate vegetation indices for both RGB, multispectral and thermal images. We included an easy mechanism to select a field column, then segment plots into images with the same dimensions and replicate the same for the whole columns.

Assessment of plant traits across the crop season: when is the best moment to measure

After dissecting what to measure and how to do it, another important issue is decide when to measure. The crop phenology varies due its growth dynamics; likewise, the potential trait estimation of the different VI shifts in time (Fernandez-Gallego et al., 2019). While in early stages VIs might be driven mainly by differences in early vigor, crop establishment and in general crop density; in more advanced phenological phases, when the canopies have a higher cover density, differences in VIs will respond to differences in crop status. Initial crop vigor measurements would help to monitor a better crop establishment and growth, but during more advances stages the measurements are more affected by how photosynthetically active the crop is. This is the case for example of the stay green, which occurs during the last part (usually the reproductive one) of the crop. However, and unless a determined phenotypic trait is targeted, it may be worth to explore the application of these VIs across the phenology of the crop and identify which VIs and in what moment may be key to predict final yield. Therefore the power of these

traits predicting yield could vary, not only across crops, but also across environments, which have to be taken into consideration (Gracia-Romero et al., 2019).

The high correlations against grain yield obtained in the VIs measured at seedlings stages of the maize studies of Chapters 1 and 2, highlight the importance of cultivars with a good early establishment under unfavorable soil conditions such as phosphorus limitations. Otherwise, Chapter 4 reported also good correlations against yield using crop coverage and canopy greenness measurements, by detecting those plants with better nitrogen status.

Finally, the wheat studies performed in Chapters 3 and 5 permitted the evaluation of different phenological moments. The performance of the proposed approaches as phenotyping methodologies was tested during the stages of heading, anthesis and grain filling, and the yield prediction reported varied significantly in each environment. Such variability can be related to differences in crop development, due to the wide range of environmental and growing conditions associated to the combination of location, year and agronomical trials factors on the environment. Climatic variability in precipitation and temperature is responsible of affecting crop development, and thus, the timing of the stress affects the accuracy of a trait assessing GY. The first symptoms of drought stress experienced by the wheat cultivars were related to leaf expansion and crop growth. Therefore, during heading and anthesis the most useful selection traits for yield improvement were biomass measurements, as the RGB indices like GA or multispectral like NDVI. In most cases assessed, the spectral-resolution precision of the multispectral VIs performed well assessing genotypic differences in GY, but when canopies were found to be very dense (for example under support irrigation), VIs were saturated. In these cases, higher spatial resolution of the RGB images allowed indexes like the NGRDI or TGI to perform close to or even surpass the multispectral VIs. A low crop area growth of the

cultivars assessed through VIs have been reported to be significant for limiting yields due a marked reduction in growth caused by stress, whereas cultivars with higher aboveground biomass may be related to a better water and nutrient availability. Moving to anthesis and early phases of grain filling, measures of the actual photosynthetic capacity of the cultivars were highlighted as critical traits for GY. At the final stages of grain filling, results reported the delay of the ripening process and maintaining the canopy greenness as one of the most important traits of the high-yielding phenotypes. Despite this was quite regular among the trials assessed, the performance of the measurements depends directly on the environmental conditions. In certain conditions as the rainfed N limited trials of Valladolid, the detection with VIs of shorter phenology cycles was correlated with higher yields, letting cultivars scape drought. Therefore, it is necessary to dissect all these data to determine what needs to be measured, when it needs to be measured, and how it should be measured in relation to our purpose, which in this instance is forecasting yield. A better understanding of the strengths and limitations of these indices may help to forecast production, but also to improve crop monitoring associated with management practices.

Application of stable isotopes for plant phenotyping

In addition to proximal sensing approaches, the analysis of stable isotopes may complement direct phenotyping under field conditions. The stable carbon ($\delta^{13}\text{C}$) and nitrogen ($\delta^{15}\text{N}$) isotope compositions, when analyzed in plant matter, inform on the water regimen and nitrogen metabolism conditions, respectively, of the plant (Yousfi et al., 2012). When breeding for yield potential and adaption to abiotic stresses such as drought, $\delta^{13}\text{C}$ in dry matter is a promising tool estimating the effect of water status on stomatal conductance thorough the crop cycle (Monneveux et al., 2007).

For both maize, $\delta^{13}\text{C}$ positively correlated with yield, and for wheat correlations were reported negative, whatever the growing conditions. It is important to note that the fractionation of maize, as a C4, plant is less severe than wheat, as a C3, and thus, $\delta^{13}\text{C}$ values will be more negative in wheat than in maize (Farquhar et al., 1989). For maize, in Chapter 1, 2 and 4, significant differences were not found in $\delta^{13}\text{C}$ from the cob leaf between the P fertilization treatments nor the CA and CP practices, as those conditions did not affect the water status of the crops. However, in Chapter 4, higher N concentration in leaves caused a decrease in $\delta^{13}\text{C}$, as result of rather increase of biomass and then increase stress or as response of a photosynthetic capacity boost (Vergara-Díaz et al., 2016). For wheat, in Chapter 5, high negative correlations between $\delta^{13}\text{C}$ analyzed in mature grains and GY suggested that the best genotypes in all tested environments were these exhibiting better water status and thus higher stomatal conductance. The $\delta^{15}\text{N}$ has been used to study the dynamics of N in soil–plant systems (Choi et al., 2003), reporting values closer to zero when the origin of the N-fertilizer is synthetic. This effect was reported in maize in Chapter 4, as the $\delta^{15}\text{N}$ was higher as the top-dressing rate of N fertilization increased. For wheat, in Chapter 5, positive significant correlations were reported between $\delta^{15}\text{N}$ and GY in the rainfed and low-N conditions, suggesting those cultivars with better ability to uptake soil N.

Challenges and opportunities of grain yield prediction models based on phenotyping data

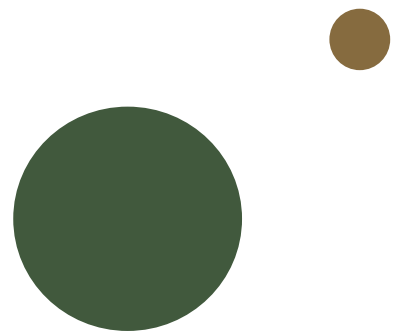
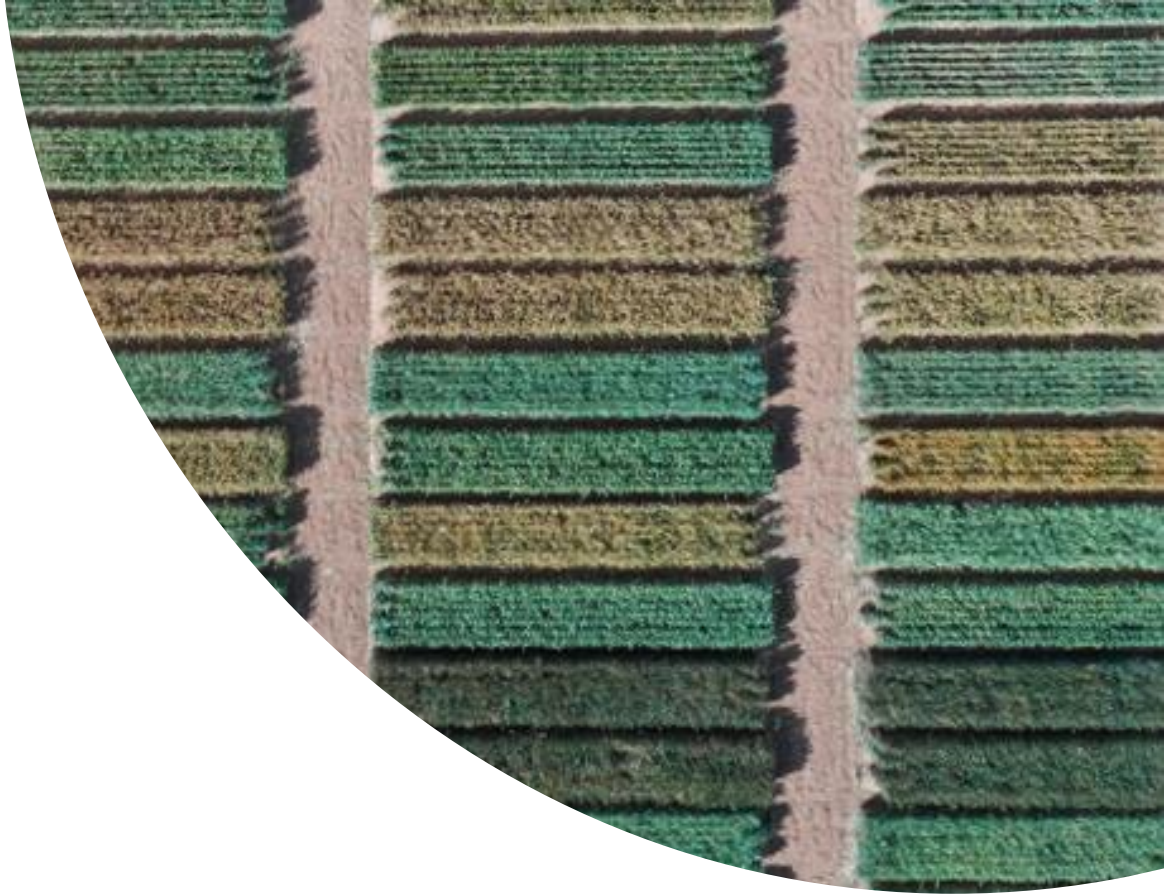
Unlocking the potential of the amounts of data collected from HTP is one of the major challenges of phenotyping (Coppens 2017). Since the main goals of most breeding programs focuses on increasing grain yield, most of the efforts for the extraction of useful information from the phenotyping assessments relies on the development of algorithms of GY forecasting. Conventionally, crop yield models are based in response functions

between yield and some input variables. In our studies with both maize and wheat, GY prediction models were built by the combination of different variables into step-wise regressions models, which the choice of predictive variables is carried out by an automatic procedure. In Chapters 1 and 2, the ability of remote sensing indices measured from the UAV platform was tested using multivariate linear models built using the step-wise regression approach. The combination of different indices improved the strength and accuracy of the assessment of grain yield of simple correlations using a single trait. In Chapter 3, step-wise regressions performed combining indices measured at different phenological stages of wheat reported higher accuracies than the predictions using information of the same phenological stage.

Owing to the needs of achieving accurate prediction models, recent approaches are involving the use of machine learning to aid the interpretation of data by the development of algorithms built from training sets (van Klompenburg et al., 2020). In the wheat study of Chapter 5, a feature selection method regression was performed across all the measurements along the phenology to assess which measurements were more critical to predict GY. To do so, the method used was the least absolute shrinkage and selection operator (LASSO). LASSO is a method for the estimation of linear models proposed by (Tibshirani, 1996) that minimizes the sum of square errors and performs an automated feature selection as part of the estimation procedure. The performance prediction yield of all the variables measured was estimated across 100 repetitions and the more times selected variables were used to build the models.

Several empirical and mathematical yield modeling using machine learning methods have been implemented for different crops (Dourado-Neto et al., 1998), and given its flexibility and the limited number of inputs required, LASSO-based approaches are reported as one with the highest potential for being operationally used to support

breeders in the identification of the best varieties for production (Ogutu et al., 2012). Vergara-Diaz et al., 2020 proven the performance of LASSO models with metabolic data to predict yield as well as providing relevant information to the understanding of wheat physiology.



CONCLUSIONS

CONCLUSIONS

The development of field-based phenotyping technologies with the capability to non-destructively capture of plant traits and their incorporation into aerial based platforms to improve high throughput capacities should become an integral and key component in the breeding pipeline. However, to correctly implement these methodologies in phenotyping studies, it is important to determine which parameters to measure and the optimal phenological moments to measure them for obtaining the best predictors of genotypic variability. The advances on phenotyping will help to develop accurate yield predictions models, fundamental to accelerate the selection process.

- Advances in remote sensing technologies have enhanced the phenotyping process through the development of low-cost and easy-to-handle tools. Field deployment of various sensors enhances the capacity and impact of agricultural studies by increasing the number and variety of genotypes tested. The use of devices like the GreenSeeker to assess NDVI, infrared thermometers or chlorophyll and other pigments using leaf-clip sensors help to characterize biomass parameters, water status or photosynthetic capacity easily, and were reported as good indicators of maize and wheat yield.
- Increasing the throughput capacity of phenotyping platforms is key for reducing the efforts associated to measuring elevated numbers of plots in a frequent basis. In that sense, UAVs present an excellent opportunity to monitor large areas with high spatial and temporal resolution. In the cases that the adoption of UAV technology can be limited, the attachment of a camera to a pole represents an innovative option for canopy assessments of tall crops such as maize.
- Imaging methodologies play a vital role for the phenotyping data collection of complex traits related to the growth, yield and adaptation to abiotic stress. Ground

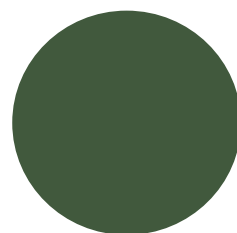
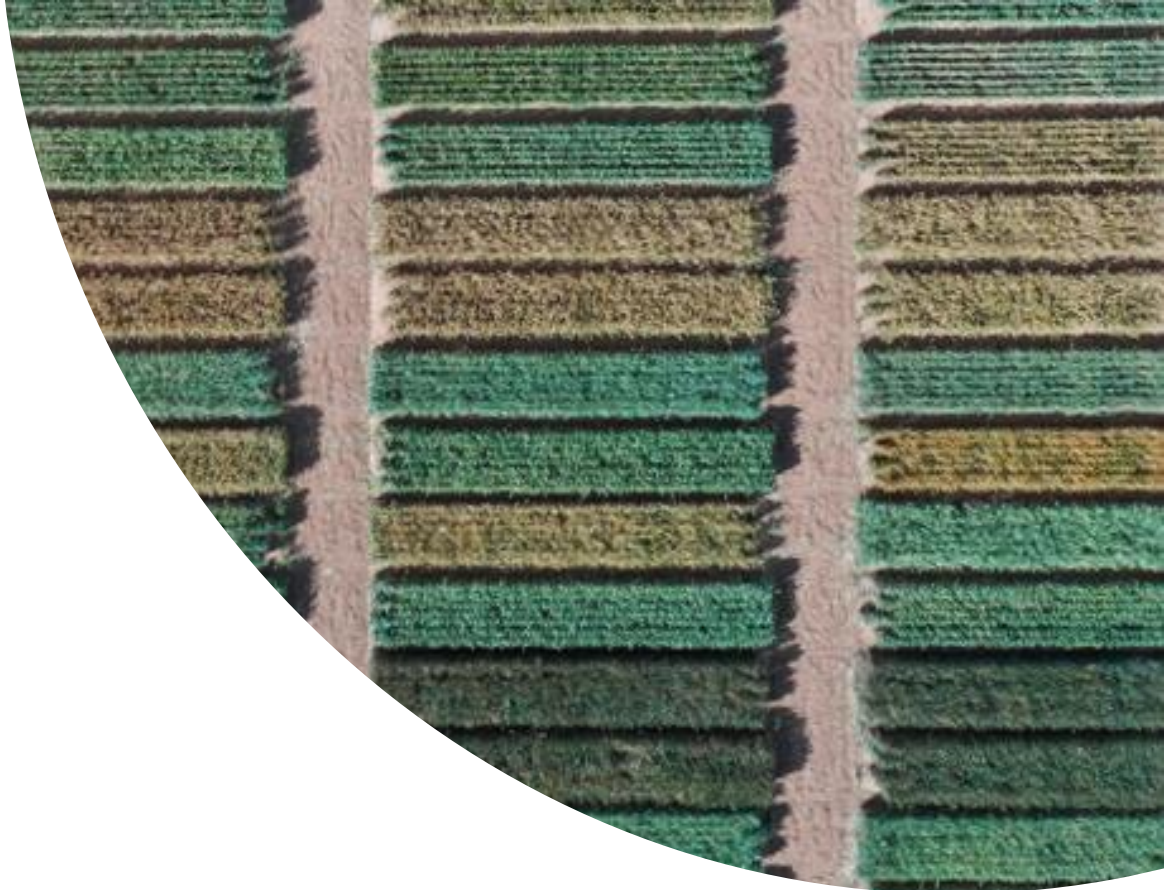
and aerial assessments of the same traits performed very similarly assessing genotypic GY differences. Nevertheless, incorporating imaging methodologies into aerial-based platforms permits to cover larger experimental areas in less time, minimizing the temporal variation in environmental variables, like occurrence of clouds, while the effect platform distance to the target canopy on the image resolution have a low impact on the measurements. Most clear benefits were reported in the canopy temperature assessments, which aerial measurements performed better predicting GY than the ground evaluations.

- There is a need for phenotyping tools which increase the selection efficiency and to understand mechanisms of nutrient deficiency tolerance. In that sense, the calculation of above-ground biomass VIs of maize development will help in the selection of better performing cultivars and to monitor yields.
- Significant yield benefits in Sub-Saharan Africa are possible under conservation agriculture practices with an adequate nitrogen and residue cover management. Here, remote sensing tools could help to monitor N fertilizer input efficiency to optimize GY, but the application of these techniques under CA can be affected by the noise of the soil cover with stover. The application of a vegetation mask based on NDVI values helped to overcome that limitation and improved the grain yield predictions.
- A better understanding of the strengths and limitations of the measurements across crop phenology will help to find the best moments to perform the samplings and thus improve the GY forecasting. Increasing wheat yield potential under water-limited environments is possible through delaying leaf senescence and extending the duration of grain filling. Stay-green traits derived from higher values of Vis,

particularly during grain filling, reported to be indicative of higher grain yields in the Mediterranean type climates where the trials were conducted.

- Independently of the measurement of green biomass amounts, which informs on the potential photosynthetic capacity, differences in photosynthetic efficiency reported to be of great importance while assessing genotypic differences in wheat yield. Changes in concentration of leaf pigments, canopy multispectral VIs like PRI and water status indicators like CT were key traits for estimation of the photosynthetic variability induced by heat and drought when measured during flowering and reproductive stages.
- Since data collection is no longer considered as a bottleneck concern partly thanks to the use of UAVs platforms, new tools to overcome the data analysis barrier are needed. The goal is about automating the image processing and analysis for the extraction of VIs. In the case of image segmentation for UAV plant phenotyping studies, in this thesis we developed the MosaicTool software, that permitted the semi-automatic segmentation of the complete field images (RGB, multispectral and thermal) and then the rapid formulating of VIs.
- Despite being a low-cost tool, VIs derived from conventional RGB cameras are presented as a robust alternative to the use of other more expensive and sophisticated methodologies. The colour properties calculations of the canopy in high resolution images are valuable information of crop variability, even performing better than the multispectral and thermal approximations.
- Yield forecasting statistical models, aside from predict crop production, can be practical for exploring the opportunities of different cultivars on specific cultivation areas. Models based on phenotypic data help to understanding the interactive effects of genotypes with the agronomic and environmental factors on

crop performance by the description on ideotypes for specific agro-climatic conditions.

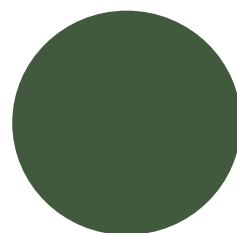
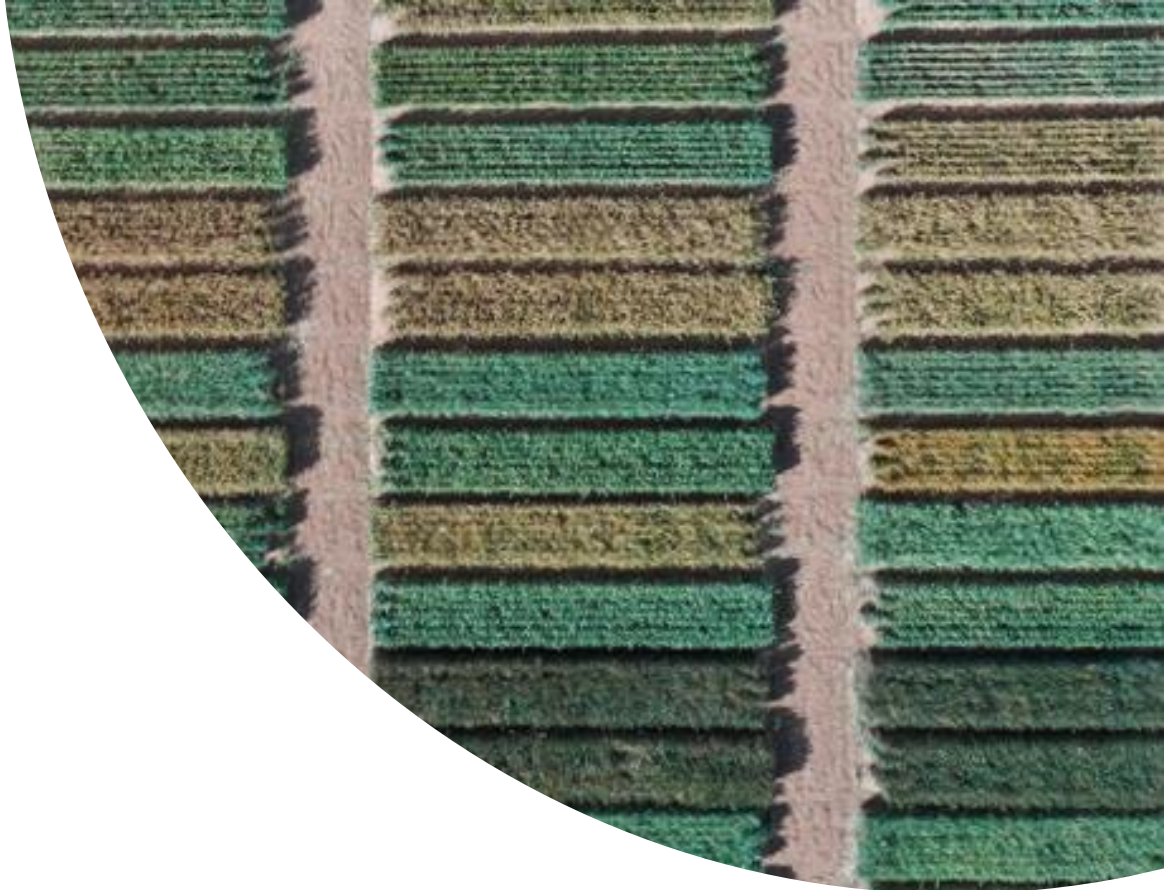


RESUM GENERAL DE LA TESI

RESUM DE LA TESI

La producció de suficient aliment per a una població cada cop més gran és un dels reptes més importants per al pròxim segle. Per assolir la demanda, la productivitat dels cultius han d'augmentar alhora que fan front als efectes del canvi climàtic com increment de les temperatures i la intensitat dels períodes de sequera. La millora de la capacitat dels cultius és un element clau per a l'adaptació a aquestes condicions més exigents i la selecció de varietats més productives sota ambients específics requereix una millor comprensió de l'aclimatació dels cultius als estressos. La recerca en fenotipatge de cultius té com objectiu el desenvolupament de noves metodologies d'alt rendiment capaces de caracteritzar característiques d'interès de les plantes d'una manera no destructiva. Sota condicions de camp, l'aplicació de metodologies tradicionals en experiments grans laboriós i requereix molt de temps. El principal objectiu d'aquesta tesi ha estat el desenvolupament i estudi diferents metodologies de caràcter versàtil, precises i d'alta capacitat per a millorar les mesures de com es desenvolupen els cultius, alhora de que es redueixen els costos i el temps requerit per a fer els mostrejos. El treball es basa en dos dels principals cereals: el blat i el blat de moro. L'ús de vehicles aeris no tripulats (UAV, del anglès *Unmanned Aerial Vehicles*) equipats amb càmeres i sensors (RGB, multiespectrals i termals) permet mesurar simultàniament hectàrees de camps experimentals d'una manera ràpida, precisa i sense la destrucció de mostra. Tot i així, les mesures a nivell de terra també són una alternativa prou potent pel que fa el cost i la resolució espacial. La capacitat d'aquestes metodologies per a mesurar diferències genotípiques en el rendiment del blat de moro i el blat ha estat analitzada sota diferents condicions de creixement com la deficiència de nutrients, pràctiques de agricultura de conservació, sequera i altes temperatures. Per una banda, els estudis de blat de moro es van desenvolupar a Zimbabwe i estaven focalitzats en l'avaluació de genotips sota

condicions diferents de fòsfor o en l'aplicació de l'agricultura de conservació per combatre la pobresa mineral dels sòls. En aquests estudis, les mesures relacionades amb paràmetres de biomassa aèria durant estadis primerencs de desenvolupament va funcionar bé com a indicadors de rendiment. A més, durant estadis fenològics més avançats, mesures de color de la capçada del cultiu van estar associats tant amb el rendiment com amb el contingut de nitrogen en les fulles. En el cas del blat, les evaluacions es van dur a terme a diferents latituds d'Espanya, cobrint un ampli rang de condicions climàtiques i agronòmiques. Els mostrejos es van realitzar en diferents estadis fenològics. En termes generals, els indicadors de biomassa i d'estat hídric del cultiu han estat de les mesures més correlacionades amb el rendiment. L'endarreriment de la senescència del cultiu en els ambients on l'aigua era el factor més limitant i el potencial fotosintètic mesurat per index multispectrals durant la floració del cultiu han estat rellevants sota condicions de sequera i sembra tardana, respectivament.



REFERENCES

REFERENCES

- Araus, J. L., and Cairns, J. E. (2014). Field high-throughput phenotyping: The new crop breeding frontier. *Trends Plant Sci.* 19, 52–61.
- Araus, J. L., and Kefauver, S. C. (2018). Breeding to adapt agriculture to climate change: affordable phenotyping solutions. *Curr. Opin. Plant Biol.* 45, 237–247.
- Araus, J. L., Cabrera-Bosquet, L., Serret, M. D., Bort, J., and Nieto-Taladriz, M. T. (2013). Comparative performance of $\delta^{13}\text{C}$, $\delta^{18}\text{O}$ and $\delta^{15}\text{N}$ for phenotyping durum wheat adaptation to a dryland environment. *Funct. Plant Biol.* 40, 595–608.
- Araus, J. L., Kefauver, S. C., Zaman-Allah, M., Olsen, M. S., and Cairns, J. E. (2018). Translating High-Throughput Phenotyping into Genetic Gain. *Trends Plant Sci.* 23, 451–466.
- Asseng, S., Ewert, F., Martre, P., Rötter, R. P., Lobell, D. B., Cammarano, D., et al. (2015). Rising temperatures reduce global wheat production. *Nat. Clim. Chang.* 5, 143–147.
- Atzberger, C. (2013). Advances in remote sensing of agriculture: Context description, existing operational monitoring systems and major information needs. *Remote Sens.* 5, 949–981.
- Bateman, A. S., Kelly, S. D., and Jickells, T. D. (2005). Nitrogen isotope relationships between crops and fertilizer: Implications for using nitrogen isotope analysis as an indicator of agricultural regime. *J. Agric. Food Chem.* 53, 5760–5765.
- Baudron, F., Delmotte, S., Corbeels, M., Herrera, J. M., & Tittonell, P. (2015). Multi-scale trade-off analysis of cereal residue use for livestock feeding vs. soil mulching in the Mid-Zambezi Valley, Zimbabwe. *Agric. Syst.*, 134, 97–106.

- Berger, B., Parent, B., & Tester, M. (2010). High-throughput shoot imaging to study drought responses. *J. Exp. Bot.*, 61(13), 3519–3528.
- Buchaillet, M. L., Gracia-Romero, A., Vergara-Diaz, O., Zaman-Allah, M. A., Tarekegne, A., Cairns, J. E., et al. (2019). Evaluating maize genotype performance under low nitrogen conditions using RGB UAV phenotyping techniques. *Sensors*, 19.
- Buerkert, A., Moser, M., Kumar, A. K., Fürst, P., & Becker, K. (2001). Variation in grain quality of pearl millet from Sahelian West Africa. *Field Crops Res.*, 69(1), 1–11.
- Bullock, D. G., and Anderson, D. S. (1998). Evaluation of the Minolta SPAD-502 chlorophyll meter for nitrogen management in corn. *J. Plant Nutr.* 21, 741–755.
- Calzadilla, A., Rehdanz, K., Betts, R., Falloon, P., Wiltshire, A., and Tol, R. S. J. (2013). Climate change impacts on global agriculture. *Clim. Change* 120, 357–374.
- Carstensen, A., Herdean, A., Schmidt, S. B., Sharma, A., Spetea, C., Pribil, M., et al. (2018). The impacts of phosphorus deficiency on the photosynthetic electron transport chain1. *Plant Physiol.* 177, 271–284.
- Casadesús, J., Kaya, Y., Bort, J., Nachit, M. M., Araus, J. L., Amor, S., Ferrazzano, G., Maalouf, F., Maccaferri, M., Martos, V., Ouabbou, H., & Villegas, D. (2007). Using vegetation indices derived from conventional digital cameras as selection criteria for wheat breeding in water-limited environments. *Ann. Appl. Biol.*, 150(2), 227–236.
- Cerovic, Z. G., Masdoumier, G., Ghazlen, N. Ben, and Latouche, G. (2012). A new optical leaf-clip meter for simultaneous non-destructive assessment of leaf chlorophyll and epidermal flavonoids. *Physiol. Plant.* 146, 251–260.

Charles, H., Godfray, J., Beddington, J. R., Crute, I. R., Haddad, L., Lawrence, D., et al. (2010). Food Security: The Challenge of Feeding 9 Billion People. Available at: <http://science.sciencemag.org/>.

Chivenge, P., Vanlauwe, B., & Six, J. (2011). Does the combined application of organic and mineral nutrient sources influence maize productivity? A meta-analysis. *Plant and Soil* 342(1):1-30.

Choi, W.-J., Lee, S.-M., Ro, H.-M., Kim, K.-C., and Yoo, S.-H. (2002). Natural ¹⁵N abundances of maize and soil amended with urea and composted pig manure. *Plant and Soil* 245, 223–232

Christopher, J. T., Veyradier, M., Borrell, A. K., Harvey, G., Fletcher, S., and Chenu, K. (2014). Phenotyping novel stay-green traits to capture genetic variation in senescence dynamics. *Funct. Plant Biol.*, 1035–1048.

Cole, M. B., Augustin, M. A., Robertson, M. J., and Manners, J. M. (2018). The science of food security. *Sci. Food* 2, 1–8.

Condon, A. G., Richards, R. A., Rebetzke, G. J., and Farquhar, G. D. (2004). Breeding for high water-use efficiency. *J. Exp. Bot.* 55, 2447–2460.

Coppens, F., Wuyts, N., Inzé, D., & Dhondt, S. (2017). Unlocking the potential of plant phenotyping data through integration and data-driven approaches. *Curr. Opin. Syst. Biol.* 4, 58-63.

Costa, C., Schurr, U., Loreto, F., Menesatti, P., and Carpentier, S. (2019). Plant phenotyping research trends, a science mapping approach. *Front. Plant Sci.* 9, 1–11.

- Crain, J., Reynolds, M., and Poland, J. (2017). Utilizing high-throughput phenotypic data for improved phenotypic selection of stress-adaptive traits in wheat. *Crop Sci.* 57, 648–659.
- Deery, D. M., Rebetzke, G. J., Jimenez-Berni, J. A., James, R. A., Condon, A. G., Bovill, W. D., Hutchinson, P., Scarrow, J., Davy, R., & Furbank, R. T. (2016). Methodology for high-throughput field phenotyping of canopy temperature using airborne thermography. *Fron. Plant Sci.*, 7, 1808.
- Diffenbaugh, N. S., and Giorgi, F. (2012). Climate change hotspots in the CMIP5 global climate model ensemble. *Clim. Change* 114, 813–822.
- Dourado-Neto, D., Teruel, D. A., Reichardt, K., Nielsen, D. R., Frizzone, J. A., & Bacchi, O. O. S. (1998). Principles of crop modeling and simulation: I. uses of mathematical models in agricultural science. *Sci. Agric.*, 55, 46–50.
- Evans, J. R. (1983). Nitrogen and Photosynthesis in the Flag Leaf of Wheat (*Triticum aestivum* L.). *Plant Physiol.* 5, 297–302.
- FAO, IFAD, UNICEF, WFP, W. (2020). Food Security and Nutrition in the World.
- Farquhar, G. D. (1983). On the Nature of Carbon Isotope Discrimination in C4 Species. *Funct. Plant Biol.*, 10(2), 205-226.
- Farquhara, G. D., and Richardsb, R. A. (1984). Isotopic Composition of Plant Carbon Correlates with Water-use Efficiency of Wheat Genotypes. *Funct. Plant Biol.*, 11(6), 539-552.
- Fernandez-Gallego, J. A., Kefauver, S. C., & Vatter, T. (2019). Low-cost assessment of grain yield in durum wheat using RGB images. *Eur. J. Agron.*, 105, 146–156.

- Fiorani, F., & Schurr, U. (2013). Future Scenarios for Plant Phenotyping. *Annu. Rev. Plant Biol.*, 64(1), 267–291.
- Fischer, R. A., Rees, D., Sayre, K. D., Lu, Z.-M., Condon, A. G., and Saavedra, A. L. (1998). Wheat Yield Progress Associated with Higher Stomatal Conductance and Photosynthetic Rate, and Cooler Canopies. *Crop Sci.* 38, 1467–1475.
- Frels, K., Guttieri, M., Joyce, B., Leavitt, B., and Baenziger, P. S. (2018). Evaluating canopy spectral reflectance vegetation indices to estimate nitrogen use traits in hard winter wheat. *F. Crop. Res.* 217, 82–92.
- Gamon, J. A., Peñuelas, J., & Field, C. B. (1992). A narrow-waveband spectral index that tracks diurnal changes in photosynthetic efficiency. *Remote Sens. Environ.*, 41(1), 35–44.
- Gitelson, A. A., Merzlyak, M. N., and Chivkunova, O. B. (2001). Optical Properties and Nondestructive Estimation of Anthocyanin Content in Plant Leaves. *Photochem. Photobiol.* 74, 38.
- Good, A. G., & Beatty, P. H. (2011). Fertilizing nature: A tragedy of excess in the commons. *PLoS Biol.*, 9(8).
- Gracia-Romero, A., Kefauver, S. C., Fernandez-Gallego, J. A., Vergara-Díaz, O., Nieto-Taladriz, M. T., & Araus, J. L. (2019). UAV and ground image-based phenotyping: A proof of concept with durum wheat. *Remote Sens.*, 11(10).
- Hassan, M. A., Yang, M., Rasheed, A., Yang, G., Reynolds, M., Xia, X., et al. (2019). A rapid monitoring of NDVI across the wheat growth cycle for grain yield prediction using a multi-spectral UAV platform. *Plant Sci.* 282, 95–103.

Idso, S. B., Jackson, R. D., Pinter, P. J., Reginato, R. J., and Hatfield, J. L. (1981). Normalizing the stress-degree-day parameter for environmental variability. *Agric. Meteorol.* 24, 45–55.

International Panel on Climate Change (2019). The IPCC and the Sixth Assessment cycle. Sixth Rep.

Jackson, R. D., Reginato, R. J., and Idso, S. B. (1988). Wheat canopy temperature: A practical tool for evaluating water requirements. *Water Resour. Res.* 13, 651–656.

Jaleta, M., Kassie, M., & Shiferaw, B. (2013). Tradeoffs in crop residue utilization in mixed crop – livestock systems and implications for conservation agriculture. *Agric. Syst.*, 121, 96–105.

Jones, H. G. (2002). Use of infrared thermography for monitoring stomatal closure in the field: application to grapevine. *J. Exp. Bot.* 53, 2249–2260.

Juliana, P., Montesinos-López, O. A., Crossa, J., Mondal, S., González Pérez, L., Poland, J., Huerta-Espino, J., Crespo-Herrera, L., Govindan, V., Dreisigacker, S., Shrestha, S., Pérez-Rodríguez, P., Pinto Espinosa, F., & Singh, R. P. (2019). Integrating genomic-enabled prediction and high-throughput phenotyping in breeding for climate-resilient bread wheat. *Theor. Appl. Genet.*, 132(1), 177–194.

Khush, G. S. (1999). Green revolution: Preparing for the 21st century. *Genome* 42, 646–655.

Kuhlgert, S., Austic, G., Zegarac, R., Osei-Bonsu, I., Hoh, D., Chilvers, M. I., et al. (2016). MultispeQ Beta: A tool for large-scale plant phenotyping connected to the open photosynQ network. *R. Soc. Open Sci.* 3.

- Lamers, J., Der Meer, T. Van, and Testerink, C. (2020). How plants sense and respond to stressful environments. *Plant Physiol.* 182, 1624–1635.
- Lukina, E. V, Stone, M. L., & Raun, W. R. (1999). Estimating vegetation coverage in wheat using digital images. *J. Plant Nutr.*, 22(2), 341–350.
- Markwell, J., Osterman, J. C., and Mitchell, J. L. (1995). Calibration of the Minolta SPAD-502 leaf chlorophyll meter. *Photosynth. Res.* 46, 467–472.
- McKersie, B. (2015). Planning for food security in a changing climate. *J. Exp. Bot.* 66, 3435–3450.
- Mittler, R. (2006). Abiotic stress, the field environment and stress combination. *Trends Plant Sci.* 11, 15–19.
- Moran, M. S., Clarke, T. R., Inoue, Y., and Vidal, A. (1994). Estimating crop water deficit using the relation between surface-air temperature and spectral vegetation index. *Remote Sens. Environ.* 49, 246–263.
- Mosa, K. A., Ismail, A., and Helmy, M. (2017). *Plant Stress Tolerance An Integrated Omics Approach.* Cham, Switzerland: Springer.
- Mueller, N. D., Gerber, J. S., Johnston, M., Ray, D. K., Ramankutty, N., and Foley, J. A. (2012). Closing yield gaps through nutrient and water management. *Nature* 490, 254–257.
- Mupangwa, W., Twomlow, S., & Walker, S. (2008). The influence of conservation tillage methods on soil water regimes in semi-arid southern Zimbabwe. *Phys. Chem. Earth*, 33(8–13), 762–767.

- Ogut, J. O., Schulz-Streeck, T., & Piepho, H. P. (2012). Genomic selection using regularized linear regression models: ridge regression. *BMC Proceedings*, 6(Suppl 2), S10.
- Osakabe, Y., Osakabe, K., Shinozaki, K., and Tran, L. S. P. (2014). Response of plants to water stress. *Front. Plant Sci.* 5, 1–8.
- Penuelas, J., Filella, I., Biel, C., Serrano, L., & Save, R. (1993). The reflectance at the 950-970 nm region as an indicator of plant water status. *Int. J. Remote Sens.*, 14(10), 1887–1905.
- Piepho, H. P., & Möhring, J. (2007). Computing heritability and selection response from unbalanced plant breeding trials. *Genetics*, 177(3), 1881–1888.
- Pinto, R. S., Molero, G., and Reynolds, M. P. (2017). Identification of heat tolerant wheat lines showing genetic variation in leaf respiration and other physiological traits. *Euphytica* 213.
- Quintero, A., Molero, G., Reynolds, M. P., & Calderini, D. F. (2018). Trade-off between grain weight and grain number in wheat depends on GxE interaction: A case study of an elite CIMMYT panel (CIMCOG). *Eur. J. Agron*, 92, 17–29.
- Reynolds, M., and Langridge, P. (2016). Physiological breeding. *Curr. Opin. Plant Biol.* 31, 162–171.
- Smith, R. C. G., Barrs, H. D., and Steiner, J. L. (1986). Alternative models for predicting the foliage—Air temperature difference of well irrigated wheat under variable meteorological conditions. I. Derivation of parameters II. Accuracy of predictions. *Irrig. Sci.* 7, 225–236.

- Snape, J. W., Butterworth, K., Whitechurch, E., and Worland, A. J. (2001). Waiting for fine times: genetics of flowering time in wheat. In *Wheat in a global environment* (pp. 67-74). Springer, Dordrecht.
- Thierfelder, C., & Wall, P. C. (2009). Effects of conservation agriculture techniques on infiltration and soil water content in Zambia and Zimbabwe. *Soil Tillage Res*, 105(2), 217–227.
- Thierfelder, C., Rusinamhodzi, L., Ngwira, A. R., Mupangwa, W., Nyagumbo, I., Kassie, G. T., et al. (2015). Conservation agriculture in Southern Africa: Advances in knowledge. *Renew. Agric. Food Syst.* 30, 328–348.
- Thierfelder, C., Rusinamhodzi, L., Setimela, P., Walker, F., & Eash, N. S. (2016). Conservation agriculture and drought-tolerant germplasm: Reaping the benefits of climate-smart agriculture technologies in central Mozambique. *Renew. Agric. Food Syst.*, 31(5), 414–428.
- Tibshirani, R. (1996). Regression Shrinkage and Selection Via the Lasso. *J. R. Stat. Soc. Series B Stat. Methodol.*, 58(1), 267–288.
- Torres-Sánchez, J., Peña, J. M., de Castro, A. I., & López-Granados, F. (2014). Multi-temporal mapping of the vegetation fraction in early-season wheat fields using images from UAV. *Comput. Electron. Agric.*, 103, 104–113.
- Tucker, C. J. (1979). Red and photographic infrared linear combinations for monitoring vegetation. *Remote Sen. Env.*, 8(2), 127–150.
- Valbuena, D., Erenstein, O., Homann-Kee Tui, S., Abdoulaye, T., Claessens, L., Duncan, A. J., Gérard, B., Rufino, M. C., Teufel, N., van Rooyen, A., & van Wijk, M. T. (2012).

Conservation Agriculture in mixed crop-livestock systems: Scoping crop residue trade-offs in Sub-Saharan Africa and South Asia. *Field Crops Res.*, 132, 175–184.

van Klompenburg, T., Kassahun, A., & Catal, C. (2020). Crop yield prediction using machine learning: A systematic literature review. *Comput. Electron. Agric.*, 177, 105709.

Vergara-Díaz, O., Vatter, T., Obata, T., Fernie, A., & Araus, L. (2020). Metabolome Profiling Supports the Key Role of the. *Cells*, 9, 1025.

Vergara-Díaz, O., Zaman-allah, M. A., Masuka, B., Hornero, A., Zarco-Tejada, P., Prasanna, B. M., et al. (2016). A Novel Remote Sensing Approach for Prediction of Maize Yield Under Different Conditions of Nitrogen Fertilization. *Front. Plant Sci.* 7, 1–13.

Vicente-Serrano, S. M., Lopez-Moreno, J. I., Beguería, S., Lorenzo-Lacruz, J., Sanchez-Lorenzo, A., García-Ruiz, J. M., et al. (2014). Evidence of increasing drought severity caused by temperature rise in southern Europe. *Environ. Res. Lett.* 9.

Voltas, J., van Eeuwijk, F. a, Igartua, E., García Del Moral, L. F., Molina-cano, J. L., & Romagosa, I. (2002). Genotype by environment interaction and adaptation in barley breeding: Basic concepts and methods of analysis. *Barley Science: Recent Advances From Molecular Biology to Agronomy of Yield and Quality*, 205–241.

Von Braun, J. (2007). The World Food Situation: New Driving Forces and Required Actions. *Intl. Food Policy Res. Inst.*

Xie, Y., Wang, C., Yang, W., Feng, M., Qiao, X., and Song, J. (2020). Canopy hyperspectral characteristics and yield estimation of winter wheat (*Triticum aestivum*) under low temperature injury. *Sci. Rep.* 10, 1–10.

Yousfi, S., Gracia-Romero, A., Kellas, N., Kaddour, M., Chadouli, A., Karrou, M., et al. (2019). Combined Use of Low-Cost Remote Sensing Techniques and $\delta^{13}\text{C}$ to Assess Bread Wheat Grain Yield under Different Water and Nitrogen Conditions. *Agron.* 9.

Yousfi, S., Kellas, N., Saidi, L., Benlakehal, Z., Chaou, L., Siad, D., et al. (2016). Comparative performance of remote sensing methods in assessing wheat performance under Mediterranean conditions. *Agric. Water Manag.* 164, 137–147.

Yousfi, S., Serret, M. D., Márquez, A. J., Voltas, J., and Araus, J. L. (2012). Combined use of $\delta^{13}\text{C}$, $\delta^{18}\text{O}$ and $\delta^{15}\text{N}$ tracks nitrogen metabolism and genotypic adaptation of durum wheat to salinity and water deficit. *New Phytol.* 194, 230–244.



UNIVERSITAT^{DE}
BARCELONA

April 2021